CRANFIELD UNIVERSITY

ABDULLAHI OBONYEGBA ABU

INTEGRATED APPROACH FOR STRESS BASED LIFING OF AERO GAS TURBINE BLADES

SCHOOL OF ENGINEERING
DEPARTMENT OF POWER AND PROPULSION

PhD

Academic Year: 2013 - 2014

Supervisors: Dr. Panagiotis Laskaridis

Professor Riti Singh

December, 2013

CRANFIELD UNIVERSITY

SCHOOL OF ENGIEERING
DEPARTMENT OF POWER AND PROPULSION

PhD

Academic Year 2013 - 2014

ABDULLAHI OBONYEGBA ABU

INTEGRATED APPROACH FOR STRESS BASED LIFING OF AERO GAS TURBINE BLADES

Supervisors: Dr. Panagiotis Laskaridis

Professor Riti Singh

December, 2013

This thesis is submitted in partial fulfilment of the requirements for the degree of Doctor of Philosophy

ABSTRACT

In order to analyse the turbine blade life, the damage due to the combined thermal and mechanical loads should be adequately accounted for. This is more challenging when detailed component geometry is limited. Therefore, a compromise between the level of geometric detail and the complexity of the lifing method to be implemented would be necessary. This thesis therefore focuses on how the life assessment of aero engine turbine blades can be done, considering the balance between available design inputs and adequate level of fidelity. Accordingly, the thesis contributes to developing a generic turbine blade lifing method that is based on the engine thermodynamic cycle; as well as integrating critical design/technological factors and operational parameters that influence the aero engine blade life. To this end, thermo-mechanical fatigue was identified as the critical damage phenomenon driving the life of the turbine blade.

The developed approach integrates software tools and numerical models created using the minimum design information typically available at the early design stages. Using finite element analysis of an idealised blade geometry, the approach captures relevant impacts of thermal gradients and thermal stresses that contribute to the Thermo-mechanical Fatigue damage on the gas turbine blade. The blade life is evaluated using the Neu/Sehitoglu Thermo-mechanical Fatigue model that considers damage accumulation due to fatigue, oxidation, and creep. The leading edge is examined as a critical part of the blade to estimate the damage severity for different design factors and operational parameters. The outputs of the research can be used to better understand how the environment and the operating conditions of the aircraft affect the blade life consumption and therefore what is the impact on the maintenance cost and the availability of the propulsion system. This research also finds that the environmental (oxidation) effect drives the blade life and the blade coolant side was the critical location. Furthermore, a parametric and sensitivity study of the Neu/Sehitoglu model parameters suggests that in addition to four previously reported parameters, the sensitivity of the phasing to oxidation damage would be critical to overall blade life.

All thanks and praises belong to Allah, the almighty creator.

ACKNOWLEDGEMENTS

I wish to sincerely thank my supervisor Dr Panagiotis Laskaridis for his guidance, support and invaluable advice, throughout my PhD research. Many thanks to my advisor, Professor Riti Singh, for his support and assistance. My appreciation also goes to Prof Pilidis, and to all the Department of Power and Propulsion staff at Cranfield University.

I am very grateful to the Chief of the Air Staff of the Nigerian Air Force for sponsoring the course. Also, the efforts and contributions by Samir Eshati, Esmail Najafi Saatlou, Panos Giannakikis, Godwin Abbe, Luis Conssolino and Angelinas Stamatis are highly appreciated. To Alice and the MSc students I worked with: Alex, Pablo, Jose, Alvaro, Jon and Mazhar, I say a big thank you for your cooperation.

Lastly, this project would not have been successfully completed without the prayers of my parents, and the patience, endurance and painful sacrifices of my wife and kids. Words can therefore not express my profound gratitude to my dear parents and family.

Publications

A . Abu, S. Eshati, P. Laskaridis, R.Singh “Aero-engine turbine blade life assessment using the Neu/Sehitoglu damage model” *International Journal of Fatigue*, *In Press**, Available online 28 November 2013.*

A. Abu, S. Eshati, P. Laskaridis, A. Haslam “*Physics based approach to gas turbine blade thermo- mechanical fatigue life assessment”*. 21st International Symposium on Air breathing Engines, ISABE 2013. 9 -13 September, Busan South Korea.

S Eshati, A. Abu, P. Laskaridis, Firoz Khan “Influence of humidity on the heat transfer and creep life of high pressure gas turbine blade” *Applied Thermal Engineering*, *Volume 60, Issues 1–2*, *2 October 2013*, *Pages 335-347.*

Samir Eshati, Abdullahi Abu, Panagiotis Laskaridis, Anthony Haslam, “Investigation Into The Effects of Operating Conditions and Design Parameters on The Creep Life of High Pressure Turbine Blades In A Stationary Gas Turbine” *Mechanics and Mechanical Engineering*.Vol. 15, No. 3 (2011) 237–247, Technical University of Lodz.

Samir Eshati, Abdullahi Abu, Panagiotis Laskaridis, Anthony Haslam, “*Investigation Into the effects of operating conditions and design parameters on the creep life of high pressure turbine blades in a stationary gas turbine engine*” 10th international symposium on compressor and turbine flow systems-theory and application areas, SYMKOM, 2011, Lodz, 26-28 October, 2011

E. Najafi Saatlou, K.G. Kyprianidis, V. Sethi, A.O. Abu, P. Pilidis, • ‘On The Trade-Off Between Minimum Fuel Burn And Maximum Time Between Overhaul For An Intercooled Aero Engine’ *Proc*. *IMechE Journal of Aerospace Engineering*, *In Press*

W. Mohamed, V. Sethi, P. Pilidis, A.O. Abu ,A.Nasir, O. Lotfi, , ‘*Evaluation of Electricity Cost in a Growing Market’ GT2013-95466* Proceedings of ASME Turbo Expo 2013: Power for Land, Sea and Air, Texas, June 03-07,2013.

TABLE OF CONTENTS

LIST OF FIGURES

LIST OF TABLES

LIST OF SYMBOLS

A	Blade surface area	m^2
A_{Ch}	Cross section area of cooling channel	m^2
A_{cr}	Scaling constant for creep	
b	Fatigue strength exponent	
C		
c	Fatigue ductility exponent	
CG	Centre of Gravity	
CF	Centrifugal stress	
CompEff	compressor efficiency	
C_P	Specific heat	$J/Kg^o\ K$
CwSec	Cool side wall section	
C_{oxid}	Oxidation life constant	
D	Damage	
D_O	Scaling constant for oxidation	
D_i	Damage fraction	
D_h	Hydraulic diameter	*m*
$\mathrm{D}^{\mathrm{creep}}$	Creep damage	
$\mathrm{D}^{\mathrm{fat}}$	Fatigue damage	
D^{ox}	Oxidation damage	
$\mathrm{D}^{\mathrm{tot}}$	Total damage	
d_{CG}	Distance between the rotation axis and Centre of Gravity	
E	Elastic modulus	*Pa*
g_{Sec}	Gas side section	
Hcr	Critical oxide, thickness constant	
h_f	Critical thickness	$W/m^2\ ^oK$
h_{sec}	Blade section height	
K	Blade thermal conductivity	$W/m\ ^oK$
Kr	Rate constant	s^{-1}
Li	Estimated service life	

$_{LE}$	Leading edge	
L_i	Estimated service life	
Li Ref	Reference remnant life	
m_{cb}	Blade cooling mass flow	*Kg/s*
m_{cc}	Channel cooling mass flow	*Kg/s*
N	Number of cycles to failure	
Nu	Nusselt number	
N_{cc}	Number of cycles to creep failure	
N_p	Pure fatigue life at strain-range	
N_{pi}	Pure fatigue life at specific fatigue conditions	
N_{cp}	Number of cycles to mixed creep – fatigue failure	
N_f	Number of cycles to fatigue failure	
${N_f}^{creep}$	Creep life term	
${N_f}^{fat}$	Fatigue life term	
${N_f}^{ox}$	Oxidation life term	
N_i	Limit number of cycles to failure	
n_i	Number of applied cycles at a nominal stress	
P	factor Non- linear damage rule	
Po_{COMPIN}	Compressor inlet stag pressure	*Pa*
PoCOMPOUT	Compressor outlet stag pressure	*Pa*
PoNGV	NGV inlet stag pressure	*Pa*
Pr	Prandtl number	
q	Heat flux	W/m^2
Q	activation energy	*J/mol*
R	Universal gas constant	*J/mol K*
S_c	Coolant side wetted perimeter	*m*
S_g	Hot side wetted perimeter	*m*
St	Stanton number	
T_c	Time to rupture under static creep	*s*

T_{ci}	Time to rupture under specific static creep conditions	*s*
T	Temperature	*K*
Tcin	Inlet coolant temperature	*K*
Tco	Outlet coolant temperature	*K*
TE	Trailing edge	
TET	Turbine entry temperature	*K*
Tg	Hot gas temperature	*K*
T_{cool}	Cooling temperature	*K*
T_H	High temperature	*K*
T_L	Low temperature	*K*
T_m	Blade metal temperature	*K*
T_{max}	Maximum gas temperature	*K*
T_{min}	Minimum gas temperature	*K*
ToC	Coolant stagnation temperature	*K*
ToCOMPOUT	Compressor outlet stagnation emperature	*K*
ToNGV	NGV inlet temperature	*K*
ToOUT	Rotor outlet stagnation temperature	*K*
T_{TBC}	Thermal barrier coolant temperature	*K*
T_{bc}	Blade metal temperature coolant side	*K*
Tw	wall metal temperature	*K*
t_i	Hold time at given stress in cycle	*s*
t_f	Time to failure	*s*
t_r	Time to creep rupture	*s*
T_{bg}	Blade metal temperature gas side	*K*
t_b	Blade thickness	*m*
t_{oxid}	Time of oxidation	*s*
U	Overall heat transfer coefficient	
$V_{Abs\ Root}$	Absolute velocity at blade root	*m/s*
Z	Heat transfer technology level	

Greek

Symbols	Description	Units
α	Coefficient thermal expansion	
α_1	Stress state constant	
α_2	Hydrostatic stress sensitivity constant	
β	Mechanical strain range exponent	
γ	Specific heat ratio	
γ'	Gamma prime alloy content	
$\Delta\varepsilon_{cc}$	Creep inelastic strain	
$\Delta\varepsilon_{cp}$	Mixed creep – fatigue inelastic strain	
$\Delta\varepsilon_{in}$	Total inelastic strain	
$\Delta\varepsilon_{pp}$	Fatigue inelastic strain	
$\Delta\varepsilon T$	Total strain range	
ΔHcr	Activation energy for creep	
ΔH^{OX}	Activation energy for oxidation	J/mol
$\varepsilon_{cooling}$	Overall cooling effectiveness	
$\boldsymbol{\varepsilon}$	Strain	
ε_T	Total strain	
ε_e	Elastic strain	
ε_p	plastic strain	
ε'_f	Fatigue ductility coefficient	
ε_o	Instantaneous plastic strain	
ε_{th}	Thermal strain	
ε_{me}	Mechanical strain	
$\dot{\varepsilon}$	Steady-state creep rate	s^{-1}
$\eta_{cooling}$	Cooling efficiency	
λ_b	Blade thermal conductivity	W/m ^oK
μ	Dynamic viscosity	N s/m^2.
ξ^{ox}	Oxidation phasing constant	
$\boldsymbol{\xi}^{cr}$	Creep phasing constant	
ρ	Blade density	Kg/m^3
σ	Stress	Pa

σ_u	Ultimate tensile strength	Pa
σ_a	Cyclic stress amplitude	Pa
σ'_f	Fatigue strength coefficient	
$\emptyset_{cr}$	Creep phasing factor	
ω	Angular speed	rad/s

LIST OF ABBREVIATIONS

Symbols	Description
1D	One dimension
3D	Three dimension
AEA	Association of European Airlines
APS	Air plasma spray
ASTM	American Society of Testing and Materials
BC	Boundary conditions
CBM	Condition based maintenance
CC	Compressive creep
CFD	Computational fluid dynamics
CG	Centre of gravity
CP	Compressive plasticity
DE	Ductility exhaustion
DP	Design point
DS	Damage summation
FE	Finite element
FEA	Finite element analysis
FLT	Fuzzy logic tool box
FS	Frequency Separation
GI	Ground idle
HCF	High cycle fatigue
HPC	High pressure compressor
HPT	High pressure turbine
IF	Isothermal fatigue
IP	In Phase
ISA	International Standard Atmosphere
LCF	Low cycle fatigue
LE	Leading edge
LHTF	Long haul turbofan
LMP	Larson Miller parameter

LPT	Low pressure turbine
MLW	Maximum Landing weight
MTOW	Maximum takeoff weight
MZFW	Maximum Zero Fuel weight
N/S	Neu/Sehitoglu
NDT	Non destructive test
NGV	Nozzle guide vane
OD	Off design point
OEM	Original equipment manufacturer
OP	Out – of – phase
PC	Plasticity creep
PCN	Relative rotational speed
PP	Compressive plasticity
RPM	Revolutions per minute
RTDF	Radial temperature distribution factor
SEP	Strain energy partitioning
SFC	Specific fuel consumption
SHTF	Short haul turbofan
SRP	Strain range partitioning
TBC	Thermal Barrier Coating
TE	Trailing edge
TGO	Thermal grown oxide
TMF	Thermal-mechanical fatigue
TS	Total strain
WAR	Water Air Ratio

1 INTRODUCTION

1.1 Research Background

The environment and the operating conditions of the aircraft affect the life consumption of engine components and therefore impact on the safety, maintenance cost and the availability of the propulsion system. Consequently, developing adequate and reliable lifing methods to assess the life of aero engines under various operating conditions related to the environment and flight profile gives huge benefits to OEMs and operators alike.

In the gas turbines, the turbine blades are subjected to severe thermal and mechanical loads during operation. At these severe conditions, the blades are prone to failure. Generally, failure due to the contribution of both thermal and mechanical loading is termed Thermo-mechanical fatigue (TMF) [1]. TMF has become more critical to the life of gas turbine blades; due to the use of improved blade cooling technologies that enable higher gas temperatures, thereby improving gas turbine efficiencies. TMF conditions produce significant damage contributions from creep, low cycle fatigue and oxidation mechanisms [2]. This is mainly due to the effect of thermal stresses from thermal gradients and transients in the blade, as well as from the different coefficient of expansion between the blade material and coatings (for coated blades). Adequate modelling of these TMF effects is therefore vital for gas turbine blade lifing assessments.

1.2 Scope, Aim and Objectives

- **Research Scope**

This study focuses on developing a robust lifing approach for physics based TMF life assessment of aero engine turbine blades. The approach is multidisciplinary and generic requiring the minimum design information typically available at the early design stages. Hence, without detailed component

geometry, a life assessment can be easily conducted to further the design space exploration, as well as enable lifetime prediction for maintenance scheduling.

In essence, the lifing approach will establish how software tools and models can be integrated to capture the appropriate thermal and mechanical loads that influence the TMF damage in the turbine blade. To this end, the current study examines what are the critical TMF factors to be considered; why and how an enhanced heat transfer analysis is conducted, How the critical TMF factors could be adequately modelled using finite element analysis of an idealised blade geometry, as well as the inherent limitations .What are the influences of material parameters and how the effect of environment and the operating conditions can be studied in terms of severity (defined as the relative damage sustained by the engine while operating under various conditions).

- **Aim and Objectives**

The aim of this research is to develop a generic Physics based method for evaluating the influence of design characteristics, technology level and aircraft operating conditions on the life and severity of high pressure turbine blades in jet engines. The following define the objectives of the research:

a. To identify the appropriate damage mechanisms, critical parameters and suitable physics based models for TMF life assessment of aero engine turbine blades. This led to the choice of the Neu – sehitoglu (N/S) TMF model in this study.

b. To integrate the software and tools that enable the modelling of thermal and mechanical loads that influence the TMF damage in the turbine blade. Entails implementing: engine and aircraft performance simulation, blade sizing, enhanced heat transfer and Finite Element Analysis (FEA) modelling.

c. Create a simplified turbine blade leading edge FEA model, accounting for critical regions – leading edge, internal cooling hole and root fixing. Deeper analysis of complex systems as the Thermal Barrier Coating (TBC) is enabled. Based on minimum number of design inputs; a generic representation of HPT blades that capture thermal and mechanical behaviour for TMF is explored. In addition to reducing computational cost and time, this will allow easy modification for design studies and sensitivity analyses.

d. Implement the TMF lifing model, and verify the heat transfer analysis and lifing method with a detailed E3 NASA blade: The limitations and uncertainties in choice of geometry as well as influences of model material parameters are identified and quantified. The method is applied to the NASA blade to evaluate its suitability.

e. Study the impact of design and operational factors on TMF life using the developed approach: This is done in terms of severity

1.3 Authors Contribution

1 The present research contributes to knowledge by developing a generic turbine blade lifing method that is based on the engine thermodynamic cycle; as well as incorporating critical design/technological factors, operational parameters and variable loading cycles that influence the blade TMF life. All these being achieved using minimum design inputs and maintaining the necessary fidelity.

a) The developed approach therefore aids design space exploration by enabling improved assessment of the turbine blade durability at preliminary stages.
b) The approach provides a reliable and cost effective means for people who may not be experts in the specific fields, but are

involved in gas turbine operations and life assessment (such as performance engineers, maintenance engineers, supervisors and technicians).

2 The idealised turbine leading edge geometries devised and verified in this study can be used for thermo- mechanical analysis on complex 3D blades, and for assessing new turbine blade designs and cooling technologies. Particularly, in evaluating the thermal gradients developed in the leading edge and the associated thermal stresses. This will reduce the complexity, as well as the computational cost and time associated with such analysis.

3 The investigation into the influences of the N/S TMF model material parameters identified 5 sensitive parameters out of the nineteen model parameters. Four of these parameters were previously identified by Amaro [3], using available out - of - phase TMF experimental data. For a typical aircraft operating condition with arbitrary temperature - strain phasing histories, this research identifies the shape factor for environmental damage phasing function (ξ_{ox}) as an additional influencing parameter in the TMF life assessment of aero engine turbine blades. This finding has been published in the International Journal of Fatigue.

4 The developed method contributes to the understanding of TMF modelling and quantitative life assessment in aero engine turbine blades. It provides pertinent information on how by linking the aircraft flight and engine performance outputs with an enhanced engineering heat transfer analysis, the thermal gradient and thermal transient's inputs critical to TMF are obtained. In terms of the TMF lifing assessment, the equivalent independent variables such as effective stress; thermal strain and mechanical strain are identified and extracted from the FEA to implement the N/S model.

A rain flow cycle counting method is also implemented, such that any complex flight loading history can easily be accommodated. These procedures and engineering analysis to examine TMF lifing for aero engine turbine blades using basic design inputs, provides a unique approach not documented in the open literature.

5 The developed TMF lifing approach indicates more damage severity compared to the IF method. However, much of the available severity studies have been based on the IF methods. Hence, this work further broadens the understanding of the damage severity on turbine blade life due to operating aero engines in various OAT conditions, flight length and application of take-off derate. In terms of safety, the TMF severity results would be preferred, and these can then be factored into engine direct maintenance costs.

6 Lastly, the FEA models, procedures and steps for the TMF analysis have been formally documented to facilitate future TMF analysis on turbine blades. This also supplements the Department of Power and Propulsion's structural integrity capability.

1.4 Thesis Outline

This thesis comprises ten chapters; starting with the research outlook, including the thesis scope, aims, objectives and authors contribution in **Chapter one**. Thereafter:

Chapter 2 "Turbine Blade Damage Mechanisms, Lifing and Heat transfer"

This chapter highlights the main turbine blade damage mechanisms, lifing methods and heat transfer process. This gives a preliminary understanding of the turbine blade working environment.

Chapter 3 “Thermo-Mechanical Fatigue”

This chapter reviews thermo-mechanical fatigue (TMF). The TMF definitions are examined, as well as TMF experiments and their application to gas turbine blades. TMF models and TMF lifing approaches are summarised from previous research in the open literature, from which a suitable TMF model implemented in this study was identified; fulfilling objective 1.

Chapter 4 “Methodology”

This chapter describes the TMF lifing approach developed to achieve the second and third objectives in this thesis. The approach comprises 6 main components, namely: performance model (aircraft and engine), component sizing, stress model, heat transfer model, FEA model, and TMF damage model. Each of the main components of the approach and the link between them is explained.

Chapter 5 “Tools and Models: Result Analysis”

The implementation of the overall methodology of this work is covered: Performance simulation, turbine sizing, heat transfer analysis and the FEA implementation. The calculation of TMF life using the N/S TMF model is also highlighted. The results of a reference mission are examined showing the thermal gradients, transients and the evolution of the thermo-mechanical stresses. This achieves the fourth objective.

Chapter 6 “Geometry and Method Verification”

The rational for idealising the turbine blade is argued in this chapter and the effects of the assumptions made are verified in relation to a detailed NASA blade. What influence does the choice of a geometric shape have? And what are the uncertainties in terms of the lifing results? These questions are addressed in this chapter.

Chapter 7 “Influence of TMF Model Material Parameters”

In this chapter, the influence of the TMF model parameters is examined via a sensitivity analysis. This was necessary because the TMF parameters require detailed experiments and are not available for many materials. Hence, the need to determine the most critical parameters.

Chapter 8 “Case Studies”

This chapter demonstrates the ability of the developed approach to evaluate the impact of various design and operating conditions on the turbine blade. This is done using the concept of severity.

Chapter 9 “Thermal Barrier Coating (TBC) FEA Model”

The developed approach was further explored to examine the impact of TBC on a surface level. This chapter shows how the approach could handle the complex modelling and analysis of the impact of TBC on the blade life.

Chapter 10, “Conclusions and Recommendations for Future Work”

The final chapter of this thesis provides the conclusions of the work presented in each chapter. Also, the limitations of the model and recommendations to improve the lifing approach are suggested.

2 TURBINE BLADE DAMAGE MECHANISMS, LIFING AND HEAT TRANSFER

2.1 Common damage mechanisms

The principal individual damage mechanisms that affect the life of gas turbine hot section components include creep, fatigue, oxidation and sulphidation as depicted in Figure 2-1. In aero engines, the turbine components could continuously deform when subjected to steady loads at high temperatures (creep); as well as fail due to the impact of cyclic loading (fatigue). At operating temperatures of approximately below 800^{o}C, mechanical fatigue is usually the principal damage mechanism. Oxidation exerts little influence within this range. However, at temperatures above 1000^{o}C, creep, oxidation and thermal fatigue (acting singly or collectively), are usually the major causes of failure [4]. Nevertheless, depending on the structure, the material, and the engine cycle employed, any of the damage mechanisms may be dominant between 800^{o}C and 1000^{o}C. Furthermore, based on the possible interaction of the major damage mechanisms a region of available life may be identified as shown in Figure 2-1.

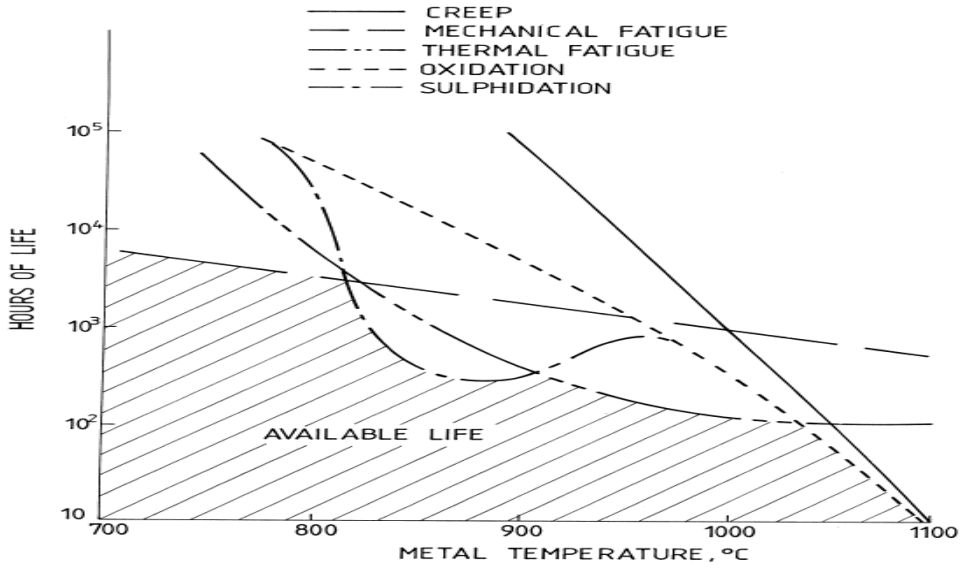

Figure 2-1: Factors influencing a turbine-component's life [4]

2.1.1 Creep

The creep process can be described as a continuous deformation that occurs at constant high temperatures due to the stress induced in an operating component over a period of time. The rate of creep deformation is a function of temperature, stress, and time. The material properties are also a major influence on creep behaviour. Being a thermally motivated phenomenon, significant creep damage would usually occur when the metal temperature reaches 40 – 50% of its melting point [5][6]. Creep estimation is usually done by using parametric techniques that incorporate time stress and temperature test data into a single expression. Some of the widely used time-temperature parameters include Orr-Sherby-Dorn parameter (OSD), Goldhoff- Sherby parameter (GSP), Manson-Haferd parameter (MHP), Manson-Succop parameter, (MSP) and Larson Miller parameter (LMP). A succinct summary of these parameters is provided in [7]. Figure 2-2 gives a schematic representation of constant – stress lines and the underlying equations for the common parametric techniques. Amongst the aforementioned parametric techniques, the LMP is still considered the most favourable because it is simple to use and popular [8][9].

2.1.1.1 Larson Miller Parameter (LMP)

The LMP combines temperature and creep life data for evaluating the effects of stress on creep life over a range of temperatures. It is expressed as:

$$\mathrm{LMP} = \frac{\mathrm{T}}{1000}(\log t_f + \mathrm{C}) \qquad 2\text{-}1$$

Where: T is the absolute operating temperature (K), t_f the time to rupture, and C is a constant value generally taken as 20 [10]. When using the LMP approach to calculate time to failure, a factor of safety is normally applied.

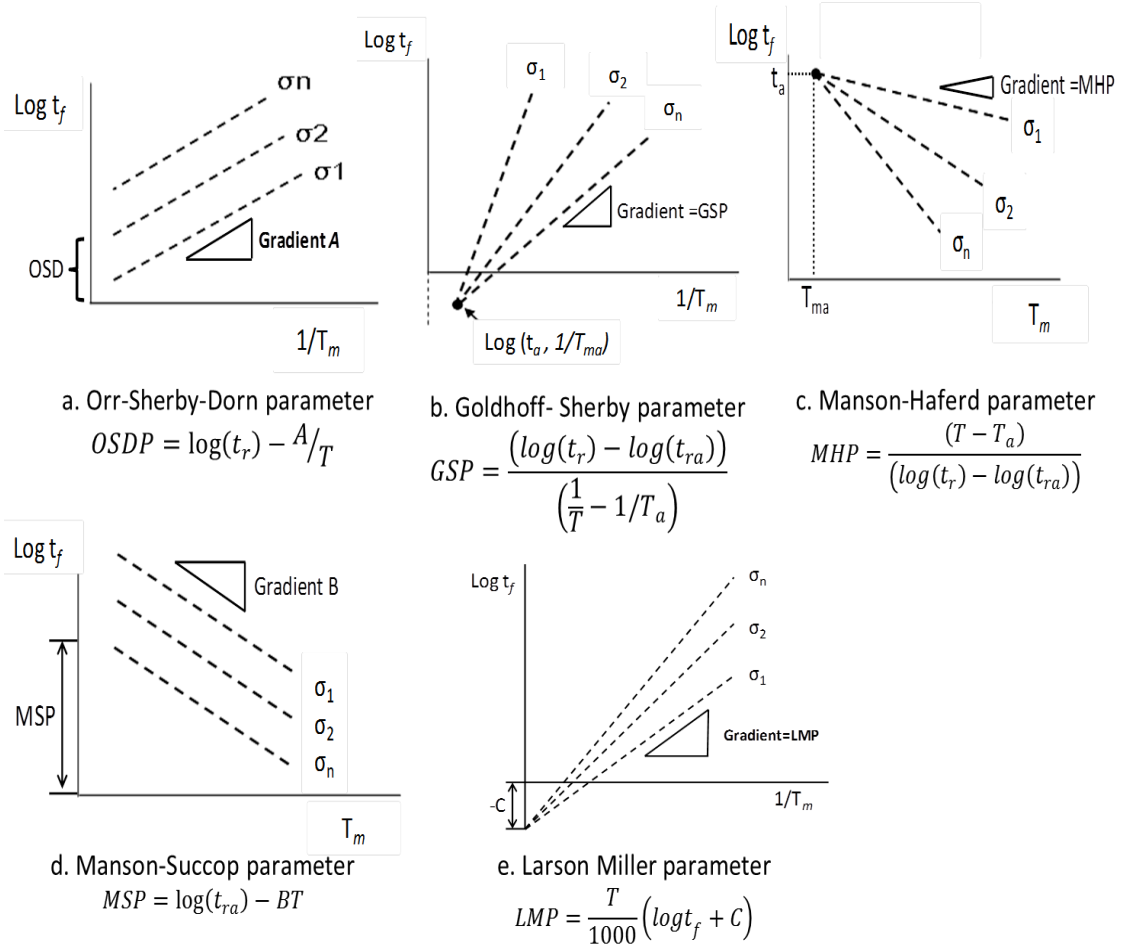

Figure 2-2 Schematic representations of constant- stress lines for commonly used parametric techniques [9].

2.1.2 Fatigue

Fatigue damage will usually occur in a component subjected to repeated or non-steady loads that cause stress and strain variation. Even though the maximum applied stress could be well below the static strength of the material, sufficiently large changes in the stresses could cause fatigue damage in the component. Fatigue damage is characterised by a crack initiation that propagates and eventually leads to fracture. Thus, fatigue failure is usually characterised by three distinct stages as shown in Figure 2-3. Generally, in fatigue analyses, only the crack initiation phase (Stage I) and the crack growth phase (Stage II) are considered. The crack initiation phase is usually analysed

using either a stress-life or strain-life approach. However, the dominant method usually employed for the crack initiation phase is the strain-life approach. The crack growth analysis is done by a fracture mechanics based approach. A total fatigue life prediction could therefore be obtained by combining the crack initiation phase and the crack propagation phase. However, since most engineering components spend their time at either the crack initiation phase or the crack propagation phase, it is normal to conservatively consider only one stage. Furthermore, the inclusion of one phase or another largely depends on the nature of the component under investigation. For gas turbines, both crack initiation and crack propagation would be included for static components such as turbine vanes and blade tip seals. On the other hand, the prediction of life to crack initiation would be important for rotating components such as the turbine blade [11]. To this end, this research mainly examines failure in terms of the life to crack initiation in the turbine blade. Crack propagation and the impact of microstructural changes are therefore not examined in any detail as regards the turbine blade life assessment in this research.

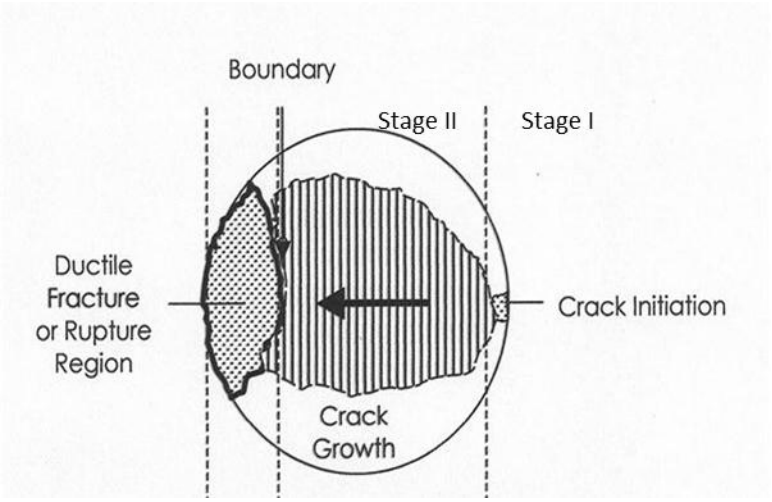

Figure 2-3: Stages of fatigue failure

Depending on the origin of the applied load, fatigue could be mechanical, thermal or thermo-mechanical (TMF). Mechanical fatigue is further divided into Low cycle fatigue (LCF) and high cycle fatigue (HCF).Conservatively, failures

that occur above or below 10^4 are termed as HCF or LCF, respectively. LCF is driven by both thermal and centrifugal stresses. It also depends on the operating temperature, applied load and material properties. LCF is significant in aero engines, considering the relatively high stresses and temperatures that occur during the engine start/stop cycle. Hence, over the years, many methods have been developed for LCF analysis. The Method of Universal slopes (MUS), based on the Coffin - Manson strain – life relationship , is one of the prominent ones used for thermal fatigue analysis [4].

2.1.2.1 Low Cycle fatigue (LCF) Analysis: Coffin- Manson and MUS Approach

In LCF analysis, test results are plotted as cycles to failure (N_f) against total strain range ΔεT, which is the sum of the plastic strain ε_p and elastic strain ε_e components. Both strain components give straight lines when plotted against the logN_f; forming the basis for the MUS. The total strain is given as:

$$\varepsilon_T = \varepsilon_p + \varepsilon_e \qquad 2\text{-}2$$

ε_e can be expressed according to Basquin as:

$$\varepsilon_e = \frac{\sigma_a}{E} = \frac{\sigma'_f}{E}\,(2N_f)^b \qquad 2\text{-}3$$

Where: σ_a the cyclic stress amplitude, σ'f fatigue strength coefficient, N_f number of cycles to failure and b fatigue strength exponent.

While, ε_p is given as [12]:

$$\varepsilon_p = \varepsilon'_f(2N_f)^C \qquad 2\text{-}4$$

Where: ε'$_f$ is the fatigue ductility coefficient, N_f number of cycles to failure and *c* the fatigue ductility exponent.

By summing the plastic and elastic components, the strain life curve equation gives:

$$\varepsilon_t = \frac{\Delta\varepsilon}{2} = \frac{\sigma'_f}{E}\,(2N_f)^b + \varepsilon'_f(2N_f)^C \qquad 2\text{-}5$$

The MUS is derived by substituting estimated parameters (obtained from tensile test data) for $\sigma' f \sim 1.75 \times \sigma_u$, *b* = -0.12 and *c* = -0.6 into Equation 2-5.

$$\Delta\varepsilon = 3.5\frac{\sigma_u}{E}\,(N_f)^b + \varepsilon^{0.6}{}_f(N_f)^{-0.6} \qquad 2\text{-}6$$

The MUS is widely used in generic studies [13], [4], [14]. The method assumes that temperature affects fatigue life by its effect on tensile properties. Effects of creep and oxidation are assumed to be absent. For non-isothermal cycles such as obtained in aero engines, the temperature in the cycle that gives the shortest calculated life is used.

2.2.1.2 High Cycle Fatigue (HCF)

HCF may be caused by higher frequency cycles of lower stresses, such as the excitation of a resonant state through variations in gas impulse loads. These variations may be created by a non – uniform temperature and pressure distribution across the face of the turbine through abnormality in the combustion process and velocity differences in the turbine nozzles [15]. Conventionally, failures that occur above 10^4 cycles are termed as HCF and failures below 10^4 cycles as LCF.

2.2.1.3 Thermo-Mechanical Fatigue (TMF)

TMF, as the name implies, is caused by the variation of heating and cooling cycles applied to a component in addition to the mechanical cyclic loading. TMF usually takes place at high temperatures in gas turbine hot section components. A scenario of TMF is the high thermal stresses that are induced in an engine, when it is shut down at a high temperature operating condition and forced to cool to ambient temperature. The rate of change of temperature between these two states induces high level of thermal stress. Combined with a high mechanical loading, these thermally – induced stresses cause localised high transient strains leading to TMF cracks in HPT blades and NGVs that are in direct contact with the hot gas path.

By adopting an adequate approach, finite element (FE) analysis could be used to examine complex thermal and mechanical cycles that induce thermo-mechanical fatigue. Whereas it is widely considered a fatigue process, TMF is uniquely different from isothermal LCF, as will be seen in Chapter 3.

2.1.3 Oxidation

Generally, the growth of oxides on the surface (surface oxidation) causing deterioration and reducing the mechanical integrity of the component describes oxidation damage. For super alloys containing γ' additives, a gamma depleted layer below the surface has been shown to exist [93]. In addition to surface oxide growth, the oxide growths along grain boundaries (intergranular oxidation) and below the external surface (internal oxidation) have also been identified.

Currently, coatings are used to protect the metal substrate from oxidation attack. Neglecting internal oxidation, the oxidation damage in the substrate would usually start after coating spallation and crack. The coating crack provides the means for oxidation attack, resulting in local oxidation in the substrate at the tip of the coating crack. Kadioglu and Sehioglu [16] proposed a model describing this phenomenon in three stages, as depicted in Figure 2-4.

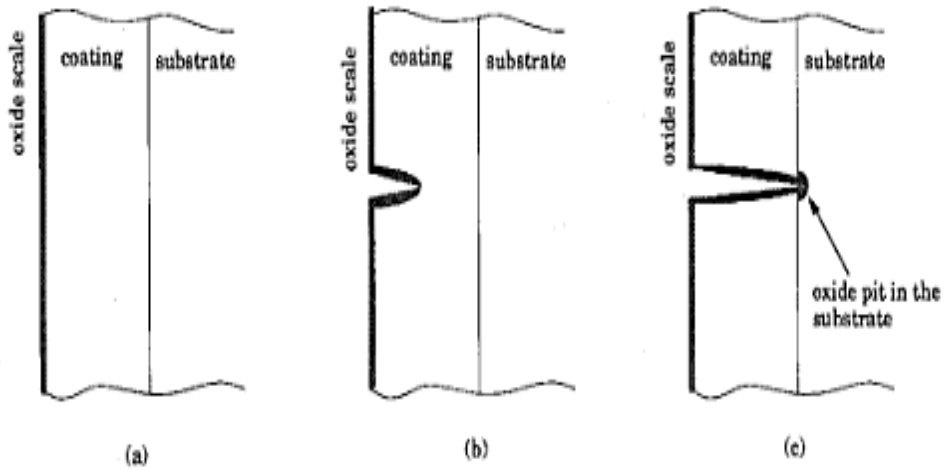

Figure 2-4: Oxide formation on the substrate: (a) oxidation of the coating surface, (b) inititiation of coating crack, and (c) oxidation of the substrate [17],p.27.

Oxidation damage is usually more severe at high temperatures and depends on the time, chemical composition of the hot gas stream, surface conditions and material properties. Different growth laws such as: Linear, parabolic, logarithmic and asymptotic have been used to characterise the oxide growth rate. However, the parabolic law is the most widely used. Over the years, several models have been developed to evaluate oxidation life of components. These models could be grouped into: mechanical, coupled, experimental, thickness evolution, and coatings. A detailed review of these oxidation models can be found in [18]. What can be observed is that many of these models use the Arrhenius equation that relates the dependence of the rate constant of chemical reactions on the temperature, T (K) and activation energy.

$$Kr = A\exp\left(-\frac{Q}{RT}\right) \qquad 2\text{-}7$$

Where: *Kr* is the rate constant, *A* is the pre-exponential factor, *R* is the Universal gas constant and Q is the activation energy.

2.1.3.1 Arrhenius Behaviour of Oxidation Damage

Based on the assumption that the oxide growth is parabolic, oxidation damage (based on coating spallation only) can be modelled using the modified Arrhenius equation [19].

$$[LogC_{oxid} - Log(d^2/t_{oxid})] \times [T_{oxid} + 460] = Q/R \qquad 2\text{-}8$$

Where; C is the oxidation life constant, *d* depth of oxidation thickness (inches), *t* is time, *T* is the Temperature(K),while *Q* and *R* are the activation energy and gas constant respectively.

2.2 Cumulative Damage Rules

The aero engine undergoes variable cyclic thermal and stress loads during operation. Hence, the accruing damage cannot be accounted for using a specific stress and temperature amplitude. The damage from each of the loading cycles (damage fractions) should be calculated and then combined in order to get the total damage. This can then be used to estimate the component life. To this end, several damage accumulation theories have been proposed. A comprehensive review of these rules can be found in [20], where they are grouped into six categories: linear damage rules; nonlinear damage curve and two-stage linearization approaches; life curve modification methods; approaches based on crack growth concepts; continuum damage mechanics models; and energy-based theories. The physical basis, damage expression and the main characteristics of each of the damage models have been detailed in [20]. None of these models could be said to be universal. Each damage model accounts for either one or more phenomenological factors, which include, multiple damage stages, non-linear damage evolution, load sequence and interaction effects. Due to the complexity of the problem, it is therefore not surprising that the Palmgren- Miner Liner Damage Rule is widely used.

The Palgrem–Miner linear damage theory, also called Miner's rule, or linear cumulative damage, is considered the earliest linear cumulative damage rule. Fatigue failure is predicted when the sum of the damage fractions ($\frac{n_i}{N_i}$), equal to one.

$$\sum_i \frac{n_i}{N_i} = 1 \qquad 2\text{-}9$$

Where n_i the number of is applied cycles at a nominal stress and N_i is the limit number of cycles to failure at the same stress and for the same cycle type.

The main drawback that has been reported for the Miner's rule is that it treats each load cycle independently, and does not predict the sequence of the applied loads leading to failure. Nevertheless, Miner's rule has been the most widely used cumulative damage form, because of its simplicity and the fact that better predictions were not necessarily obtained from complicated methods [20][21][22]. It should also be mentioned that the non-linear damage rules have been proposed to overcome the shortcomings of the Miner's Rule. One of the popular non-linear rules proposed by Marco and Starkey uses a non -linear damage exponent, *P* to augment miner's rule. Hence, the damage fraction is given by:

$$D_i = \left(\frac{n_i}{N_i}\right)^P \qquad 2\text{-}10$$

Where the value of P would be greater than 0, and less than or equal to 1 [22].

The non-linear method has given good correlation to observed material behaviour. It is also suitable for summing damage in high temperature applications with creep and fatigue interaction. The main limitation of the non-linear methods is the number of tests required to determine the material constants, which may not be available for a given material or application.

2.2.1 Lifing Philosophies and Methods for Gas Turbine Engines

Broadly, three main lifing philosophies can be identified. These are the damage tolerance approach, safe life philosophy, and probabilistic lifing [6]. Based on these philosophies, two distinct lifing methods can also be discerned. These are the in –service methods and physics based methods.

2.2.1.1 Damage Tolerance Approach

The damage tolerance approach, also known as 'retirement for cause', is a newer approach that stems from the fact that most materials are not necessarily defect free and are almost certainly to have flaws. Hence, the engineer firstly declares a cyclic lifetime for each component, and after the declared life has been reached, the component may be cleared for further service after undergoing a programme of meticulous inspection. During this inspection, Non-Destructive tests (NDT) such as magnetic dye penetrant eddy current and ultra-sonic probe inspections are done on the component to evaluate the presence of cracks. Generally, the existing level of NDT technology somewhat limits the accuracy and reliability of the damage tolerance approach. Furthermore, to ensure the safe return to service of a part that may contain a crack, accurate crack propagation prediction using fracture mechanics lifing is needed [9].

2.2.1.2 The Safe Life Approach

In the safe life approach, the engine component is assumed to be effectively defect free. A safe life limit within which the component will not fail is then determined from matching the basic design with the operating conditions and the performance of the chosen material. Since it is quite impossible to be hundred per cent certain that failure would not occur in a gas turbine component, a safety factor to cater for this uncertainty is applied. On reaching the safe life limit calculated, the component is retired from service. However, it has been shown that most retired components have a considerable service life left and that a less conservative approach could reduce engine related life cycle

costs [6]. Also, the safe life approach is unlikely to take account of any possible defect, that, in conjunction with high stresses, would initiate rapid crack growth and lead to component failure before the predicted life. Nevertheless, the safe life approach has been commonly used to estimate creep and low cycle fatigue life of critical gas turbine components. A particular example is the low cycle fatigue (LCF) procedure used to determine the safe life limit of turbine discs.

2.2.1.3 Probabilistic Lifing

In probabilistic lifing, statistical distribution, probabilistic and artificial intelligence methods are applied to life prediction. The idea is to create a relationship between the driving factors, usage parameters and the estimated life. These methods are also used to reduce the level of uncertainties in the life prediction. There are a number of studies that highlight the applicability of the probabilistic approach. In the work of Zhimin [23] a statistical response surface method was used to build a direct relationship between the creep life and different operating conditions. The work considered only the temperature of the hot flow and engine rotational speed as the key operating parameters. The work was further extended by adding up to six more parameters into the response surface equation. Thermal and stress analysis were then conducted using finite element analysis (FEA) and Computational Fluid Dynamics (CFD), before the creep life was calculated using the Graham -Walles theory [24].

Developing on Zhimin work, a Monte Carlo simulation was used by Wallace [25] for further probabilistic analysis to calculate creep life. In the area of artificial intelligence, Harris [26] used a fuzzy logic method to estimate the interaction of creep and fatigue in aluminium. Philip [27] have also developed a neural networks engine model that is combined with Monte Carlo simulation to predict system damage in a NASA aircraft engine simulator.

2.2.1.4 In- Service Methods

The post service evaluation is the main in service method that is used for lifing of gas turbine components. In the post service method, access to the part is necessary. Destructive and non-destructive tests are then conducted to establish the life history of the component. In - service methods are application specific.

2.2.1.5 Physics Based Lifing Methods

Physics based methods of lifing can either be design type or operational condition monitoring. Operational condition monitoring considers the design/technology factors, alongside using the monitored engine performance and, material data to estimate the engine useful life. On the other hand, the design approach uses numerical and analytical methods to estimate component life, based on typical mission or operational profile data. The physics based methods help us better understand the complex nature of component life estimation and provide necessary inputs for other methods. This research is based on the design approach physics based lifing method.

Some of the studies relating to this method include that of Tinga [28][29]. Tinga demonstrated an integrated method to predict gas turbine hot section component life based on engine performance analysis. His method comprised engine performance model, CFD model, finite element model and the lifing model. The method used operational data from a military aircraft to calculate thermal and mechanical loads on a turbine blade, from which the combine creep and fatigue life was obtained using the Miner's rule and Robinson's life fraction, respectively. Tinga was silent on the equation or methods used in the lifing model. Nevertheless, he mentions that the tool is limited in accuracy, but can be used for relative life assessments and sensitivity studies.

Naeem [30; 31] developed a creep life estimation method that considers the effect of operating conditions and engine deterioration on the hot section creep

life of a military aircraft engine. His work included an engine performance model, thermal and stress models and the creep damage model. Unlike the works of Tinga, his stress and thermal models were analytical. For the creep life calculation, he used the Larson Miller Parameter (LMP). Pascovici [32] and Suria [33] developed a flexible lifing model using similar analytical stress and thermal models, as well as the LMP. Their lifing model was an improvement of Naeem's, in the sense that it could also calculate fatigue life. For the fatigue life calculation, the Neuber and Coffin and Manson relationships were used. However, no attempt was made to sum the effect of creep and fatigue damage. Rather, the estimated life was based on the mechanism that contributed the highest damage.

A combined creep and fatigue life evaluation for an aero engine was done by Wu [34]. He also used analytical models for stress and thermal analysis, as well as the LMP and Neuber approximations for creep and fatigue damage, respectively. However, he used two different methods, the linear summation and ductility exhaustion rules, to predict the combined damage from creep and fatigue. His results indicated that the ductility exhaustion was less conservative than the linear summation rule. He further applied his results to predict life cycle cost savings from reduced thrust operations.

Koehl [35] developed an algorithm that monitors aero engine life usage based on a reference analysis of the design mission. The reference analysis was calculated using finite element analysis to determine the temperature and stress histories for a predefined mission. The flight damage calculations were based on the linear damage rule and crack propagation rate, for crack initiation and crack propagation phases respectively. The cycle damage is then defined relative to the reference cycle.

$$Dcycle = \frac{(damage\ of\ cycle)}{(damage\ of\ \ refence\ engine)} \qquad 2\text{-}11$$

Furthermore, Corran and Williams [36] report a lifing correlation containing separate models for crack initiation and propagation developed by Rolls Royce. The method has the ability to accommodate creep – fatigue interaction.

From most of the works described above, any life prediction method will involve thermal and stress analysis, either by use of analytical or numerical tools like computational fluid dynamics (CFD) and finite element analysis (FEA) to obtain the thermal and mechanical loads acting on the blade. Then a suitable damage model would be applied to predict the remaining life of the component. The adequacy of the life prediction would usually depend on the selection of the appropriate damage mechanisms.

2.3 Turbine Blade Heat Transfer and Cooling

The heat transfer from the hot combustion gases to the blade takes place by convection and depends on the flow field, temperature distribution and the boundary layer condition around the blade [37]. Within the blade material heat transfer is by conduction, and to cool the blade, convection heat transfer takes place between the blade metal and the coolant air as shown in Figure 2-1. The heat transfer via conduction follows the Fourier law in Equation 2-12**,** while the convective heat transfer rate is governed by the Newton's law of cooling in Equation 2-13.

$$Q = AK\Delta T \qquad 2\text{-}12$$

Where: A = blade surface area, K is blade thermal conductivity and ΔT is the temperature gradient

$$q = A\, hg\, (Tg - Tw) \qquad 2\text{-}13$$

Where: q represents the heat transfer rate, hg is the hot gas heat transfer coefficient, T_g is temperature of the hot gas and Tw is the wall metal

temperature. Using a representative turbine blade heat transfer model as depicted in Figure 2-5 the overall heat balance across the blade can be obtained from Equation 2-14**.**

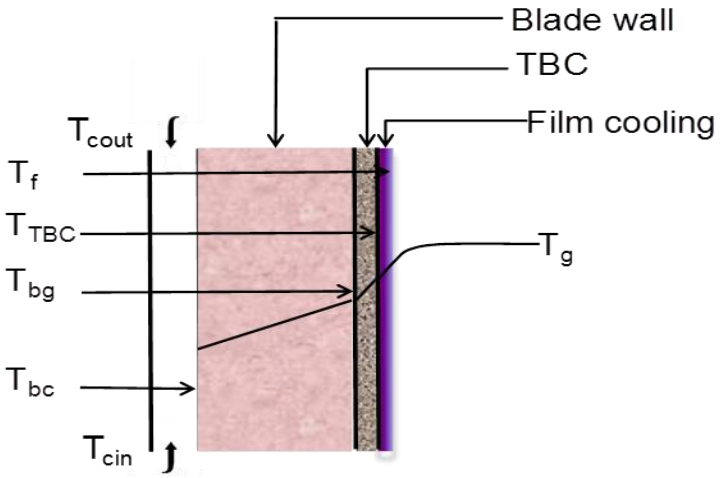

Figure 2-5: 1D representative thermal model [38] p. 102

$$q = h_g \cdot \left(T_g - T_{bg}\right) = \frac{\lambda_b}{t_b} \cdot \left(T_{bg} - T_{bc}\right) = h_c \cdot \left(T_{bc} - T_{cool}\right) = \mathrm{U} \cdot \left(T_g - T_{cool}\right) \qquad 2\text{-}14$$

Where: T_{bg} and T_{bc} are the blade temperature at the hot gas side and cold side, respectively; λ_b is the blade thermal conductivity; t_b is the blade thickness, h_c ·is coolant heat transfer coefficient, T_{cool} is the cooling temperature and *U* is the overall heat transfer coefficient.

2.3.1 Turbine Blade Cooling

Turbine blade cooling has enabled the ability to increase turbine inlet temperatures above melting temperatures of turbine blades. This has enabled gas turbines operate at higher TETs giving efficiency and performance benefits. Compressed cooling air bled from the high pressure compressor (HPC) and the application of thermal barrier coatings (TBC) are the main techniques used for the turbine blade cooling. The widely used air cooling designs are: convective internal cooling, film cooling and impingement cooling.

2.3.2 Convective Cooling

Convective cooling involves the use of compressed bleed air from the high pressure compressor to cool the blade through blade cooling passages or channels. These cooling passages have been developed from simple designs such as the single pass smooth cooling passages to complex serpentine geometries. They are usually shaped to give large internal cooled surface area. To obtain effective cooling, sufficient quantity of air is required to pass from the root to the tip at high velocity. The use of bleed air from the compressor has performance penalties, hence a balance must be achieved between the high TET advantages required and the bleed air loses.

2.3.3 Film Cooling

In order to reduce the gas temperature, a protective layer of used cooling air is created over the blade surface. This is achieved by the injection of the cooling air through holes or slots, such that a thin film of air is formed around the blade. Film cooling presents challenges in manufacturing, and blade structural strength due to the several row of holes created on the blade. It also leads to aerodynamic performance losses as a result of boundary layer distortion.

2.3.4 Impingement Cooling

In impingement cooling, air is directly ejected from the cooling holes to improve the heat transfer of particular blade critical parts. The technique is commonly applied in the leading edge and trailing edges. Figure 2-6 illustrates a cooling architecture of HP turbine blades with convective, film and impingement cooling.

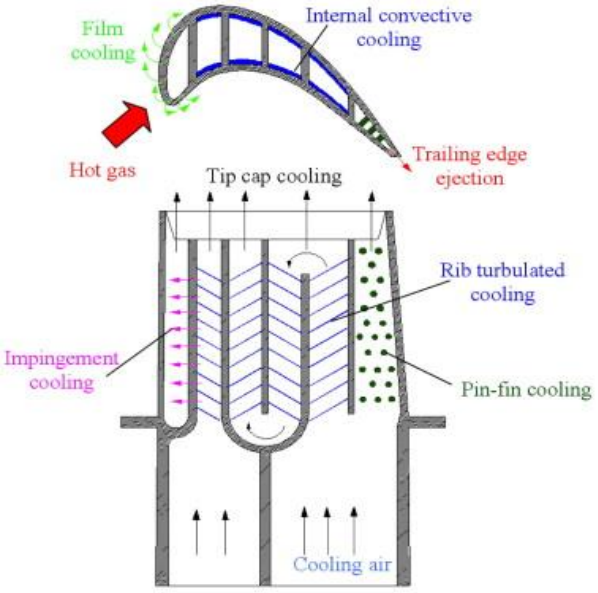

Figure 2-6: Internal blade cooling architecture [39] p.327.

2.3.5 Thermal Barrier Coating (TBC)

Turbine blades are protected with thermal barrier coatings (TBC) to reduce blade metal temperatures. The TBC is a multi-layered system comprising an insulating ceramic top layer and a metallic bond coat. A representation of the various layers in a TBC coated blade is depicted in Figure 2-7.

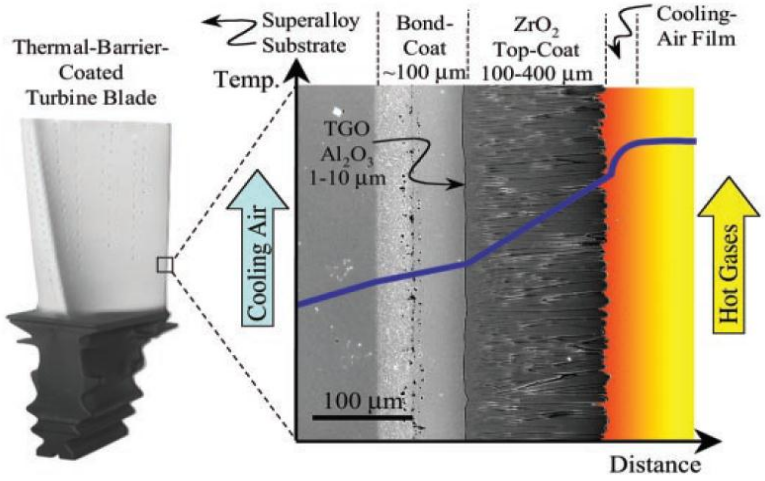

Figure 2-7: Cross section of an electron-beam physical-vapour deposited TBC, with temperature diagram [40] p. 281.

The ***substrate*** is the blade metal nickel-based superalloy. The substrate experiences a severe thermal gradient, because it is subjected to the hot combustor gases on the external surface and cooling air through the internal cooling holes. At high operating temperatures, the constituent alloy elements diffuse into the bond coat and other layers of the TBC. This diffusion can contribute to the failure of the TBC.

The ***bond coat*** is an oxidation resistant metallic coating, typically made from NiCrAlY or NiCoCrAlY alloy. The bond coat is deposited on the substrate using either the electron beam physical deposition (EB-PVD) or the air plasma spray (APS) method. Its thickness varies from 75 to 100 μm [40]. At high operating temperatures, the bond coat temperature can exceed 700 ºC leading to oxidation of the bond coat. Due to the bond coat oxidation, the thermal grown oxide (TGO) is formed between the bond coat and the ceramic top coat.

The ***TGO*** (1 to 10 μm) formation can be described as a volumetric expansion process that occurs during the high temperature exposure [41]. Ideally the TGO would form as αAl_2O_3, which serves to retard further bond coat oxidation. Due to the dimensional constraints within the multi-layered TBC, the growth of the TGO is recognised to develop compressive stresses [42], which could affect the TBC failure. Also, the type of deposition technique used influences the region where TBC failure will occur. Nissley observes that failure in an EB-PVD TBC occurs in the TGO while, APS TBC failures occur slightly above the metallic bond coat in the ceramic top coat [41]

The ***ceramic top coat*** provides the thermal insulation to the substrate. The top coat is commonly made of Yttria stabilised Zincronia (Y_2O_3 stabilised ZrO_3 , or YSZ). YSZ has a very low thermal conductivity ($\sim$2.3 $W \cdot m^{-1} \cdot K^{-1}$ at 1000°C for a fully dense material) and a high thermal coefficient of expansion, which is needed to reduce thermal expansion mismatch stresses between the ceramic top coat and substrate. With a melting point of about 2700^{o}C, YSZ is eminently suitable for high temperature applications.

The two prominent methods used for depositing ceramic coatings on the metal substrate are the air-plasma-spray (APS) deposition method and the electron beam physical vapour deposition (EB-PVD) method.

The **air-plasma-spray (APS)** deposition technique involves the spraying of molten ceramic or metallic powder material on the surface of a metal using a plasma jet produced by an electric discharge of a gas. The material is injected into a very high temperature plasma jet, where it is heated rapidly and accelerated to a high velocity. The hot material impacts on the surface of the substrate and cools rapidly to form the coating. APS TBCs have the following microstructural characteristics [40]:

i. Splat grain morphology having thickness of 1 to 5 µm and diameter of 200 to 400 µm, with inter splat boundaries and cracks parallel to the metal/ceramic interface which helps in lowering the thermal conductivity .
ii. A porosity of 15 to 25 vol % for both low elastic modulus (high strain tolerance) and low thermal conductivity.

APS TBC has an undulating nature at the interface of the metal and ceramic, which increases the interlock adhesion properties and results in out-of-plane stresses responsible for failure of the TBC in service. The orientation of the cracks and pores normal to the direction of the heat flow assists in reducing the thermal conductivity of the top-coat from ~2.3 W/m/K for a fully dense material to 0.8-1.7 W/m/K [40]. The presence of microstructural defects which are oriented parallel to the interface and the roughness of the interface results in low thermal cycle life than EB-PVD TBCs. Hence, the APS TBCs are used for less severe applications in aircraft engines such as fuel vaporizers, flame holders of after burner and combustors.

In the **electron beam physical vapour deposition (EB-PVD TBC)**, the bond-coat surface can be smooth before deposition. Thus, the interface between the bond coat aand the ceramic is smooth in contrast to the rough surface in air

plasma spray TBCs. The EB-PVD ceramic top coat (approximately 125 µm thick) has the following microstructural properties [40]:

a) Presence of thin regions of polycrystalline equiaxed grains (usually 0.5 to 1 µm) at and near the interface of metal and ceramic.
b) Columnar YSZ grains of diameter from 2 to 10 µm growing out of the equiaxed-grain region to the top-coat surface,
c) Nanometre- scale pores present within the columnar grains.
d) Channels that separate the columnar grains, perpendicular to the metal and ceramic interface.

The disconnected columns give “strain tolerance” to the TBC as they can move more freely at high temperatures, accommodating stresses due to the mismatch of thermal expansion The presence of cracks and porosity helps in reducing the thermal conductivity [~1.5 to 2 W/m/K], but not to the extent as APS TBCs because of the orientation of channels parallel to the direction of heat flow. The EB-PVD TBCs are more durable than APS TBCs; but are expensive. They are primarily used in more severe applications such as turbine blades and vanes in aircraft engines.

During service, the thermal conductivity of TBCs will change due to sintering. Hence, the suppression of sintering within the top-coats (in both EB-PVD and APS TBCs) at operating temperatures is very desirable for maintaining high strain tolerance.

2.4 Turbine Blade Cooling Approaches

In the past, practical heat transfer methods were relied upon to determine the amount of cooling flow required to maintain blade temperature within prescribed metallurgical limits [43]. Currently, several analytical heat transfer solutions are available for blade thermal analysis and design. Likewise, high fidelity methods such as finite element analysis and Computational fluid dynamics (CFD)/conjugate heat transfer simulations are now used to estimate the heat transfer from the hot gas stream to the blade [44]. This has been possible

because of the rapid developments in high performance computational resources.

Nevertheless, the turbine blade heat transfer analysis using CFD is inherently complex, computationally expensive and costly. Hence, most of the significant contributions from CFD heat transfer analysis have come from original equipment manufacturer (OEM) sponsored research and National Research Laboratories. Furthermore, CFD requires specific details about the component and the flow path; which are typically not available at the early design stages. Hence, for initial design purposes, which require much iteration, it would be suitable to use simpler engineering methods that allow an analyst to estimate the heat transfer processes [44]. Accordingly, much of the discussion in this section will focus on engineering methods that have been developed and used for turbine blade cooling and heat transfer analysis.

In Ainley's work [45], the heat transfer process was described by the standard blade concept. A constant inlet gas temperature and constant blade metal temperature along the chord was assumed. Hence, the blade temperature T_b was equal to both the gas side blade metal temperature, T_{bg} and the coolant side blade metal temperature, T_{bc}. The inlet gas temperature was also assumed to be constant along the blade span; but the blade metal temperature increased towards the tip of the blade. The blade external and internal wetted perimeters for both the hot gas S_g and coolant sides S_c were all assumed to be constant along the span.

Halls [46] and Holland and Thake [47] have also used the same assumption of the standard blade. Their analysis included convective cooling, film cooling and TBC. They also considered both the cooling effectiveness and cooling efficiency of the blade.

Consonni [48] developed a model to estimate the blade cooling flow requirement using mean temperatures and heat transfer coefficients. The method is able to calculate the flow requirements across the blade chord. The Z

parameter is applied to describe the technology level for the heat transfer coefficient and internal blade geometry. His approach followed Ainley, except that film cooling was included and finite thickness via the Biot number for TBC and metal thickness were accounted for.

The approach by Young and Wilcock [49] [50] essentially followed that of Holland. However, they deviated from the standard blade by allowing a temperature distribution through the blade wall and coating; such that the ($T_{TBC} \geq T_{bg} \geq T_{bc}$). T_{TBC} is the temperature at the TBC surface.

Based on the approach of Consonni [48] and Ainley [45], Torbidoni [51; 52] also examined the effect of the internal blade geometry on the cooling performance using the Z parameter. His work allowed for the variation of temperature along the blade span, through the blade walls and coating. This was achieved by splitting the blade into elementary cross sectional areas along the height and chord; then calculating the heat flux through each blade section.

In a bid to address the limitations in Ainley's model, Horlock and Torbidoni [53] revised the Ainley approach to include variations in the chord direction for: coolant flow and temperature; the heat transfer coefficients; and the gas and blade metal temperatures. In addition, finite blade wall and TBC thickness was allowed. The analysis also catered for multi-pass cooling channels.

Based on the works of Consonni and Torbidonni, Eshati [44; 54] accounted for the use of humid air and variable temperature dependent properties. The model directly related the operational design and technology parameters to the blade damage (creep life). Using the radial temperature distribution, the non-uniform gas temperature profiles were applied to determine the minimum and maximum gas temperatures on the blade. The model calculates the span wise temperature distributions and heat transfer coefficients for both the hot blade surface and the cooling hole. The effects of thermal barrier coatings (TBC) and the implementation of convective cooling parameters were also accounted.

In the current research, Eshati's model was further enhanced to give the temperature and heat transfer variation with time along a flight. This was achieved by linking the heat transfer design parameters to the variation of the engine thermodynamic performance along a flight path.

2.5 Chapter conclusions

- **Damage mechanisms**

In aero engines, the turbine components could continuously deform when subjected to steady loads at high temperatures (creep); as well as fail due to the impact of cyclic loading (fatigue). Oxidation at high temperatures also causes oxide growth that deteriorates the components surface.

Fatigue damage will usually occur in a component subjected to repeated or non-steady loads that cause stress and strain variation. Depending on the origin of the applied load, fatigue could be mechanical, thermal or thermo-mechanical (TMF). In general, TMF would usually take place at high temperatures in gas turbine hot section components. Where, the variation of heating and cooling cycles, in addition to the mechanical cyclic loading causes strains that induce damage. The total life to failure could be obtained by summing the life due to crack initiation and life due to crack propagation. The crack propagation phase, which is more complex and involves the use of fracture mechanics usually, starts after the crack inititiaion.In this research, a conservative approach is adopted by using the life to fatigue crack initiation as the key damage criteria for the lifing of the turbine blade.

- **Lifing approaches**

Three main lifing philosophies can be identified. These are the damage tolerance approach, safe life philosophy, and probabilistic lifing. The damage tolerance approach emphasises the management of the crack propagation processes. In the safe life approach, the engine component is assumed to be effectively defect free. The safe life approach is unlikely to take account of any

possible defect that, in conjunction with high stresses, would initiate rapid crack growth and lead to component failure before the predicted life. Nevertheless, in aero engine applications, the safe life approach is more commonly used to estimate creep and low cycle fatigue life of critical gas turbine components.

In probabilistic lifing, statistical distribution, probabilistic and artificial intelligence methods are applied to life prediction. The idea is to create a relationship between the driving factors, usage parameters and the estimated life. These methods are also used to reduce the level of uncertainties in the life prediction. The post service method involves physical assessment of the part. Destructive and non-destructive tests would usually be conducted to establish the life history of the component. These histories can also be used by the probabilistic lifing method to establish the relationship between the driving factors.

Looking at the physics based methods of lifing, it is observed that either the design or operational condition monitoring approaches are currently used. Physics based methods helps us better understand the complex nature of component life estimation and provides necessary inputs for other methods. The physics based methods help us better understand the complex nature of component life estimation and provide necessary inputs for other methods.

This research is based on the design approach physics based lifing method. Hence, numerical and analytical models to estimate component life were developed, based on a typical mission or engine operational profile data.

Overall, most lifing prediction methods will involve thermal and stress analysis, either by using analytical or numerical tools to obtain the thermal and mechanical loads of the hot section component. Then a suitable damage model would be applied to predict the remaining life of the component. The accuracy of the life prediction would usually depend on the selection of the appropriate damage mechanisms.

- **Heat transfer and blade cooling approaches**

The turbine blade heat transfer and cooling has evolved from the standard blade assumption using semi empirical data, to a more detailed approach based on the Influence of internal geometry and cooling technology factors. Based on the popular heat transfer and cooling methods developed over the years, these approaches could be classified into two: the standard blade semi –empirical approach; and approach based on Influence of internal geometry and cooling technology factors.

The relatively simple models using semi-empirical data for the heat transfer analysis of air cooled turbines blades will fall into the first category approach. The ‘standard blade’ concept is generally used. This assumes a uniform gas temperature and blade metal temperature along the blade span and chord, as well as an infinite thermal conductivity.These models were mainly concerned with estimating mass flow of the coolant required to maintain the blade temperature within certain limits. In terms of lifing, an analyst can use these methods to determine the average blade temperature of the blade and calculate the blade life using a simple parametric approach such as the Larson Miller Parameter. These heat transfer models would be inadequate to capture thermal gradients across the blade, limiting their use in higher fidelity lifing analysis.

The second approach goes beyond the standard blade assumptions and considers the influence of more detailed blade design parameters and internal geometry of the blade. Hence, the Z parameter, Biot numbers, film cooling and overall cooling effectiveness are detailed accordingly. Variations in temperature and heat transfer properties along the blade for the cooling air and blade metal are also accounted for.

Hence, a more detailed heat transfer analysis can be conducted to give the span or chord wise variations of temperatures and heat transfer predictions across the blade. Furthermore, the thermal gradients can be easily deduced; and the results are better suited for further analysis with FEA tools. This implies

that for deeper lifing analysis that reflects the appropriate operating conditions of the blade (such as TMF), heat transfer models falling under this category could be adapted to get the temperature and heat transfer predictions.

Overall the main benefit of the analytical bade heat transfer models is the ability to fairly accurately predict the effects of many geometric and aerodynamic variables affecting the blade cooling performance, using minimal effort [45].

3 THERMO-MECHANICAL FATIGUE

3.1 Thermo- Mechanical Fatigue Concept

Thermo- mechanical Fatigue (TMF) can simply be described as damage due to the combination of both cyclic thermal and mechanical loading leading to failure of a component. According to Antolovich [55], TMF, can be viewed as 'a fatigue damage process under simultaneous changes in temperature and mechanical loads'. Invariably, mechanical strains develop under the mechanical loads and additional thermal strains under the cyclic thermal loads. The thermal strains generated are mainly from the temperature gradients (thermal gradients) and temperature variations (thermal transients). Hence, the influence of temperature is a key factor in TMF behaviour. Harris, et al [1] particularly emphasises a detailed knowledge of the transient temperature distribution as a prerequisite for any stress and strain analysis in an engine cycle.

Two major TMF cycles have been identified based on the phase difference between the temperature and the total strain. These are the in – phase or out – of – phase TMF cycles, as shown in Figure 3-1. For in- phase cyclic loading, the maximum strain occurs at the peak temperature. Conversely, the maximum strain occurs at the minimum temperature for out-of-phase cycles. The strain – temperature phasing is thus another important parameter characterising TMF. This has been recognised to particularly influence TMF in turbine blades [56].

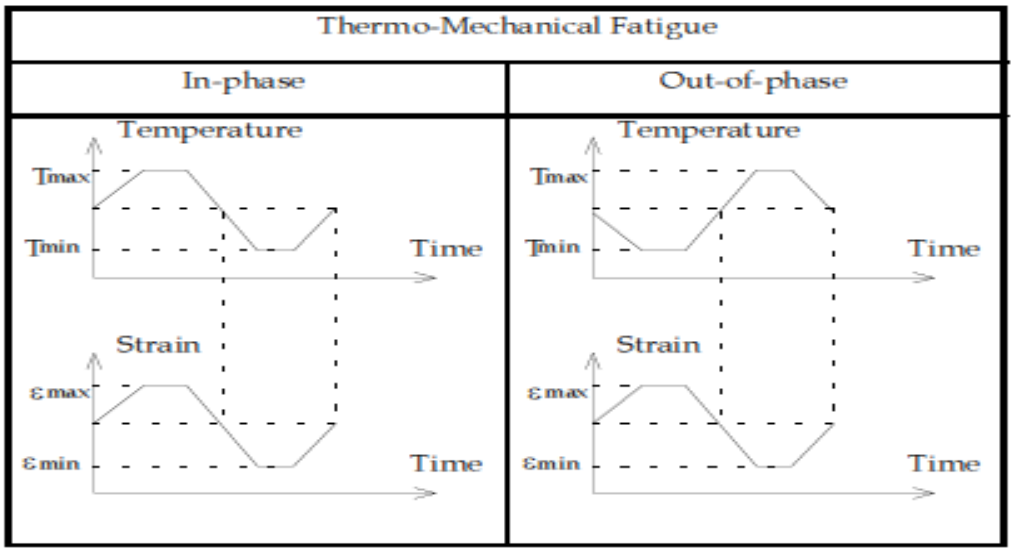

Figure 3-1: In - Phase and Out - of - Phase TMF cycles [57] p.3

3.2 TMF Experiments

3.2.1 Thermo-Mechanical Fatigue Tests

An experiment devised to study damage mechanisms under varying strain temperature histories is called the TMF test [58]. Basically, in TMF testing, temperature and strain are varied simultaneously. The changes in strain occur due to the combined effects of thermal and mechanical loading. The mechanical strain is the control parameter in a TMF test and can be obtained by subtracting the thermal strain from the total strain [59].There is yet a universally accepted TMF testing standard; although the EU has made concerted efforts towards standardisation [60]. Two of the commonly used TMF tests are: the two level approach and the bithermal tests.

3.2.1.1 Two Level Approach

In this approach, a specimen would be cycled at a given high temperature, T_H for half of the projected life, and then cycled to failure at a lower temperature, T_L. A similar experiment could be run subsequently, in which the specimen is cycled to half the life at $T_{L,}$ and then cycled to failure at T_H. This type of

experiment was done in [59] for a specimen of polycrystalline Rene 80 cycled to N_f /2 at T_H of 760^oC and then at T_L 25^oC, (maintaining the same strain range).Reversing the temperature sequence (L/H) during the experiment had resulted in an unexpected fracture. However, repeating the specimen cycling to about one quarter of the life at T_H, then cycling at T_L recorded over 6000 cycles. The experiments therefore highlighted that the damage accumulation rate is very non -linear; but sequence dependent.

3.2.1.2 Bithermal Tests

This approach is more complicated than the two level approach. It involves cycling half of the hysteresis loop at one temperature and to then change the temperature and complete the cycle. The procedure could be repeated until failure. Usually, the temperature is discretely applied at no- load conditions in between mechanical straining. Hence, when thermal straining occurs, mechanical straining is excluded. This makes the bithermal test suitable for partitioning between thermal and mechanical strain ranges [61].The approach is also better suited to simulate actual operating conditions and examining the damage interactions [59].

3.2.1.3 Multi Axial Tests

The multi axial test rig uses a rotating bending machine with high and low temperature source, permitting thermo-mechanical loading at relatively high frequencies on the test specimen. Hence, while the specimen is rotating, a heating and cooling load is alternatively applied. This enabled adequate capture of the thermal gradients within the specimen. Some other multi axial TMF tests such as [62], and [63] are based on applying both axial and torsion strains, where the controlling parameters are temperature, axial strain and torsional strain/shear strain.

3.2.2 TMF Tests for Turbine Blades

TMF tests representative of the operating conditions of the turbine blades have been conducted over the years. Beck et al, [60] gives a brief description of one of such experiments. In Figure 3-2, the principle of thermally induced loading and its experimental simulation in a TMF test of a cooled turbine blade is depicted. As a result of transient temperatures, thermal induced loads would occur in the blade during start-up and shut down phases of a service cycle. Likewise, during stationary service, thermal loads would be generated due to the temperature gradients.

The thermal strain at the hot outer side of the blade would therefore be restricted by the colder volume elements inside the blade. Hence, a compressive load is induced in the hot side, as the temperature increases. Conversely, an equilibrating tensile load is generated in the cold side. In order to simulate these loadings, the temperature-time history at either location 1 or 2 is imposed on the gage section of a laboratory specimen. The resulting mechanical loading from the constraint of the local thermal strain is then imposed on the specimen by controlling the total strain represented by:

$$\varepsilon_t = \varepsilon_{me} + \varepsilon_{th} \qquad 3\text{-}1$$

Where: ε_t is the total strain at the specimen, ε_{th} is the thermal strain in the absence of external forces and ε_{me} is the mechanical strain, exhibiting a phase shift of 180 degrees with respect to the temperature and thermal strain vs. time path in volume element 1, or a phase shift of 0 degrees in the case of volume element 2, respectively [60].

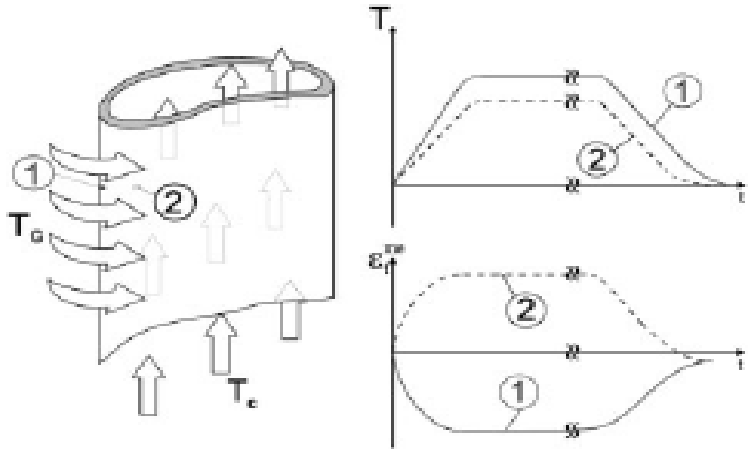

Figure 3-2: TMF testing simulation of thermally induced loadings of a cooled turbine blade [60] p.54.

3.3 TMF Damage Interactions

Essentially, TMF damage has been considered in terms of damage contributions from creep, fatigue and oxidation; as well as their interactions observed from TMF tests. The effects of any single damage mechanism, or their combination depends on the material properties, as well as several parameters that define a particular TMF cycle. The key parameters include temperature, mechanical strain range, strain rate and phasing. Therefore, different damage mechanisms would dominate for a given TMF cycle (IP, OP or diamond). For an arbitrary TMF cycle, such as would be obtained from aero engine turbine blade in - service, the need arises for a TMF model that suitably describes the TMF behaviour of the turbine blade. In Chapter 2, the individual damage mechanisms were introduced. The following sub sections are meant to highlight how TMF has been examined in relation to the interaction of the damage mechanisms. Accordingly, creep – fatigue and fatigue - oxidation interaction are discussed. Although Kraft [64] observes that the influence of creep would unlikely cause failure in modern turbine blade materials, Remy [65] suggests that the contribution of creep- fatigue interaction should not be

ignored. Nevertheless, the work of Amaro [3] indicates that satisfactory results could still be achieved without including the creep damage.

3.3.1 Creep-Fatigue Interaction

Generally, the combined creep and fatigue damage under high temperature and cyclic mechanical loads has been found to be more damaging than the addition of each separately calculated damage [66]. Under high temperature cyclic loading, the inelastic strains generated can be separated to plastic and viscous components; due to fatigue and creep contributions to micro crack growth, respectively.

The particular influence of creep-fatigue damage has been examined by several researchers in unique ways. Hales [67] describes the creep damage as a strain rate to ductility ratio, based on the fact that creep ductility depends on the strain ratio. Creep-fatigue interaction has also been considered as a propagation-controlled problem where the damage micro-mechanism considered is assumed to influence the fatigue growth or vice versa [58]. Saxena [68] considers the creep cavity growth ahead of the crack tip. The creep-fatigue damage is then examined in terms of the modified fracture mechanics parameters to account for crack tip stress strains/ strain fields.

3.3.2 Fatigue-Oxidation Interaction

The significant influences of the environment (oxidation) on turbine blade super alloys have been highlighted by researchers such as Lasalmonie [69] and Fleury [69; 70]. Likewise, under TMF loading, a time dependent cyclic damage response has been observed to occur due to environment - fatigue interaction [71]**.**

This process could be described by the growth of oxide scales on the surface and the diffusion of oxygen in the material. Neu and sehitoglu [58] illustrate two types of oxide rupture processes (Type I and Type II) that could occur under

cyclic loading. As indicated in Figure 3-3a**,** Type I mechanism describes the intrusion of an oxide formed by repeated oxide rupture, until it reaches a critical thickness h_{f1}, (a). Crack initiation is then assumed to have occurred beyond the critical oxide thickness, (b). A fresh metallic surface is then exposed to the environment and is quickly oxidised, (c). When the oxide thickness reaches the critical thickness $h_{f2,}$ the oxide ruptures again, (b). The process then continues,(e) - (f). Type II follows a similar process, except that part of the cracked layer detaches from the surface forming oxide stratifications as shown in Figure 3-3b. The transition between Type I and Type II rupture process is attributed to increase in temperature and strain range. Invariably, brittle oxide fracture would have an adverse effect on both crack initiation and growth stages in a blade material under cyclic loading. The works of Miller [72] [60] and Sehitoglu [73][79, 61] support this observation.

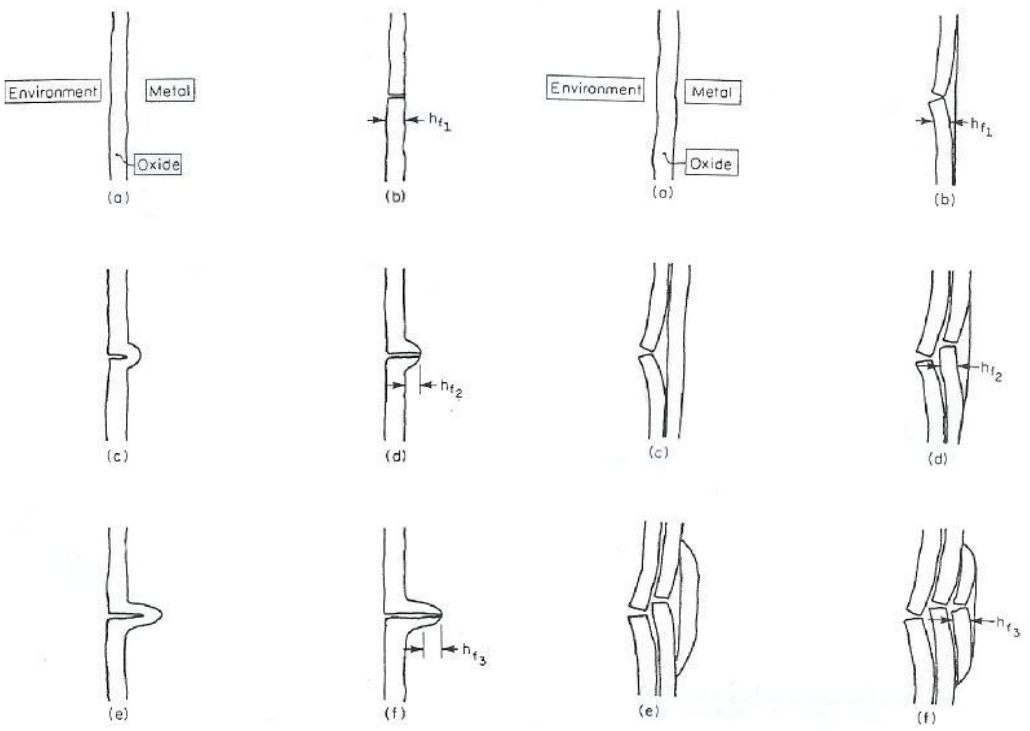

(a) Type I (b) Type II

Figure 3-3 Schematic of oxide rupture process [58]p.61.

3.4 TMF Models and Lifing Approaches

Historically, lifing methods derived from isothermal fatigue (IF) tests at the maximum operating temperature have been used for TMF life assessment. These results are not primarily suited to study: the phase relationships between temperature and mechanical loadings; thermal transients that occur in the operation of gas turbines (particularly, the cooled aero gas turbine blades); and the interaction of fatigue, creep and oxidation damage mechanisms [60]. In recent times, experiments have been done to simulate the behaviour of materials undergoing TMF, and TMF life prediction methods have been developed [74]. The methods based on TMF tests are therefore recognised to better describe the damage process under varying thermal and mechanical loading, and provide reliable results for life assessment of gas turbine blades.

Different concepts have been used to account for TMF and the complex interaction of the damage mechanisms. The following four approaches are identified by Christ [75]: (i) empirical,(ii)damage mechanics,(iii)fracture mechanics and (iv) physical. The importance of the physical approach is in providing the physical background for empirical and damage mechanics models. However, the complex physical concepts of modelling the interaction of damage mechanisms limit the significance of physical models for TMF life prediction. The damage mechanics concept is rarely applied to complex loading [76], while fracture mechanics is used, preferably, if a material contains a flaw from the start or if cracks are initiated quickly at the start of cyclic life. Nevertheless, the empirical approach is a widely used concept for TMF life prediction [45,77- 83]. Although there has been reasonable agreement between experimentally observed TMF life and the results from empirical means, the lack of a physical basis limits its use to specific conditions [75]. Koberl [84] also suggests that such lifetime calculation models are only applicable within a limited range defined by temperature, strain constraining, and their combination.

3.4.1 TMF Models

Out of the numerous crack initiation models that have been developed for TMF, the following are considered the most popular: Damage summation (DS), Frequency Separation (FS), Ductility Exhaustion (DE), Strain-range partitioning (SRP), Total – Strain Version of SRP (TS - SRP), and strain energy partitioning (SEP). A critical review of these models is contained in Zhuang [57]. A brief description of the DS, FS, DE and SRP models will be given.

The DS model was first introduced by Taira [85] and is the simplest expression for creep - fatigue prediction. It ignores the microstructural details of the damage process. The damage summation rule assumes that failure occurs when the sum of the fatigue damage and the creep damage is equal to a critical value. The DS model can adequately predict experimental behaviour for engineering applications, especially for thermal fatigue [4].The model has been adopted by the ASME Boiler and Pressure Vessel Code, Section III, Case N-47 (1974) to predict the creep-fatigue life.

The FS model adds the effect of cyclic frequency upon the creep- fatigue life. The model was developed to deal properly with very complex wave shapes. The model separates damage into tension-going and compression-going damage, thereby providing a significant error reduction in high temperature low-cycle fatigue life prediction. In developing the FS model,Coffin [86][88] obtained good agreement between fatigue life predicted from the model and actual measured life in experiments, for type 316 stainless steel. However, the frequency modification approach requires considerable input data, and is considered fairly cumbersome.

The DE Model was derived originally from the Coffin-Manson relationship between the inelastic strain-range and the number of cycles to failure. The DE model is simple to use and has been successfully used to interpret test data [87]. Nevertheless, Coffin [12] and Ellison [80] indicated that the lifetime of creep-fatigue predicted by the DE model is normally conservative.

The SRP method was developed by Manson [88] to cater for the time dependent portions of the high temperature low-cycle fatigue cycle, stress-strain cycle. The SRP life prediction model partitions the inelastic strain-range into time-independent plasticity and time-dependent creep, rather than working with the total inelastic strain-range alone. Each component contributes a certain fraction to the total damage. Under cyclic reversed loading, the SRP model needs to consider the following four possible combination cycles of inelastic strain: tensile plasticity reversed by compressive plasticity (PP), tensile creep reversed by compressive creep (CC), tensile creep reversed by compressive plasticity (CP), and tensile plasticity reversed by compressive creep (PC). In any stabilised combined cycle, a maximum of three cycle types are physically possible, PP, CC, and either PC or CP. The model is not applicable to non-ductile materials since the inelastic strain is too small to be determined correctly. It is also not successful for nickel-base superalloys which are common in aircraft engines Nitta [89]. The SRP model does not cater for oxidation attack and may over-predict the life [81].

The summary of the TMF models is presented in Table 3-1, where: *C, β, m,* and *k* are constants dependent on material, environment and temperature in the frequency separation model. v_t and v_c are reciprocals of the tension-going and compression-going times.

For the ductility exhaustion model, α is a constant approximately ½ at ambient temperature, but increases to near unity at elevated temperature for many materials. *D* is also a constant related to the tensile ductility. Hence, $D_{c\ and}\ D_p$ are the ductility constants for low band creep and plastic strain fatigue, respectively. N_c and N_p represent the life for creep dominated failure and fatigue damage dominated by plastic strain, respectively. $\Delta\varepsilon_p$ is the effective plastic strain and $\Delta\varepsilon_c$ is the tensile creep strain per cycle.

In the SRP model, N_{pp}, N_{cc}, N_{pc}, and N_{cp} are the fatigue lives produced by PP, CC, PC and CP inelastic strain cycles, respectively. Also, F_{pp}, F_{cc}, F_{pc}, and F_{cp}

are PP, CC, PC and CP strain-range fractions. The coefficients A and exponents C are experimentally determined material constants.

Table 3-1 Classification of TMF models.

	Damage Summation	Frequency Separation	Ductility Exhaustion	Strain Range Partitioning
Features	•Based on linear cumulative damage(Creep and fatigue) •Failure occurs when damage equal a critical value	•Incorporate effect of cyclic frequency •Separates tension and compression damage •Deals with complex wave shapes	•Originally from Coffin – Manson relationship between inelastic strain and number of cycles to failure •Total damage separated into creep and fatigue components	•Accounts for time dependent cyclic stress – strain behaviour •partitions inelastic strain-range into time-independent plasticity and time-dependent creep
Advantages	•Adequately predict experimental behaviour for engineering applications •Simplicity •Adopted by ASME	•Significant error reduction in life prediction	•Simple to use	•Relatively temperature independent
Drawbacks	•Ignores micro -structural details of damage process •Sequence effect of damage omitted •Non-conservative predictions •Creep properties may not be appropriate	•Invalid if compressive part of cycle influences tensile half •Requires considerable input data for material constants •Fairly cumbersome	•Conservative lifetime prediction •Difficult tests need to be conducted	•Material data need to be obtained experimentally •Difficulty in partitioning inelastic strain experimentally •Not successful for nickel based super alloys •Does not account for oxidation •May over predict life
Equations	•$D_{fatigue} + D_{creep} = D_{total}$ •$N_f\,(1/N_p + t/T_c) = D_{total}$ •$\sum N_i/N_{pi} + \sum t_i/T_{ci} = D_{total}$	•$N_f = C\,\Delta\varepsilon_{in}^{\beta} v_t^{m} (v_c/v_t)^{k}$	•$\Delta\varepsilon_{in}\,N_f^{a} = D$ •$\Delta\varepsilon_c\,N_c = D_c$ •$\Delta\varepsilon_p\,N_p = D_p$ •$1/N_f = 1/N_c + 1/N_p$	•$1/N\,f = F_{pp}/N'_{pp} + F_{cc}/N'_{cc} + F_{pc}/N'_{pp} + F_{pp}/N'_{cp}$ •$\Delta\varepsilon_{pp} = A_{pp}\,(N_{pp})^{Cpp}$ •$\Delta\varepsilon_{pc} = A_{pc}\,(N_{pc})^{Cpc}$ •$\Delta\varepsilon_{cp} = A_{cp}\,(N_{cp})^{Ccp}$ •$\Delta\varepsilon_{cc} = A_{cc}\,(N_c)^{Ccc}$
References	Taira(1962), Ellison(1994) Spera(1972), ASME (1974) Mottot et al. (1982), Ellison and Zamily (1994)	Coffin (1970),Coffin (1976) Ostergen(1979), Del Puglia and Manfredi (1979) Manson (1973)	Coffin (1967) , Priest and Ellison (1981) , Ellison (1994) , Edmunds and White (1966)	Manson et al. (1971) , Manson, Halford and Hirschberg (1971),Nitta and Kuwabara (1988), Halford and Nachtigall (1979) Nitta et al. (1983) ,Bernstein 1982

According to Cai [74] TMF prediction models can be classified into five types: general damage models, damage-rate models, Thermo-mechanical fatigue/strain-range partitioning methods, modified J integral, and the empirical models. The strain range partitioning and empirical models have been mentioned earlier. Hence, only the general linear damage accumulation model will be highlighted. The damage rate and J integral are fracture mechanics based models; a brief discussion will be given in relation to the work of Christ [75].

The prominent general linear accumulation damage model is the Neu and Sehitoglu TMF damage model [58; 90; 91]. The model was developed as a general model for high-temperature fatigue that accounts for TMF. The model considers damage accumulation due to fatigue, oxidation, and creep processes. Damages per cycle from fatigue, oxidation, and creep are summed to obtain the total damage per cycle. The model assumes that linear damage is equal to one at failure.

$$\mathrm{D}^{\mathrm{tot}} = \mathrm{D}^{\mathrm{fat}} + \mathrm{D}^{\mathrm{ox}} + \mathrm{D}^{\mathrm{creep}} \qquad 3\text{-}2$$

Equation 3-3 can be rewritten in terms of life, $\mathrm{N_f}$; where damage is taken as $\frac{1}{\mathrm{N_f}}$.

$$\frac{1}{\mathrm{N_f}} = \frac{1}{\mathrm{N_f}^{\mathrm{fat}}} + \frac{1}{\mathrm{N_f}^{\mathrm{ox}}} + \frac{1}{\mathrm{N_f}^{\mathrm{creep}}} \qquad 3\text{-}3$$

This research focuses on the life to crack initiation, so neither simulation nor analysis concerned with crack growth was conducted. However, fracture mechanics approaches to TMF have also been demonstrated to predict material life by applying crack propagation methods. In one of such studies, Christ [75] uses Equation 3.4, similar to the linear damage law, to calculate TMF life for X8019/12.5p Aluminium alloy subjected to low strain rate and varying temperature effects. The equation combines the creep, fatigue and oxidation

damage contributions, assuming that no coupling exists between the single damage mechanisms.

$$\frac{\mathrm{d}a}{\mathrm{d}N} = \left.\frac{\mathrm{d}a}{\mathrm{d}N}\right|_{\mathrm{fat}} + \left.\frac{\mathrm{d}a}{\mathrm{d}N}\right|_{\mathrm{Creep}} + \left.\frac{\mathrm{d}a}{\mathrm{d}N}\right|_{\mathrm{Oxygen}} \qquad 3\text{-}4$$

Where; $\frac{\mathrm{d}a}{\mathrm{d}N}$ represents the overall crack propagation rate, $\left.\frac{\mathrm{d}a}{\mathrm{d}N}\right|_{\mathrm{fat}}$, $\left.\frac{\mathrm{d}a}{\mathrm{d}N}\right|_{\mathrm{Creep}}$,and $\left.\frac{\mathrm{d}a}{\mathrm{d}N}\right|_{\mathrm{Oxygen}}$ represent the crack propagation rates for fatigue, creep and oxidation, respectively. The damage contribution from fatigue was calculated using the J integral cyclic crack propagation rate relationship, while the contribution from creep and oxidation was estimated from the model of Miller [72]. Figure 3.4 presents a map for X8019/12.5p alloy, showing the regimes of plastic strain amplitude and temperature/plastic strain rate where damage could be attributed to the various damage mechanisms.

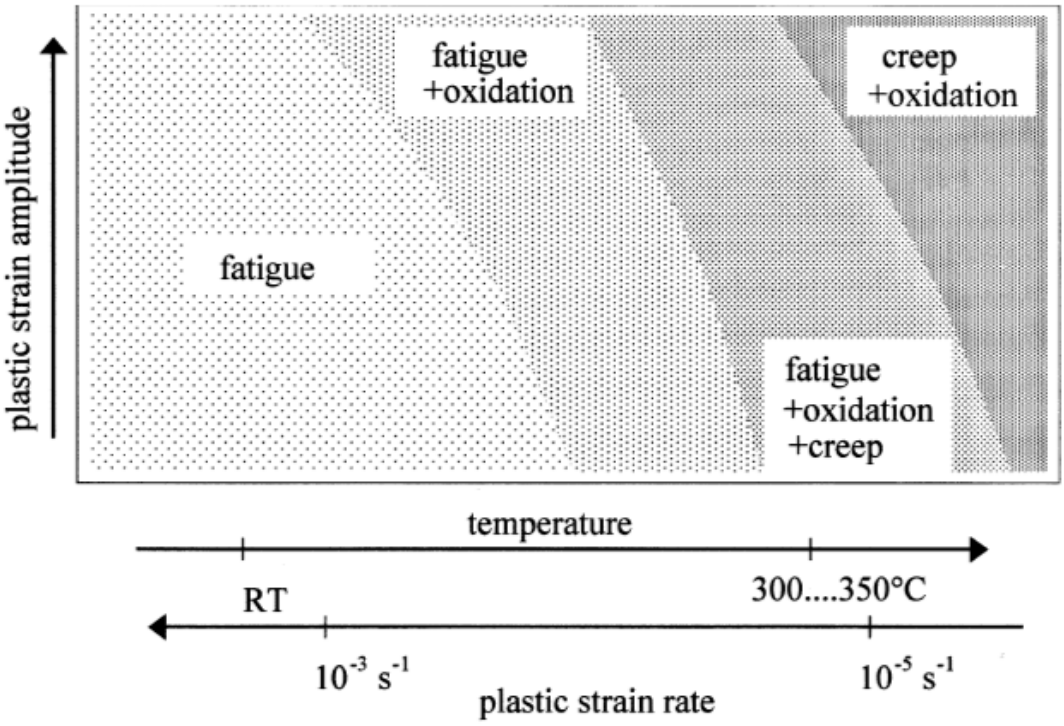

Figure 3-4 Schematic map for X8019/12.5p alloy, showing the regimes of plastic strain amplitude and temperature/plastic damage due to the damage mechanisms [75]

It would be observed that most of the TMF models are based on the interaction of creep and fatigue and no model has been found to give better prediction than the others. Hence, the choice of any model would be based on the relevant situations for which the model was verified. The challenge therefore is to develop a prediction model that can be applied over a broad range of conditions. Such a model would be inherently complicated and require several experiments to validate its usefulness.

3.4.2 Assessment of TMF Models

A review was conducted by Blanchard [92] to determine suitable TMF models for turbine blade lifing assessment. Consequently, 19 TMF models were assessed using the following essential criteria: Type of material used, parameter inputs, ability to adequately account for TMF behaviour,

reproducibility, broad range of application and reported accuracy. In terms of materials, the model should be applicable to turbine blade super alloys. The inputs to the model should also be independently generated from the engine cycle information and numerical analysis such as FEA. The model also has to account for the interaction of the three damage mechanisms in TMF behaviour and the varying temperature- strain histories. Lastly, sufficient information on model constants and parameters must be available to ensure its reproducibility. The desirable criteria were: number of material constants and ease of implementation. Once a model failed any essential criteria, it was considered unsuitable. Only the TMF model by Boismier and Sehitoglu [73; 93] met all the essential criteria and was considered for implementation in this research.

3.5 Thermo-Mechanical Fatigue in Aero Engines

In aero engines, TMF damage may accumulate over a range of temperatures and strains under both steady-state and/or transient flight conditions [55]. As flight operating conditions change during a mission, strong thermal gradients are developed. Coupled with the mechanical loads, these thermal gradients induce TMF damage in the aero engine; particularly, in the turbine blade that bears severe temperatures and high centrifugal stresses.

During straight and level flight, aero-engines are basically at constant temperatures and mechanical loading. At this condition, steady-state creep and the influence of oxidation are the primary damage mechanisms. However, at take-off and landing, the transient demand for more power causes load and temperature changes that lead to fatigue damage. Usually, each flight would be considered as one fatigue cycle with an imposed hold time, wherein creep and fatigue would be acting independently; as well as creep-fatigue interactions influenced significantly by oxidation [55]. Engine start up and shut down also present strong thermal and applied mechanical loads transients, which are fundamental to TMF damage. Some of the severest damage will therefore occur during the transient operations in aero engines. The interested reader is

referred to Harrison, et al [1] and Antolovich and Saxena [55] for detailed description of the TMF process in gas turbine engines.

3.5.1 Thermo-Mechanical Fatigue in Turbine Blades

In the turbine blade, TMF damage mainly occurs due to the cyclic thermal and mechanical loads experienced during service (particularly transient operation). The mechanical loads experienced are centrifugal stress and bending moments due to gas pressure and velocity changes. Under cyclic thermal loads, thermal gradients and transients cause thermal strains that induce thermal stresses in the blade. The thermal transients are the variation of temperature with time along a flight path; while thermal gradients are mainly due to blade cooling technologies, such as internal convection cooling and thermal barrier coatings (TBC). Lasalmonie [69] explain that the advancement of these cooling technologies are the main source of TMF in turbine blades. Zamrik [94] also emphasises that the addition of coatings complicates the TMF effect, particularly at the coatings substrate interface.

For cooled blades, the thermal strain at the hotter blade surface is partially constrained by the internal colder surface, leading to compressive and tensile thermal stresses on the hotter and colder sides, respectively. The coefficient of expansion mismatch between the blade material and TBC layers impose additional thermal stresses for coated blades. The complex geometry of the turbine blade also imposes stress concentrations that contribute to the TMF damage.

The blade regions mostly affected by TMF are areas that would experience high thermal stresses and gradients, particularly in transient operations. The leading edge would therefore be a critical region because of the nearby cooling holes and film cooling features that induce high thermal gradients. Moreover, the leading edge experiences the highest gas temperatures and heat transfer coefficeints. In transient operation, the leading edge would also exhibit a quicker

response to any variation in temperature. Accordingly, TMF cracks in the leading edge have been observed by [95]. Substantial TMF cracks were also observed at the mid chord in the pressure and suction sides. Similarly, the same TMF crack regions were identified by [96] as shown in Figure 3-4**.** Invariably, the root and the region at three quarters of the blade span would also be critical in the leading edge. The highest stresses are experienced in the root, and a combination of stress and the highest temperature would occur at the mid to about three quarter's span of the blade.

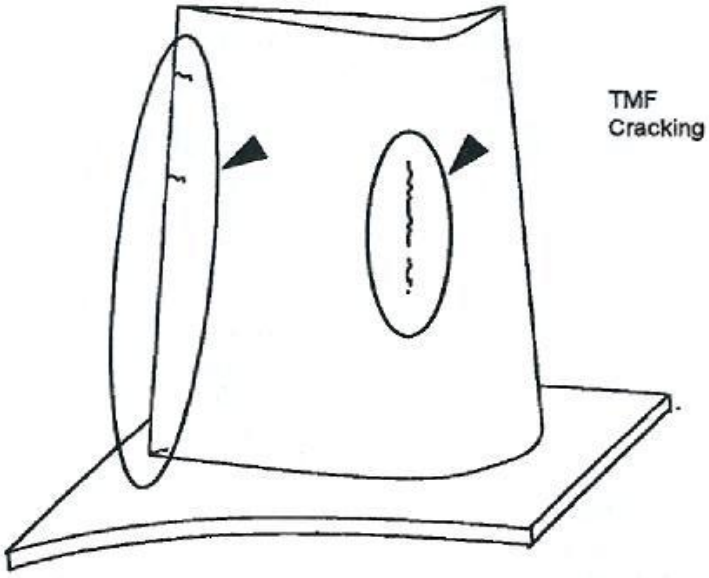

Figure 3-5 TMF crack locations observed in anisotropic blade [96],p.20-3.

3.6 Chapter Conclusions

From the foregoing, TMF damage in the turbine blade is influenced by creep, fatigue and oxidation; acting individually and in combination. The dominant damage mechanism in TMF also changes as a result of variation in the strain-temperature phasing history (in – phase or out-of-phase TMF). The effect of coatings and the influences of temperature, mechanical and thermal stresses induced due to the strain – temperature phasing are key factors that drive the

TMF damage in a gas turbine blade. Accounting for these effects is essential in the TMF life prediction of the turbine blade.

Over the years many TMF models have been developed. However, many of these models were based on isothermal tests and do not account for: the phase relationships between temperature and mechanical loadings; thermal transients that occur in the operation of gas turbines (particularly, the cooled aero gas turbine blades); and the interaction of fatigue, creep and oxidation damage mechanisms. The methods based on TMF tests more accurately describe the damage process under varying thermal and mechanical loading. Hence, these TMF based methods would provide reliable life assessments of gas turbine blades.

Nevertheless, care must be taken to apply the appropriate model for the specific conditions it was developed for. A TMF model that can be applied over a broad range of conditions is highly desired. However, such a model could be inherently complex. One of such models identified from the literature is the Neu /Sehitoglu TMF model. The model accounts for damage accumulation due to creep, fatigue and oxidation influences. It can also be applied over a broad range of temperature strain histories. However, its main drawback is the high number of material parameters that have to be experimentally determined. Hence, to apply this model, there would be the need to consider alternative, but satisfactory means to account for the material specific parameters. This model was chosen for implementation in this research because of its generic feature and its ability to more accurately capture the TMF behaviour of creep, fatigue and oxidation interactions in the turbine blade.

4 METHODOLOGY

4.1 Integrated Lifing Approach: Overview and limitation

The focus of the current research is to develop a life assessment approach that gives a physical basis linking the impact of operational and design choices on the life of the turbine blade. In this regard, the developed approach identifies the key parameters involved and how these can be suitably modelled. The developed method is implemented by integrating appropriate software tools, as well as building suitable numerical models. The approach is generic, using the minimum design information typically available at the early design stages. Hence, with minimum component design inputs, a life assessment can be conducted to further the design space exploration. It should be noted that as an initial lifing approach, the main purpose is not necessarily to obtain a definitive time – to – failure value, but to provide a means for the analyst to assess the effectiveness of design and operational decisions, as well as examine trends.

The turbine blade lifng approach developed in this thesis comprises six main modules. These are: performance model (aircraft and engine), component sizing, stress model, heat transfer model, FEA model, and TMF damage model. The flow chart relating the main components of the approach is shown in Figure 4.1. Where: TET is the turbine entry temperature; $T_{coolant}$, $W_{coolant}$ and $h_{coolant}$ are the temperature, mass flow and heat transfer coefficient of the turbine blade cooling air, respectively. RPM represents the high pressure turbine shaft rotational speed; while σ , ε , T and q represent the FEA stress, stain, temperature and heat flux distributions.

Limitation

The lifing approach developed in this research considers TMF damage to the turbine blade due to the applied temperature and mechanical loads during service. The TMF damage is based on the assumption that the blade failure occurs at the initiation of a crack. It is assumed that the TMF damage can be

predicted from the accumulation of time spent under different stress levels; based only on the thermal and mechanical stresses generated under steady thermal conditions. Thus, the stresses generated during any form of transient operation are not taken into account. Furthermore, in calculating the blade life, the stress predictions were based on purely elastic behaviour. In reality, the plastic flow would affect the evolution of the blade stress fields; but this was not considered due to its complexity and inherent uncertainty in modelling the material constitutive behaviour.

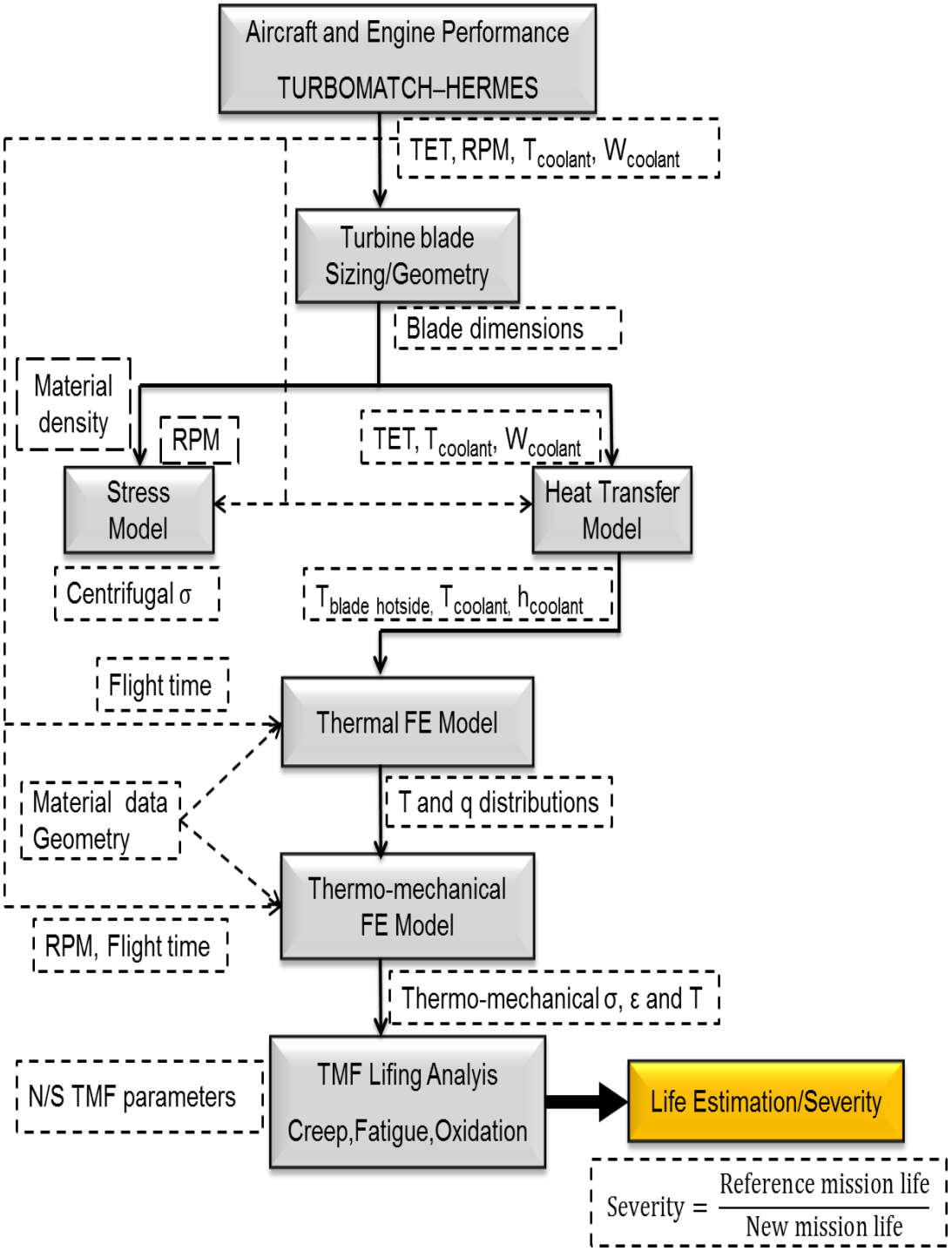

Figure 4-1: Integrated Lifing Method

4.2 Engine and Aircraft Performance Simulation

A typical history that gives adequate information of the temperature and stress variation throughout the engine cycle is a pre-requisite for any turbine blade stress and strain analysis. Since the transient changes in temperature and stress in the turbine blade influence the TMF damage, an accurate and reliable representation of their history is required. Furthermore, component aero thermal data including inlet and outlet temperature, pressure, mass flow rate and rotational speeds from the engine cycle performance are needed to size the turbine blade annulus. These can be obtained using an engine performance simulation tool. For a typical aero engine, an aircraft performance tool coupled to the engine performance would give further information on the overall engine flight performance at various segments of the flight mission. The ability of the coupled performance tool to capture both steady state and transient performance is highly desirable, as TMF damage is recognised to be severe during the transient phases of operation (start- up and shut down, as well as rapid acceleration and deceleration).

The calculated duration of each flight segment, along with the associated engine operational conditions such as component rotational speed, TET, cooling air temperature and cooling mass flow are the essential outputs needed. The temperature and mass flow outputs would then be used in a heat transfer analysis to estimate the heat transfer coefficients and temperature distribution along the turbine blade. The rotational speed can be used directly to estimate the centrifugal stress (CF stress) on the blade. Furthermore, using the gas pressure and velocity outputs across the turbine, the stress due to the bending moments can be evaluated and added to the CF stress. The performance models developed in this research are discussed in the following sub sections.

4.2.1 Engine Performance

The engine performance model developed in this research is similar to a high bypass turbofan engine configuration for a short/medium haul aircraft. The

engine model and performance simulation was done using Turbomatch; a component based gas turbine performance tool developed at Cranfield University [97] . This software was used to model the design point and study the off-design performance of the engine. The design point of the engine was selected at take-off conditions based on the performance parameters obtained from open literature [98-100] **.** Table 1.1 gives some of these parameters, while a representative Turbomatch model layout of the reference engine is shown in Figure 4 2.

Table 4-1: Engine performance parameters take-off**.**

Parameter	**Value**
Take-off Thrust	121.4 kN
Bypass ratio	5.1
Pressure ratio	32.8
Shaft speed	15183 rpm
Mass flow	354.7 kg/s

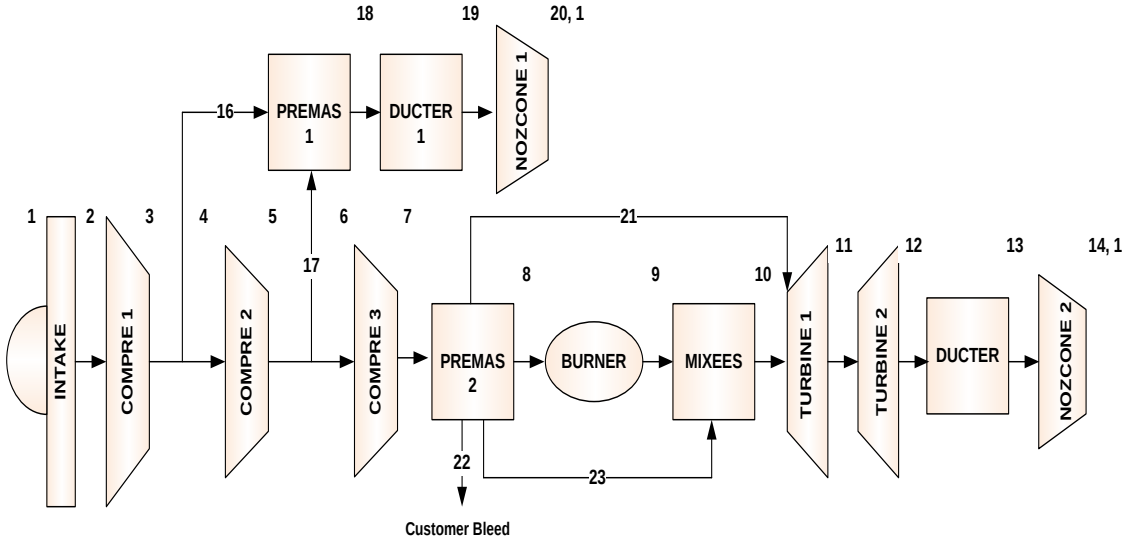

Figure 4-2: General layout of the reference engine.

4.2.2 Aircraft Performance

The overall engine flight performance for a given flight condition and mission profile was simulated using Hermes. Hermes is aircraft performance software also developed at Cranfield University [101]. The Hermes aircraft model developed is representative of the characteristics of a short – medium range, twin-engine aircraft from information in the public domain [102; 103]. The user provides the basic information to define the shape, geometry and required performance of the aircraft; including the engine design point information earlier modelled in Turbomatch. Other inputs include the specification for the climb schedule, cruise speed and altitude, as well as descent schedule. Hermes calculates the aerodynamic characteristics of the aircraft and combines this with the engine data from Turbomatch to determine the overall aircraft performance at various segments of the flight mission. The calculated duration of each flight segment, along with the associated engine operational conditions such as component rotational speed, TET, and cooling flow temperature are used as inputs to the FEA model and lifing calculations. The following table gives some basic characteristics of the reference Hermes aircraft model:

Table 4-2 Aircraft specifications

Parameter	**Value**
No of engines	2
Airframe Weight Kg.	33837
Weight per engine Kg.	3654
Operational Empty Weight Kg.	41413
Maximum Payload Kg.	20276
Maximum Zero Fuel weight (MZFW)Kg.	61689
Maximum takeoff weight (MTOW) Kg.	79016
Maximum Landing weight (MLW) Kg.	251,290
Fuel Capacity L.	26022
Cruise Mach	0.785

4.3 Turbine Sizing

The HPT blade would usually be sized at take-off conditions were the TET and shaft rotational operating conditions are highest. A free vortex design is commonly used; but in cases where large twisted blades should be avoided, the constant nozzle method is preferred. The sizing process starts with the turbine component specifications obtained from the engine performance simulation. Then initial rotational speed, inlet Mach number, and hub-to-tip ratio of the turbine are selected. The velocity diagrams would be calculated at the blade mean diameter and the stage loading, flow coefficient and blade angles assessed. Engineering judgement is essential to select some design data from the open literature, as well as data previously used by other studies. Also, assumptions such as constant axial velocity and 50% degree of reaction at mean height are usually made to simplify the process. Turbine sizing procedures are well documented and refs [104-106] give detailed guides for this.

In this research, the single stage high pressure turbine blade was sized at take-off conditions using the constant nozzle method. Figure 4.4 shows a flow chart of the sizing process comprising engine performance simulation, inlet/outlet annulus geometry sizing, stage efficiency prediction, rotor inlet velocity calculation; constant (NGV) blade design calculation and preliminary blade design at the root, mean and tip locations.

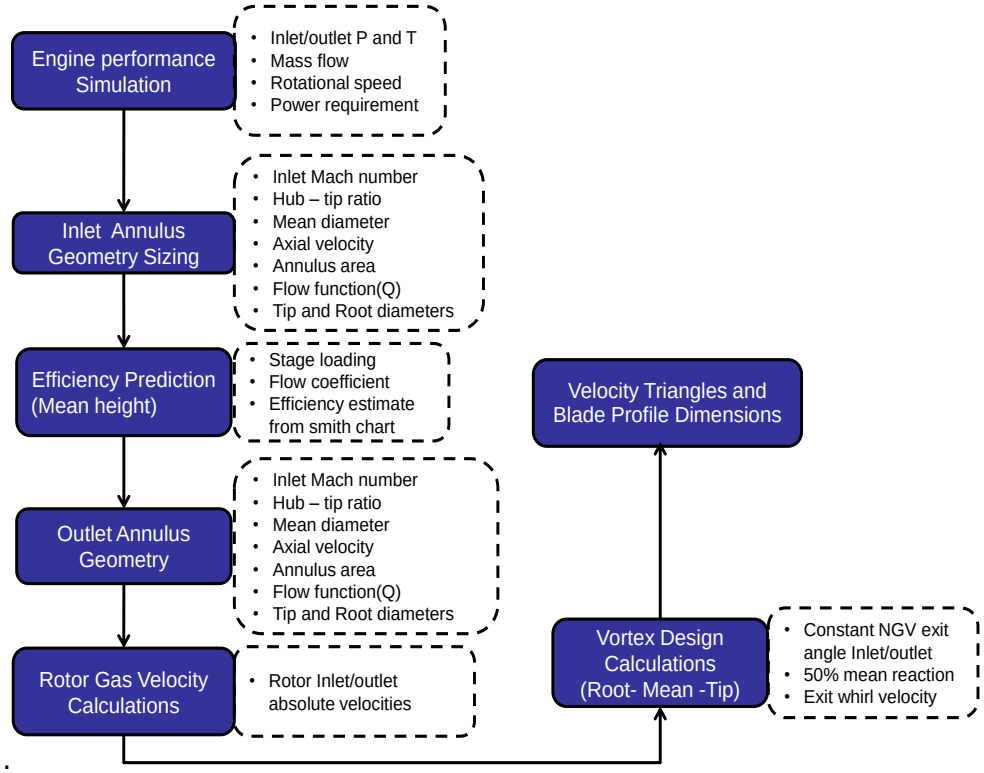

Figure 4-3:Turbine blade sizing flow chart.

4.4 Stress Model

Gas turbine blades undergo high stresses due to: centrifugal load, gas bending moments, and thermal stresses. The gas bending forces would usually be conterbalanced by measures such as blade leaning;so their effects are very small compared to the centrifugal and thermal loads. Furthermore, only a minimum set of design information is typically available when examining the life of turbine blades at the initial design stages. Hence, blade stress analysis could be done using the centrifugal stresses and thermal stresses, ignoring the bending moments . Centrifugal stress would always exists because the blade material has mass.Usually, because the blade operates in an inertial field, upto about 80 percent of the blade material strenght is used in over coming centrifugal stress[107] . The thermal stresses are due to the variation of thermal gradients on the turbine blade. This can be very destructive and actually characterise TMF behaviour. An FE model using a simplified 3-D model of the turbine blade would therefore be necessary to capture these effects.

For the life assessment in this research, gas bending moments and gas pressure loads where ignored. Only the centrifugal stresses on the blade from the root to tip as shown in were considered. The rotational speed is generated from the engine design point data, while the blade height is obtained from the sizing analysis. Table 4.3 summarises the input data for the stress model. An un-shrouded blade of constant area is assumed and the axial gas velocity remains constant along the span of the blade. Also, it is assumed that the forces on the blade act at the blade section centre of gravity (CG). The blade was divided into sections, and the centrifugal stress, $\sigma_{CFSec}$was calculated at each section using Equation 4.1

$$\sigma_{CFSec} = \rho \times h_{sec} \times \omega^2 \times d_{CG} \qquad 4\text{-}1$$

Where: ρ is the blade density, h_{sec} is the blade section height, ω is the angular speed, and d_{CG} is the distance between the rotation axis and the section centre of gravity (CG). The results serve as initial estimates and verification for the FEA structural analysis.

Table 4-3 Basic inputs for the stress model.

h_{blade}(m)	PCN	N in DP (rpm)	ω (rad/s)	h_{shroud}	ρ_{blade} (Kg/m^3)	r_{hub} (m)
0.04	1.004	15122.51	1589.96	0	8525.41	0.2275

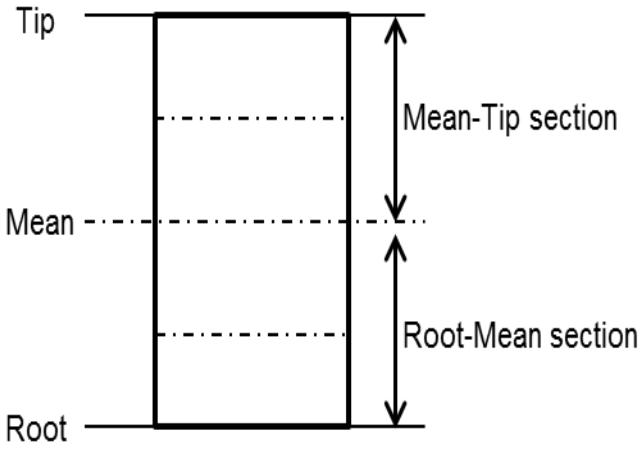

Figure 4-4: Blade sections for centrifugal stress calculation.

4.5 Heat Transfer Model

Adequate modelling of transient temperatures and the thermal gradient across the turbine blade is a major requirement in determining the thermo-mechanical stresses that influence TMF damage. Again depending on the available inputs, the heat transfer analysis can range from a low fidelity 1D heat exchanger model consisting of hot gas and coolant convection, to a 2D or 3D detailed CFD heat transfer analysis as depicted in Figure 4.5.

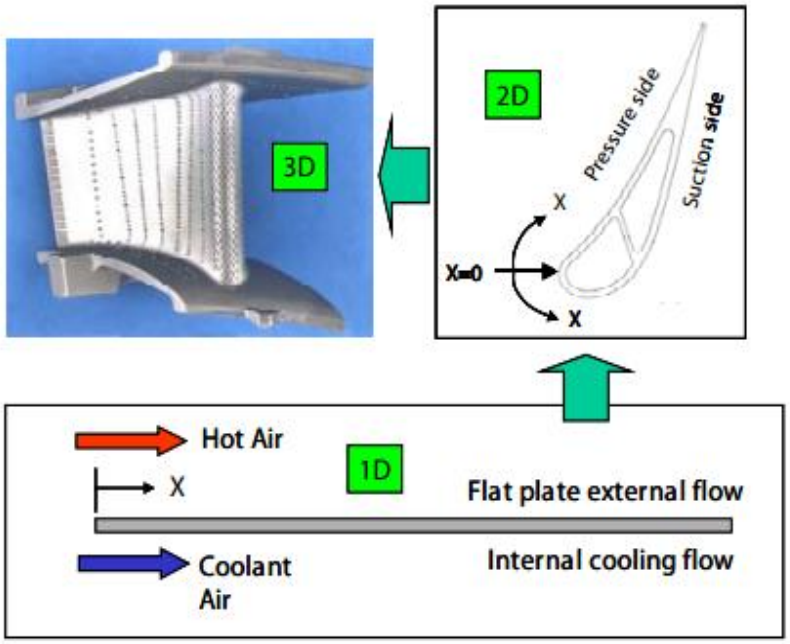

Figure 4-5 Simplified to complex cooling design analysis [108], p. 297

Although a CFD analysis would give the highest fidelity, the complexity and huge computational costs makes it unattractive as an initial design option. Moreover, it would require detailed blade geometry, which is usually not available at the initial design stages. It is arguable that existing blade geometry could be adapted, but this removes the generic benefit in such a developed model. An analytical heat transfer model that captures the salient blade cooling design details, yet giving the right balance in terms of depth of analysis and reduced complexity is therefore a proposed option.

This model would be similar to the 1D heat exchanger, but include the effects of film cooling convection and conduction through the TBC; by means of derived analytical expressions. Empirical correlations can be used in estimating the heat transfer coefficients. The blade model will be split into span wise sections, with each section treated as a single blade. Hence, the outlet temperature and heat transfer coefficient from the preceding section form the inlet conditions to the next section. This way the span wise variations of temperature and heat transfer coefficients are considered. The model would also consider the non-uniform total temperature pattern exiting the combustor, as well as the relative temperature experienced by the blade. Accordingly, this can be accounted for by using the radial distribution factor (RTDF) and temperature recovery factors

Two blade sections could be defined for the hot surface in contact with the combustor gas and the cold surface in contact with the cooling air. A heat balance to account for the internal cooling can then be performed allowing for the rise in cooling temperature along the blade span. The calculated temperature distribution and heat transfer coefficients would then be used as boundary conditions for a transient heat transfer analysis using a finite element package.

In view of the foregoing, An analytical model developed by Eshati [54] [44] for heat transfer and creep analysis to investigate the influence of Water Air Ratio (WAR) on an industrial gas turbine was adapted for aero engine application in this research. The model evaluates the heat transfer to the leading edge (hot side) and cooling hole (cold side), using non-dimensional parameters such as: Reynolds number, Nusselt number, Stanton number, and Prandtl number. The model comprises two sub-models: the coolant heat transfer model and the hot side heat transfer model as depicted in. Figure 4.6 and Figure 4.7. The aero-thermal data from Turbomatch, and the blade sizing details are the inputs used in the model. The outputs include the span wise temperature distribution of for the blade metal, cooling air and TBC. The heat transfer coefficients for the hot

and cold sides are also calculated. These outputs are used in the FEA thermal model as boundary conditions.

Furthermore, the model was enhanced in this research to account for the time dependent variation of temperature and heat transfer along a given flight path. This was done by linking the aero-thermal data from Hermes to the heat transfer model; such that for every TET and cooling temperature variation along the mission, the model calculates the associated heat transfer coefficients.

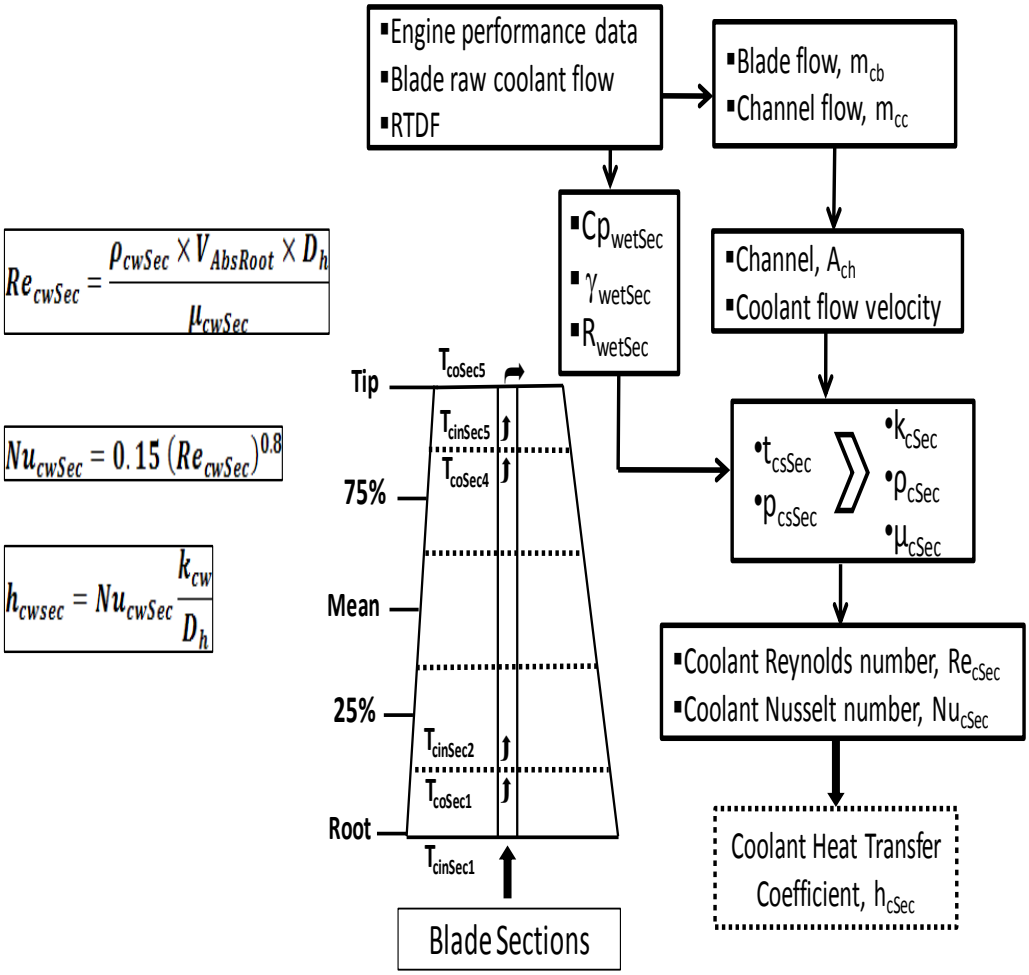

Figure 4-6 Flow chart for cool side heat transfer analysis [54] p.4

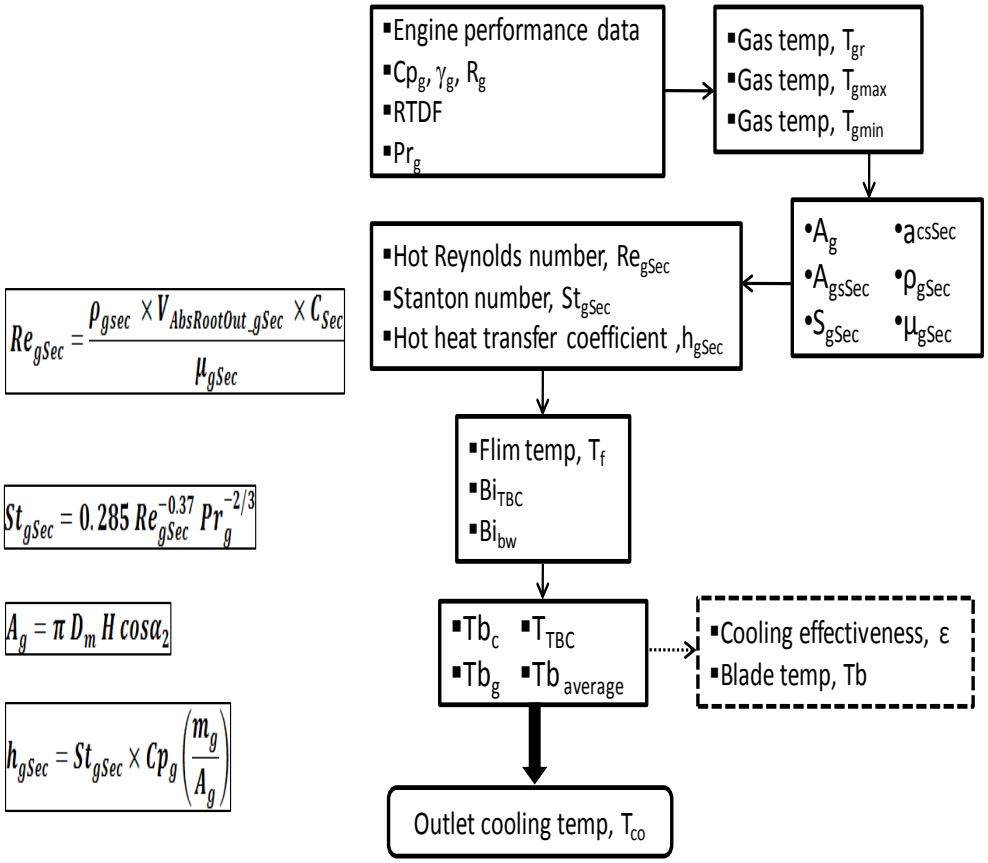

Figure 4-7 Flow chart for hot side heat transfer analysis [54] p.6

4.6 Idealised LE blade Geometry

The turbine blade leading edge experiences the maximum temperature within the blade. It also suffers from severe thermal gradients which induce thermal stress that contribute to TMF damage. Thus, the leading edge is considered a critical region for lifing of the turbine blade. However, the cooled turbine blade geometry is complex, consisting of multi- channel cooling holes and thin curved surfaces. These introduce stress concentrations, and substantial changes in temperature across small regions of the blade, thereby complicating accurate blade life determination. Hence, a generic representation of the HPT blade that would capture the thermal and mechanical behaviour for TMF could be evolved. This idealisation would be based on minimum number of basic inputs and easily modified for sensitivity analyses. The identified critical regions to be accounted

for are the LE hot gas surface and internal cooling hole, as well as the blade root for stress calculations.

To this end, this research proposed that the cross section of the turbine blade could be simplified to two parts as depicted in Figure 4-8. A hemi-cylindrical shape with a hole to account for cooling represents the leading edge, while a flat plate wedge represents the remaining portion of the blade and trailing edge.

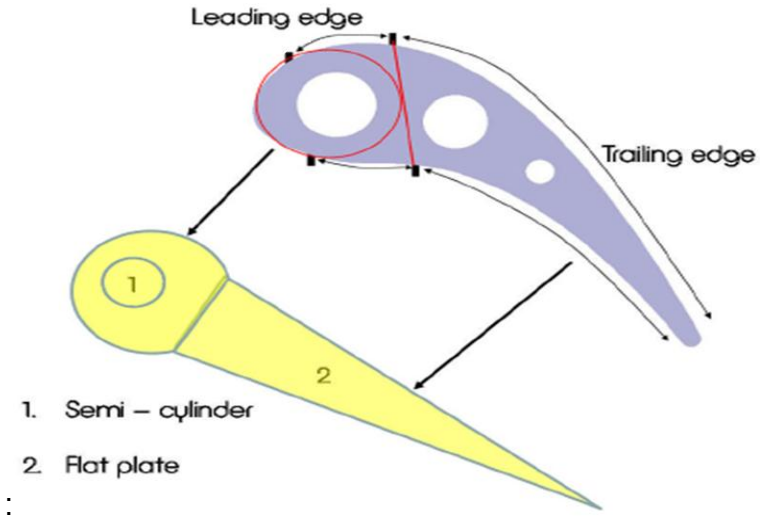

:

Figure 4-8 Blade geometry simplification

This kind of model is needed to develop a generic method for the life assessment of the turbine blade, using basic sizing inputs such as the blade span and annulus radii. It also gives benefits of reduced computational time and complexity in FEA thermal –mechanical modelling. The trade-off between simplicity and accuracy is accounted for by incorporating the effects of thermal barrier coatings (TBC) and convective cooling in the thermal analysis of the LE .The method could serve as an initial model for thermal analysis on complex 3D blades, as well as evaluating new turbine blade designs and cooling technologies. Figure 4.9 shows an outline of the proposed geometry. Chapter 6 assesses the effect of the simplifications and assumptions of the idealised blade geometry with respect to a NASA detailed blade design [109].

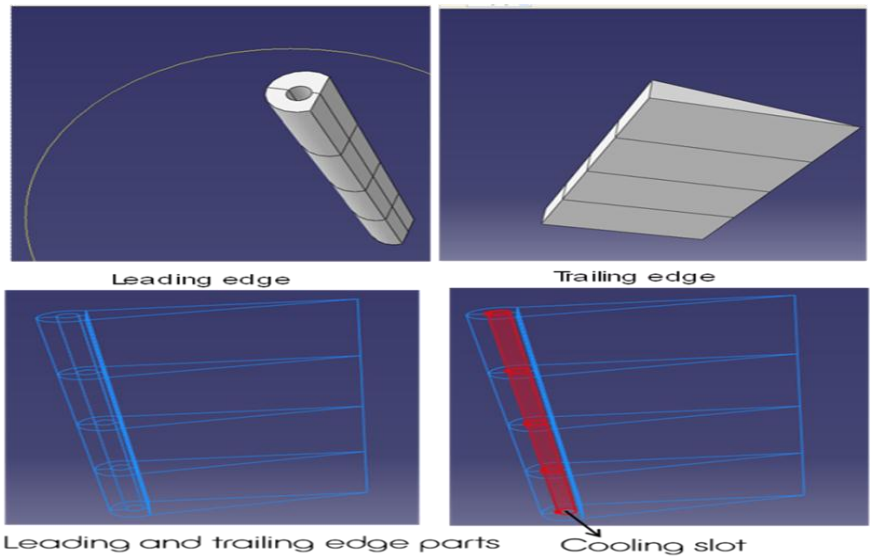

Figure 4-9 Outline blade geometry for FEA analysis.

4.7 FEA Model

Blade TMF cycles for typical aero engine operating conditions need to be determined by finite element analysis [81] . A sequential coupled thermal stress analysis would be required to obtain the thermal stress and strains outputs for the TMF life assessment. This involves developing a separate FE thermal model and thermo-mechanical model. The thermal model is implemented with a heat transfer analysis procedure, while the thermo-mechanical model uses a static stress analysis.

First, a transient thermal analysis would be conducted on the blade model. The previous analytical heat transfer analysis enables the blade hot and cold surfaces temperature distributions and heat transfer coefficients to be obtained. These would form the main boundary conditions. It is necessary that a means to apply the span wise variation of both the temperature and heat transfer coefficient in the thermal FEA is evolved. The resulting temperature distribution can now be used as a pre-defined field for running the static stress analysis. Temperature dependent material properties of thermal conductivity, specific heat, coefficient of thermal expansion, yield stress and Young's modulus are essential to be included in the material definitions. In addition, the time

dependent variations in temperature and stress would have to be accounted for by relating the engine flight performance results to the FEA. An elastic analysis is quite sufficient and is usually performed [81].

The results of the thermo-mechanical stress and strain components along a given flight can then be extracted as the main outputs for a TMF lifing analysis. in this research, the FEA considered only the blade leading edge. two main sections were defined: the leading edge hot side (HS) in contact with the combustor gas and the internal cooling hole, cold side (CS) as shown in Figure 4.10. The FEA therefore assumes that there is no conduction from the leading edge to the trailing edge of the blade. This is a necessary conservative assumption in using this idealised FEA model. The thermal and thermo-mechanical models developed in this research were implemented using abaqus CAE, a commercial FEA package.

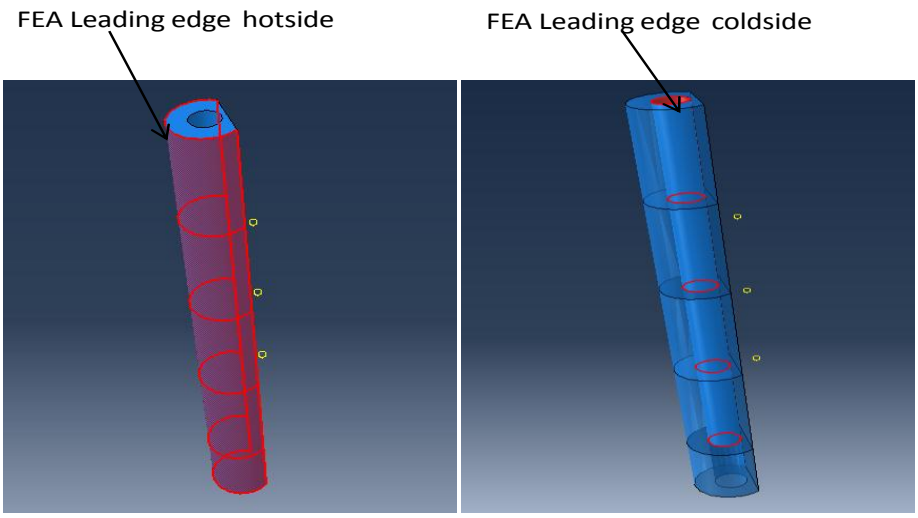

Figure 4-10: Leading Edge hot and cold sides in FEA model

4.7.1 ABAQUS Thermal Model

A transient thermal analysis was conducted using linear heat transfer elements (DC3D8) and an average mesh size of 0.0005m. Temperature dependent material properties obtained from open sources for Mar M247 were specified for thermal conductivity, density, specific heat and thermal expansion [110].

Thermal boundary conditions (BC) were applied by specifying the blade metal temperature profile on the hot side and surface film temperature (cooling air) and heat transfer coefficients on the cold side. These BCs were obtained at take –off conditions from the analytical heat transfer model. The blade metal temperature profiles were integrated in ABAQUS using analytical fields and varying amplitude factors for both the cooling air temperature and heat transfer coefficients to account for the variation with time for the given flight profile. The flight profile was broken into four steps: Ground idle (GI) and taxi, GI – take off – climb, cruise, and descent – landing. An initial temperature equal to the taxi temperature was also applied uniformly to the whole model. The boundary conditions implemented for the thermal analysis are detailed in Chapter 5.

4.7.2 ABAQUS Thermo-Mechanical Model

A static stress analysis was performed using an elastic –plastic material behaviour. Linear stress elements (C3D8R) with the same mesh size used in the thermal analysis were employed. Although turbine blade materials are usually anisotropic, a simplified isotropic case was implemented. The temperature dependent material properties defined were Young's modulus, Poisson's ratio and yield strength and specific heat capacity. Thermal loads were applied via a predefined temperature field calculated previously from the thermal analysis. Mechanical loads (centrifugal) were applied as uniformly rotational body forces. Similar to the thermal analysis, time variations were included by means of amplitude factors. The blade root was restrained by applying the mechanical boundary condition "Encastre". This means that the nodes at the blade root will have zero translation and rotation. Further details of the thermo-mechanical analysis and the boundary conditions used are contained in Chapter 5.

4.8 Lifing Model

As previously highlighted in Chapter 3, the turbine blade experiences a combination of cyclic thermal and mechanical loads that result to damage

described as TMF. Hence, TMF could be appropriately considered as the primary failure mode for turbine blades. In the same vein, the lifing methods based on TMF tests are considered to better describe the damage process under varying thermal and mechanical loading, thereby providing reliable results for life assessment of gas turbine blades.

Generally, a TMF lifing model should directly relate the impact of the applied loads to the component life. The ability to capture the arbitrary stain – temperature loading histories is essential, particularly for aero-engine blade life assessment. The model has to account for the major damage mechanisms such as fatigue, creep and oxidation, and their interaction that characterise TMF. Essentially, the choice of a TMF model will depend on the model's ability to be applied over a broad range and accommodate the expected damage mechanisms in the turbine blade.

The Neu/Sehitoglu (N/S) TMF model has been implemented in this research. Although the N/S model was originally developed for 1070 steels [90] , the model has been successfully applied to turbine blade materials [3; 73; 111] . Unlike most models that are based on isothermal tests, the N/S model is a physics-based damage model developed from observed creep, fatigue and environmental effects (both in terms of oxidation and γ' depletion), as well as their interaction in TMF experiments. The N/S model is able to account for the arbitrary temperature-strain phasing due to the varying thermal gradients and transients experienced by the blade. This is achieved in the model via cycle period normalised phasing factors for oxidation and creep .The phasing factor being a function of the ratio of the thermal and mechanical strain rates. Furthermore, the influence of other factors that influence the severity of the damage mechanisms, such as strain rate and mechanical strain range have been incorporated in the model; thereby providing a generic approach to examine TMF.

However, the draw back with this model is the large number of constants that have to be determined experimentally. Nevertheless, the ability of the N/S

model to account for the various damage mechanisms, as well as the influence of temperature, mechanical and thermal stresses induced due to any arbitrary strain – temperature histories makes it a suitable choice for life prediction in this research. The description of the N/S model is detailed in Appendix A.

4.8.1 Neu/Sehitoglu Model Implementation

Whereas, the N/S TMF model [93] has been derived from standard experiments conducted under uni-axial applied loads, real life components experience multi-axial and complex cyclic loading. To cater for multi-axial loads, the model is implemented using equivalent 3D stress and strain variables from the FEA Thermo-mechanical model, as shown in Table 4.3. Furthermore, a rain flow cycle counting method was applied in the developed lifing approach to cater for the complex mission histories that occur in service. The model calculates the damage for each extracted cycle, and sums the total damage via the linear damage rule. The TMF life distribution along the leading edge is then obtained for the total life and for each of the three damage terms. However, in using the linear summation rule for complex histories, it is assumed that the damage calculated for each extracted cycle is independent of previous component deterioration, regardless of the sequence. The N/S model was coded in MATLAB by Blanchard [92]. The flow chart for the model implementation is illustrated in Figure.4.11.

Due to the many variables required in the TMF model, three cycle counting variables were identified. These are the nodal temperatures, Von mises stress and mechanical strain extracted from the FEA. The influence of each these cycle counting variables on the TMF life was evaluated and are presented in Appendix B. Although, the Von mises stress gave the most conservative results, temperature was selected as a suitable cycle counting variable for this study; because it was considered simpler to measure and control .The material used in the model was MAR-M247 nickel supper alloy. The properties and TMF model constants were obtained from [2].

Table 4-4: Equivalent TMF model Parameter variables

Uniaxial parameter (TMF model)	**Equivalent parameter (FEA outputs)**
Total strain (ε)	Maximum principal strain(ε_3)
Thermal strain(ε_{th})	Maximum principal thermal strain (ε_{th3})
Mechanical strain (ε_{mech})	$\varepsilon_3 - \varepsilon_{th3}$
Effective stress ($\bar{\sigma}$)	Von Mises stress (σ_{Mises})

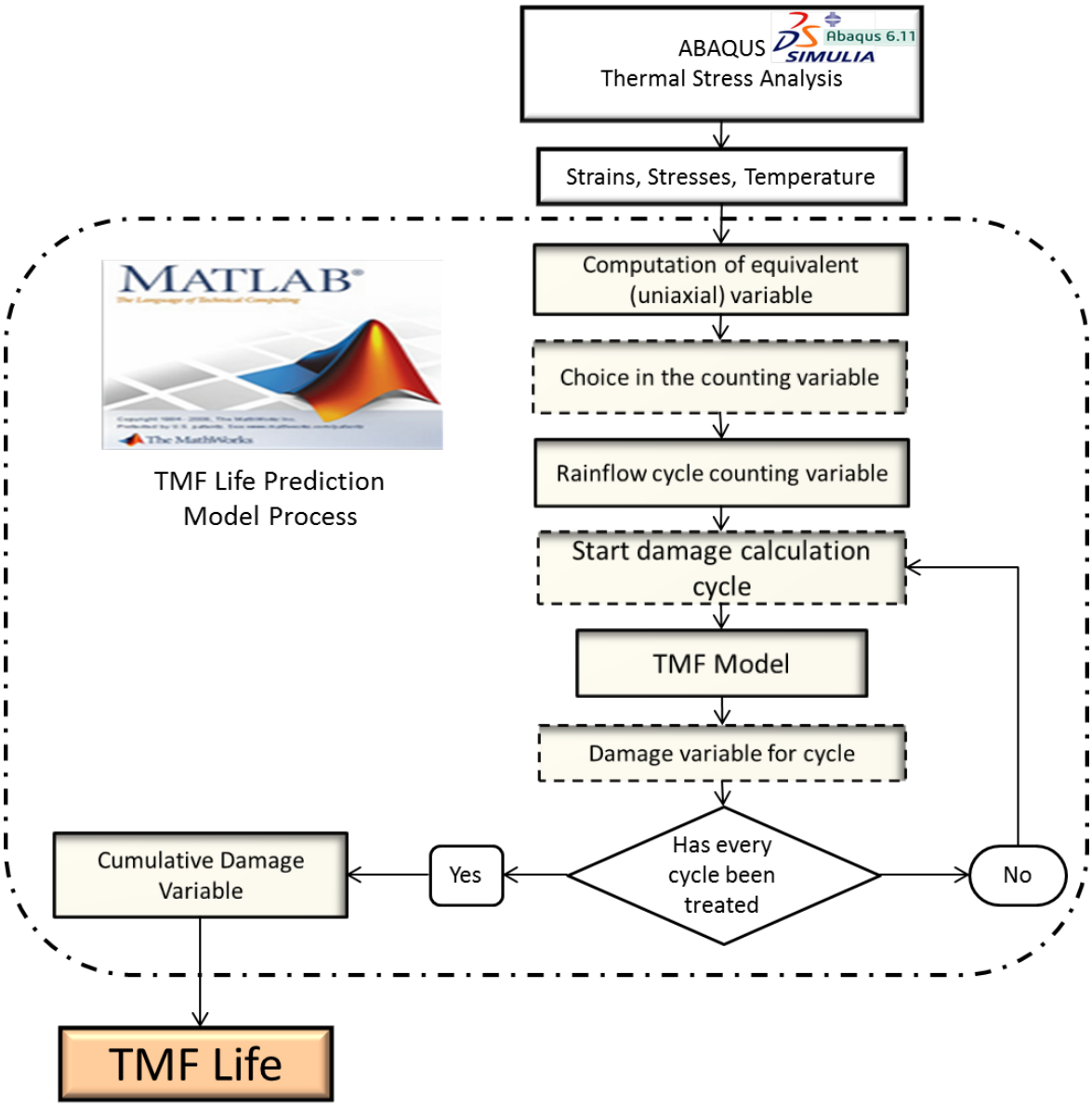

Figure 4-11: N/S TMF Implementation Chart

4.9 TMF Life Extraction

The TMF lives for the analyses in this research were further extracted at a centre line equivalent to the stagnation points of the turbine blade leading edge. The minimum life of the cold side or the hot side of the centre line (as shown in Figure 4.12 and later referred to as critical/stagnation line) is taken as the blade TMF life.

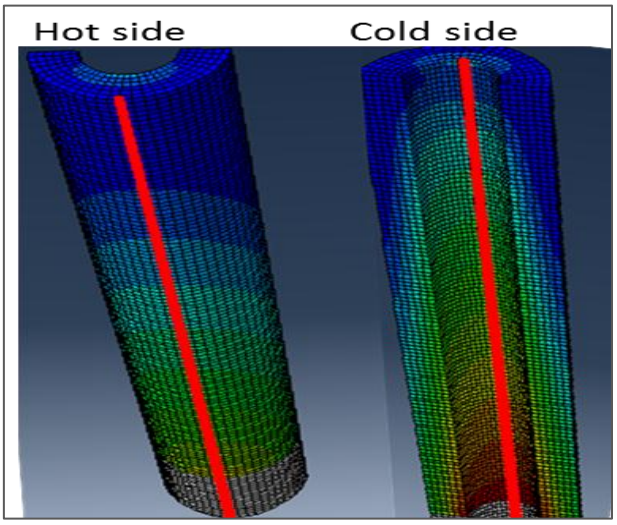

Figure 4-12: LE Hot side and cold side critical lines.

4.10 Severity Study

In examining case studies later in this thesis, the blade TMF life values are converted to relative factors and compared in terms of severity. Severity (*S*) can simply be defined as the ratio of total damage due to a given mission to the total damage of the reference mission [13]. In terms of life cycles, the inverse of the total damage is utilised as shown in Equation 4.2**.**

$$Severity = \frac{New\ mission\ damage}{Reference\ mission\ damage} = \frac{\frac{1}{New\ mission\ life}}{\frac{1}{Reference\ mission\ life}} = \frac{Reference\ mission\ life}{New\ mission\ life} \quad 4\text{-}2$$

Basically, a TMF severity of less than one indicates an increase in blade life, while a severity greater than one shows a reduction in the life. The turbine blade damage severity depends on various operational parameters and design/technology factors. The operational parameters include take-off derate, OAT, TET and engine shaft speed; while design parameters include cooling effectiveness, RDTF, and TBC. These parameters are examined in terms of TMF severity in Chapter 8.

4.11 Chapter Conclusions

The overall methodology developed in this thesis was described in this chapter. TMF has been identified as the critical damage mechanism affecting the turbine blade. Hence, the impact of the thermal gradients and transients, as well as the mechanical loads experienced by the turbine blade need to be accounted for in developing a lifing method for gas turbine blades. What key parameters are involved and how these could be captured is the key concern. Nevertheless, an appropriate balance is required between the level of fidelity of the lifing method on one hand, and the design inputs available on the other.

The lifing approach developed in this thesis is based on this premise. The approach is therefore generic and uses the minimum design inputs typically available at the conceptual design stages. Numerical models were therefore created and integrated with appropriate software in developing the current lifing approach. The developed methodology comprises 6 main modules. These are: performance model (aircraft and engine), component sizing, stress model, heat transfer model, FEA model, and TMF damage model.

The engine performance is first carried out using a representative aero engine and aircraft model. The engine and aircraft performance results provide inputs to the turbine sizing and heat transfer models. Turbine sizing is performed to obtain the basic design dimensions, while a heat transfer analysis gives the spanwise blade metal temperature distribution and heat transfer coefficients across the blade. A sequentially coupled thermal-stress analysis on an idealised

blade is then performed with Abaqus FEA software. The FEA was needed to evaluate the variations of temperature along the flight path (thermal transients); the thermal gradients between the hot gas surface and the cooling hole; the thermal induced stresses and the mechanical stresses (due to centrifugal loads). From the FEA stress and strain inputs, the blade life is evaluated based on the Neu-Sehitoglu TMF damage model. The model implicitly and explicitly captures the damage due to creep, low cycle fatigue and oxidation. The model also accounts for the phasing of temperature and mechanical strain, which dictate the damage, induced in the turbine blade. Furthermore, material properties and TMF model parameters form major inputs to the approach.

Lastly, the impact of operational and technological factors that affect the blade TMF damage can be examined in terms of severity. The output from the developed methodology enables such severity analysis.

5 TOOLS AND MODELS: RESULT ANALYSIS

This chapter explains the details of the results obtained from implementing the developed lifing approach for a given flight profile. The performance and sizing results are first highlighted. Then, the derivation of the FEA boundary conditions from the heat transfer analysis. The thermal gradients, stress and strain outputs from the FEA are also assessed. The life results are then examined for the individual damage mechanisms and the overall TMF life.

5.1 Performance Simulation and Turbine Sizing

The engine and aircraft performance in this analysis are for a reference mission (RM) of 1.4 hours,with take-off OAT=ISA+3 and 10% take-off derate. The mission segments modelled using Hermes are taxi-out, take-off, climb cruise, descent, approach, landing, reverse thrust, and taxi-in. The main take-off performance data from Turbomatch are given in Table 5-1. These are the inputs required to apply the heat transfer model. Other performance and HPT characteristics in terms of variations with time of the flight altitude and Mach number; the TET and HPT relative shaft speed; and the HPT cooling air temperature and cooling mass flow for this mission are shown in Figure 5-1 – Figure 5-3, respectively. These results are all as expected and consistent with the normal trends.

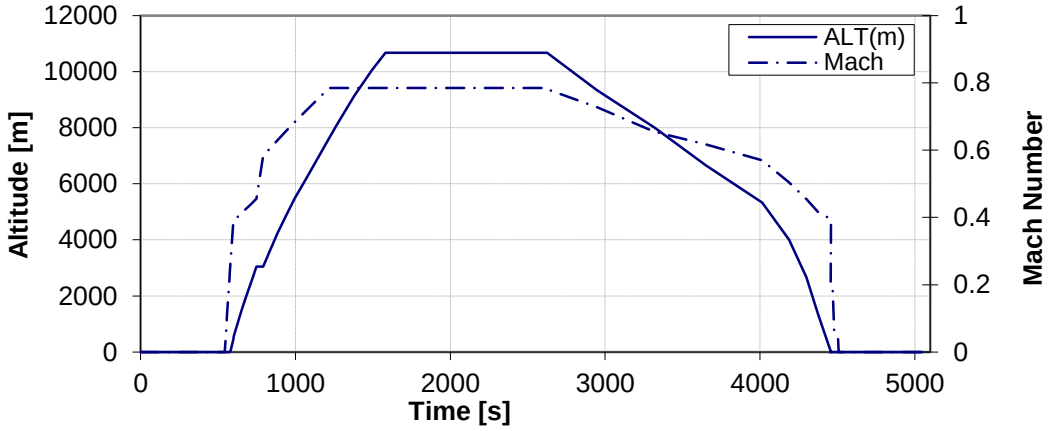

Figure 5-1: Flight altitude and Mach number variation

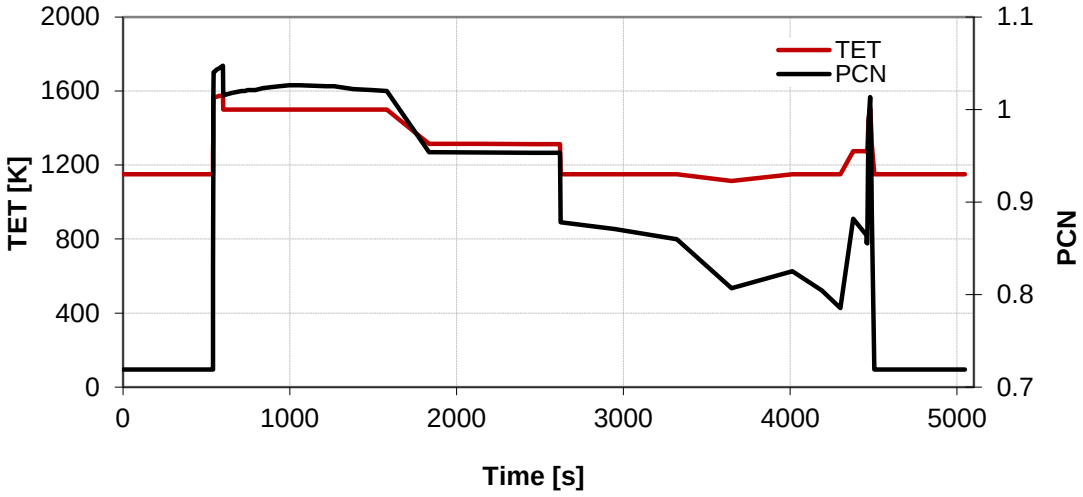

Figure 5-2: HPT shaft relative rotational speed (PCN) and TET Variation.

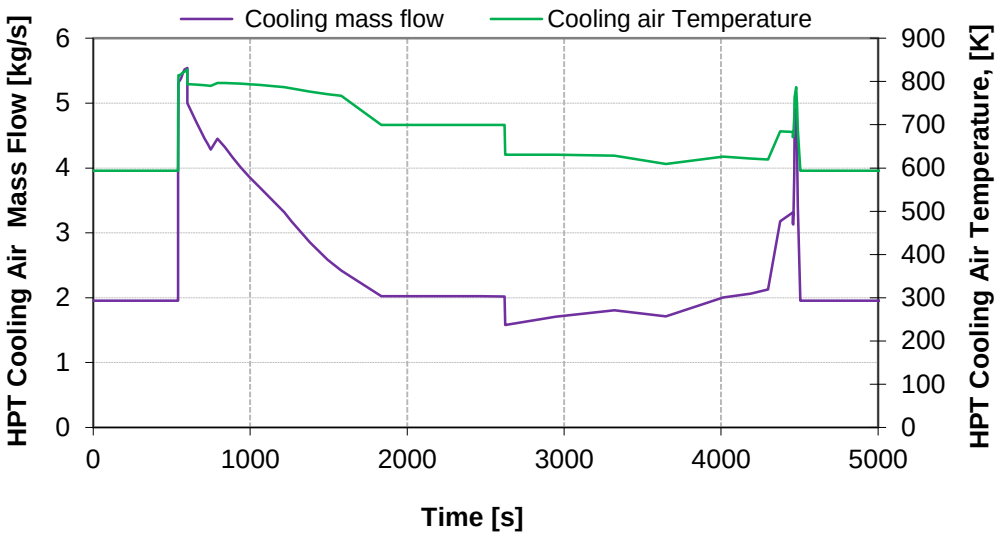

Figure 5-3: Coolant Temperature & Mass flow variations

Based on the take-off performance, the sizing of the idealized blade leading edge is modeled as shown in Figure 5-4. The baseline technology parameters used are in Table 5-2. These parameters are used in conjunction with the

turbine blade sizing dimensions for the heat transfer analysis and as reference values for severity investigation of technology parameters later in Section 10.

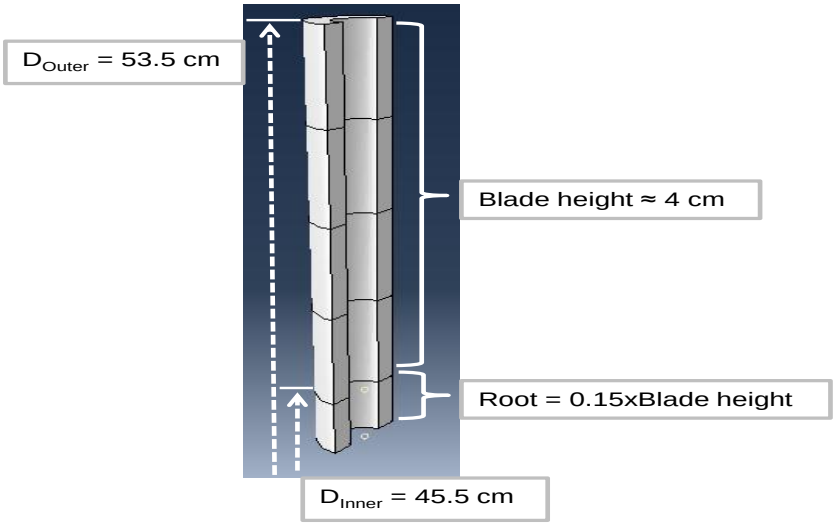

Figure 5-4: Idealised blade leading edge sizing

Table 5-1: Turbomatch Engine performance outputs: Take-off

Turbomatch		
Relative speed, PCN	1.0	
Inlet mass flow	59.3	kg/s
Overall compressor efficiency CompEff	0.9	
Overall turbine efficiency	0.9	
Compressor inlet stag temp, To_{COMPIN}	288.2	Kelvin
Compressor inlet stag pressure, Po_{COMPIN}	101.3	kPa
Compressor outlet stag temp, $To_{COMPOUT}$	820.9	Kelvin
Compressor outlet stag pressure, $Po_{COMPOUT}$	2988.7	kPa
Burner inlet temperature	820.9	K
Gas mass flow, mg	54.4	kg/s
NGV inlet stag temp, $To_{NGV\ (TET)}$	1562.0	Kelvin
NGV inlet stag pressure, Po_{NGV}	2872.9	kPa
Rotor outlet stag. temp, To_{OUT}	1138.3	Kelvin
Rotor outlet stag. pressure, Po_{OUT}	797.4	kPa

Coolant mass flow, mc	5.9	kg/s
Coolant stagnition temperature, To_C	820.9	Kelvin

Table 5-2: Reference Technology parameters

Technology /Design Parameters					
Cooling effectiveness	TBC thickness (μm)	TBC thermal conductivity $(W/(mK)$	RTDF	Hydraulic diameter (m)	LE wall thickness (m)
0.69	125	1.5	0.08	0.004	0.002

5.2 Heat Transfer Analysis

The heat transfer analysis on the HPT is done to obtain approximate heat transfer coefficients for the hot and cold sides, as well as the blade temperature distributions across the blade. The specified RM take-off performance (Table 5-1), sizing and technology parameters were the inputs used in the heat transfer model. The model calculates the temperature profile along the span of the blade for film cooling, TBC, blade metal hot and cold sides, and the coolant temperature. The spanwise temperature profiles and heat transfer coefficients are presented in Figure 5-5 and Figure 5-6, respectively.

From these results, the blade hot side temperature, cooling air temperature and cooling heat transfer profiles are implemented as Thermal BCs in the FEA model. The calculated blade temperatures increase from root to the tip. This trend is recognised; as the blade metal temperature significantly depends on the cooling air temperature which becomes hotter as the cooling flow rises from the root to tip sections of the blade. Assuming a negligible change in blade cooling effectiveness, the metal temperature would tend to progressively increase from the root to the tip section due the increase in coolant temperature along the span of the blade. Hence, the coolant temperature at the tip section would be highest. This drives the overall increase in metal temperature towards the blade tip.

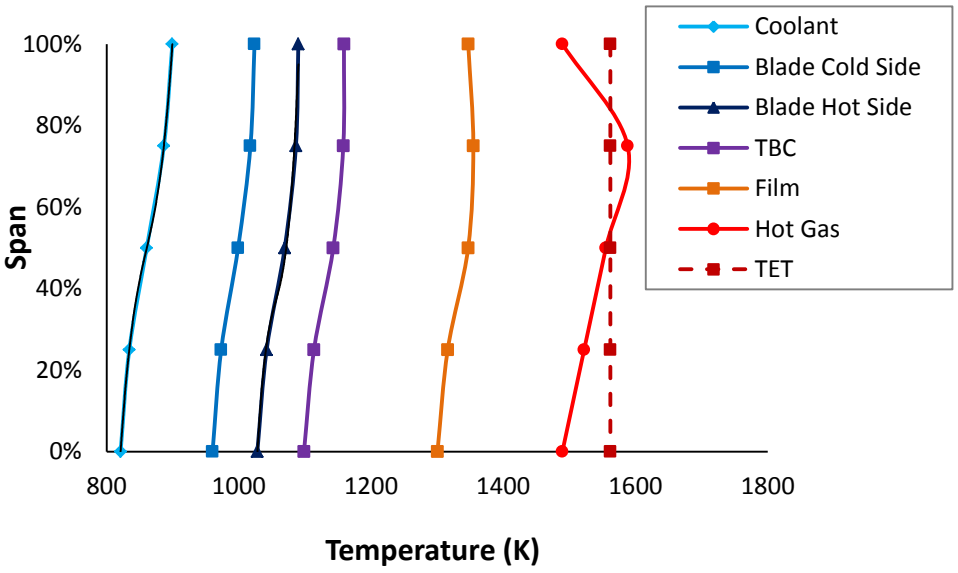

Figure 5-5: Spanwise Temperature profiles – RM Take off

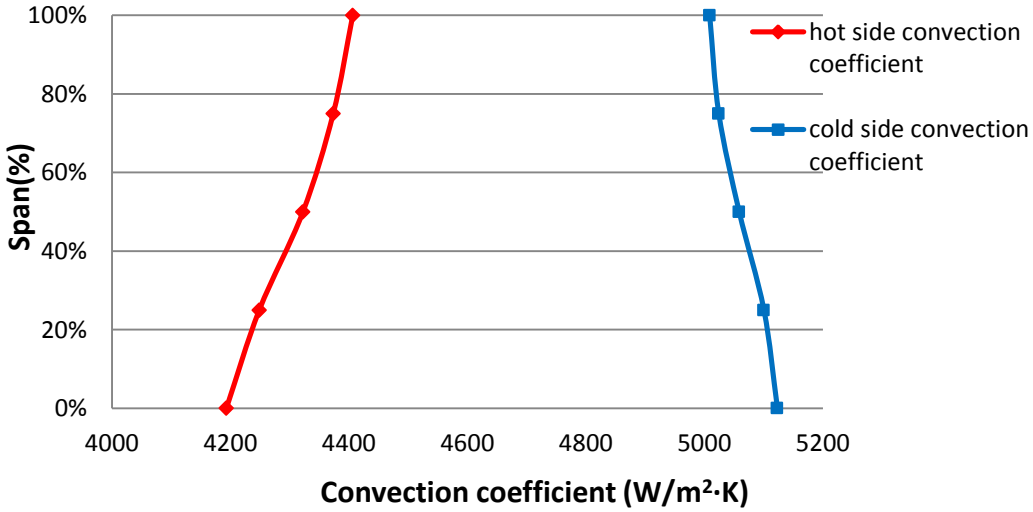

Figure 5-6 Heat transfer coefficients - RM Take off

5.2.1 Heat Transfer Model Verification

The analytical heat transfer model developed by Eshati et al [44] was used in this research as a trade-off between accuracy and the availability of design inputs. The model calculates the time dependent variation of blade metal

temperature and heat transfer along a given flight path, as well as accounts for the coolant loss along the span of the blade due to film cooling ejection. Despite the model simplifications, it provides a generic and reliable means to calculate heat transfer coefficients and blade temperature distribution along the blade. When compared to the results extracted from the detailed NASA E3 HPT thermal design, the model calculates the cooling effectiveness and the temperature distribution within 10% accuracy, as depicted in Table 5-3and Figure 5-7. Hence, the model is well suited for relative blade cooling design assessments and sensitivity case studies; particularly, at the conceptual design stages where very little information is available about the component.

Table 5-3: Cooling effectiveness and blade temperature distribution for NASA and heat transfer model,p.342

	NASA	**Generic thermal model**	**Accuracy %**
Cooling effectiveness	~0.60[1]	0.64	6.7%
Average Blade metal temperature at mid span	1227K	1217K	0.82%(10K)

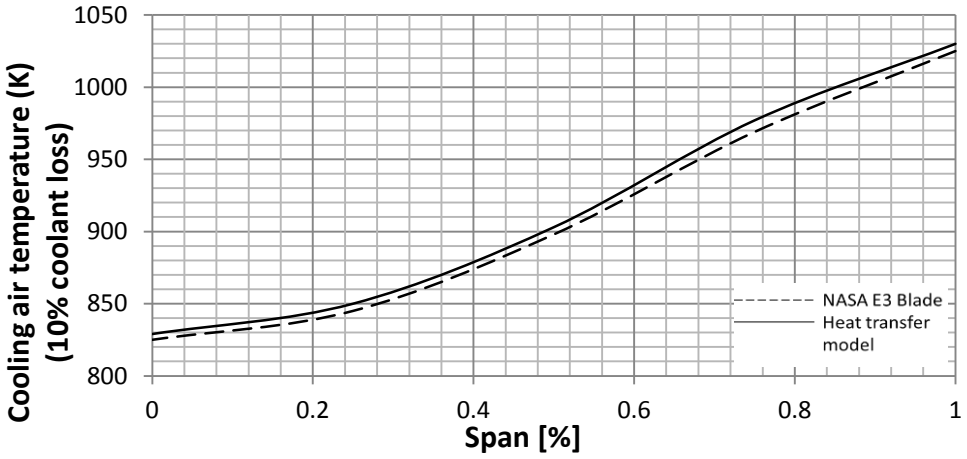

Figure 5-7: Cooling air temperature comparison between NASA E3 HPT and heat transfer model,p.343.

[1] Evaluated from the TET, average blade temperature and cooling air temperatures provided in ref[109].

5.3 Finite Element Analysis (FEA)

5.3.1 Thermal Analysis

The results for the spanwise blade temperature distribution and heat transfer coefficient from the heat transfer analysis give 3rd order polynomial correlations. These correlations are implemented in the FEA thermal model as analytical fields that give the span wise temperature variation along the blade leading edge. The hot side temperature correlation is applied to the external leading-edge surface (hot side), while on the internal cooling hole (cold side), both the cooling air temperature and the cold side heat transfer coefficient are applied as shown in Figure 5-8. To account for the temperature variation during the flight, the results of the temperature variation with time (from Hermes) for the hot gas and cooling air are converted to non- dimensional factors. Likewise, the cooling air heat transfer coefficient for every temperature variation along the flight path was calculated and expressed in non-dimensional factors. These factors were implemented as 'amplitudes' in the FEA. Figure 5-9 details the implemented amplitudes for the given flight.

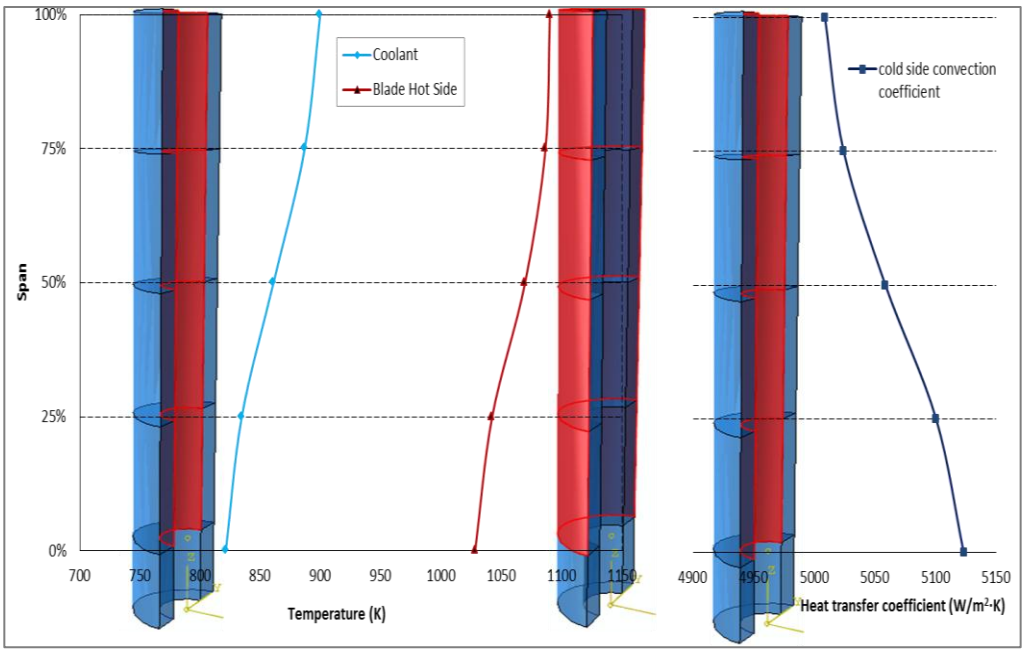

Figure 5-8 Thermal FEA model BCs

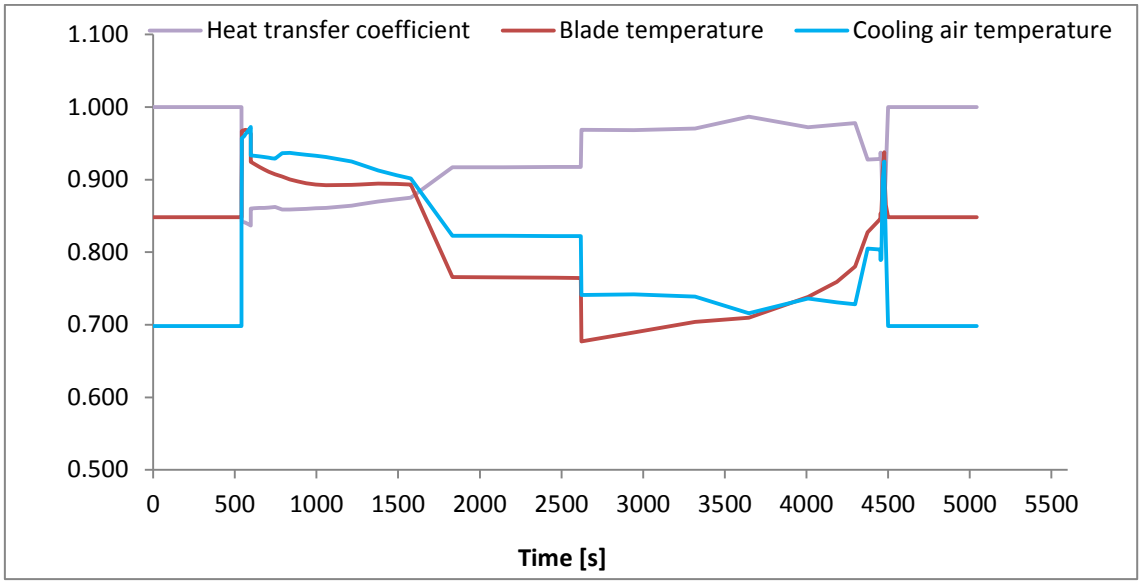

Figure 5-9: Thermal FEA amplitudes.

5.3.1.1 Thermal FEA Outputs

The outputs from the thermal FE model are the spatial time dependent blade metal temperature and heat flux distribution of the leading edge. The temperature distribution is used as input for the subsequent stress analysis. On the hot side, the temperature distribution should be close to that of the boundary condition applied as shown in Figure 5-11**.** On the other hand, for the cold side, the temperature distribution is computed by ABAQUS, based on the heat transferred to the coolant from the heat transfer coefficients and the cooling temperature specified. Hence, the temperature distribution is dependent on the heat conduction from the hot side, leading to a thermal gradient between the hot and cold sides. The span wise temperature distributions on both the hot and cold sides of the leading edge model for various flight segments are shown in Figure 5-10. The profiles are taken at the commencement of each flight segment.

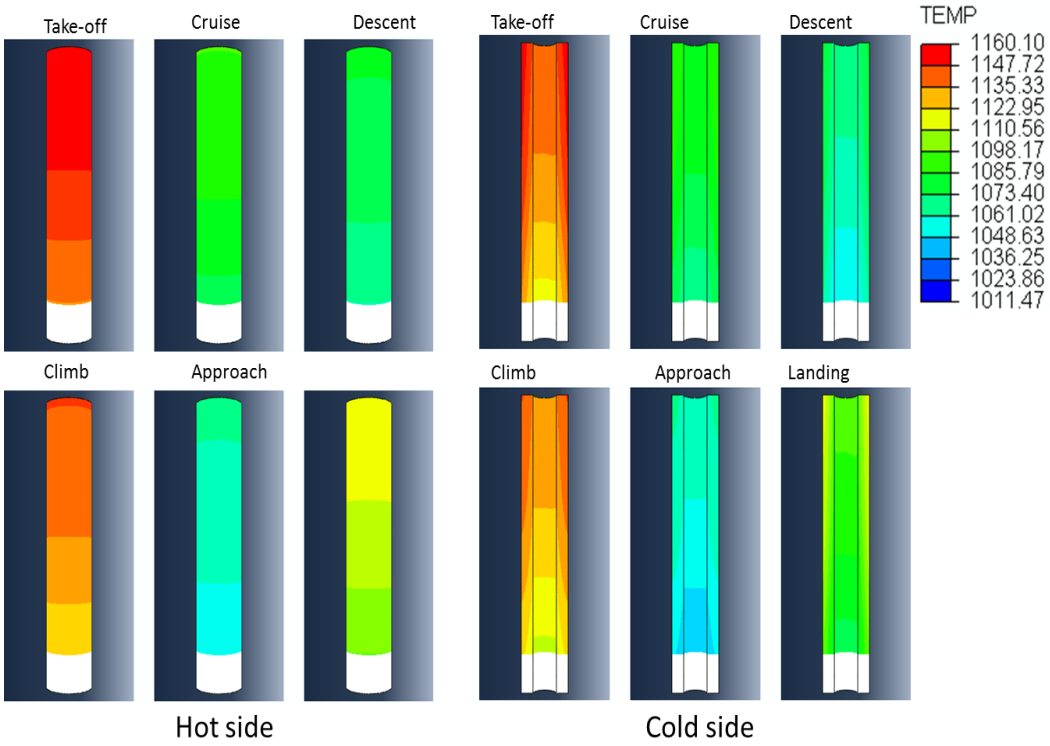

Figure 5-10: Blade LE temperature distribution at various flight segments.

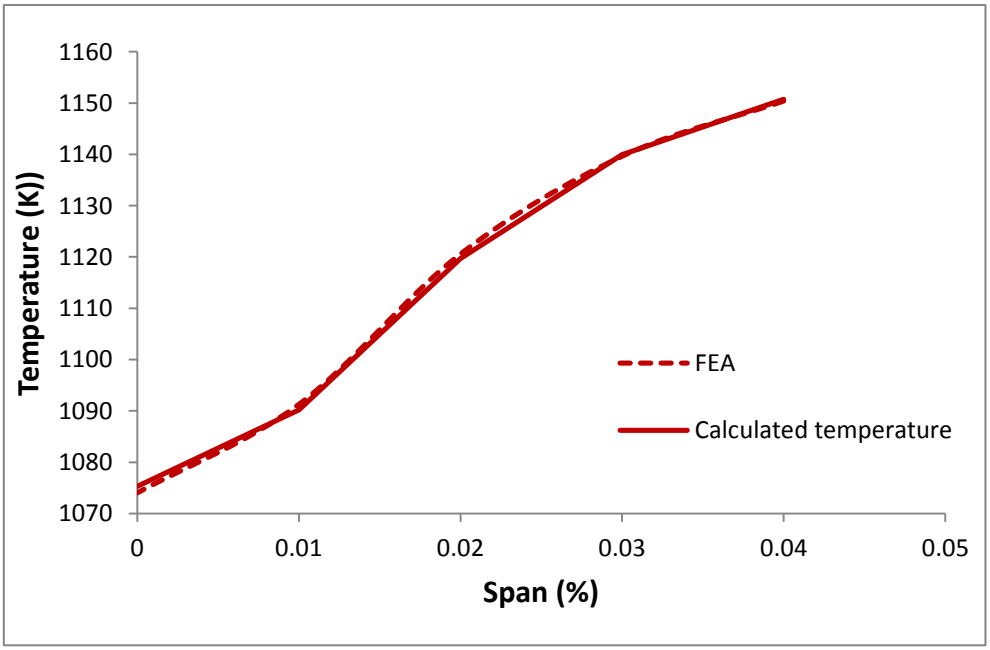

Figure 5-11: FEA and analytical model LE blade temperature comparison.

5.3.1.2 Thermal Gradients

During a given flight, the turbine blade experiences the hot gas temperatures on the hot side of the leading edge and the cooling air in the internal cooling hole (cold side). Thus, a thermal gradient (ΔT), which varies along the blade height, is imposed on the blade because of the temperature differential between the hot and cold sides. Figure 5-12 shows the temperature variation for the hot and cold sides, and the resulting thermal gradient at the take –off segment of the given flight. The highest thermal gradient occurs within the 25%- 50% region of the blade, and then reduces along the blade span. This is because the blade temperature is lowest at the root but increases to the maximum at about 50-75% blade height. Consequently, the cooling air temperature also increases span wise taking up heat from the blade metal as it passes from the root. This progressively reduces the coolant effect on the hot side temperature. Hence beyond the blade mid height the temperature difference between the hot and cold sides (the thermal gradient) becomes progressively smaller.

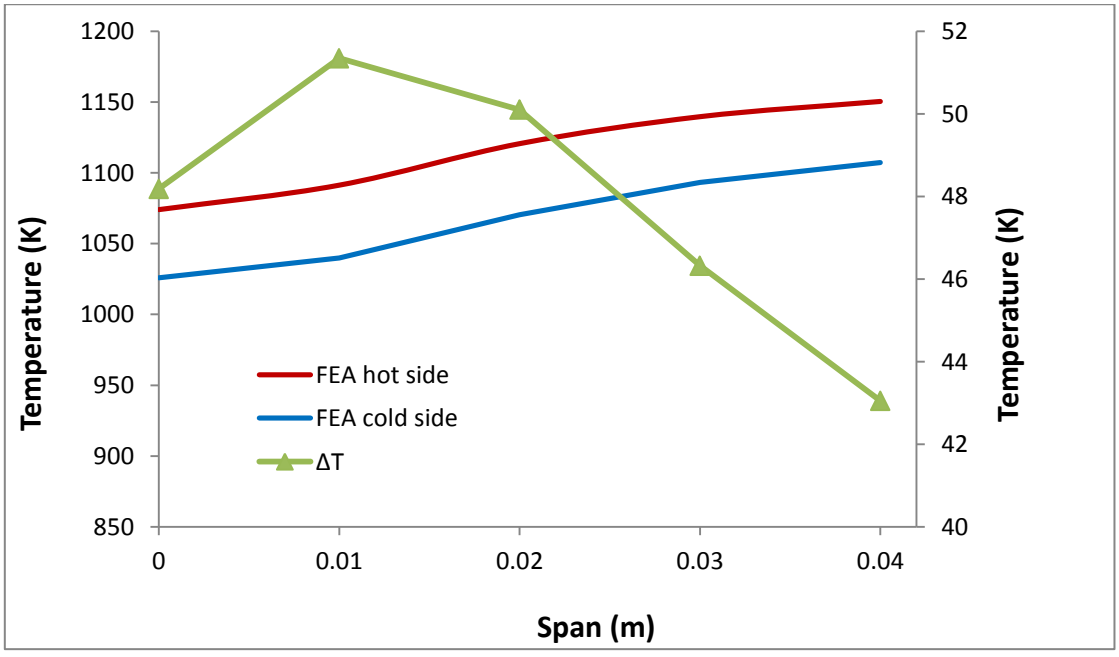

Figure 5-12: Temperature profile and thermal gradient take off

The thermal gradients vary with time along the flight path, which cause thermal transients. The impact of thermal gradients and transients are critical factors

affecting TMF in turbine blades. It should be noted that the transients referred to here are not due to fast acceleration or deceleration transient engine performance behaviour. Only the steady state changes in temperature and stress loads with time along a flight history are being considered. These are effectively accounted for in the current approach using the thermal FEA results. Figure 5-13 shows the variation in thermal gradient with time for the given flight profile; where from ground idle to take –off (points 1- 2) and reverse thrust to landing phases (3-4) are recognised to experience the highest thermal gradients. This is consistent with actual aero engine operation; where the demand for more power induces high load and temperature changes in the take-off and landing segments. The spanwise variation of thermal gradient for the various flight segments is also presented Figure 5-14. The overall effect of these variations in thermal gradients is that during a given flight mission, different regions of the blade section will undergo varying thermal strains and stresses leading to TMF damage.

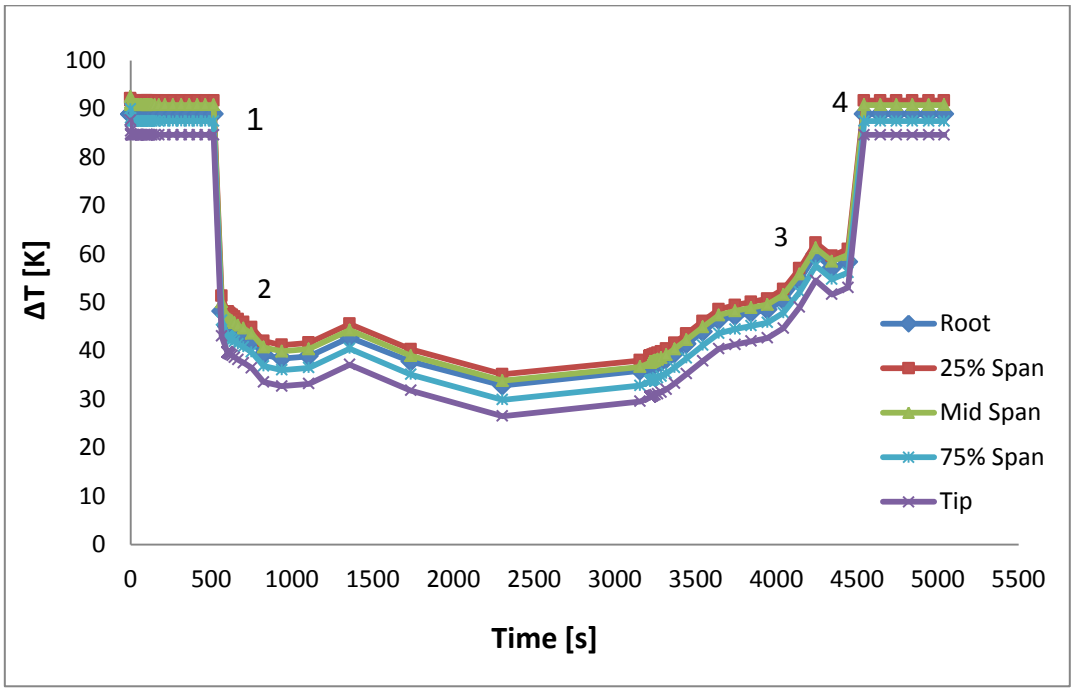

Figure 5-13: Variation in thermal gradient along a flight path.

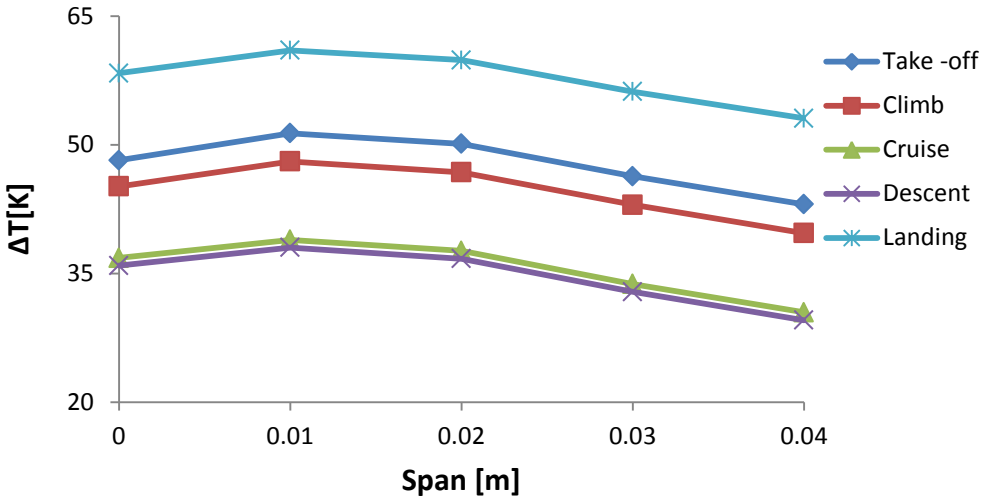

Figure 5-14: Spanwise thermal gradient profile for various filght segments.

5.3.2 Thermo-Mechanical Analysis

The thermo-mechanical model FEA gives the thermo-mechanical stress and strain results along the blade leading edge. The temperature distribution from the thermal FEA was applied to the LE blade model as a predefined field. Additionally, a centrifugal force of 1589 rad/s (equivalent to the HP shaft rotational speed) was applied as load, while the root was restrained with the encastre BC (Figure 5.15). Similar to the thermal FEA, the rotational speed amplitudes are added to account for the variation in centrifugal load with time along the flight path.

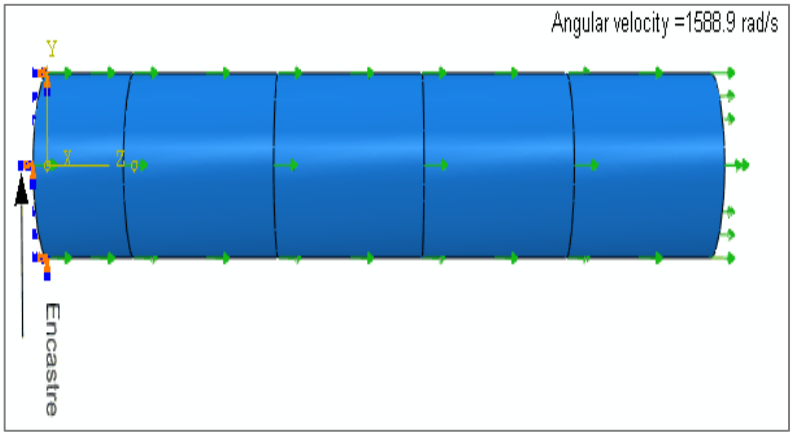

Figure 5-15: Centrifugal load and encastre constraints on thermo-mechanical model.

The thermo-mechanical stress distribution along the blade leading edge model for the various flight segments are shown in Figure 5-16. The maximum stresses occur at the root, and progressively decrease towards the blade tip as expected. However, the impact of the span wise increase in temperature causes a parabolic distribution of the stresses towards the tip; indicating the influence of the thermal stresses.

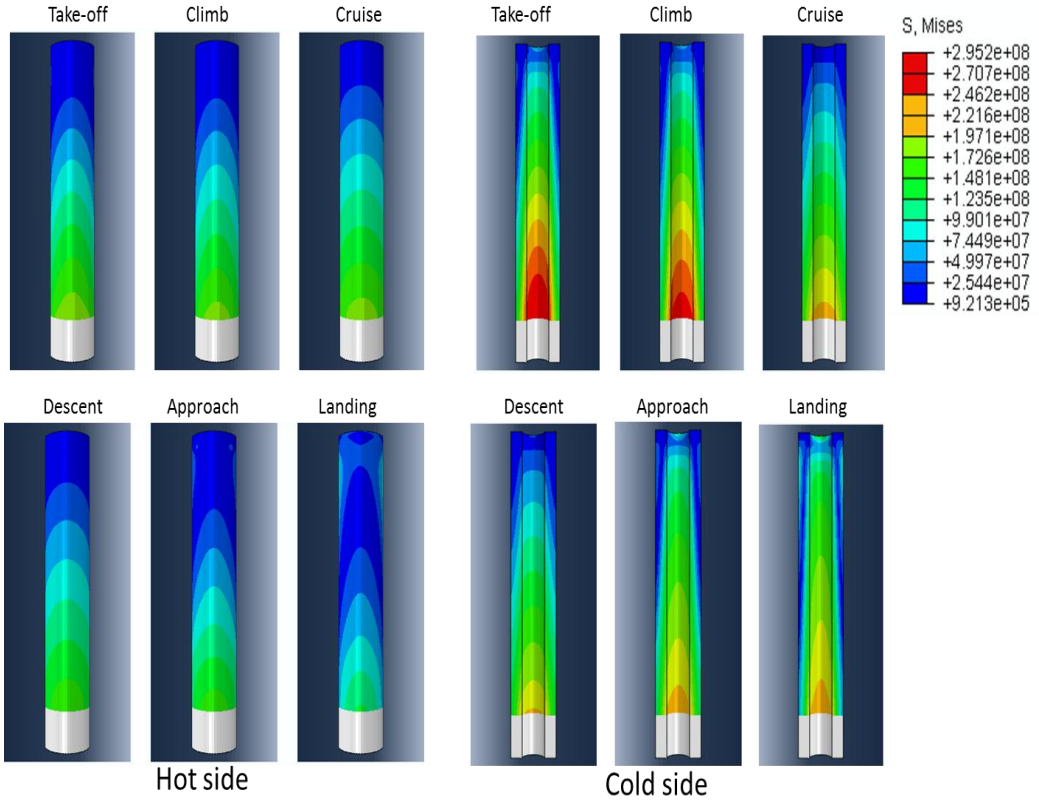

Figure 5-16: Thermo-mechanical stress distribution along the blade leading edge model for the various flight segments.

The results of the thermo-mechanical model were verified in two steps. First, the stress distribution from a pure mechanical model (excluding temperature loads) was compared with the analytical centrifugal stress calculations. Then, a combination of the results of the mechanical model and a separate thermal stress model (the mechanical loads excluded), was compared to the thermo-mechanical model stress distribution. Figure 5-17 shows the very good agreement between the FEA stress values and the analytical calculation. It is

also observed from Figure 5.18 that the combination of the mechanical and thermal stresses is equivalent to the thermo-mechanical stress distribution.

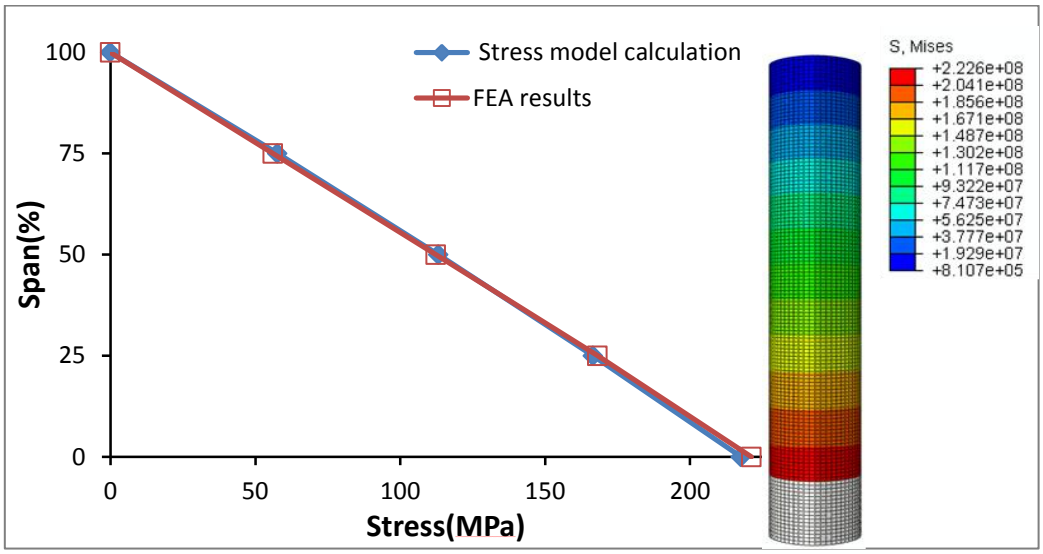

Figure 5-17: Comparison of the CF stress values from FEA and the Stress model

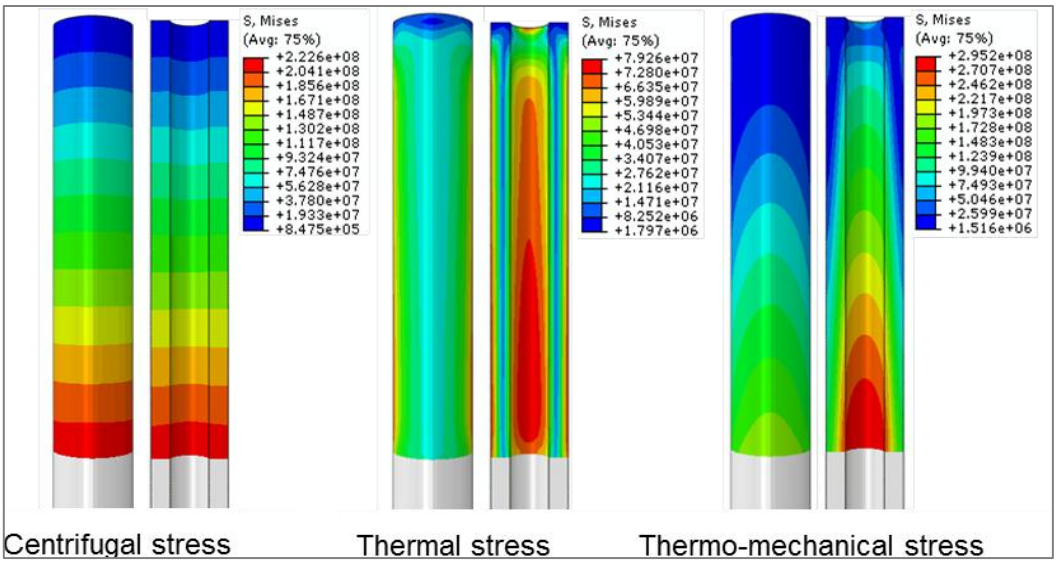

Figure 5-18: Mechanical, thermal and thermo-mechanical hot and cold sides contour plots.

The blade cold side was observed to experience a higher thermo-mechanical stress than the hot side. Since both the hot and cold sides experience the same

centrifugal stresses, the increase in thermo-mechanical stress in the cold side is mainly due to the higher cold side thermal stresses as depicted in Figure 5.19. Invariably, the evolution of thermal stresses in the cooled turbine blade will therefore drive TMF damage and the blade life. This is examined in the following sub section.

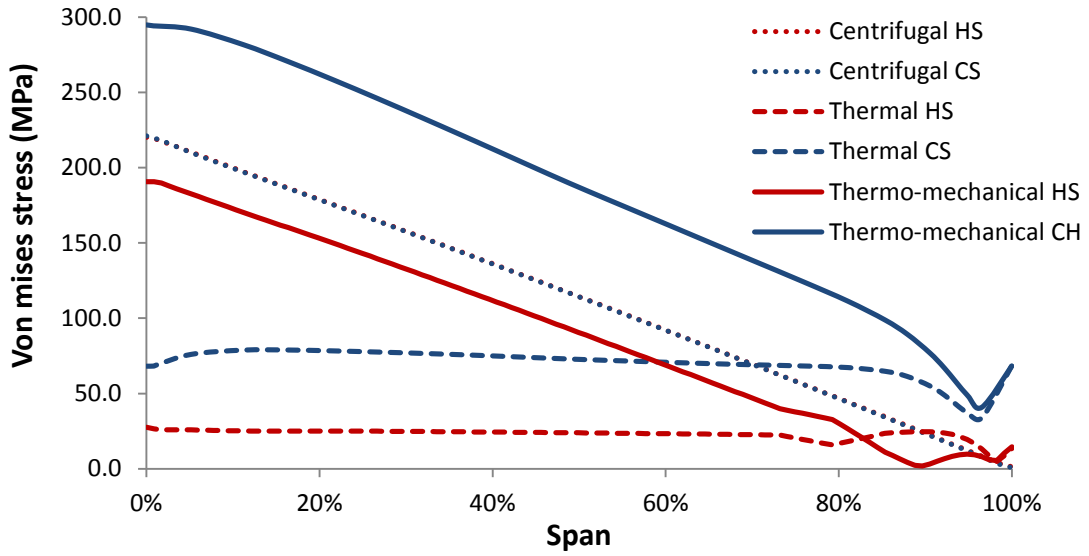

Figure 5-19: Mechanical, thermal and Thermo-mechanical stress distributions

5.3.2.1 Thermal, Mechanical and Thermo-Mechanical Stress Evaluation

The damage resulting from the effect of temperature could be examined in terms of the thermal gradient, and resulting thermal strain (ε_{th}) imposed in the material.

$$\varepsilon_{th} = \alpha(\Delta T) \qquad 5\text{-}1$$

Where; α is the coefficient of thermal expansion and ΔT is the total change in temperature between the hot and cold sides. The thermal strains due to the variation of thermal gradients between the hot and cold sides will vary considerably along the flight path, as well as along the blade span, as shown in Figure 5-20 and Figure 5-21, respectively.

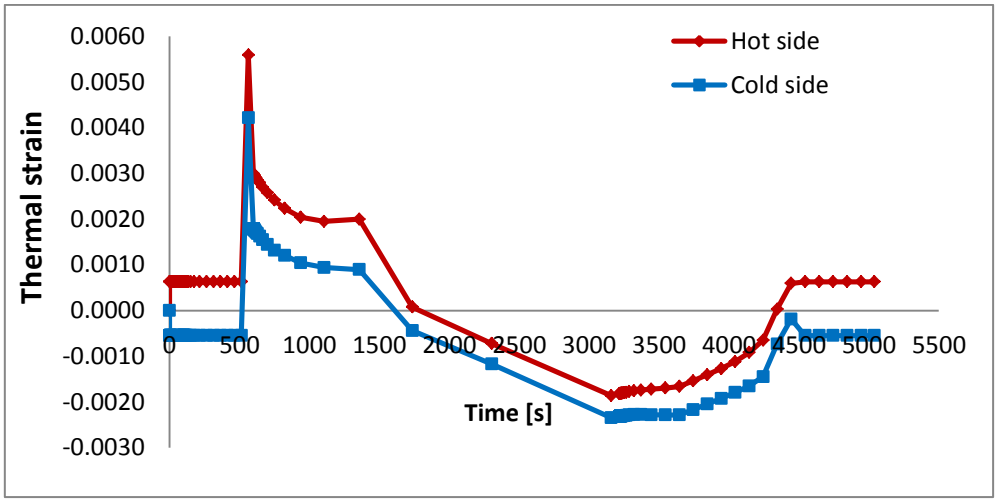

Figure 5-20: Variation of thermal strain along the flight path.

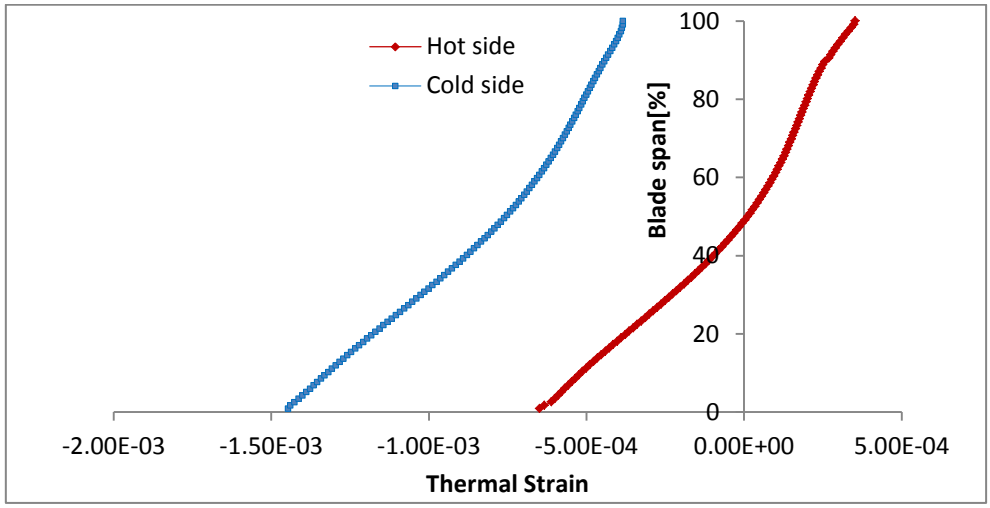

Figure 5-21: Thermal strain distribution along the span in the Take- off phase.

In Figure 5-22 two root nodes (one on each of the blade surfaces) on the simplified FEA blade model during the ground idle to maximum take-off phase are shown; where thermal strains in the hot side are tensile and in the cold side, compressive. This indicates the extent to which the thermal gradient imposed by the presence of blade cooling slots restricts the resultant thermal expansion within the turbine blade material. The resultant thermal stresses influence the predominant damage mechanism on the blade at the different operating profiles typical of jet engines.

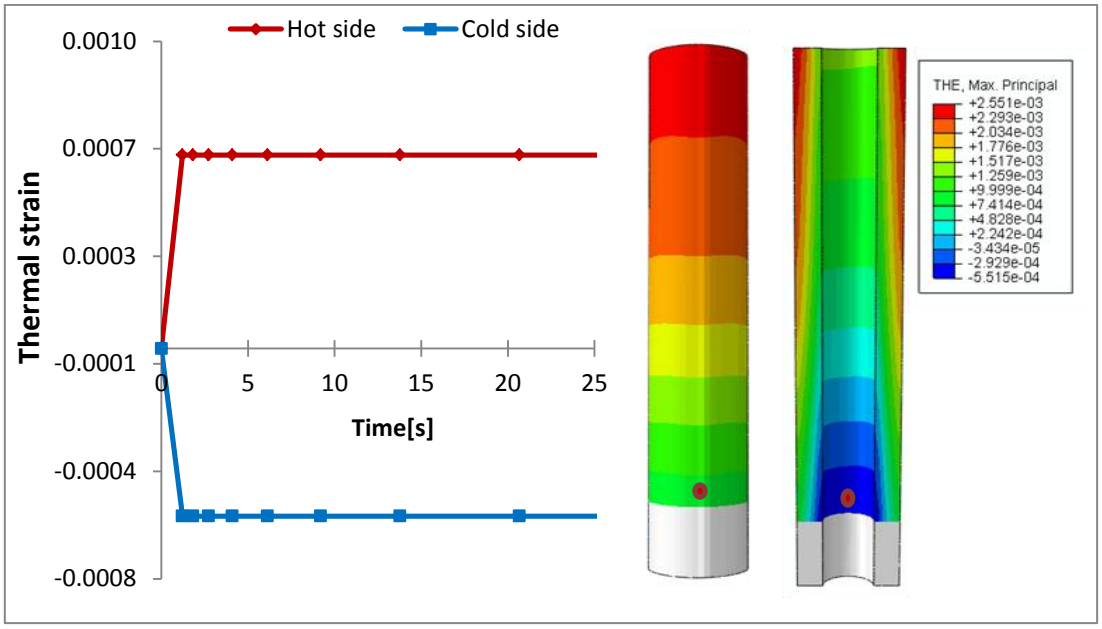

Figure 5-22: Thermal strain profile at the blade root for selected hot and cold side nodes

Regarding the evolution of the thermal stresses across the blade, the hot and cold sides show different behaviour. Although the hot side is at a higher initial temperature than the cold side, the thermal strain of the hot outer side of the blade is partially constrained by the cold side of the blade. This leads to compressive thermal stresses with increasing temperature at the hot side, and tensile thermal stresses on the cold side due to the equilibrium of stresses (Figure 5-23). Furthermore, the blade hot side would benefit from the subtractive influence of the compressive thermal stresses against the tensile centrifugal stresses. On the other hand, the thermal and centrifugal stresses are both tensile on the cold side, hence an additive influence leading to higher thermal-mechanical stresses experienced by the cold side as seen earlier.

The above observations are consistent with what obtains in practice during acceleration from ground idle to take – off phase, and the landing – shutdown sequence. In the cooled turbine blade, the surface temperature increases rapidly as TET increases. However, the temperature rise of the cooled internal surface is lagging. Hence, the cold surface constrains the expansion of the hot surface inducing a compressive stress; while experiencing a tensile thermal

stress. As the thermal gradient reduces along the blade, these stresses are also reduced. The thermal stresses produced are internal to the blade and self-equilibrating. They are either added to or subtracted from the centrifugal loadings.

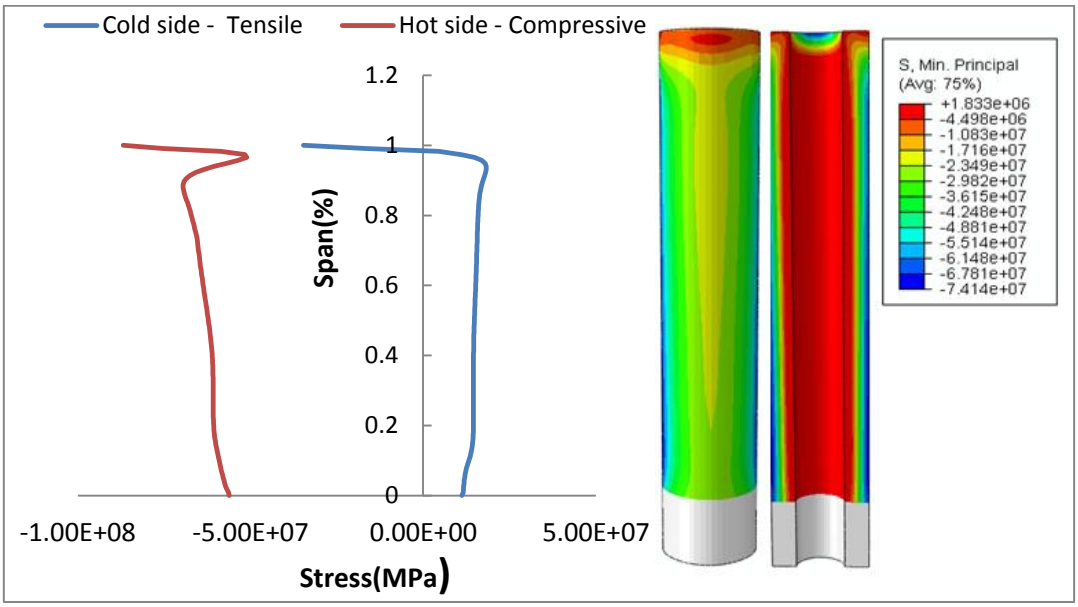

Figure 5-23: Thermal stress distribution along the blade span

5.4 Life Estimation Using N-S Model

The TMF life estimates for the reference mission have been calculated from the time dependent stress, strain and temperature FEA outputs. The results are presented in Figure 5-24. The influence of oxidation damage is observed as the main driver of TMF life. This has consistently been identified by researchers for OP TMF. Generally, an increase in applied stresses will lead to an increase in oxidation damage. Hence, since the cold side experiences a higher thermo-mechanical stress than the hot side, it is expected that the oxidation damage in the cold side would be higher than that of the hot side. The cold side therefore has a lower TMF life than the hot side. In addition, the cold side experiences predominantly tensile stresses, which could lead to oxide fracture. Tensile oxide fracture has been recognised to be very damaging in crack initiation and growth. Nevertheless, the lower activation energy and Arrhenius temperature

relation in the oxidation model formulation also contribute to the dominance of oxidation damage in TMF life calculation. Also, Antolovich et al [] has shown that in many cases, despite the emphasis on creep- fatigue interactions, the most damage under TMF result from the interaction of slip bands with oxidised boundaries.

Considering only the life at the cold side, the estimated life for this reference mission is about 16500 flight cycles (23000 hours). This is quite conservative, but very realistic compared to the results from using the LCF coffin manson method and LMP creep estimation, which gave 1.15E+06 flight cycles and 5.9E+06 flight cycles, respectively. It could also be discerned that out-of-phase TMF would significantly dominate the TMF life in aero engines, since oxidation is the driving damage mechanism.

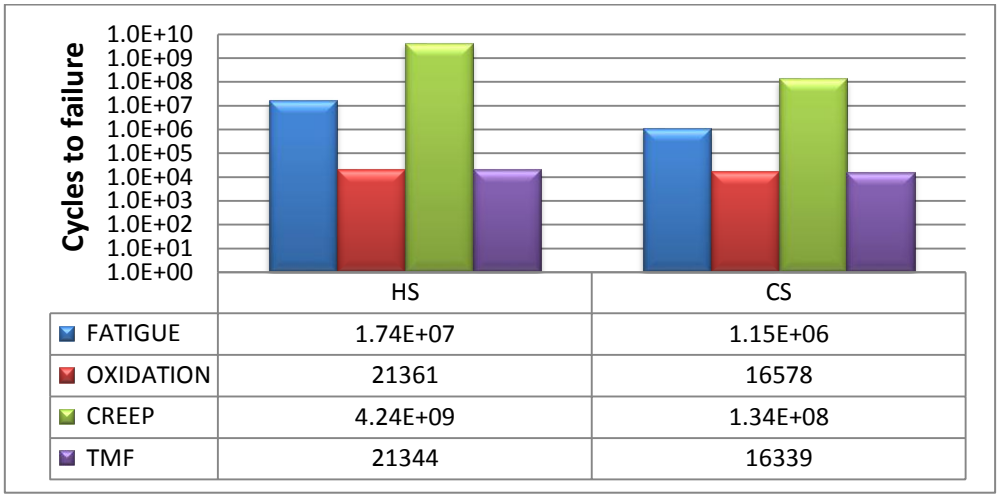

	HS	CS
FATIGUE	1.74E+07	1.15E+06
OXIDATION	21361	16578
CREEP	4.24E+09	1.34E+08
TMF	21344	16339

Figure 5-24: Hot and Cold sides life distribution.

The blade life distribution for each of the damage mechanisms is presented In Figure 5-25**.** The root region, despite having a lower temperature, experiences the highest thermo-mechanical stress. Hence, it could be identified as a critical location for the damage mechanisms. It would be expected that the critical region would shift upwards to about mid span for an actual blade with span wise reduction in thickness. This is because at the mid span region, a combination of sufficiently high temperature and stresses results in greater damage.

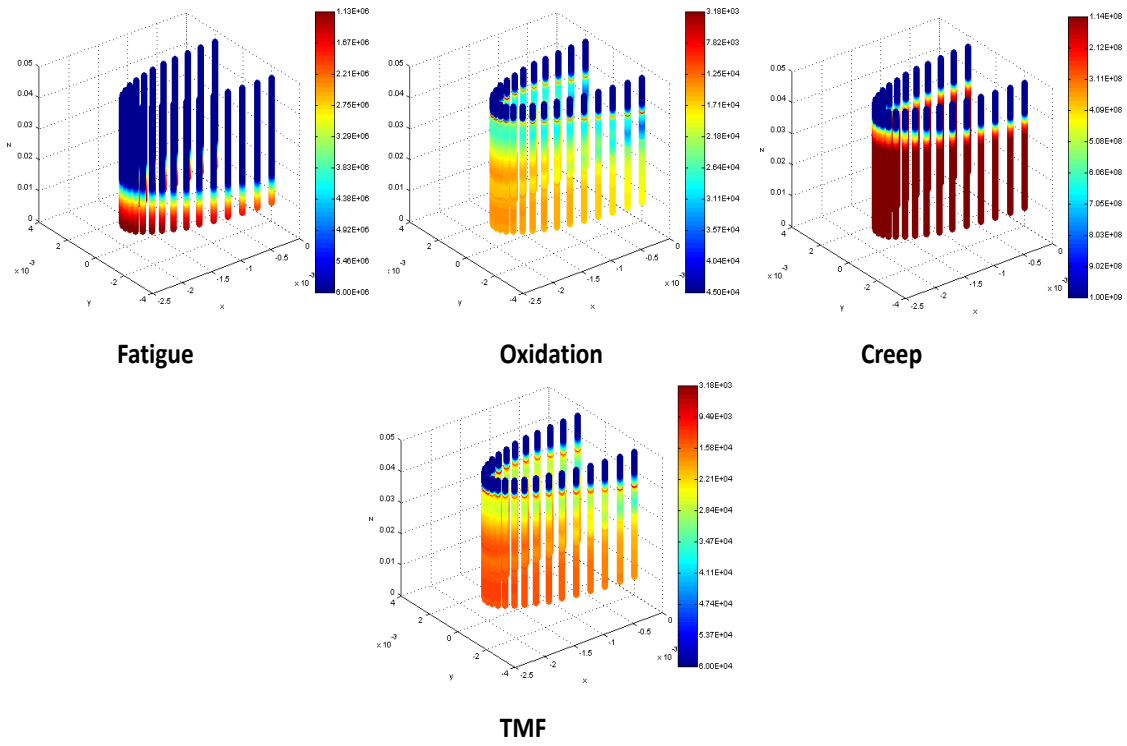

Figure 5-25: life distribution for damage mechanisms

For the pure fatigue damage, although the temperature is increasing along the span of the blade, the impact of fatigue damage is reducing because the overall thermo-mechanical stress is decreasing along the blade span. Hence, fatigue damage is highly influenced by the applied stress, relative to the temperature.

In addition to the root, the LE mid region is observed to be highly affected by oxidation damage. This region experiences sufficiently severe impact of both the thermo-mechanical stresses and increasing blade temperature; which are the main factors that influence oxidation damage. The impact of oxidation is then considerably reduced as the thermo-mechanical stresses reduce toward the blade tip. Creep is highly influenced by temperature as well as applied the stress. Hence, as the stresses along the blade span reduce, the influence of higher metal temperatures drives impact of the creep damage further above the blade mid span.

5.5 Chapter Summary

The implementation and results of the developed lifing approach have been examined in this chapter. From the engine and aircraft performance simulation, a set of basic aero-thermal data inputs were derived and applied as inputs to an enhanced heat transfer model. The outputs from the heat transfer model are used as thermal BCs for the FEA. The thermal BCs are time dependent span wise metal temperature distribution for the blade hot side, and the cooling air temperature and heat transfer coefficients for the cold side. These are applied as 3rd order polynomial correlations in the thermal FEA model. The results of the FEA are verified by comparing with the temperature profiles from the analytical heat transfer model. From these temperature distributions the variation of thermal gradients along the blade span and throughout the given flight are determined. The approach is able to adequately capture the transient thermal gradients, which is fundamental to any TMF assessments – as these transient changes bring about associated thermal stresses.

For the FEA thermo-mechanical stress analysis, the blade temperature distribution calculated from the FEA thermal model is used as input. In addition, a rotational body force equivalent to the HPT shaft speed is applied to generate the mechanical stresses (only centrifugal stress is considered). The FEA stress results are verified with the hand calculation from the analytical stress model, as well as quantitative and qualitative assessment of the separately applied stress and thermal loads.

The blade stress distribution from the thermo-mechanical model is expected, with the highest stress occurring in the root and progressively reducing along the blade span. Also, the thermal stress was identified to be critical in the evolution of the overall blade stresses. The cold side experienced more stress. This is because the thermal stresses generated are predominantly tensile in the cold side, while compressive in the hot side. Hence, while the hot side stress are subtracted from the centrifugal stress. The tensile cold side stresses are added; giving a higher stress distribution in the cold side. These counteracting

thermal stresses influence the blade TMF life, as well as the impact of the dominant damage mechanisms.

Using the N/S TMF model, the blade TMF life of about 16,500 cycles calculated is conservative compared to IF methods (coffin-manson and LMP). The oxidation damage is the main mechanism driving the blade TMF life, while the blade cold side was identified as the critical damage region.

6 GEOMETRY AND METHOD VERIFICATION

6.1 Rationale for Simplified Geometry

In examining life cycle cost against design knowledge, Figure 6-1 suggests that up to 70% of a given product's life cycle cost could be determined when about 5% of that product's design is known, [112]. Hence, examining the influence of design choices when very little information is available becomes a challenge, particularly as those choices affect the success of the final product. In this regard, a key focus in this study is to provide a means to assess the turbine blade life when no detailed geometric data or only basic design inputs are available. To this end, the need arises to use simplified geometries that include critical features of the turbine blade for initial lifing assessments.

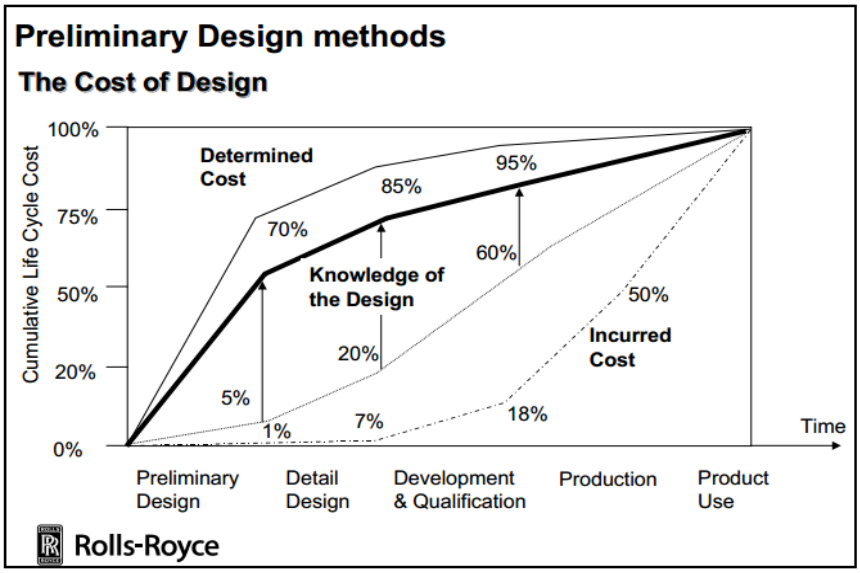

Figure 6-1: Design cost against knowledge [112] p. 52-2

In the design of turbine blades, particularly in the aero-engine, the blade shape and dimensions are critical geometric considerations to meet weight and space constraints. The turbine blade leading edge geometry also influences both the flow and heat transfer characteristics to the blade. In addition, the complex

blade curvatures influence the equilibrium of stresses between the hot gas side and the cooling holes of the turbine blade. This contributes to the blade thermo-mechanical fatigue damage; but introduces complications and uncertainties in assessing the blade thermal and structural stresses. Furthermore, the detailed blade geometric data, aerodynamic flow and the heat transfer characteristics are often unavailable; requiring complex CFD analysis to get acceptable estimates.

The present work does not seek to analyse a particular blade. The focus is developing a lifing approach to evaluate the influences of different design and operational conditions that affect TMF of jet engine blades. Hence, it was necessary to simplify the turbine blade geometry for the lifing assessment.

When investigating blade life, high operating temperatures have always been identified as a critical factor in turbine blade damage [113]. Invariably the leading edge, which experiences the highest gas temperatures, and thermal gradients becomes a critical part of the blade susceptible to damage. Furthermore, experiments suggest that the maximum external heat transfer usually occur in the blade leading edge, as illustrated in Figure 6.2. It is also noteworthy that compared to the rest of the blade, the turbine blade leading edge gas temperatures are the most easily discerned from basic performance inputs. Therefore, this study presumes that the analysis of the thermo-mechanical loads on the blade leading edge would give a valid representation of the damage and TMF life assessment of the blade.

In view of the foregoing, the blade was idealised into basic geometries characterising the leading edge. This was necessary because of the generic requirement in this current approach and the need to use only basic engine design inputs/ data available in open source. This also reduces computational time and complexity in FEA thermal modelling. Using these simplified geometries allow a direct assessment of the thermal and mechanical loads on the blade critical regions, as well as the TMF life; without the additional

influences of stress concentrations due to a complicated blade aerofoil shape. This analysis could therefore be applied to any blade leading edge geometry.

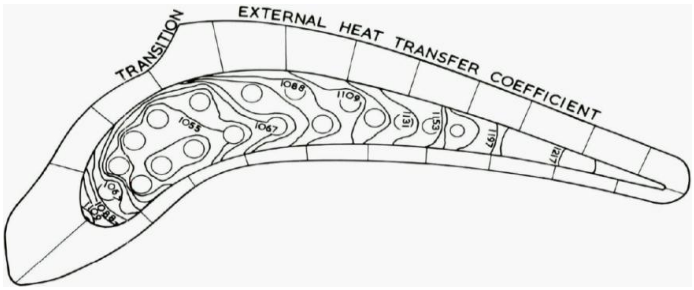

Figure 6-2: Predicted heat transfer coefficient pattern for a HP turbine rotor blade [114] p. 4-17

6.2 Idealised Blade Leading Edge Geometries

The idealised leading geometries examined in this thesis are depicted in Figure 6.3. The external surface denotes the - hot side, while the cooling hole is termed the cold side. Geometry 0 (Geom 0) depicts a hemi cylindrical shape with half of the cooling hole. Geometry 2 (Geom 2) is also hemi cylindrical, but with a full cooling hole and further portion of the blade leading edge. Geometry 3 (Geom 3) is similar to Geometry 2, but with an elliptical cooling hole instead. Geometry 1 (Geom 1) and Geometry 4 (Geom 4) are elliptical with part of the cooling hole and full cooling hole, respectively. Geometry 5 (Geom 5) is also elliptical, but with a full elliptical cooling hole. These shapes were selected similar to geometries that have been used to experimentally determine the heat transfer correlations for flow over a cylindrical body, as established in literature [115; 116]. They are therefore considered realistic basic geometries for idealising the turbine blade leading edge.

For the hemi cylindrical shapes, a leading edge thickness of 2mm and a cooling hole diameter of 4mm was maintained. For the elliptical geometries, the ratio between the major and minor axis, d1/d2 = 4 was used for the cooling hole. A

leading-edge height of ~40mm determined from the turbine sizing was used for every geometry.

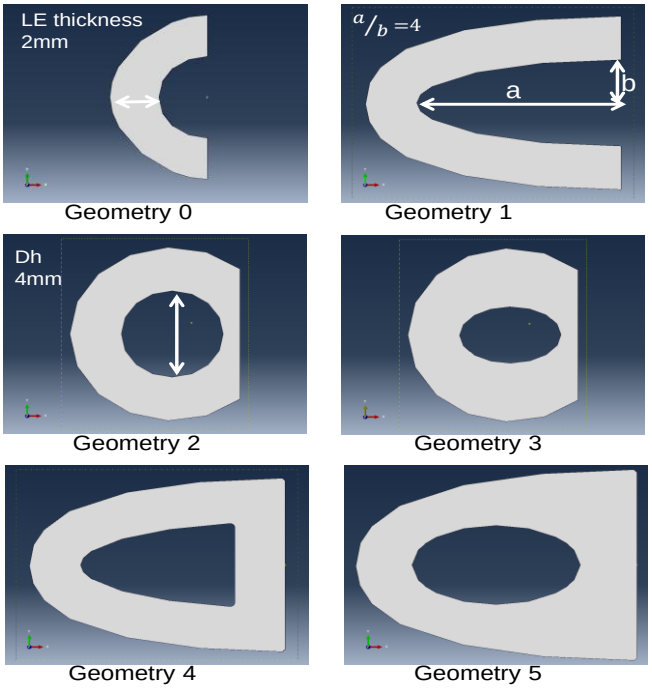

Figure 6-3: Idealised LE Geometries.

6.3 Comparison of FEA Results for Idealised Geometries

6.3.1 Temperature and Stresses Distribution

The evaluation of the FEA results for the idealised blade geometries is meant to identify possible influences that the choice of a geometric shape could have in the lifing approach. Hence, a thermal and thermo-mechanical FE analysis was conducted on the idealised blade geometries. The reference mission for this analysis was a 4-hr flight at ISA conditions. The procedure for deriving the BCs for the FE analyses was previously described in Section 4.7; and Section 5.3.

Accordingly, the results of maximum centrifugal stress (CF) stress, maximum temperature and thermo-mechanical stress at take-off for the various geometries are compared in this section. The results for all the other geometries were normalized with the values for Geometry 0.

In Figure 6.4, the temperature distribution increases along the span from the root to the tip for all the geometries as expected; and the comparison of the temperature values give a very good agreement as shown in Figure 6.5.

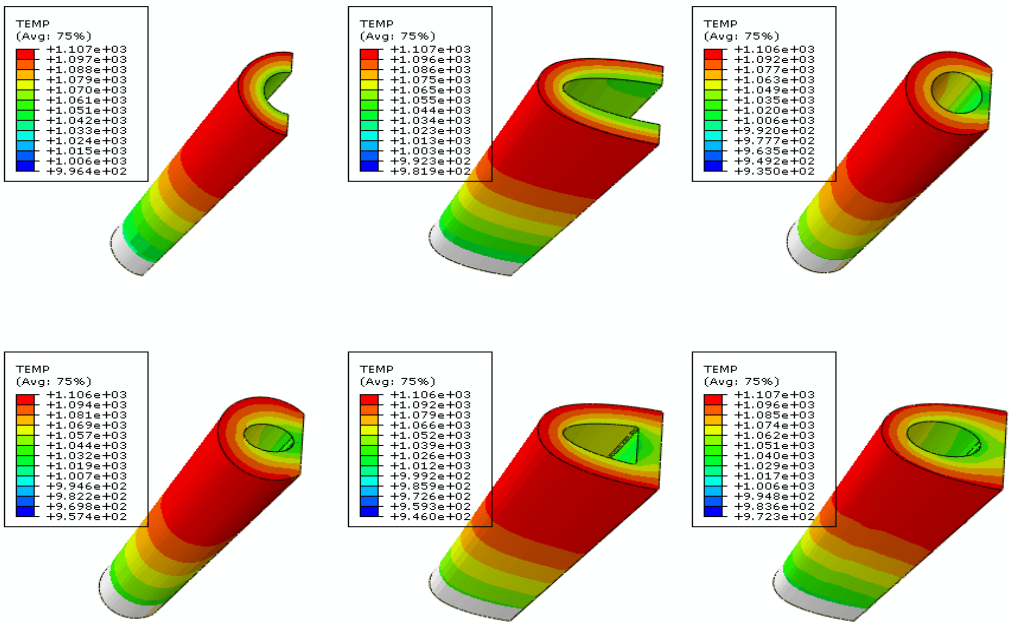

Figure 6-4: Temperature contour plots for idealised geometries.

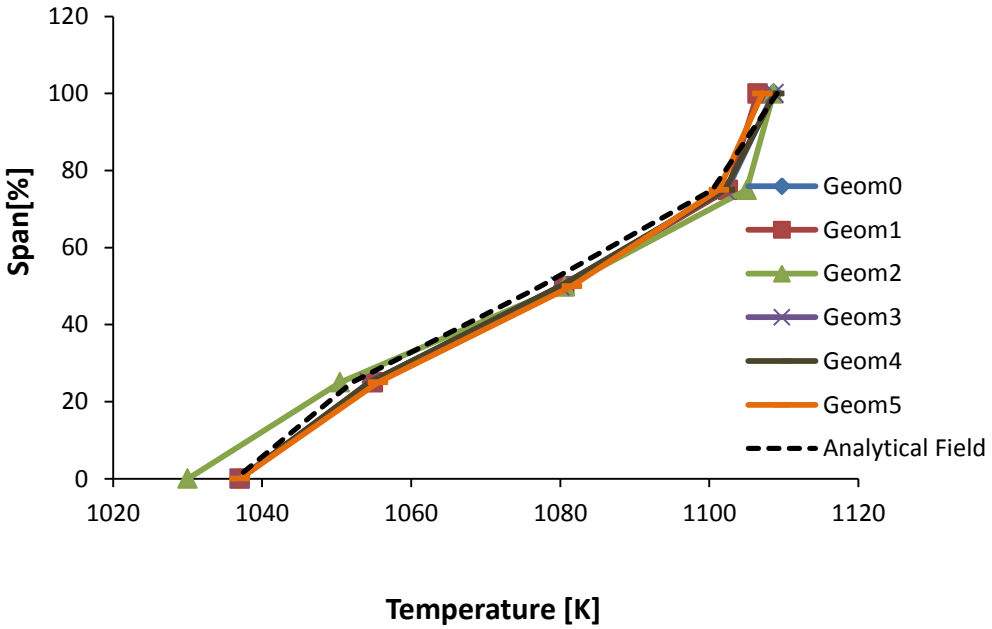

Figure 6-5: Temperature distributions for idealised geometries.

The trend in CF stress is normal as shown in Figure 6.6. The maximum stress is located at the root and the stress progressively decreases along the blade span towards the tip, where it is assumed to be zero. A uniform distribution of the stress as expected from the constant cross section blade model is also observed from the contour plots. Again, very good agreement is obtained from the CF stress comparison between the geometries in Figure 6.7.

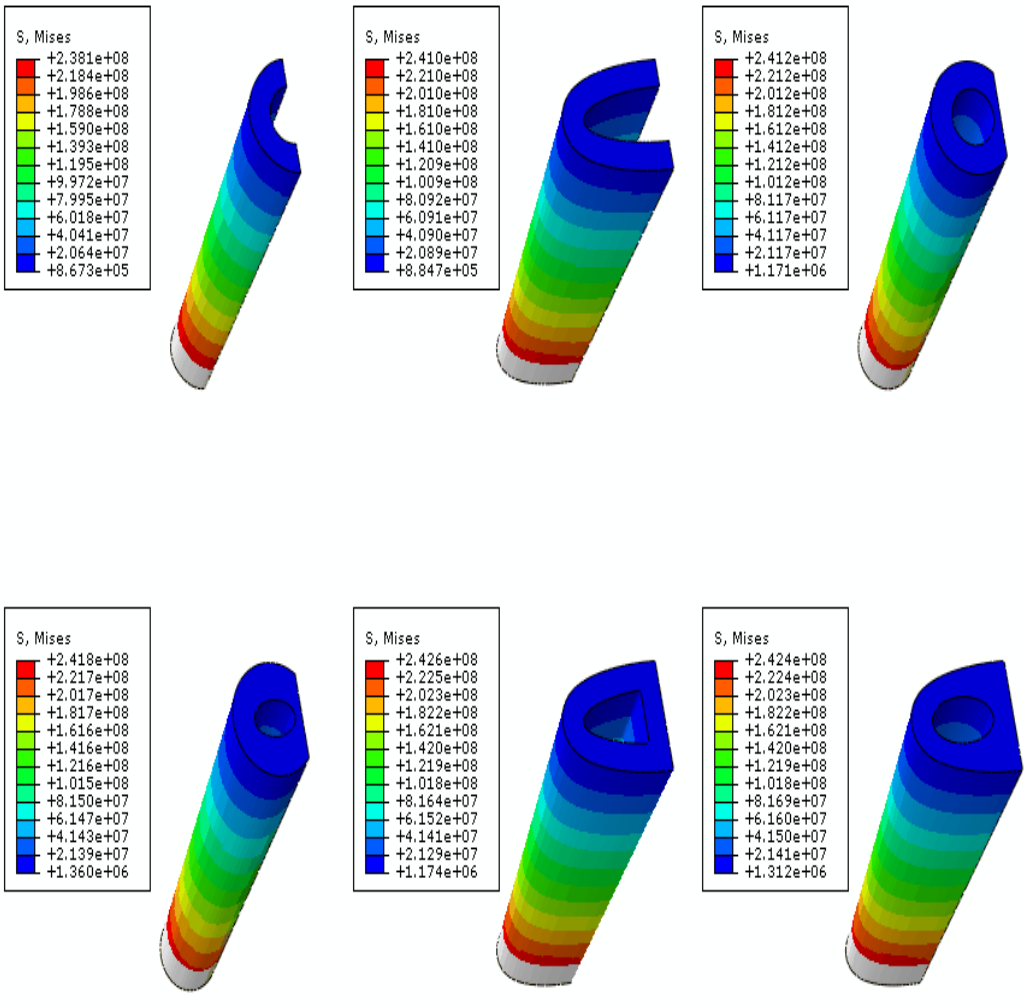

.

Figure 6-6: Centrifugal stress distributions for geometries.

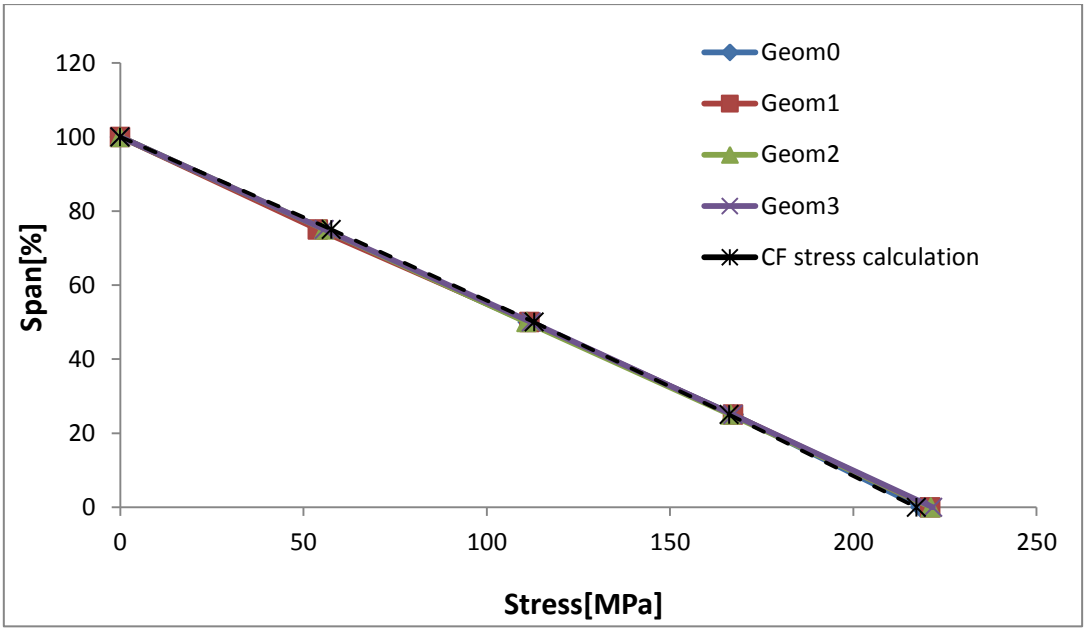

Figure 6-7: Centrifugal stress distributions for geometries

In Figure 6.8, the thermo-mechanical stress distributions show some peculiar variations, which is attributed to the effect of increasing temperature along the blade span, and the thermal stresses generated due to the thermal gradients. This impact is also seen by the change from the uniform distribution in the CF stress contour plot to a parabolic contour plot, due to the effect of the increasing temperature along the blade span. It is also apparent that geometrical singularities influence the stress fields. In particular, regions with sharper corners increase the local stress concentration. In addition to the thermal stresses, this stress concentration would also add to the variation in thermo-mechanical stress distributions for the various geometries as shown in Figure 6.9

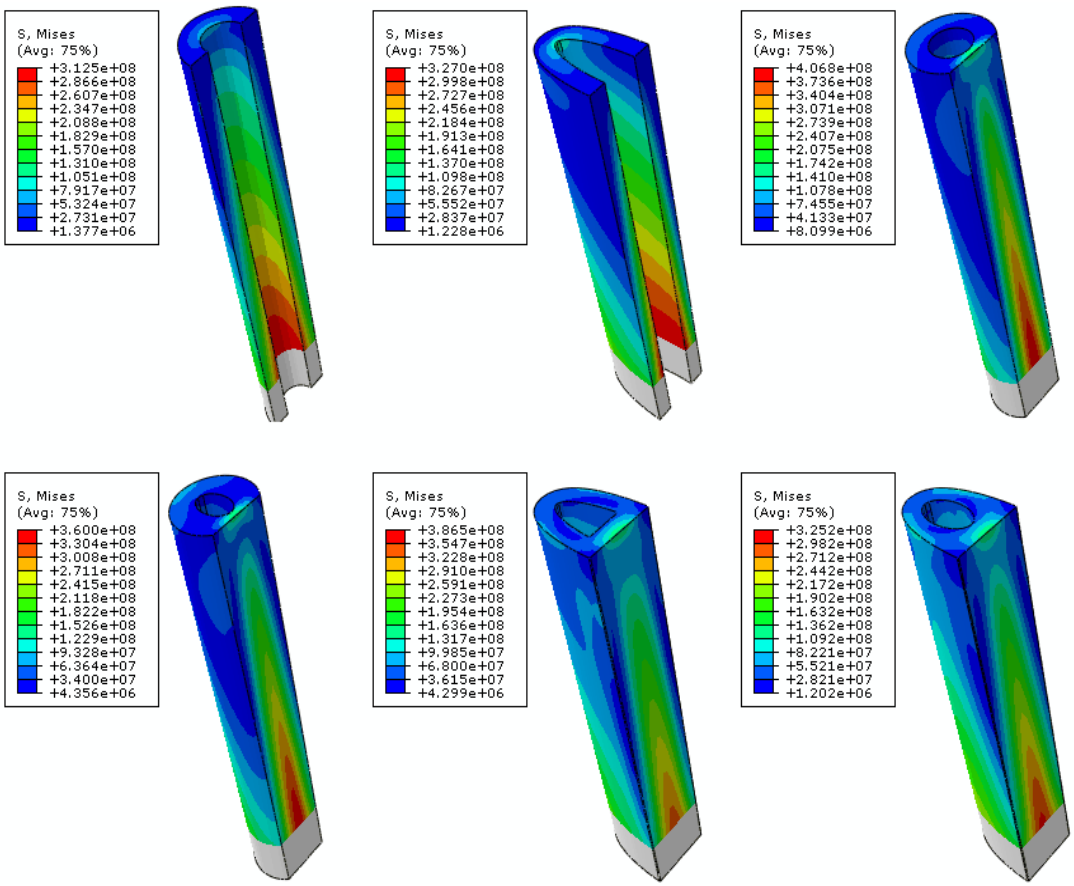

Figure 6-8: Thermo-mechanical stress contour plots for idealised geometries.

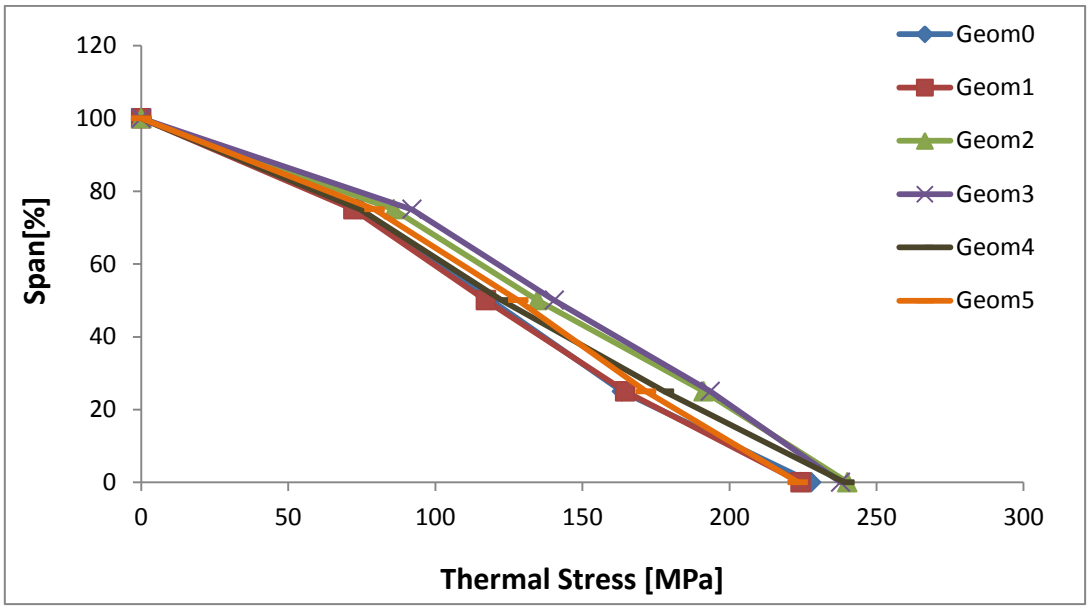

Figure 6-9: Thermo-mechanical stress distributions for idealised geometries.

Nevertheless, as summarised in Figure 6.10, the variation in temperatures and CF stresses are negligible, while the thermal-mechanical stress varies within a maximum factor of 1.07. The satisfactory comparison of the results from the various geometries implies that the TMF life for the various geometries should be quite similar. The TMF lives for the various geometries are examined in the following section.

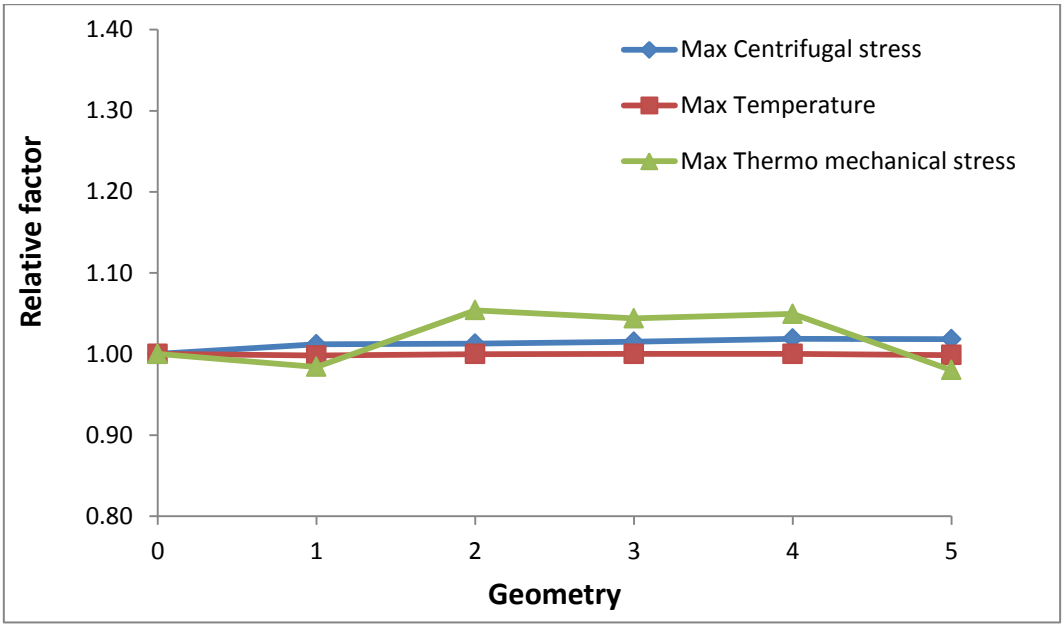

Figure 6-10 Comparison of stress and temperatures for idealised geometries.

6.3.2 Analysis of TMF Life

The overall lifing approach was applied to the geometries and the TMF life assessed in relative terms. The same reference boundary conditions were implemented in order to examine the effect of the geometric shape on the TMF life calculated. The calculated life for fatigue, oxidation, creep and TMF are shown In Figures 6.11 and 6.12 for the cold and hot sides, respectively. The absolute values are presented to show the magnitude of the calculated life results from the tool. For all the geometries, the oxidation influence is driving TMF life in the hot and cold sides of the blade. The calculated TMF life values for the six geometries are observed to be within the same order of magnitude.

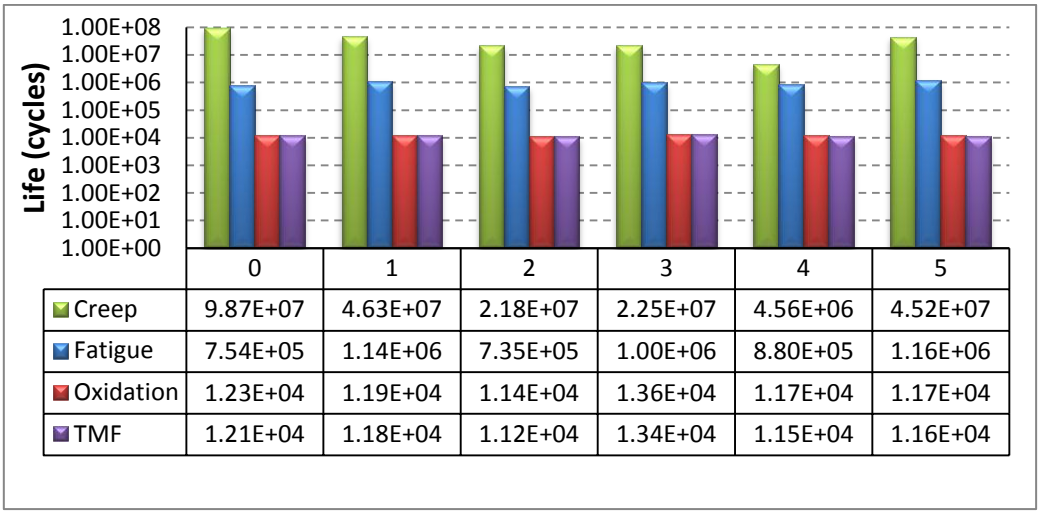

	0	1	2	3	4	5
Creep	9.87E+07	4.63E+07	2.18E+07	2.25E+07	4.56E+06	4.52E+07
Fatigue	7.54E+05	1.14E+06	7.35E+05	1.00E+06	8.80E+05	1.16E+06
Oxidation	1.23E+04	1.19E+04	1.14E+04	1.36E+04	1.17E+04	1.17E+04
TMF	1.21E+04	1.18E+04	1.12E+04	1.34E+04	1.15E+04	1.16E+04

Figure 6-11: Cold side life for different geometries.

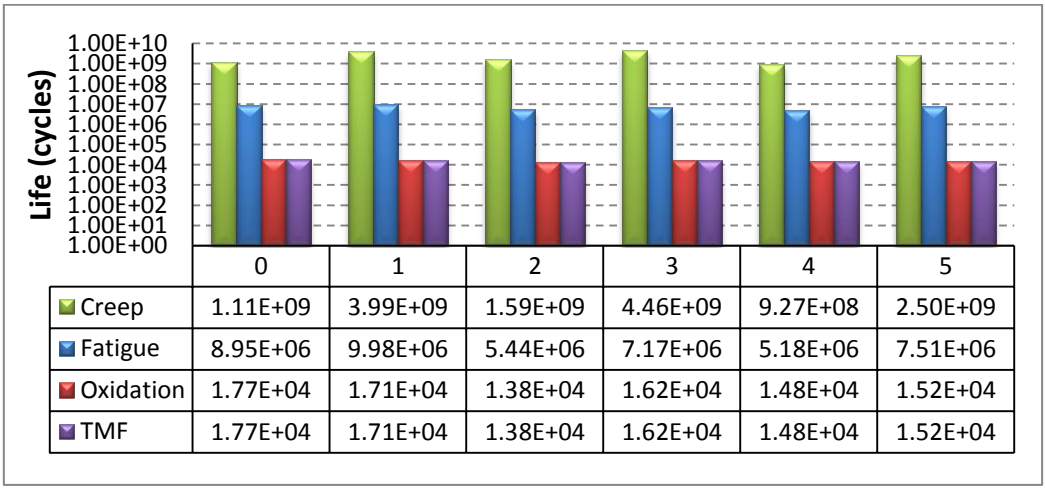

	0	1	2	3	4	5
Creep	1.11E+09	3.99E+09	1.59E+09	4.46E+09	9.27E+08	2.50E+09
Fatigue	8.95E+06	9.98E+06	5.44E+06	7.17E+06	5.18E+06	7.51E+06
Oxidation	1.77E+04	1.71E+04	1.38E+04	1.62E+04	1.48E+04	1.52E+04
TMF	1.77E+04	1.71E+04	1.38E+04	1.62E+04	1.48E+04	1.52E+04

Figure 6-12: Hot side life for different geometries

In relative terms, Figure 6-13 shows the variation in the estimated TMF lives for the various geometries. Geometry 0 was taken as reference geometry for both the cold and hot sides. The TMF lives calculated for the various geometries are within a relative factor of 0.9 and 1.3 for the cold and hot sides, respectively. This is a good agreement; giving that In lifing studies, It is generally acceptable to have variation in life estimates up to a factor of +/-2 [73]. This therefore suggests that the selection of a particular shape would not severely affect the TMF life prediction using the developed lifing approach. What becomes more significant is the accurate definition of the thermal and stress boundary conditions.

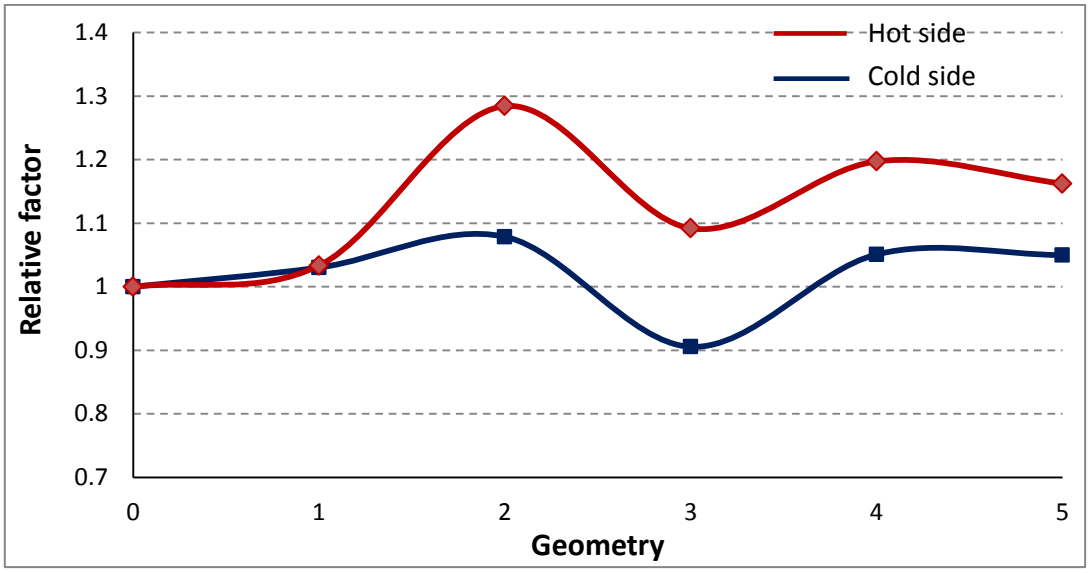

Figure 6-13: Relative comparison of TMF lives for geometries.

Figure 6.14 compares the hot and cold side lives for each of the geometries. It is observed that the cold side has the lower lives in all the geometries indicating that the cooling hole would be the critical region particularly affected by TMF. This would be attributed to the higher thermal stresses experienced in the cold side as shown in Figure 6.15 for one of the Geometries. Hence, the cold side is subjected to higher thermo-mechanical stresses, leading to greater TMF damage.

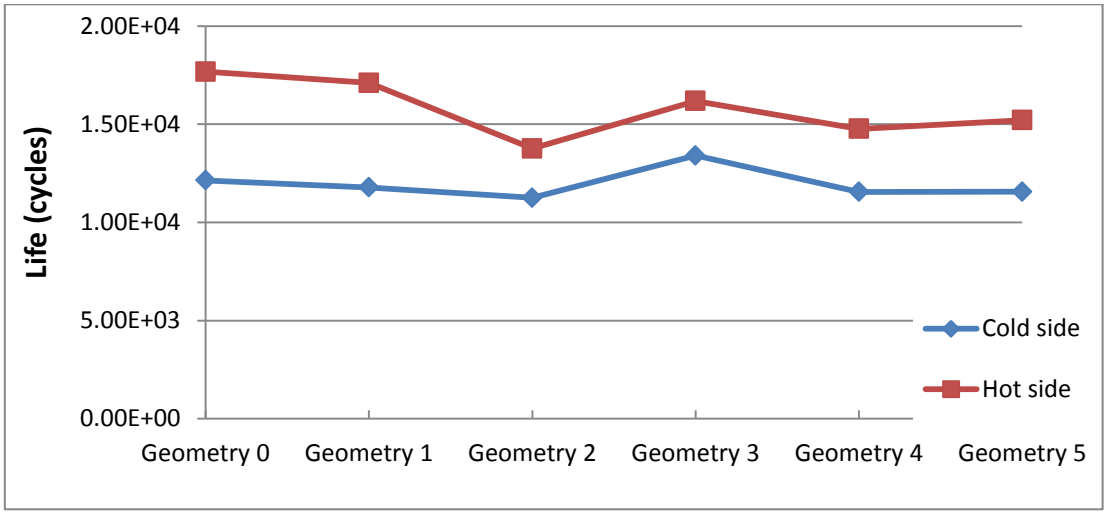

Figure 6-14: Hot and cold side TMF life for various Geometries.

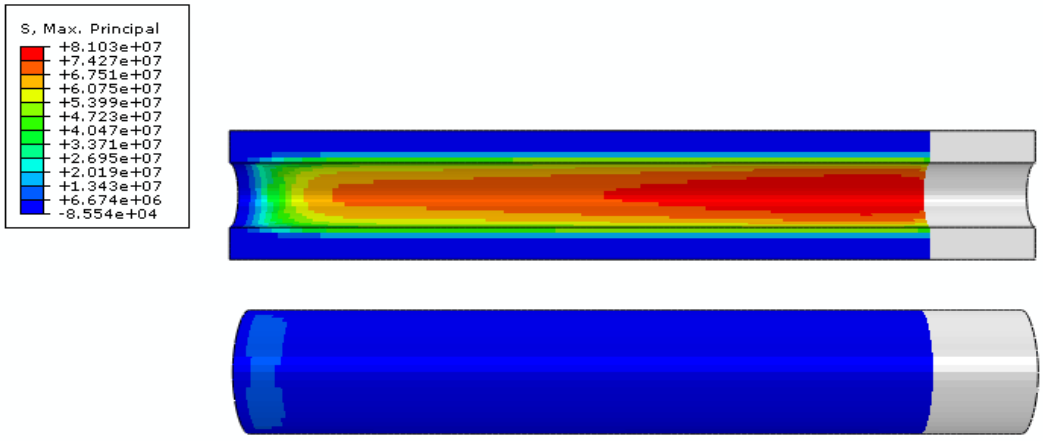

Figure 6-15: Maximum principal thermal stress for cold side (top)and hot side(bottom).

6.4 Blade Geometry Verification

To verify the developed methodology, as well as the choice of geometry, the methodology was implemented on a NASA Energy Efficient Engine turbine blade (NASA E3 blade), using data extracted from NASA report [109]. The NASA E3 blade was then modelled in CATIA and imported to ABAQUS CAE (Figure 6.16). The FEA procedure was conducted on the NASA E3 blade and the other geometries using the same boundary conditions as the NASA E3 blade. The blade temperature boundary conditions were derived from the heat transfer model using the engine cycle data from the NASA report, while only the centrifugal stress was applied using the HP shaft rotational speed ,blade height and hub diameter.

The idealised geometry of the E3 blade was created by increasing the height of the proposed simplified geometries to match the blade height and sizing data of the NASA E3 Blade. A thermal and thermo-mechanical analysis is then conducted on both models. The simplified blade geometry FEA results (in terms of temperature and stresses) were then compared to those of the detailed E3 blade to assess the impact of the geometric simplification. The temperature

distribution for the geometries agree very well with that of the NASA E3 blade as shown in Figure 6.17

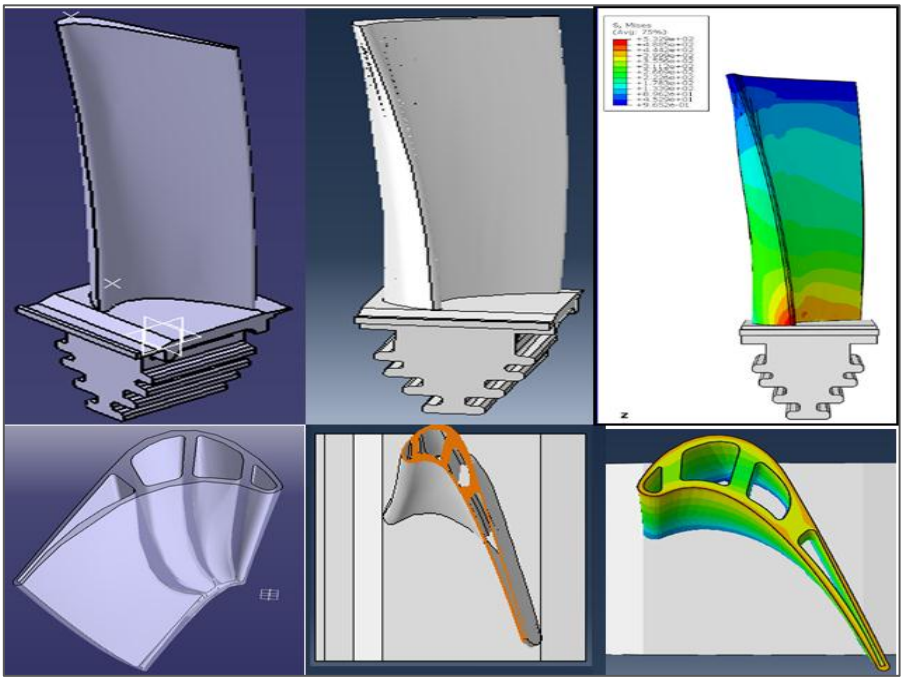

Figure 6-16: NASA E3 blade model.

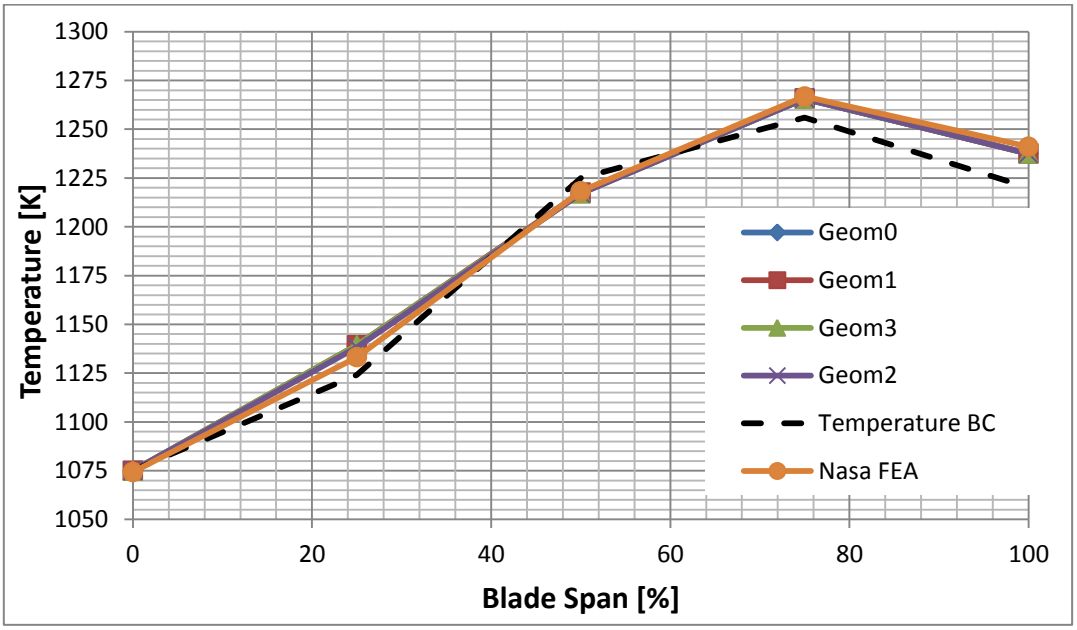

Figure 6-17: Metal temperature comparison NASA E3 model and geometries.

In terms of the centrifugal stress, all the geometries give very satisfactory agreement in the stress distribution (Figure 6.18) and contour profiles (Figure 6.19) relative to each other. On the other hand, the E3 blade model shows a large reduction of centrifugal stress around the mid span region. This is attributed to the effect of the downward taper and the leaning of the blade. This generates a bending moment as a result of the misalignment between the section centre of gravity and the centroid of the blade root. Hence, in the absence of any applied gas bending forces the bending moments counteract the centrifugal stress leading to the progressive reduction of stress shown at the E3 blade mid region. Nevertheless, the magnitudes of the maximum centrifugal stresses generated are very close. However, this comparison suggests that the use of the idealised geometries could lead to conservative results, as no stress reducing design features are included.

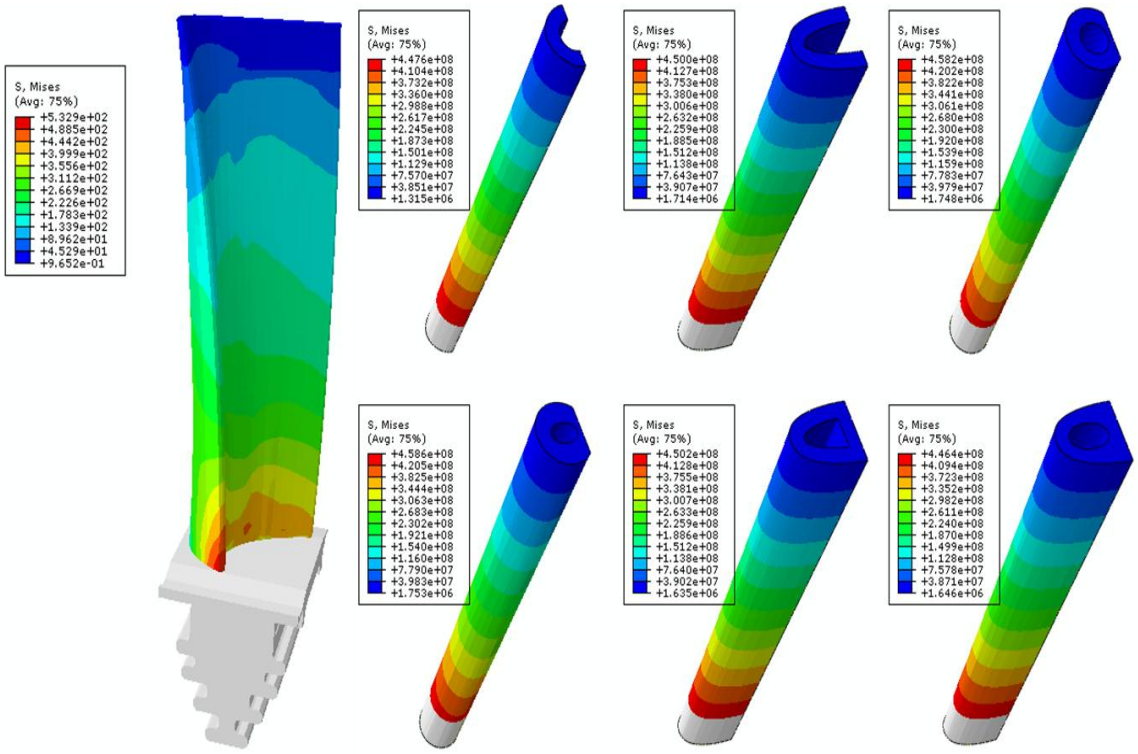

Figure 6-18: Centrifugal stress contour plots for NASA E3 blade and Idealised geometries.

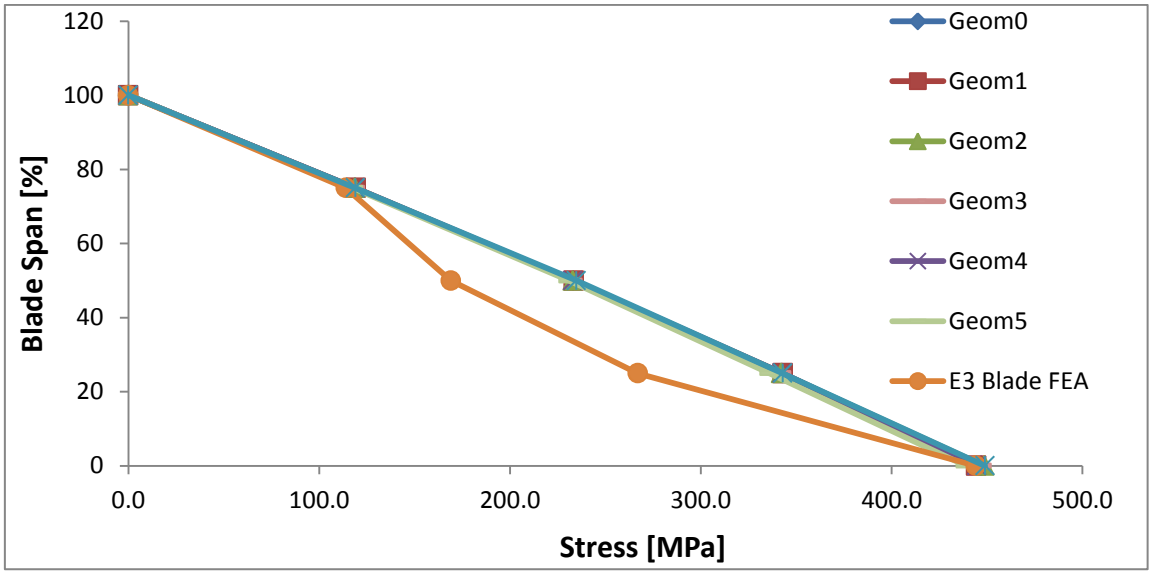

Figure 6-19: Centrifugal stress comparison NASA E3 blade and Idealised geometries.

In Figure 6.20, the thermo-mechanical stress comparison shows similar variations between the idealised geometries as earlier seen in Section 6.3.1, with the highest relative factor of 1.08. The same trends for the centrifugal stress behaviour earlier in Figure 6.19 are also observed for the E3 blade.

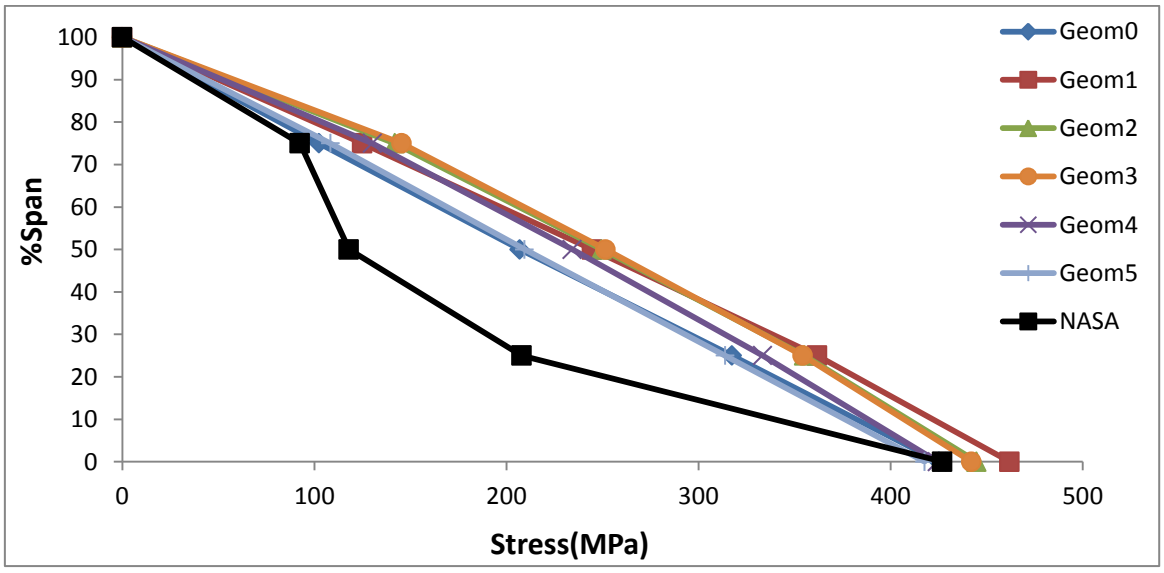

Figure 6-20 Thermo-mechanical stress comparison NASA E3 model and Idealised geometries.

6.5 Lifing Method Verification

The developed lifing approach was implemented on the HP Turbine blade of the NASA Energy Efficient Engine (NASA E3 blade) using data extracted from NASA report [109], as highlighted in Section 6.4. The TMF lives obtained from analysing the NASA E3 blade was now compared to that of the equivalent idealised model . However, two iterative procedures had to be implemented to match the E3 blade life of 10000 flight hours reported in [109] . Although the E3 blade material used is PWA1484, MAR-M247 was used for this analysis due to the availability of TMF model data for this material.

6.5.1 Thermal Analysis

Figure 6.21 shows the thermal boundary conditions obtained from the heat transfer model, using the blade sizing data available in the NASA report [109]. The thermal boundary conditions were used in the FE thermal analysis for both the NASA E3 blade and its equivalent idealised model.

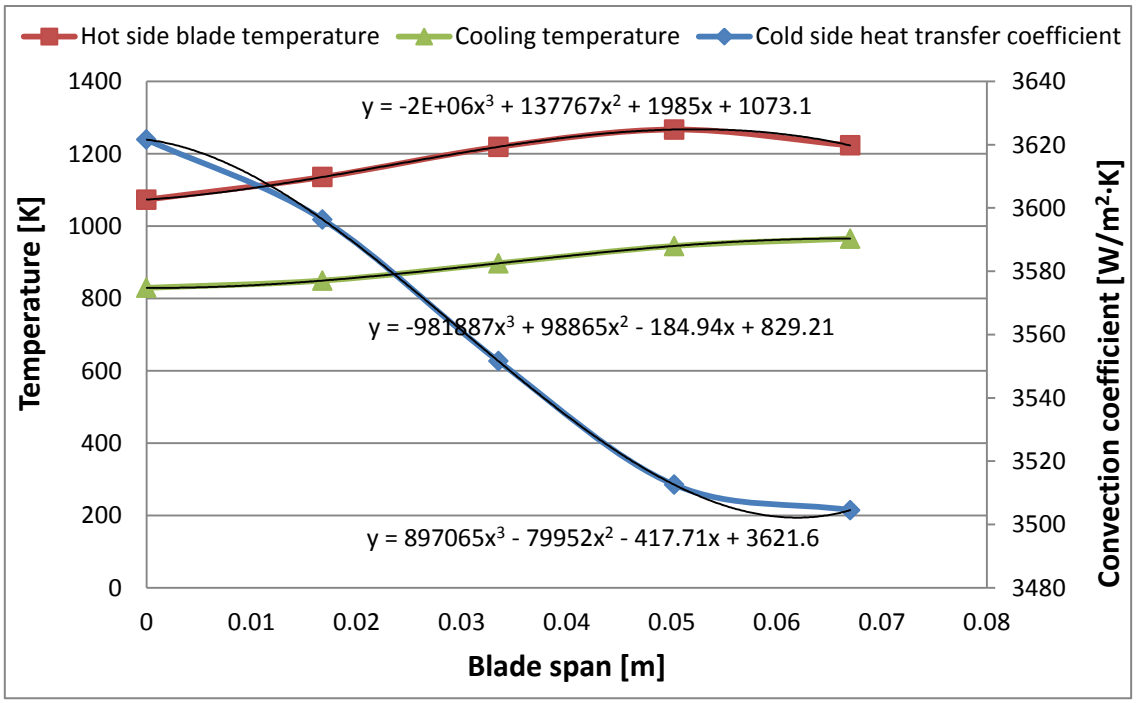

Figure 6-21: FEA thermal boundary conditions for method verification.

6.5.2 Thermo-Mechanical Analysis

The thermo-mechanical analysis was conducted using the temperature results from the thermal analysis and a rotational speed of 735.9 rad/s. This speed gave the thermo-mechanical stress values that produced a TMF life close to the value of 10,000 hours reported for the E3 Nasa blade [109]. The TMF analysis and comparison of the results are based on the equivalent stagnation lines described in Chapter 4. The hot side and cold side stagnation line for the NASA E3 blade are depicted in Figure 6-22.

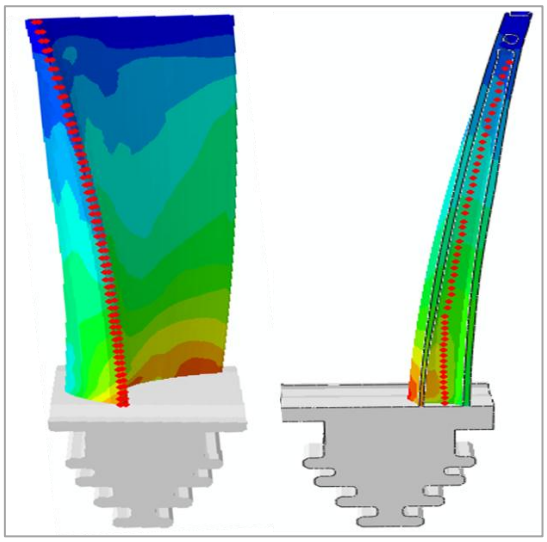

Figure 6-22: Hot and Cold side span lines for NASA blade leading edge.

6.6 TMF Life Comparison

An estimated life of 10,000 hours was given for the E3 NASA blade in [109] . Using a 4- hour flight mission in this analysis, the equivalent estimated life would be 2500 flight cycles. The first iteration was then done on the detailed E3 NASA blade by varying the rotational speed to obtain the thermo-mechanical stress that would give the equivalent life of 2500 flight cycles. Consequently, a rotational speed of 735.39 rad/s, equivalent to a thermo-mechanical stress of 152MPa was obtained. This produced a TMF life of 2551 flight cycles for the E3

NASA blade. Figure 6-23 summarises the iteration procedure conducted; where ω is the angular rotational speed in rad/s.

The second iterative process was done on the idealised model of the E3 NASA blade by varying the rotational speed to match the thermo-mechanical stress value of 152 MPa obtained in the first Iterative procedure. This was to ensure that both the E3 NASA blade and its idealised model had equivalent thermo-mechanical stress distribution. This could be viewed as an accurate boundary condition being defined for the idealised geometry.

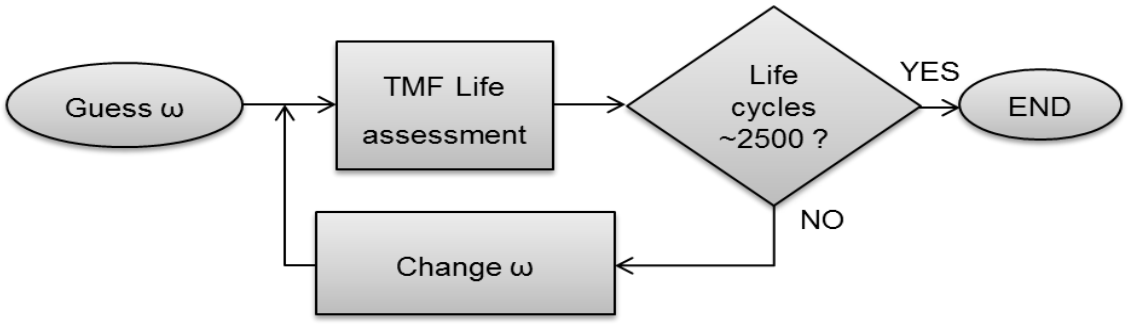

Figure 6-23: Iterative process for determining thermo-mechanical stress required to match NASA E3 blade life .

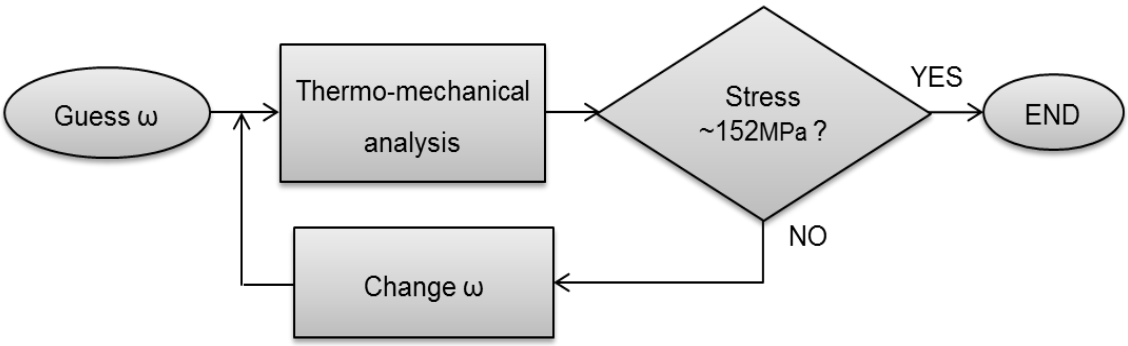

Figure 6-24: Iterative process for determining $\boldsymbol{\omega}$ required to match thermo-mechanical stress

From the iterative procedure (Figure 6-24), a rotational speed of 805 rad/s, which gave a thermo-mechanical stress of 151.86 MPa was obtained for the idealised NASA geometry.

6.6.1 Result Comparison

The TMF life of the idealised NASA geometry was evaluated; based on the obtained thermo-mechanical stress. Table 6-1 summarises the results for the verification, where the life calculated for the idealised geometry is within a relative factor of 1.1. The lives for other geometries compared to the NASA E3 blade also give good results, as shown in Figure 6.25. The maximum relative factor is about 1.3 for Geometry 1, while Geometry 2 matches the target life of 2500 flight cycles.

Table 6-1 Results of method verification.

	NASA E3 Blade Model	**Geometry 0**	
Rotational Speed	735.39	805	(rad/s)
Max Thermo-mechanical stress(MPa	152	151.86	(MPa)
Max Blade Temperature(K	1,267	1,267	K
TMF life	2,551	2,829	(Flight cycles)

Figure 6-25 TMF life summary for E3 blade model and idealised geometries.

6.7 Chapter Conclusions

The leading edge experiences the highest gas temperatures, and thermal gradients in the turbine blade. The leading edge is therefore identified as critical part susceptible to damage. In this research, it was necessary to idealise the turbine blade leading edge for the following reasons: limitation of design inputs; to reduce the complexity and computational cost of modelling; to enable a generic blade life assessment. The idealisation also allows a direct assessment of the thermal and mechanical loads on a critical region of the blade, without influences of stress concentrations from a complicated aerofoil shape. Consequently, six basic cylindrical and elliptical shaped models were created incorporating critical features such as the cooling hole and root fixing.

The developed methodology was applied using each of these models to investigate the influence of the choice of shape on the lifing assessment. The results indicate that the variation in temperatures and CF stresses are negligible, while the thermal-mechanical stress varies within a maximum factor of 1.06.

The TMF lives calculated for the various geometries are within a maximum relative factor of 1.3. This is considered a very good agreement; giving that In lifing studies, It is generally acceptable to have variation in life estimates up to a factor of +/-2. The results therefore suggest that the selection of a particular shape would not severely affect the TMF life prediction using the developed approach. What becomes more significant is the accurate definition of the thermal and stress boundary conditions.

Giving the geometric simplifications introduced in the current approach, the TMF lifing assessment above is considered very satisfactory. The different mesh sizes and model fidelity are some of the visible factors that could contribute to the variations in the FEA results and consequent lives obtained. However, this is not considered a major limitation, as the prediction accuracy could be easily improved by increasing the mesh densities and model fidelity;

but this has computational cost and time penalties. The developed lifing approach has been successfully implemented; and the use of the proposed idealised geometry verified by comparing with a detailed NASA E3 blade model. The results indicate that the TMF life obtained from the idealised geometries could vary within a relative factor of 1.3, when compared with the use of detailed blade geometry. Although, the blade shape would particularly affect stress distribution, the adequate determination of the boundary conditions is the key consideration in using any idealised geometry.

7 INFLUENCE OF TMF MODEL MATERIAL PARAMETERS

7.1 Motivation

The parameters for the N/S TMF model implemented in this thesis are only available for few materials. Furthermore, the model parameters for each of the damage mechanisms generally depend on the specific material that is used. Hence, for a given material, several experiments would be conducted to obtain about nineteen parameters needed to implement the N/S TMF model. This is time consuming and costly. Moreover, it is impractical to conduct sufficient tests that could cover all possibilities of load/temperature variations. Hence, researchers have performed sensitivity analysis to identify the critical parameters that drive the TMF life; as well as estimating optimum values for these parameters [3][117]. The number of parameters to be experimentally determined would now be reduced to the number of critical parameters identified in the sensitivity analysis. If experimental determination of the critical parameters is precluded, optimisation techniques could be applied to the sensitive parameters to obtain values that fit experimental data [3; 59].

7.2 Sensitivity of TMF Model Parameters

Using the lifing methodology developed in this thesis, a similar sensitivity analysis to Amaro et al [3]was done on the N/S model parameters. This was found necessary because the typical aero engine mission being analysed was derived from a performance simulation; permitting a wider range of temperature – strain phasing history than would be obtained from experimental data. Hence, using such flight mission history, the sensitivity of the of the life estimation results to the various N/S model parameters had to be examined. This was done using a simple parameter variation method, in which a parameter was varied by a specified amount, while holding all other parameters at nominal values. This analysis will be important at the early design stages, where the effects of design and operating parameters can be analysed in relative terms; in

the event of limited information about the N/S TMF parameters for a given nickel super alloy.

The model parameters for bare Mar M-247 used for this study are summarized in Table 7.1. Except α_1 and α_2, all the other parameters were each varied by a minimum of +/- 20% up to a value were no significant changes in the result occurred. The results from this analysis show that five oxidation damage terms had significant impact on the total TMF life, while the constants for creep and fatigue damage terms influence only their respective mechanisms. The five influential parameters are:

- *b*; Strain rate sensitivity constant of the average thickness of oxide+ γ' depleted layer at rupture, $\bar{h}_f$.
- *β;* Exponent on time in oxide+γ' depletion growth.
- Q_{ox}; Activation energy for oxidation.
- $Q_{\gamma'}$, Activation energy for *γ'* depletion.
- ξ_{ox}; Shape factor for environmental damage phasing function.

The strain rate sensitivity constant, *b*

The strain rate sensitivity constant, *b*, was varied from -70% to 90% obtaining the representation in Figure 7.1. The variation in the total life was similar to the oxidation life, within a range of a 0.1%. Significant increase in life variation begin to manifest at about 40% increase over the reference value, while reducing the value of *b* produce no significant change in life variation. The results of the variations in the hot side follow the same trend with the cold side.

Exponent on time in oxide+γ' depletion growth constant, *β*

As shown in Figure 7-2, the exponent on time *β* in oxide+γ' depletion growth constant, was varied by -40% to 40% from the original value. The same trend as highlighted from the comparison between the total and oxidation life results was observed. Also, the hot and cold sides both follow similar trends. In this

case, decreasing the value of β by over 20% resulted in significant increase in life, while increasing the value had negligible changes.

Activation energy for oxidation, Q_{ox}, and γ' depletion $Q_{\gamma'}$

The activation energies for oxidation Q_{ox} and for γ' depletion $Q_{\gamma'}$ were varied by 30% to 50%, and 25% to 50%, respectively. The variation for the total and oxidation life results were relatively constant and the same trends were seen for the hot and cold sides as shown in Figure 7.3 and Figure 7.4, respectively.

Table 7-1: Neu/Sehitoglu model parameters/constants for bare M-247 alloy.

Parameter	Value
Fatigue terms constants	
C	0.0137
d	-0.149
Oxidation term constants	
b	**0.75**
β	**1.5**
B ($s^{-0.5}$)	6.93E-03
δ_0 ($\mu m*s^{-0.75}$)	1.12E-10
D_0^{ox} (μm^2*s)	1.54E04
Q^{ox} (kJ/mol)	**175.9**
$D_0^{\gamma'}$(μm^2*s)	8.57E03
$Q^{\gamma'}$(kJ/mol)	**163.3**
h_{cr} (μm)	461.4
ξ^{ev}	**0.44**
Creep term constants	
A(s^{-1})	7E25
m	11.6
ΔH (kJ/mol)	536.4
ξ^{creep}	0.34
α_1	0.333
α_2	1.0

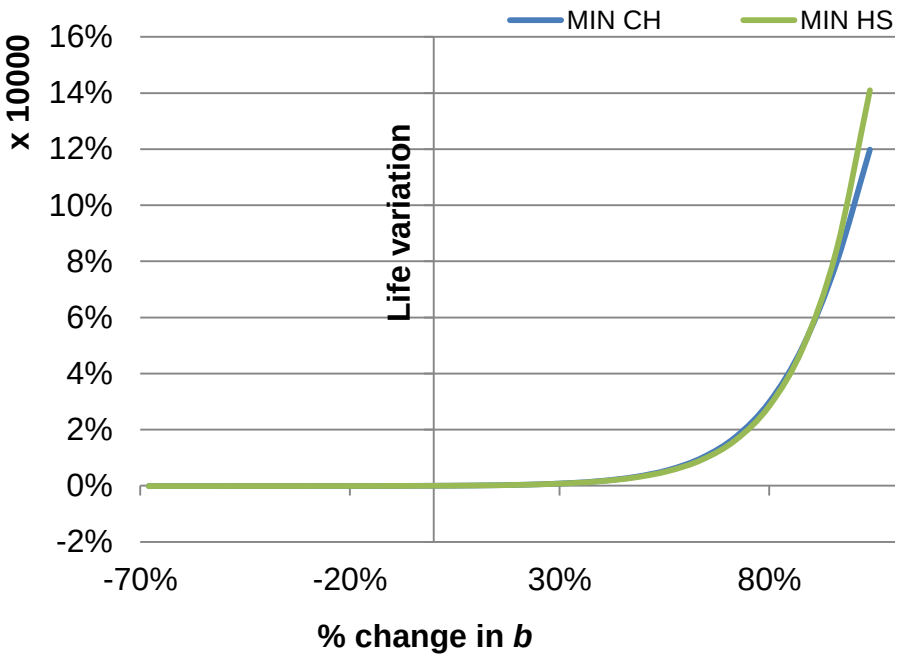

Figure 7-1: Variation of the total life for changes in *b*

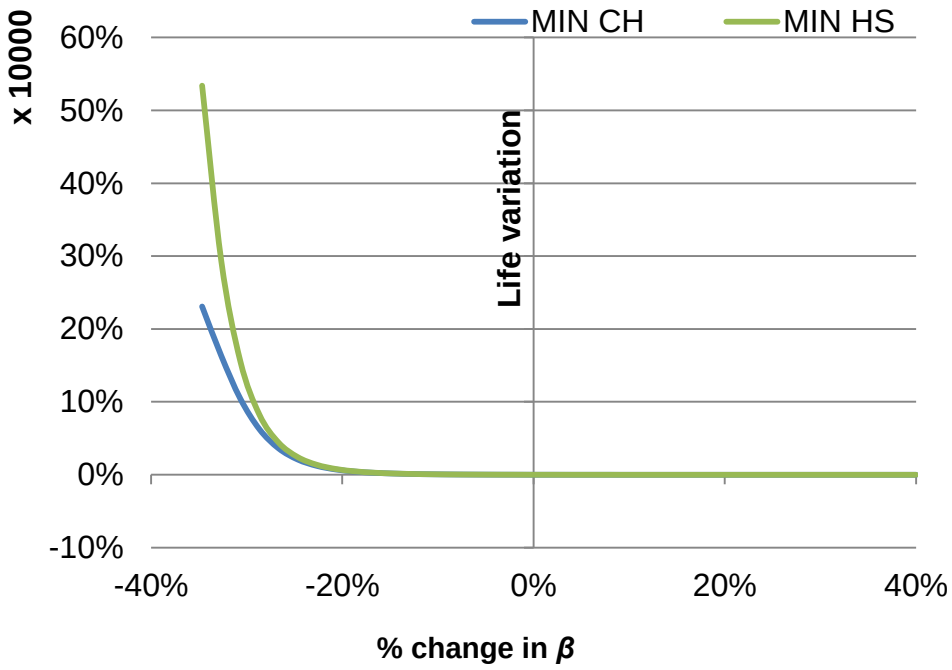

Figure 7-2: Variation of the total life for changes in *β*

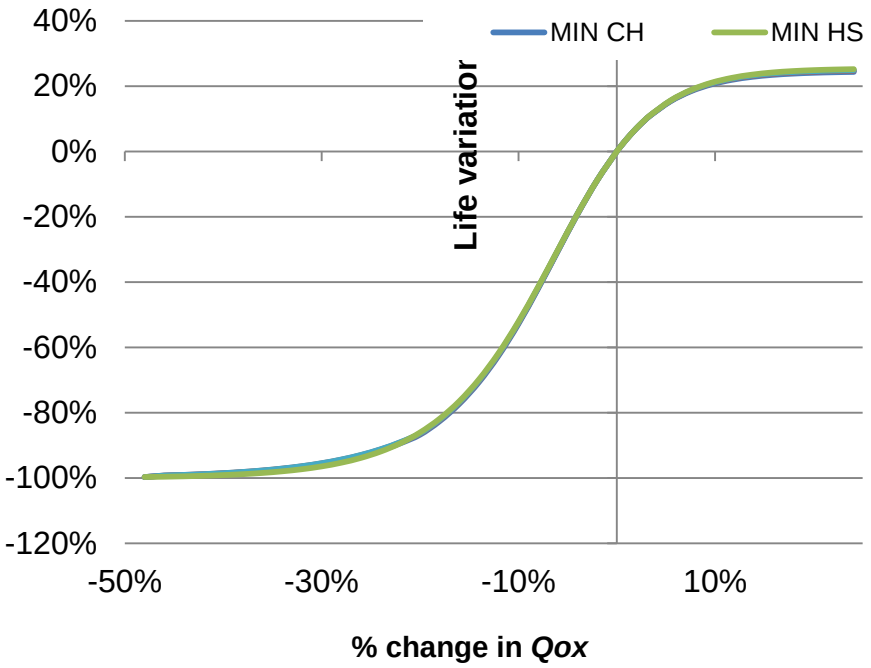

Figure 7-3: Variation of the total life for changes in *Qox*

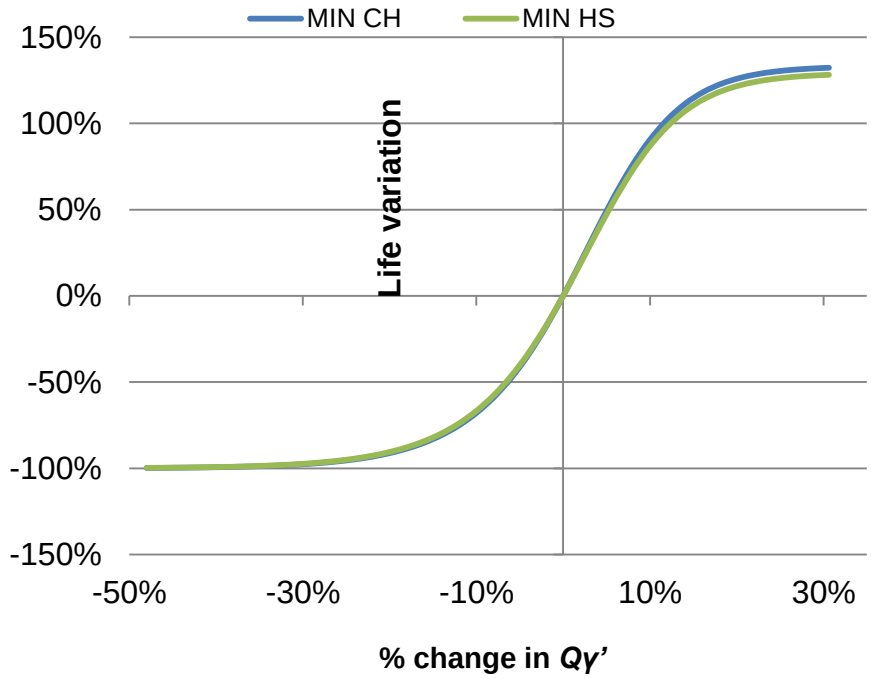

Figure 7-4: Variation of the total life for changes in *Qy'*

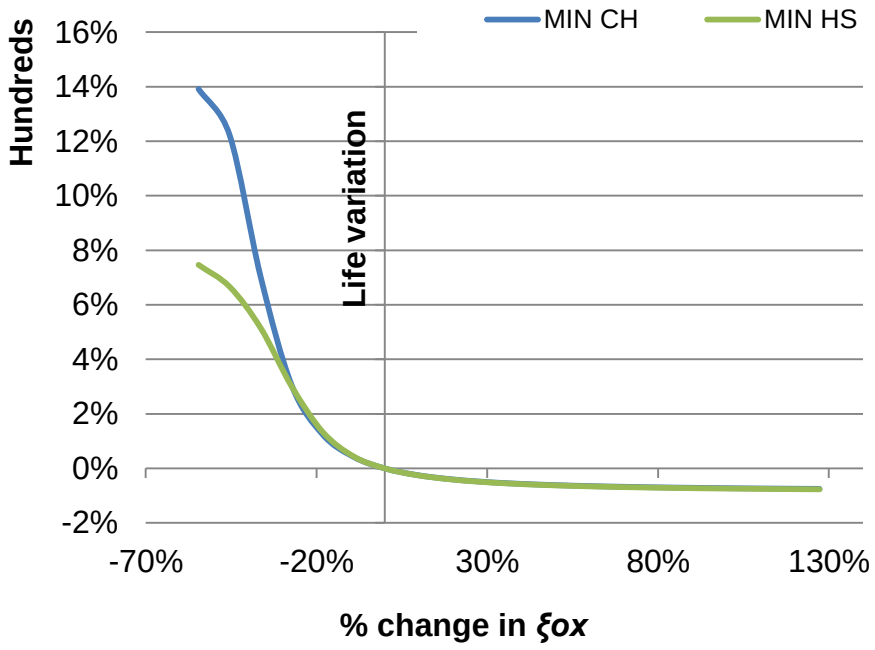

Figure 7-5: Variation of the total life for changes in ξox

The shape factor for environmental damage phasing function, ξ_{ox}, was varied between -60% and 130%; and as in the previous cases, the influence in the oxidation life is translated entirely into the total life. The trends of the cold and hot sides are also similar, but at lower values of ξ_{ox} the hot side exhibits lower life estimates. This suggests that due to the reduced phasing factor, the impact of the temperature strain phasing, as well as the thermal gradient between the hot and cold sides is reduced. This would lead to lower estimation of the tensile thermal stresses on the cold side that influence the oxidation damage in OP-TMF. The higher temperatures on the hot side begin to dominate oxidation damage; driving the life.

Overall, it was observed that the exponent on time β in oxide+γ' depletion growth constant had the most impact on the life estimation (about 6600:1 relationship), followed by strain rate sensitivity constant, b (1550:1), shape factor for environmental damage phasing function, $\xi_{ox.}$(25:1), activation energy for γ' depletion $Q_{\gamma'.}$ (4:1) and lastly, the activation energy for oxidation, $Q_{ox.}$ (1:1).

Except environmental damage phasing function, $\xi_{ox,}$ the other four parameters were also observed by Amaro, et al [3] as significant oxidation parameters. In [3], only out-of-phase TMF lives were examined from the results of controlled experiments. However, in a typical aero-engine mission as studied in this work, several phase changes in both thermal and mechanical load could be experienced from start-up to shut down cycles and during changes in flight segment. This seems to have been sufficiently captured in the lifing method, particularly in the variations that would occur between the cold and hot sides of the turbine blade. Hence, the influence of the environmental damage phasing constant had a significant effect on the total life.

7.3 Severity of TMF Model Parameters

7.3.1 Influence of TMF Material Parameters on Severity

In the preceding section, 5 critical parameters from the sensitivity analysis on the influence of the N/S TMF model parameters were identified. This was based on how changes in the parameters affected the TMF life using a reference operating condition. This section further examines, in terms of severity, the uncertainty and the importance of accurate TMF material regarding changes in operating condition.

Using the same material (MAR-M247), with constant material properties (density, thermal expansion, and thermal coefficient), the sensitivity in terms of severity of the critical TMF parameters to a change in operating condition from the reference mission was investigated. This was done for different TETs and HPT relative shaft speeds by varying each of the five critical TMF variables one after the other, while keeping the other four variables constant. The life calculated for the reference mission was used as the baseline for severity calculation in relation to the life calculated for each change in TET and PCN.

The TMF parameters were varied from 1% to 5% for changes in the reference TET (TET+5K to TET+15K in steps of 5K). The impact on severity was then

evaluated for both the cold surface (CS) and the hot surface (HS) of the leading edge. Both sides showed the same severity trends. Figures 7.6 - 7.11 detail the severity characteristics obtained from this analysis for the cold side.

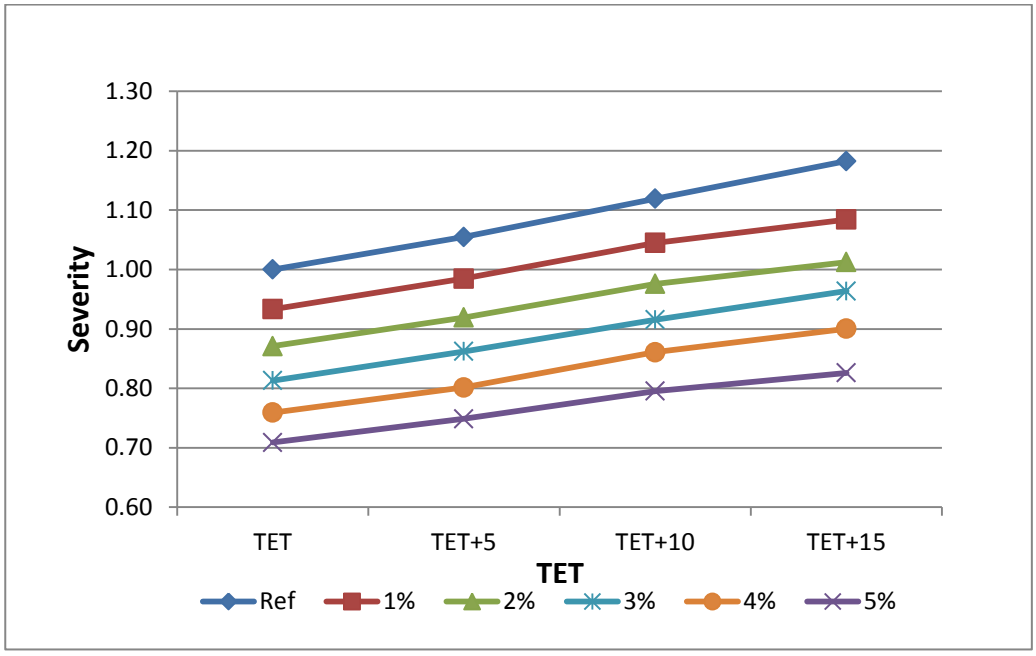

Figure 7-6: Severity Vs TET and 'b'

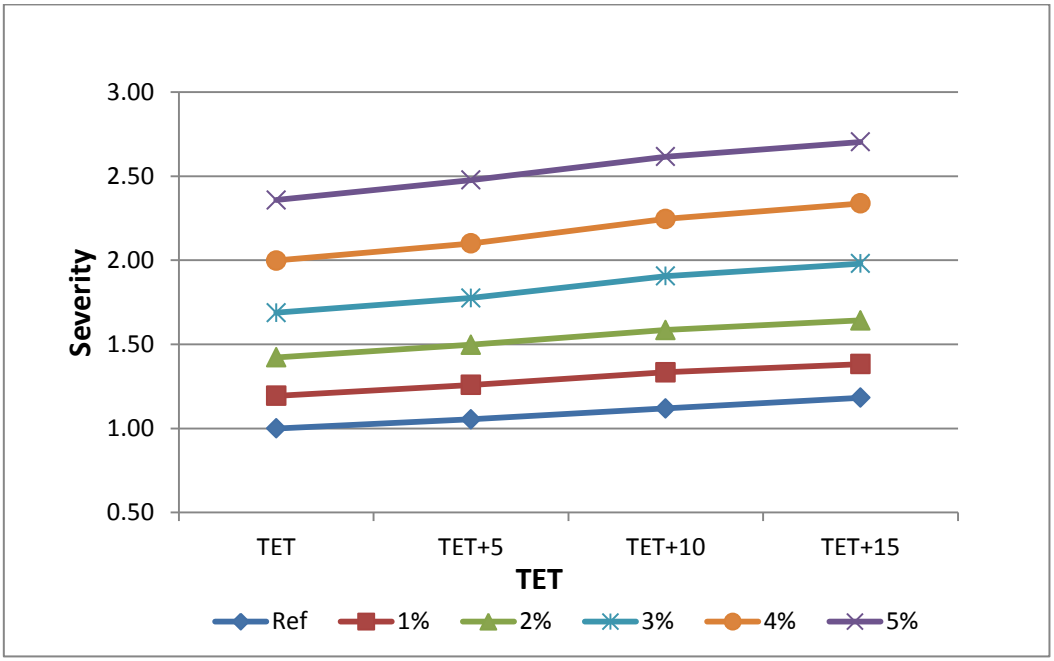

Figure 7-7: Severity Vs TET and ‘β’

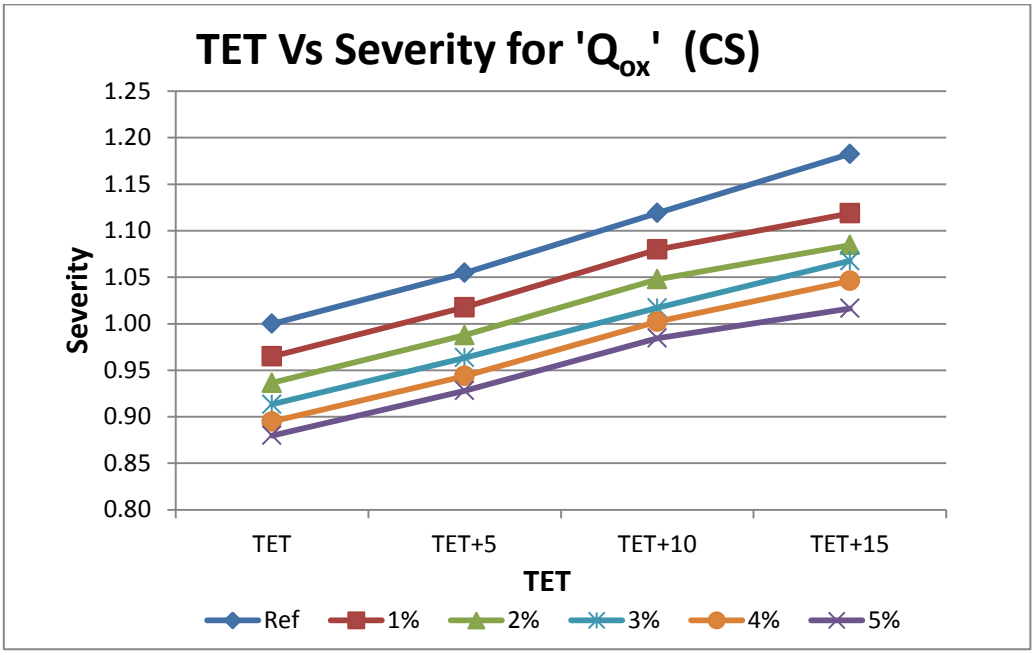

Figure 7-8: Severity Vs TET and ‘Q_{ox}’

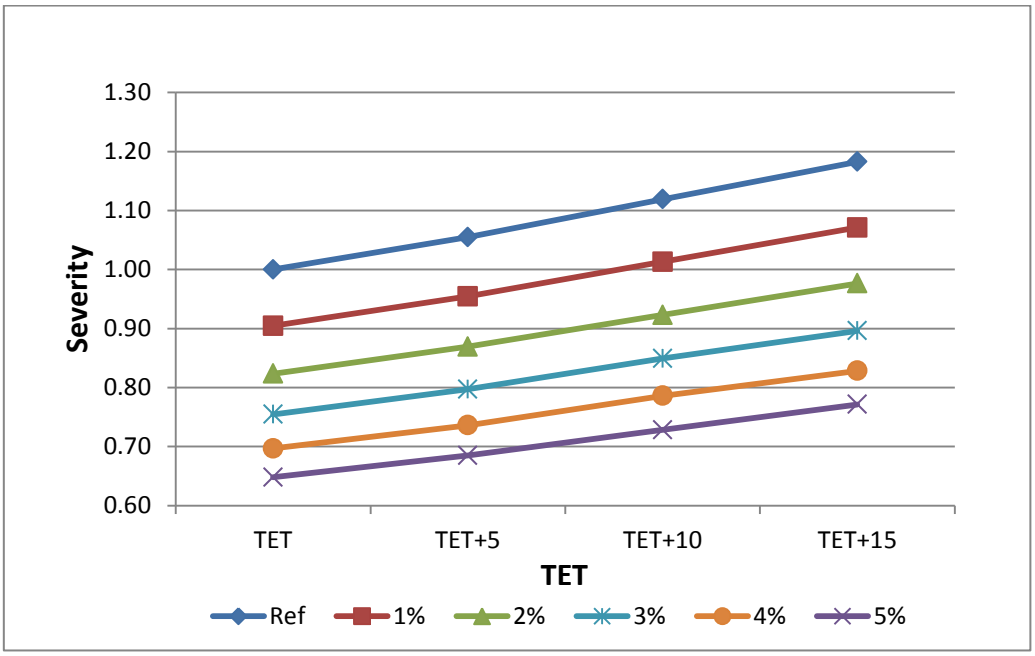

Figure 7-9: Severity Vs TET and '$\boldsymbol{Q}_{\gamma'}$'

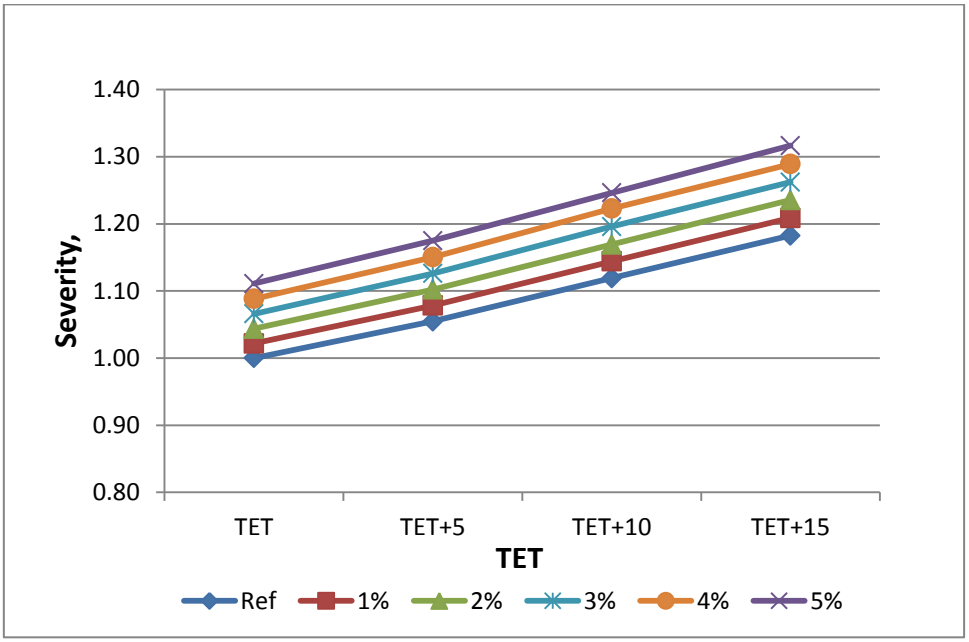

Figure 7-10: Severity Vs TET and '$\boldsymbol{\xi_{ox}}$'

It is observed that the severity of the turbine blade increases with the increase in TET. This is normal as the TMF damage mechanisms such as creep and oxidation become more severe at higher temperatures. Also due to the influence of higher blade temperatures, the hot side shows more sensitivity than the cold surface.

An increased value of the strain rate sensitivity constant (*b),* activation energy for oxidation (Q_{ox}) and activation energy for γ' depletion ($Q_{\gamma'}$) resulted in a reduction in the severity. Usually, as observed in [73], when the strain rate increases, the critical thickness $\bar{h}_f$ will decrease thereby reducing the damage severity. Likewise, higher activation energy means that the effect of temperature on the damage is also reduced.

On the other hand, the increase of time exponent (*β) and* environmental shape factor (ξ_{ox}) corresponded to an increase in the severity. Invariably, an Increase

in the value of β leads to increased oxidation induced crack length, while increase in ξ_{ox} translates to a higher oxidation phasing factor (function of the thermal to mechanical strain ratio); resulting in more oxidation damage.

It was also observed that, β had the highest influence on the severity, followed by '*b' and* 'ξ_{ox}' respectively.Lastly, for a unit change in TET (5K) and TMF parameters (1%), the TMF parameters (excluding for 'ξ_{ox}',) show more influence on the severity calculations.The same trends in the severity characteristics were obtained from the analysis on changes in HPT relative shaft speed. In this case, the shaft speed is varied from 100% to 115% (in increments of 5%).

It is noteworthy, as presented in Figure 7.11, that using the life calculated for each change in TET as the reference (instead of the TET for the reference mission) , exactly the same severity characteristics is obtained for any of the ranges of TET or PCN considered.

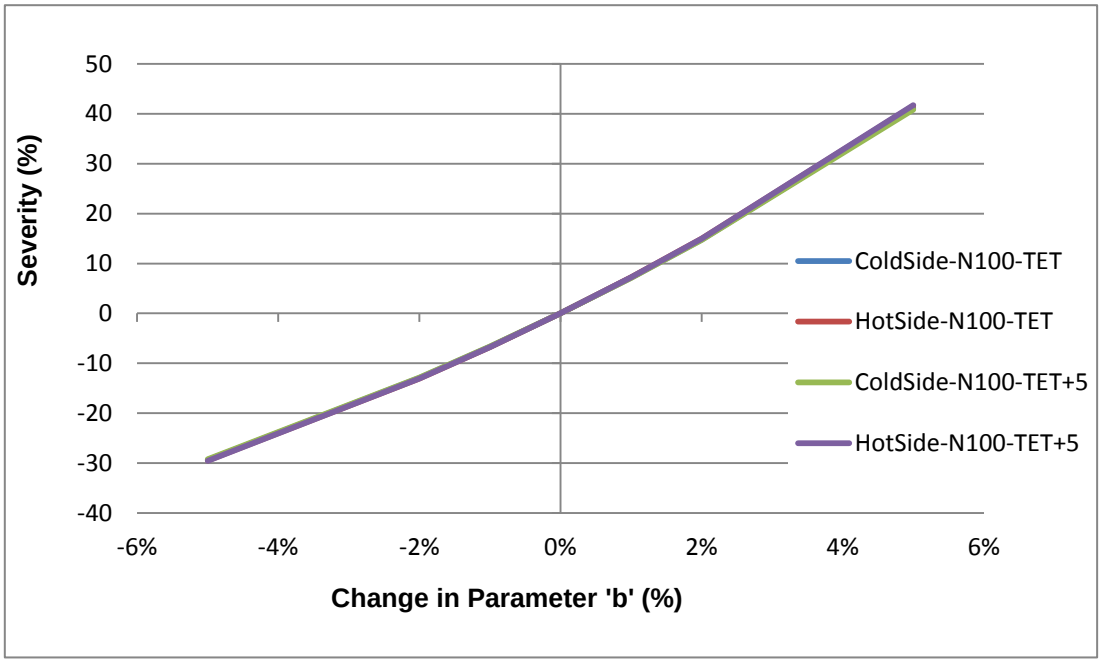

Figure 7-11: Severity Vs TET and 'b'

7.4 Chapter Conclusion

Five constants within the oxidation damage term in the N/S TMF model were found to significantly influence the calculation of the TMF life. This suggests that these five parameters are highly material specific. Therefore, the tests to determine the N/S TMF model parameters could be focused on only these critical parameters. Also, as conducted in Amaro, et al [3], an optimisation method could be used to determine a best engineering fit for the parameters.

The five sensitive parameters identified are consistent with previous findings in Amaro, et al [3]. However, in Amaro, et al, only four critical constants were considered as influential. For a typical flight operating condition, this study identifies the shape factor for environmental damage phasing function, ξ_{ox}, as an additional influencing parameter in the TMF life assessment of aero engine turbine blades.

Furthermore, the impact of a deviation in TMF parameters has more influence on damage severity than changes in the operating conditions considered (TET and PCN). Nevertheless, using a given set of TMF parameters, the same severity characteristics can be predicted for different operating conditions. This tool therefore becomes very useful at the preliminary design stages were design choices in operating parameters such as TET and PCN could be investigated in terms of severity with some degree of certainty.

8 CASE STUDIES

The impact on the HPT blade life due to changes in certain initial design parameters, as well as operating conditions can be quantified through a severity study (previously described in Chapter 4). To this end, the developed lifing approach enables the investigation of the impact of the variation of key influencing parameters on the blade life – in terms of severity factors. This ability would help gas turbine operators in making maintenance decisions relating to the physical operation of their assets, as well as help engine designers evaluate the impact of design factors at an early stage; using minimum inputs. The TMF lives, presented in terms of severity, are obtained from the root node of the leading edge stagnation line.

8.1 Operational Parameters

The time on wing (TOW) of an aero engine is significantly influenced by its thrust rating, operational severity; such as flight length, take-off derate and environment [118]. These factors affect the engine's direct operating costs. It is therefore important to evaluate how the variations in these operational parameters affect the blade severity and therefore time on-wing and engine maintenance cost estimations.

Invariably, the thermal and mechanical loads imposed by the operational conditions of the aircraft and engine are the main cause of damage to the HPT blade. The changes in operational parameters therefore directly influence the severity. Accordingly, the impact of variations in the following identified operational parameters on the HPT blade damage severity is examined in this section:

a. Take off derate (TO derate)

b. Flight time

c. Outside air temperature(OAT)

In the following cases, the reference mission is a 1.4hr flight, at ISA+3 and 10% de-rated thrust. This is similar to that of MRO baselines for severity calculations [13].The technology parameters used are given in Table 8.1.

Table 8-1: Technology parameters for operational parameters case study

Technology /Design Parameters					
Cooling effectiveness	TBC thickness (μm)	TBC thermal conductivity $(W/(mK)$	RTDF	Hydraulic diameter (m)	LE wall thickness (m)
0.69	125	1.5	0.08	0.004	0.002

8.1.1 Take-Off (TO) Derate

Derate entails the reduction by a certain percentage of the thrust produced by an aero engine. Hence, derate at take-off significantly reduces the thermal and mechanical loads that impact on the HPT blade damage severity.

For a given mission, the damage severity could be directly related to the change in blade metal temperature, exhaust gas temperature, shaft speed and the centrifugal load experienced by the HPT. The use of derate at take-off will therefore reduce the peak temperature and shaft speed on the engine. The resultant reduced thermal and centrifugal stresses lead to a lower damage impact on the blades. Thus, TO derate is beneficial and extensively used in aircraft to reduce component damage, thereby reducing engine maintenance cost [13; 118] .Using the developed methodology, the effect of varying take off derate from -10 percent to 20 percent on the TMF severity characteristics is examined subsequently. The technology factors and operational parameters are kept constant during this investigation.

It is expected, as shown in Figure 8.1**,** that the EGT and HPT shaft speed (PCN) will decrease as take-off derate is increased. The reduction in gas temperatures and PCN means the blade would experience a reduced thermal gradient and mechanical stresses at take-off. This translates to a lower thermal

strain and thermo-mechanical stresses on the blade. Consequently, the damage on the blade is reduced and the severity decreases with increasing TO derate. The resultant TMF severity characteristic is presented in Figure 8.2, where the curves for various geometries fall within the relative factor of 1.3.

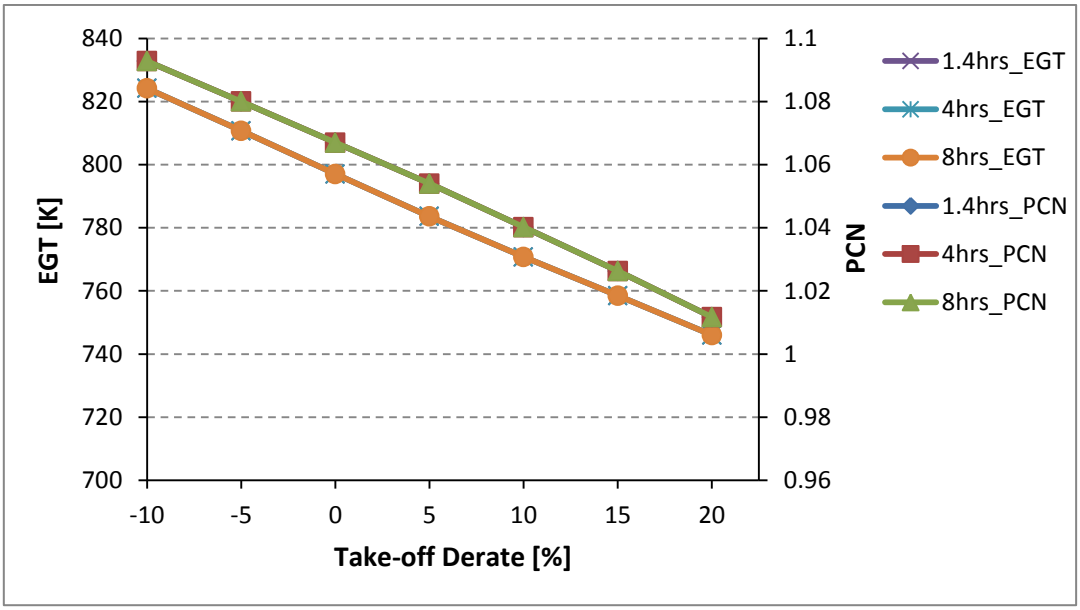

Figure 8-1: EGT and HPT shaft speed characteristics with take-off derate.

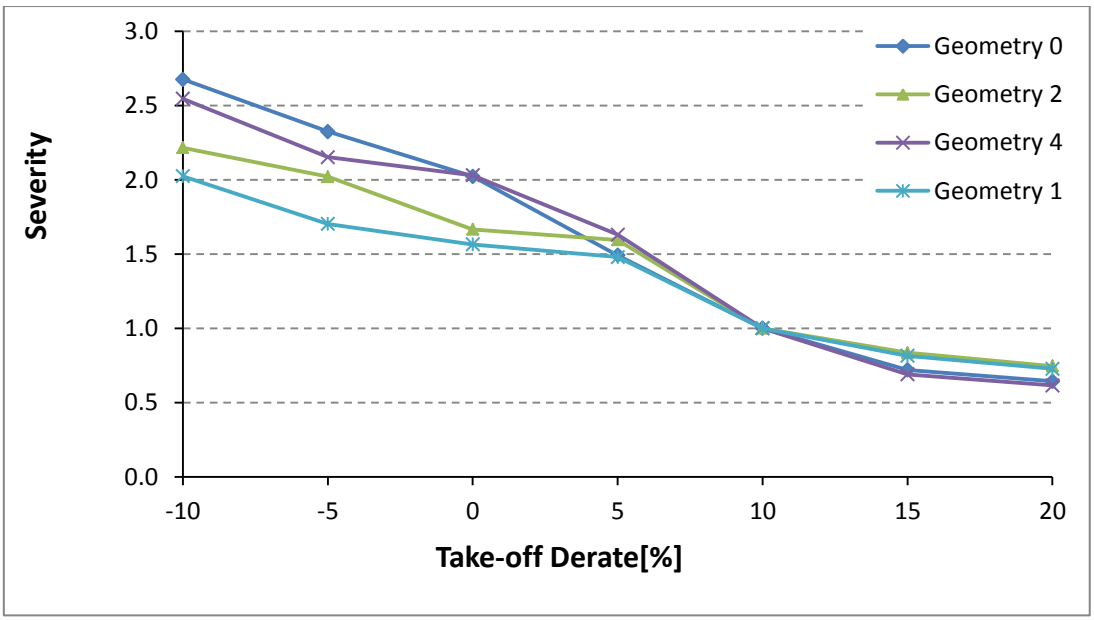

Figure 8-2: Severity characteristics for take-off derate.

Invariably, a less demanding operational condition reduces the TMF damage severity on the engine and increases the life. However, It is further observed that operating T-O derate above 10% , the severity starts to flatten because the reduction in thermal gradient becomes quite small leading to reduced effect of the thermal strain and stresses on the blade. This suggests that below a certain temperature and stress limit, not much benefit will be further derived from derate at take-off.

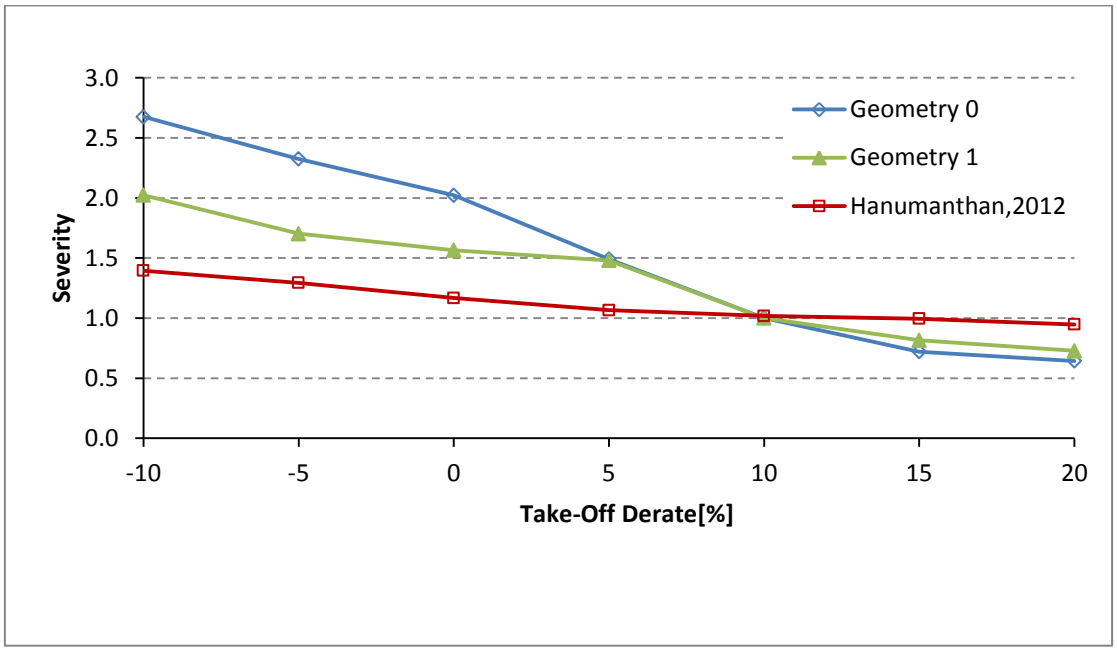

Figure 8-3: Severity comparison with Hanunmanthan,et al [13].

Furthermore, the TMF severity is compared In Figure 8.3 to the severity obtained by Harnumanthan, et al [13], using a similar engine model**.** However, following Taira [85], the severity calculated in [13], was based on summing the blade lives due to isothermal formulations for fatigue (MUS), creep (LMP) and oxidation (Arrhenius equation). The higher TMF severity characteristics obtained in Figure 8.3 corroborates the observation that, compared to TMF lifing methods, the lives predicted by isothermal methods would usually be non-conservative [73; 81]. A conservative approach such as demonstrated by the results of this current approach would appear to be more appropriate in terms of safe operation and reliability, but may be costly maintenance wise.

Overall, applying derate at take-off for a given flight mission reduces the peak temperatures and shaft speed, thereby reducing the thermal and mechanical stresses on the blade. This results in a reduction in engine damage severity, leading to maintenance savings and extended operational life. There is also an increased safety incentive in operating an engine below its critical limits. However, the penalty will be mainly the increased fuel consumption, and take off time (none of which are examined in the current research).

8.1.2 Flight Length

The severity characteristics for various flight lengths, with respect to take-off derate is usually used to represent the MRO curve for an engine [119]. As the flight length reduces, large parts of the total flight are spent on take-off and climb power settings [118]. Thus, the engine experiences a greater portion of the flight under the severest thermal and mechanical loading associated with the take-off and climb phases. Figure 8.4 shows that for the three trip lengths examined, the shortest flight length of 1.4 hrs has the largest portion of about 25% of the total flight for TO and climb. This decreases to approximately 11% and 7%, for the 4hrs and 8hrs trip lengths, respectively.

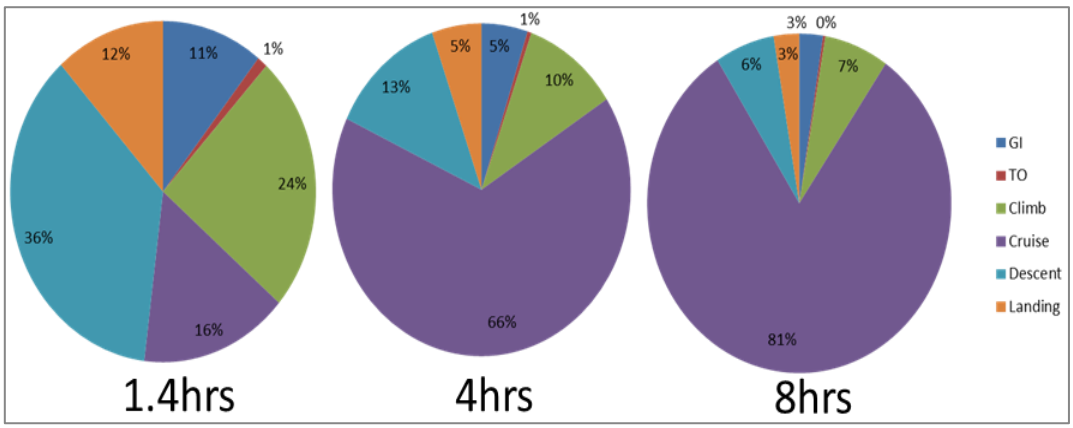

Figure 8-4: Proportion of flight segments for trip lengths.

Accordingly, in calculating the TMF life, the impact of the time parameter in the creep, and oxidation terms dominate the thermal and mechanical stress parameters (which have relatively the same magnitudes for the flight lengths as

indicated in Figure 8.5). Hence, in Figure 8.6**,** the shorter flight lengths show more damage severity; leading to a higher deterioration rate of the HPT blade and reduced time on wing of the engine. On the other hand, longer flight lengths will result to less wear and tear over the flight mission, thereby increasing the on-wing time.

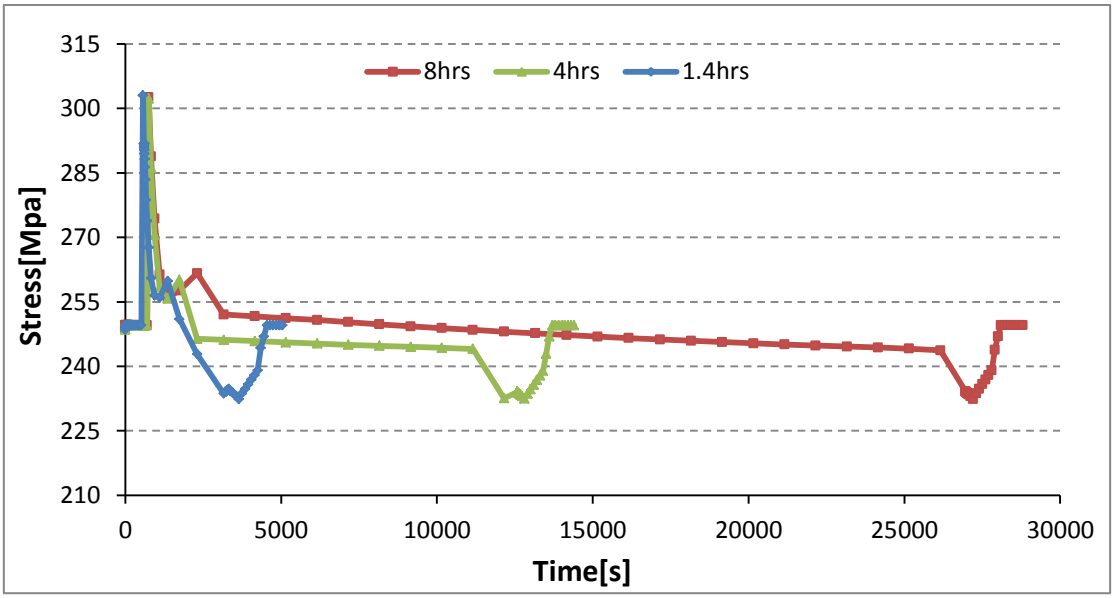

Figure 8-5: Thermo-mechanical stress variation for trip lengths 1.4, 4 and 8 hrs

Furthermore, irrespective of flight length, applying take- off derate is beneficial in reducing the damage severity. However, unsurprisingly, the impact of TO derate is greater for the shorter flights, because a larger portion of the flight is spent at the higher power setting compared to the longer trip lengths. Hence, the 1.4hrs flight shows the steepest curve; with a significant impact of TO derate up to about 15%, when the curve flattens. The steepness of the severity curves progressively reduces for the 4hrs and 8hr trip lengths as the trip length increases, flattening out at about 10% and 5% TO derate, respectively. Also, the impact of Take - off derate in reducing severity is greater at the higher thrust settings (higher temperatures and shaft speeds), as reflected in the steeper curve within the -10 to 5% TO derate region. Conversely, a flatter fall in severity is observed for the reduced thrust regions.

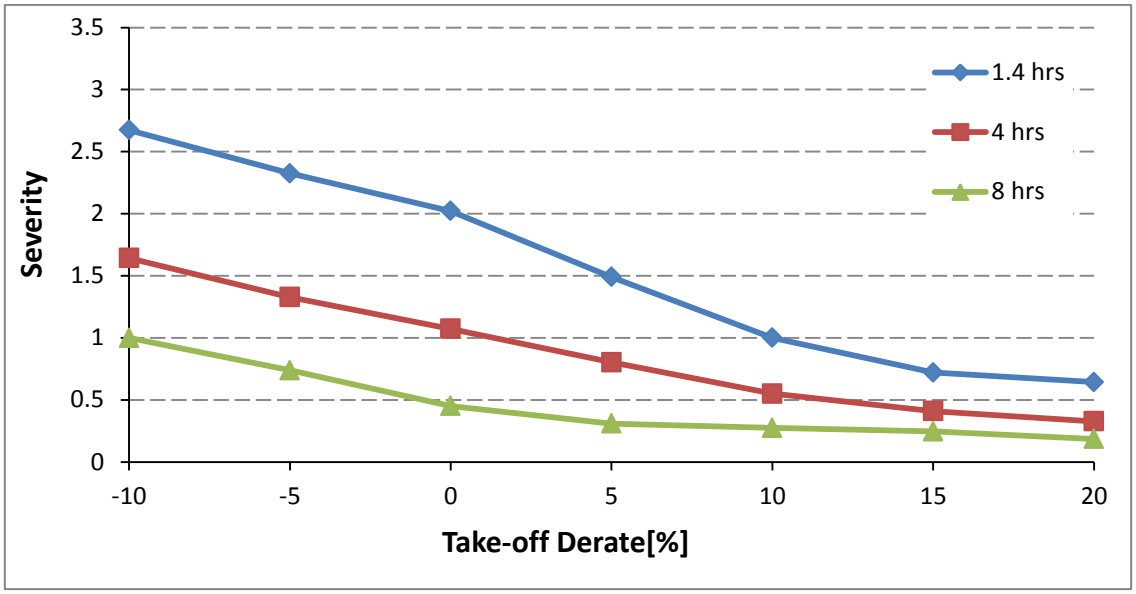

Figure 8-6: TMF Severity characteristics for Flight lengths.

The TMF severity for the flight lengths was also compared to Hanumanthan[119]. The same trends are observed, where the shorter flight lengths show more severity in Figure 8.7.

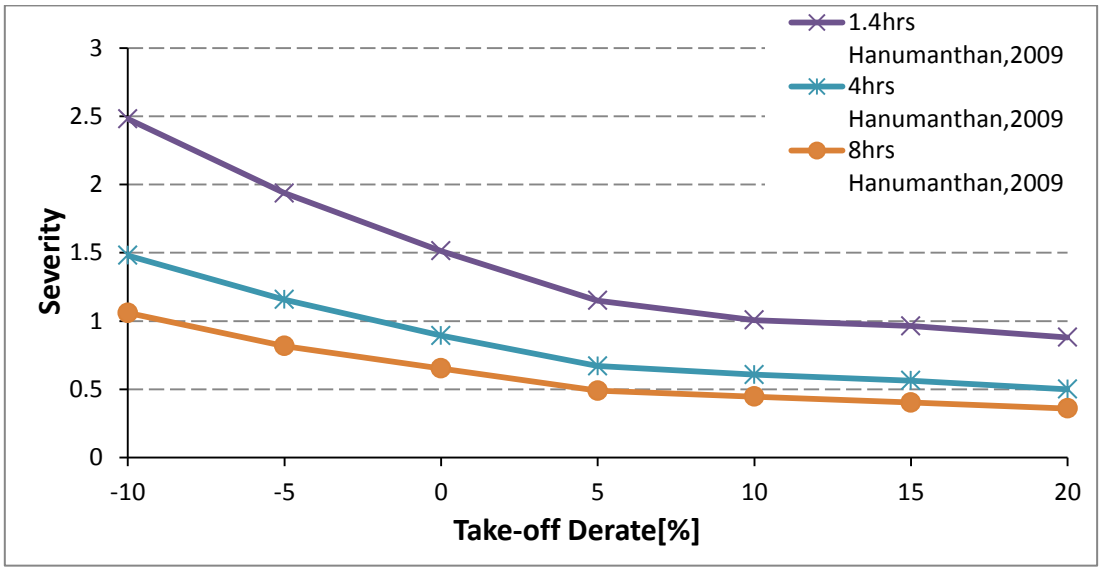

Figure 8-7: Comparison of derate severity curves for trip lengths

8.1.3 OAT at Take-Off Conditions

An aircraft engine will inevitably be operated in various environments over its service life. The outside air temperature (OAT) in a particular environment will therefore influence both the performance of the aero engine and its useful life. As the OAT increases the air density reduces. This leads to a decrease in the total thrust due to the reduction in pressure ratio and mass flow to the engine. To compensate for this effect, turbofan engines are flat rated to a specific OAT limit. To maintain the rated thrust, the TET at take-off and maximum climb ratings increase as OAT increases up to the rated limit. Consequently, the EGT and relative HP shaft speed increase, causing damage to the HPT blades.

The effect of OAT on the TMF severity of the turbine blade was examined by varying the OAT at TO conditions from ISA -15 to ISA +15; while keeping the rated TO thrust constant. Figure 8.8 and Figure 8.9 depict the expected increase in the EGT and HPT shaft speeds, respectively, as OAT is increased. This means that an engine exposed to higher OAT will experience a lower EGT margin, higher thermal and mechanical stresses that results to a higher impact of damage on the blade.

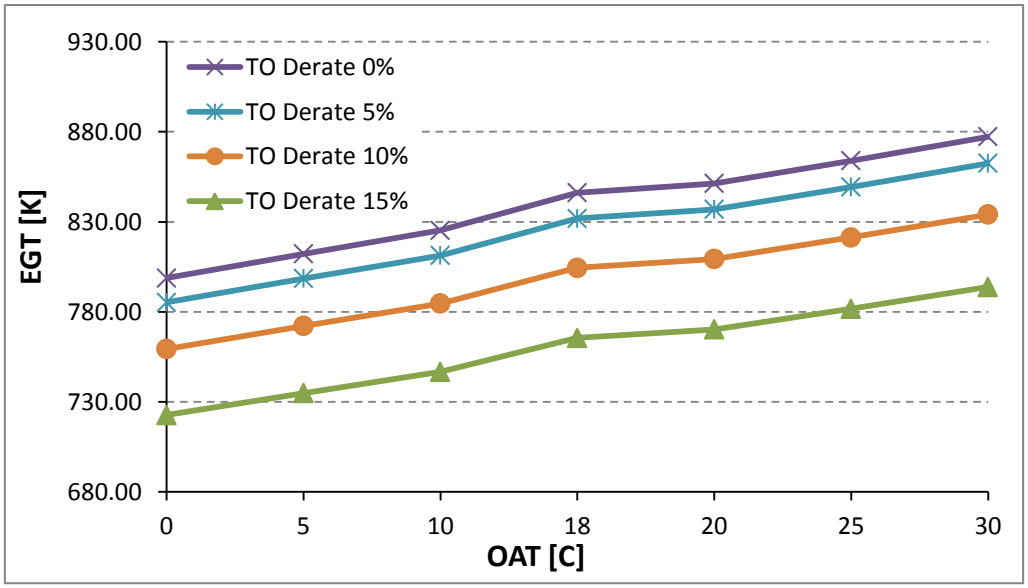

Figure 8-8: EGT characteristics with OAT

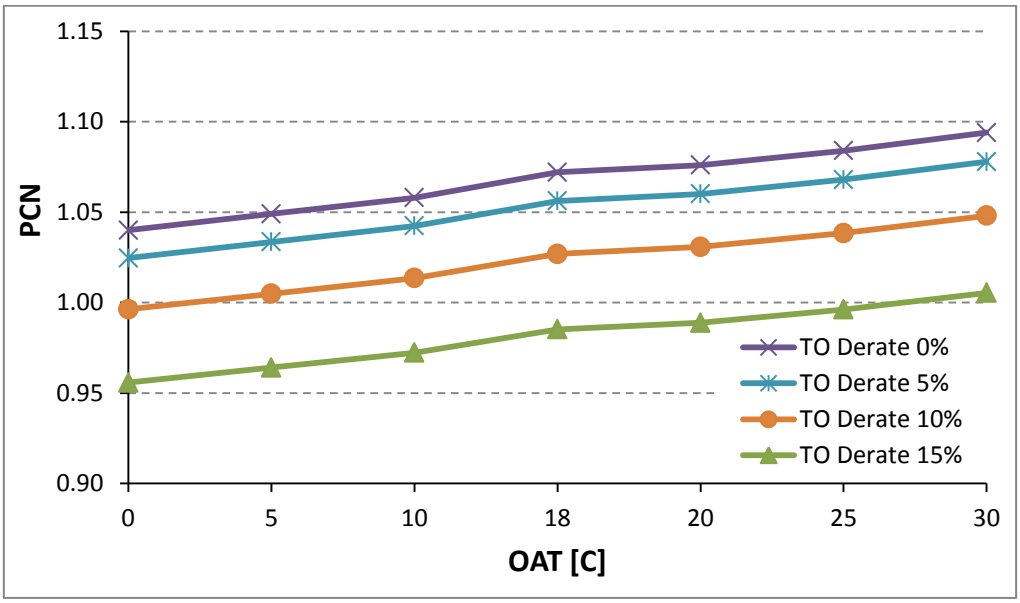

Figure 8-9: HPT shaft speed characteristics with OAT

In Figure 8.10, the severity characteristics confirm that an engine operated in higher OAT environment will experience more damage. For instance, using the 0% TO derate curve, the severity increases from about a factor of 0.5 to 3.0, as OAT increases from 0 to 30^{o}C. Furthermore, when TO derate is applied, the severity factor progressively decreases from around 3.0 to 1.0,at TO derate of 15%. Hence, the use of take-off derates at airports with high OAT would help reduce the blade damage, thereby increasing the engine TOW. However, applying higher percentage of TO derate would be marginally beneficial at lower OATs. This is shown by the very flat regions between OAT ranges 0^{o}C to 10^{o}C of the 10% and 15% TO derate curves.

The TMF severity characteristics compares very well with the trends observed in Figure 8.11**,** where the severity increases with increasing OAT. However, there is more impact of reduced TMF severity when take- off derate is applied. At lower OATs.

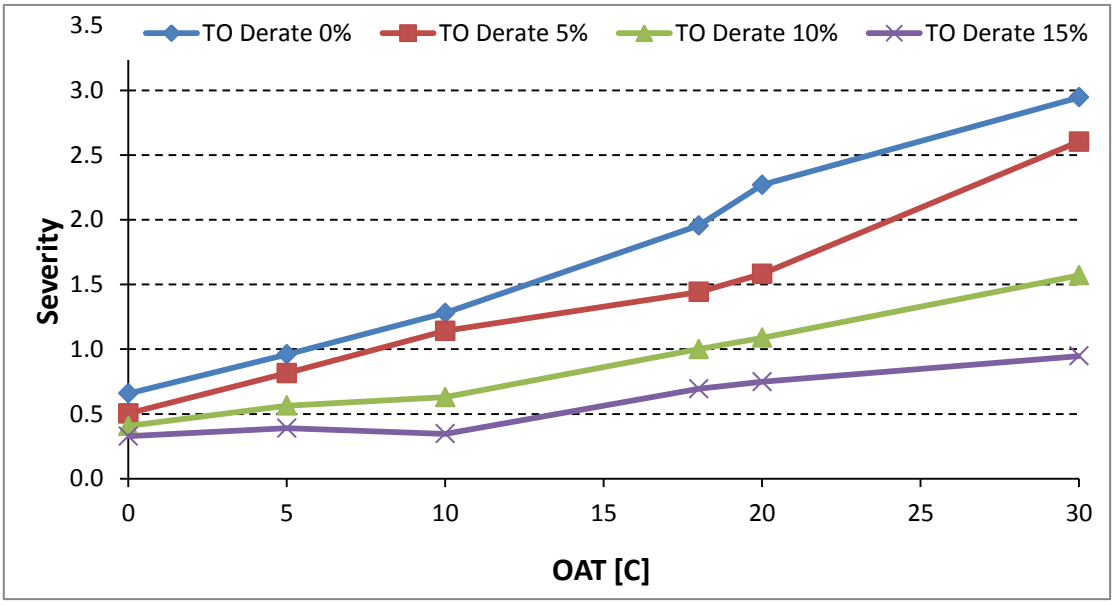

Figure 8-10: TMF severity characteristics with OAT.

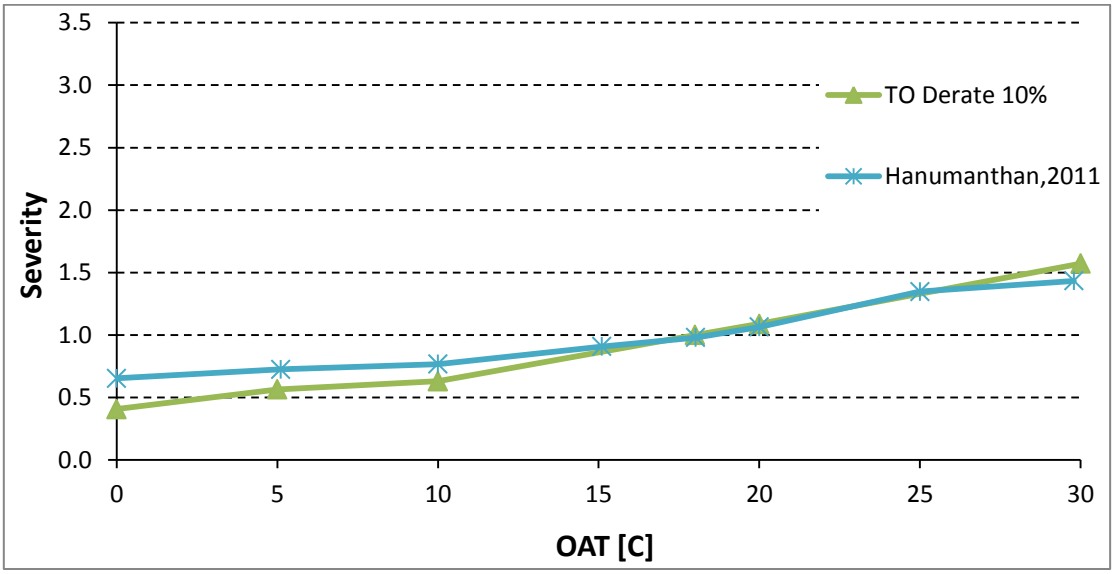

Figure 8-11: severity characteristics with OAT [Hanumanthan,2011].

8.1.3.1 Environment

In addition to the effect of OAT, the engines operated in dusty, sandy or corrosive environments will undergo additional damage, which will reduce the blade life. For instance, in dusty or sandy environments, turbine blades could be eroded and the cooling holes blocked[118]. Damages due to these factors,

including FOD, are not easily modelled and there is yet any reliable TMF lifing model developed for this [81].

8.2 Design parameters

The effects of some engine component design parameters on the HPT blade life of an aero gas turbine engine are investigated in this section for various RTDF, TET, and cooling effectiveness (ε). A reference baseline for TET, cooling air temperature, RTDF, ambient temperature, cooling effectiveness and relative rotational speed (PCN) was set at 1562K, 821K, 0.08, 288.15K, 0.7 and 100%, respectively. The reference mission (RM) is for a 4hr flight at ISA conditions. The reference design/technology parameters used are in Table 8-2

Table 8-2: Reference values for design parameters

Technology /Design Parameters					
Cooling effectiveness	TBC thickness (μm)	TBC thermal conductivity (W/mK)	RTDF	Hydraulic diameter (m)	LE wall thickness (m)
0.70	125	1.5	0.08	0.003	0.0018

8.2.1 The effect of RTDF on blade life

The effect of RTDF on TMF life is investigated by changing its value from 0.08 to 0.1 and then 1.5. During this investigation, the TET, the relative rotational speed (PCN), and ε were maintained at the baseline values. The blade inlet temperature profile and associated blade metal temperature distribution along the span of the blade at different RTDF values are shown in Figure 8-12 and Figure 8-13 , respectively. In Figure 8-12, as the value of RTDF is increased from 0.08 to 0.15, the maximum gas temperature increased by about 3.3%, from 1588K to 1640K at a point 75% along the span of the blade. On the other hand, it reduces by about 2.3% from 1489K to 1455K at the root and tip. Lower RTDF values result in higher gas temperatures at the root and at the tip of the blade. However, as shown in Figure 8-13 , this translates to higher metal temperatures only at the root, where there is an increase of 6K (about 0.6%), as

RTDF value reduces from 0.15 to 0.08. At the tip there is a slight increase in metal temperature as the value of RTDF is increased.

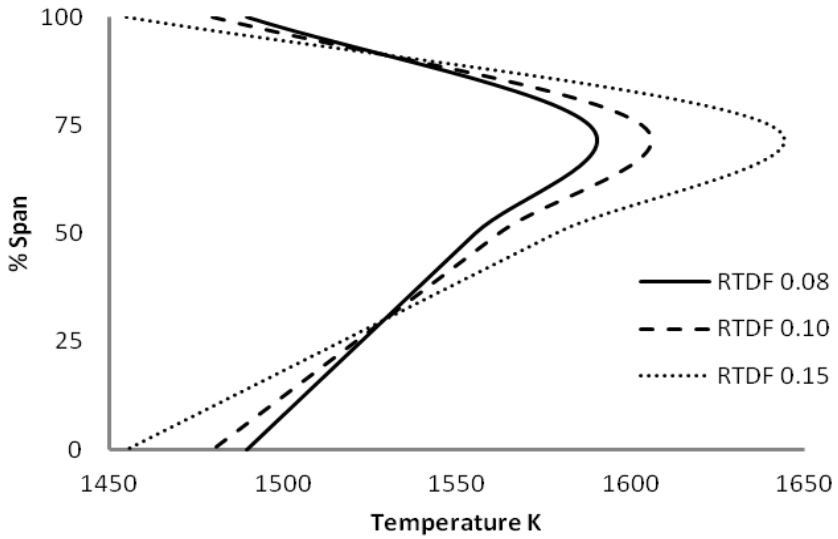

Figure 8-12**:** Blade inlet temperature profile for different RTDFs.

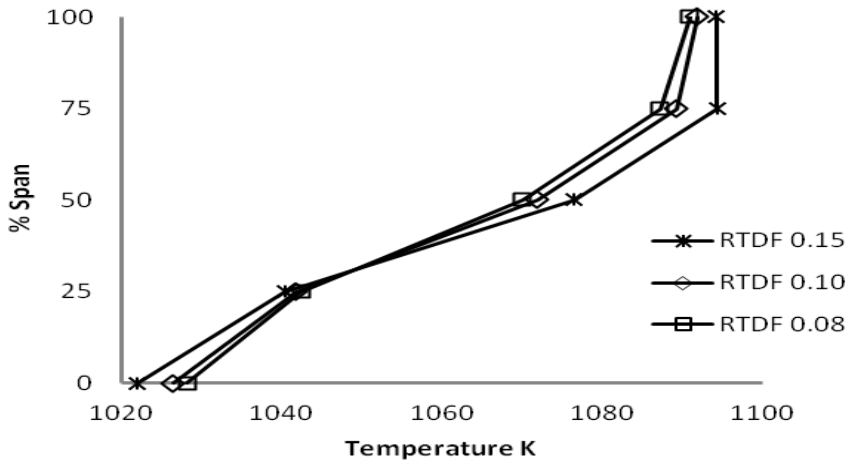

Figure 8-13**:** Blade metal temperature distribution along the span of the blade at different RDTF.

Generally, high temperatures at the root and tip should be avoided; since the roots of turbine blades already bear the largest stresses, and at the blade tip there is the need to prevent damage due to overheating. Hence, for a given TET requirement, it would be necessary to choose an RTDF that gives lower

blade temperatures, especially at the root and tip of the blade, for better blade life.

Figure 8-14 shows the severity characteristics for RTDFs of 0.08, 0.1 and 0.15 for the cold and hot sides of the leading edge. Considering the life at the CS for the reference mission (RTDF = 0.08), the severity increases to about 2.1, and then 3.7 for RTDFs of 0.1 and 0.15, respectively. The increase in severity with increasing RTDF is mainly because of the higher thermal gradient, and associated thermal strain resulting from the higher blade metal temperatures. Hence, more blade damage is experienced as thermal strain is increased.

Regarding the damage mechanisms, oxidation has the major influence on the total life followed by fatigue and creep. Figure 8-15 shows the details of the contribution of each of these damage mechanisms for the cold side. Overall, careful consideration should be given to the selection of the combustor RTDF to better control blade life.

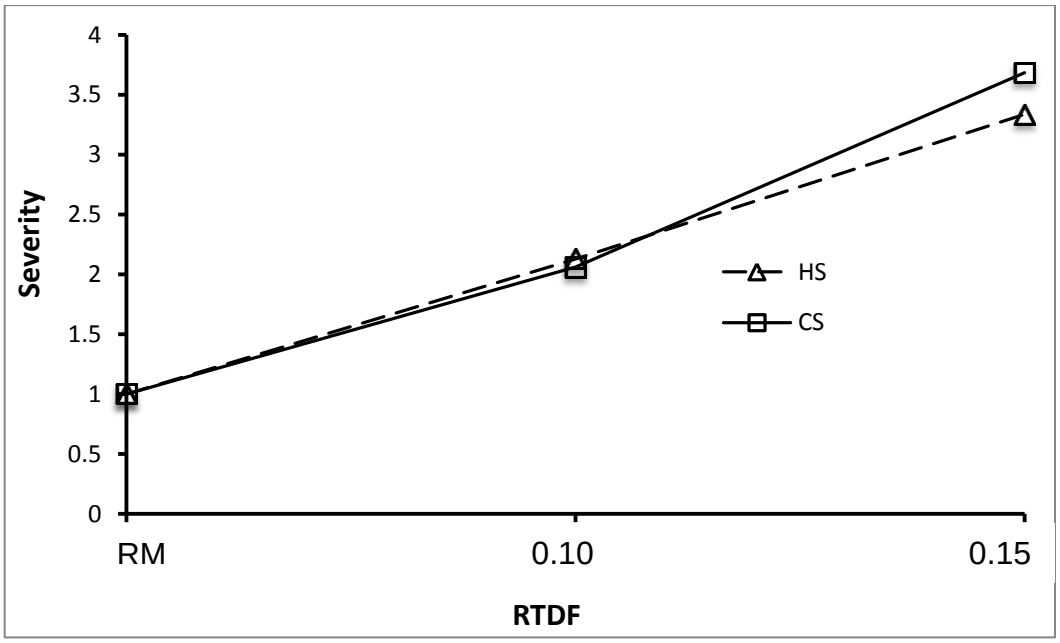

Figure 8-14: Blade severity for RTDF=0.08(RM), 0.10 and 0.15.

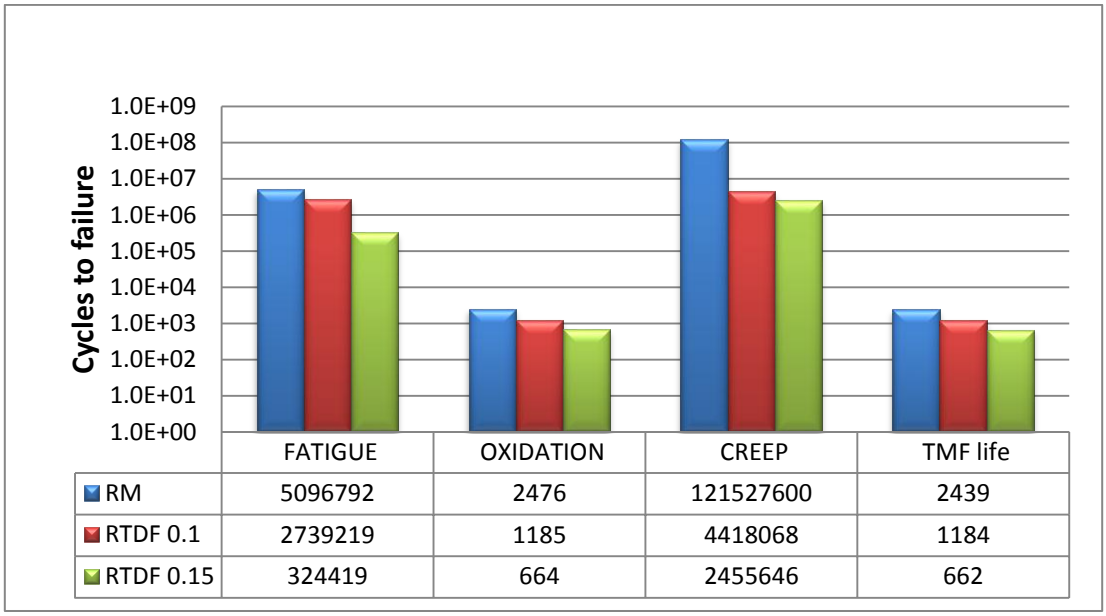

	FATIGUE	OXIDATION	CREEP	TMF life
RM	5096792	2476	121527600	2439
RTDF 0.1	2739219	1185	4418068	1184
RTDF 0.15	324419	664	2455646	662

Figure 8-15: Variation of life with RTDF

8.2.2 The Effect of Cooling Effectiveness

Cooling effectiveness (ε) is one of the main drivers of turbine blade temperature. The reduction of ε could be due to any combination of the following factors: increase in air cooling temperature, increase in TET and /or degradation in the cooling system [120]. For this investigation, the effect of cooling effectiveness on blade life is evaluated using the reference baseline parameters. In the analysis, ε was degraded from 0% (ε =0.7) to 5% (ε = 0.665) to assess the variation of the blade life and severity. The results for cooling effectiveness degradation of 1%, 3% and 5% are presented subsequently.

Figure 8-16 shows the expected progressive increase in blade metal temperatures as ε reduces by 1% to 5%. The maximum metal temperature along the blade span increases at an average of about 5K per percentage ε degradation, from 1093K to1116K.

Figure 8-17 shows that reduction in ε increases the severity, leading to a reduced blade life. This is mainly due to the increase in blade metal temperature, and the associated thermal gradient along the span of the blade. The effect of the increased blade metal temperature also influences the impact

that the various damage mechanisms have on blade life. From Figure 8-18, it is observed that although oxidation is the damage mechanism driving the overall blade life, the effect of creep starts to be felt at higher temperatures. Hence, at 5% reduction in ε, where the metal temperature is highest relative to the RM, the creep reduction in life is about 98%, compared to oxidation and fatigue with approximately 55% each.

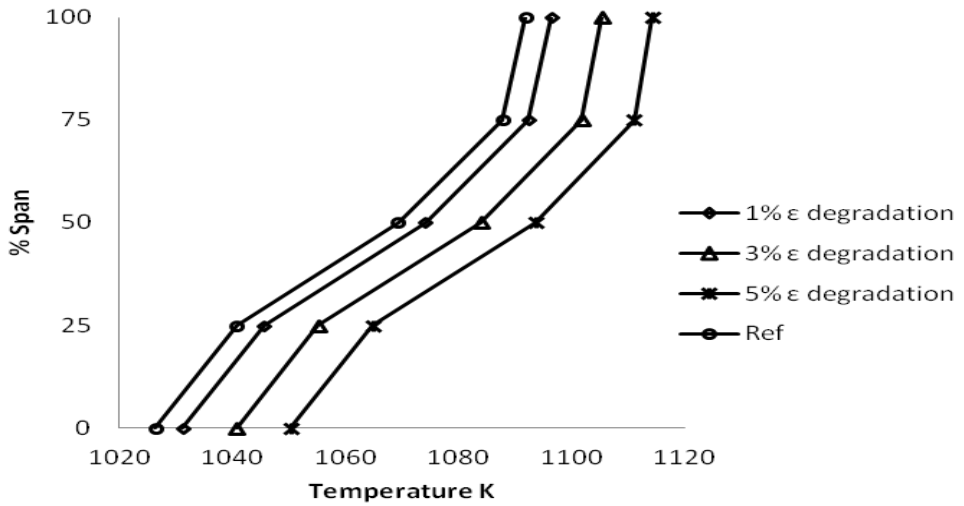

Figure 8-16: Blade metal temperature profile for different cooling effectiveness.

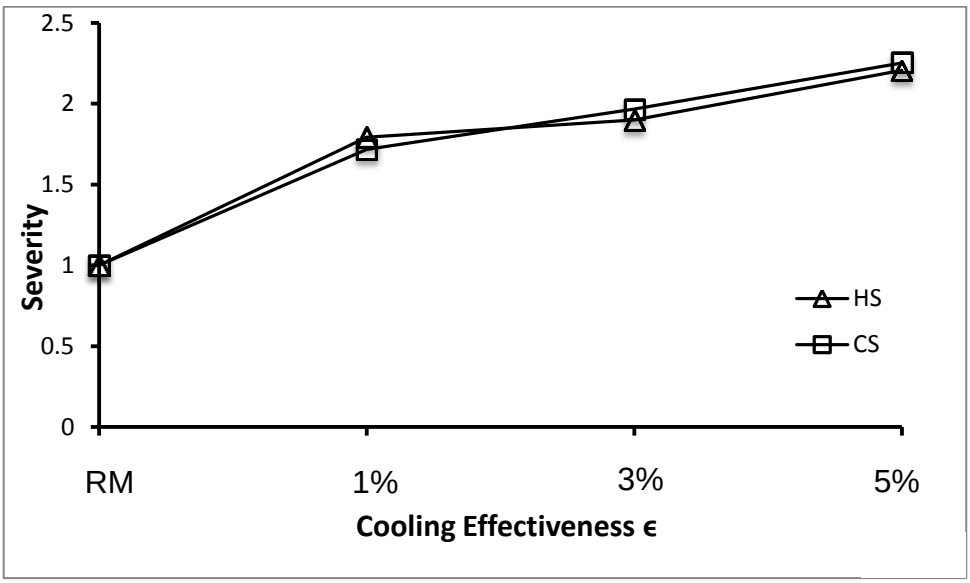

Figure 8-17: Severity characteristics for different cooling effectiveness.

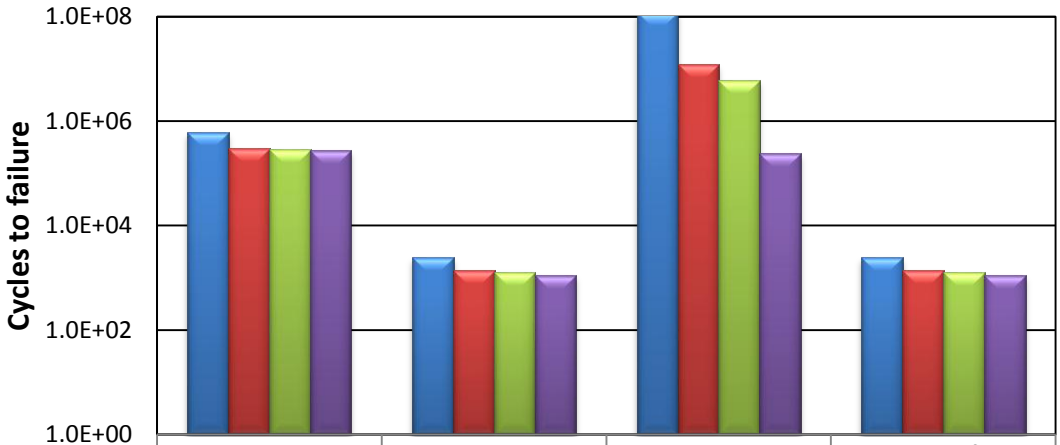

	FATIGUE	OXIDATION	CREEP	TMF life
RM	596792	2448	121527600	2439
1%	298859	1366	12051280	1360
3%	284295	1290	6010201	1284
5%	270358	1115	237410	1105

Figure 8-18: Variation of life with different cooling effectiveness.

8.2.3 The Effect of TET

Temperature is recognised to strongly affect the life of turbine blades. The increase in thermal gradient across the blade and creep damage at higher temperatures are the main concerns .The effect of TET on blade life is examined by varying the baseline TET from 1562K to 1640K in increments of 1%. An increase in TET would generally increase the effect of the damage mechanisms, increased severity and lead to reduced life. As shown in Figure 8-19, one per cent rise in TET causes the blade severity factor to increase to about 1.45. However, the effect of creep damage was found to increase significantly with a high rise in TET. Hence, at 5% increase in TET, where the temperature is highest relative to the RM, creep starts to dominate, with a reduction in life of about three orders of magnitude, as depicted in

Figure 8-20. Generally, a component operating at a lower TET will have a longer service life than a component operating at a higher TET. However, increasing TET gives a better performance in terms of thrust and power outputs. Hence, the trade-off between increased performance and better component life

are important considerations at the initial design stage for gas turbine designers/users.

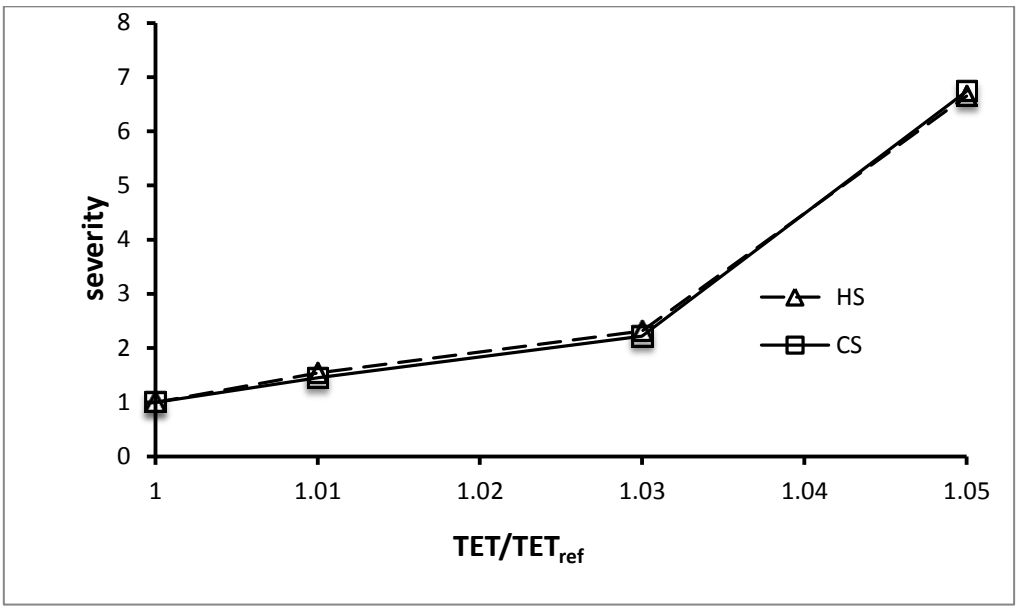

Figure 8-19: Turbine Blade TMF severity for different TETs.

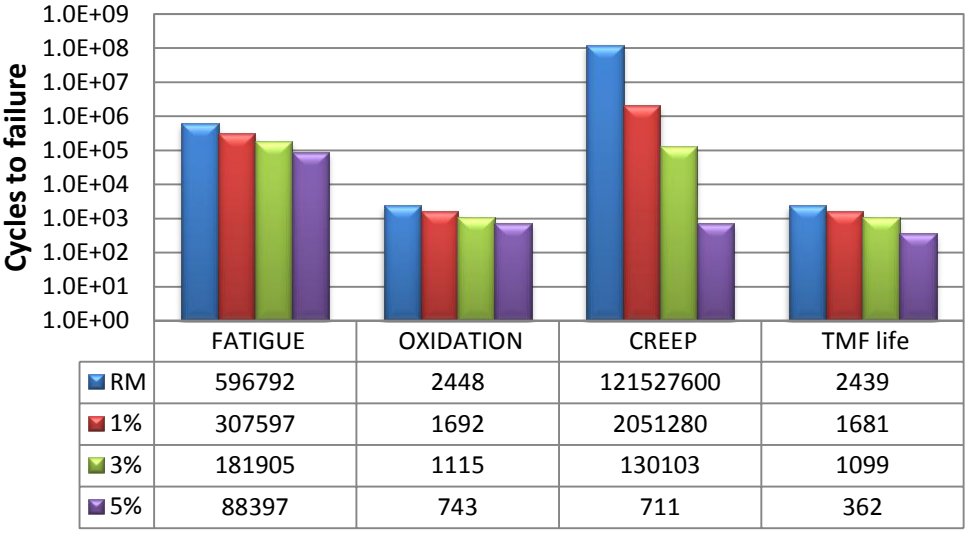

	FATIGUE	OXIDATION	CREEP	TMF life
RM	596792	2448	121527600	2439
1%	307597	1692	2051280	1681
3%	181905	1115	130103	1099
5%	88397	743	711	362

Figure 8-20: Variation of life with increasing TET.

8.3 Chapter Summary

The effects of engine operational parameters such as TO derate, trip length and OAT have been successfully investigated using the developed methodology in

this thesis. The results presented in terms of severity give the gas turbine analyst or operators a physical basis related to the exact operation of the engine. Hence, any merits or demerits from taking a design or maintenance decision can readily be evaluated and quantified. In this investigation, for a given reference condition – 1.4hr flight at ISA +3, and 10% take off derate, the following were observed:

a. Higher severity results were obtained from using the current approach.
b. Damage on the blade reduces and the severity decreases with increasing TO derate. However, below a certain temperature and stress limit, not much benefit will be further derived from derate at take-off.
c. The shorter flight lengths show more damage severity than longer flight lengths. Irrespective of flight length, applying take- off derate is beneficial in reducing the damage severity.
d. Engines operated in higher OAT environment will experience more damage severity. The use of take-off derate at airports with high OAT would help reduce the severity, but, applying higher percentage of TO derate would be marginally beneficial at lower OATs.

For the design parameters, the impact on blade life was investigated for different RTDF, TET, and cooling effectiveness (ε). A reference baseline for TET, RTDF, ambient temperature, cooling effectiveness and relative rotational speed (PCN) were set at 1562K, 0.08, 288.15K, 0.7 and 100%, respectively for a 4hrs reference mission (RM). The blade severity increased as RTDF was increased. The severity also increased as cooling effectiveness was reduced. The critical region remained the cold side as the blade life reduced with reduction in cooling effectiveness. Increasing the TET increased the severity impact of the damage mechanisms and reduced the blade life accordingly. However, creep started to drive the total failure at higher TETs, compared to the effects of fatigue and oxidation. Pure fatigue damage had the least influence on the overall TMF life calculation.

Ideally, the results from the lifing approach in this research should be validated against experimental/operational data. However, such data are not readily accessible. Hence, the results in these case studies were compared with data available in the open literature as a means of verification. The operational severity results showed were generally higher and the trends were as expected. In the design parameters cases, the life of 2440 flight cycles (9760 hours) calculated for the reference mission is quite conservative for a civil aero-engine, but this compares very well to the life of 10,000hrs estimated for the NASA E3 blade[109]. The severity trends were also as expected. Overall, the capability of the developed approach has been demonstrated to suitably conduct relative blade life and severity assessment; as well sensitivity case studies – particularly, at the conceptual design stages where very little information is available about the component.

9 THERMAL BARRIER COATING MODELLING AND ANALYSIS

TBCs are essentially used to provide thermal insulation to aero engine blades. The use of TBCs in modern aero engines, has enabled higher gas operating temperatures, thereby improving engine efficiency and performance When coupled with internal cooling technologies, the use of TBCs has helped to reduce the turbine blade surface temperatures (100-300 °C) ; thereby Improving the blade life. Despite these benefits the premature in- service failure of TBCs, which exposes the blade metal to severe gas temperatures, presents a concern. The complex and diverse TBC structure and the severe operating environment make the understanding of TBC failure difficult. Nevertheless, the thermal expansion mismatch stresses have been recognised to significantly impact on the attached blade metal interface. Hence, it is important to consider this effect in the lifing of the turbine blade.

The bare model in this research considers the effect of TBC addition in the analytical heat transfer model. This gives the expected temperature reduction on the blade metal hot surface. The effect of the stresses developed due to the TBC addition could further be captured using a FEA model that incorporates the layers of the TBC attached to the substrate. This necessitated the TBC blade model created in this research.

9.1 Limitations

The TBC structure is inherently complex and further complexity is introduced by the interactions at the interface between the TBC and substrate. In addition to thermal conduction and expansion, several phenomena that include diffusion, oxidation, creep, and fatigue, elastic and plastic deformation are occurring within the TBC layers. These effects are not presently captured, and are not examined in the current research. How the lifing methodology developed in this research can be further applied to examine the effects of TBC addition on the blade life is being explored. Accordingly, the impact on blade life due to the

thermo-mechanical stresses generated by the mismatch in thermal expansion between the substrate and the TBC is examined. In addition, the influence of changes in properties of the TBC such as thermal conductivity and TBC thickness (ceramic top coat) are also studied.

9.2 TBC FEA Modelling

The TBC FEA model was created from the bare model by including the bond coat, TGO and ceramic top coat layers as shown in Figure 9-1.Table 9-1 gives the material properties from open sources used to implement the model [40, 125]. The surfaces of the TBC layers were attached using tie interactions and surface constraints in Abaqus.

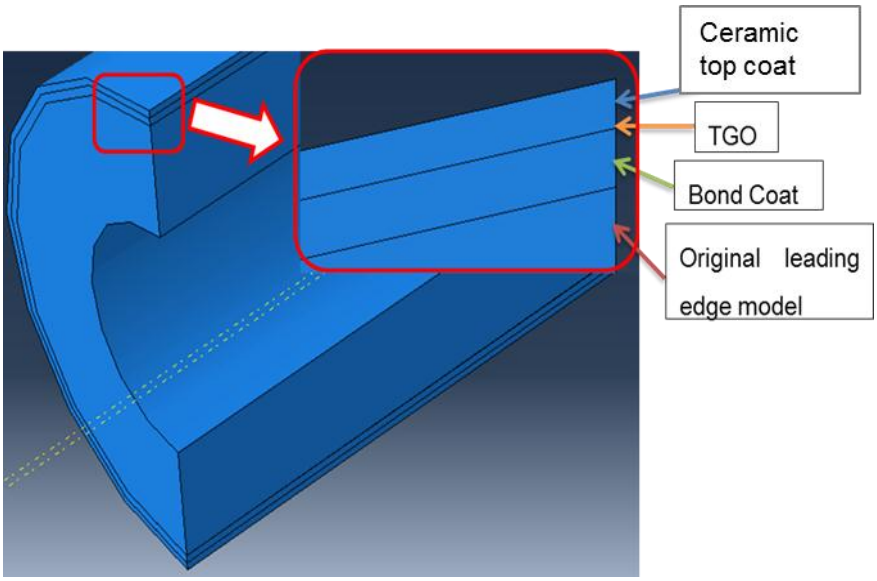

Figure 9-1: FEA TBC model Layout

9.2.1 FEA TBC Thermal Model

The boundary conditions (BCs) for the TBC thermal model are similar to the bare model. However, in the TBC thermal model it is the span wise TBC surface temperature obtained from the heat transfer model that is used. This is applied to the ceramic top coat surface, as shown in Figure 9-2.

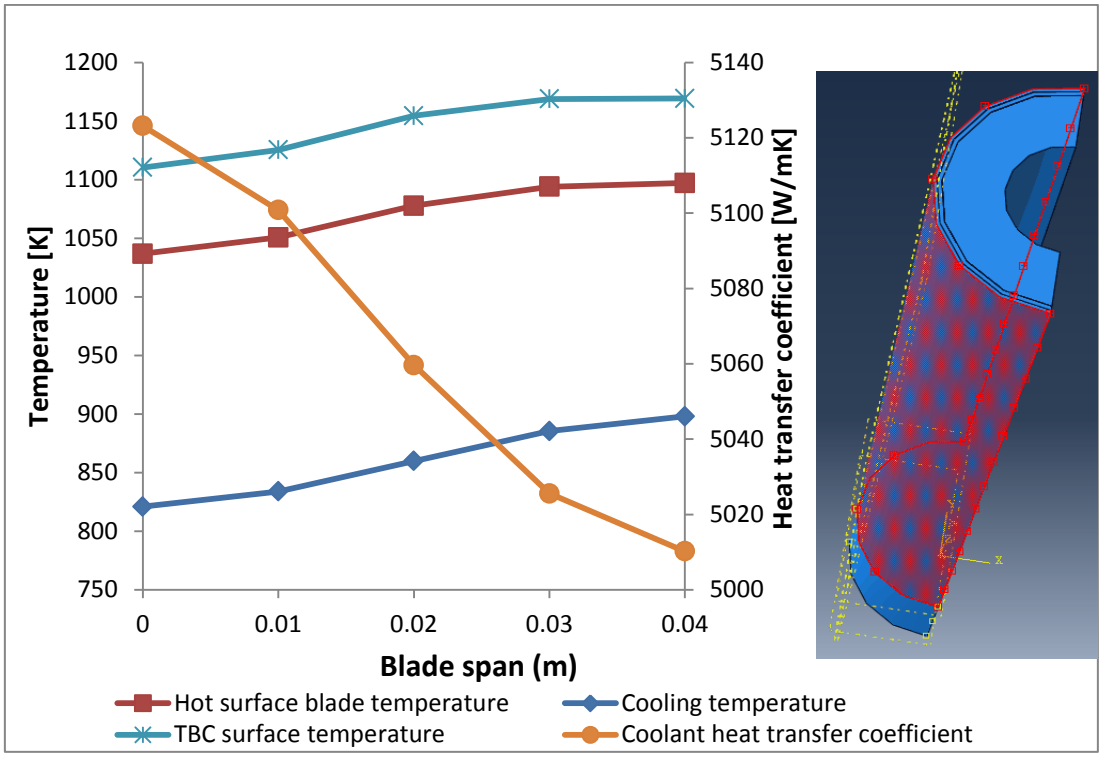

Figure 9-2: Thermal BCs for TBC FEA model

9.2.2 Thermo- Mechanical Model

The same constant rotational body force BC in the bare blade was maintained for the TBC blade model. The change from the bare model is the 'Encastre' constraint that was extended to cover all the layers of the TBC system.

9.3 Impact of TBC on TMF Life

To examine the effects of the TBC addition on blade life, the coated blade TMF life was calculated and compared to that of the bare blade. A linear elastic analysis was assumed for this analysis. Also it was assumed that the bare and coated blades had the same metal surface temperature distribution. Hence, the blade hot side temperature distribution had to be matched for both the bare and coated blade models. This required some iteration in the thermal analysis until the same temperature distribution was obtained for the blade metal hot side of both models. This isolates any influence of temperature; allowing the

investigation of only the TBC thermal expansion stresses on the blade life. Furthermore, this analysis does not account for the cracking or failure of the TBC system, Hence, the blade lives calculated and compared are for the metal surface (substrate) of each of the bare and coated models. It was observed that the blade life improved due to the application of the TBC, in contrast to the bare blade as shown in Figure 9-3.

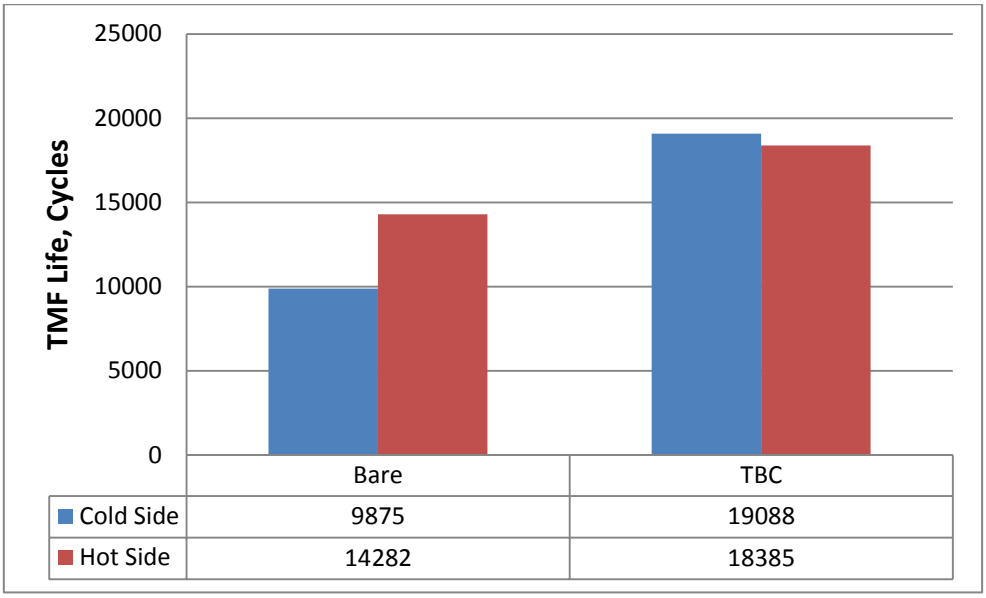

Figure 9-3: Comparison of TMF life for TBC and Bare blade

The increase in the coated blade TMF life could be linked to the impact of the generated strains and associated stresses. The substrate surface of the coated blade model was found to experience reduced strain and stress, when compared to the bare blade model. This is attributed to the opposing expansion of the adjacent TBC layers, which affects the expansion of the attached substrate surface. Compressive stresses are then imposed on the hot side of the substrate of the coated blade; which equilibrates with an opposing tensile stress. The overall compressive stress on the hot side surface in contact with the TBC increases. The increased compressive stresses are beneficial to the blade life, because they are subtracted from the tensile centrifugal stress. Furthermore, the equivalent constraint imposed by the tensile cold side is decreased due to the reduced expansion of the hot side surface interacting with

the cold side. Hence, in the coated blade, the benefits of the increased compressive stresses in the hot side, and the reduction of the cold side thermal stresses led to an improvement in life over the bare blade.

The impact of the reduced stresses can be observed through the blade thickness direction. This is represented by the minimum principal stress (S1) as depicted in Figure 9-4 and Figure 9-5, for the maximum stress at take-off, and the stress variation along the flight path, respectively**.** These results are indicated for a critical node at the root of both the coated and bare blade.

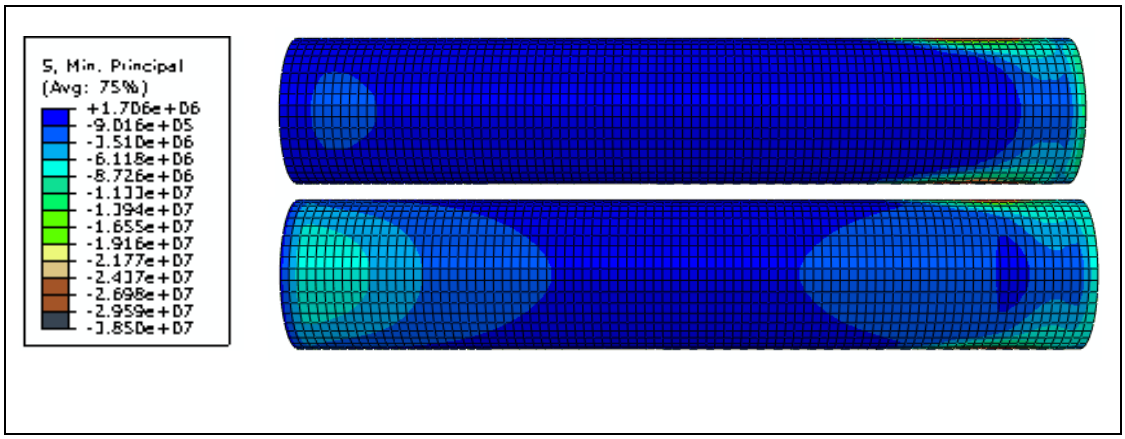

Figure 9-4: Minimum principal stress at take- off phase for bare (top) and TBC (bottom) blade models

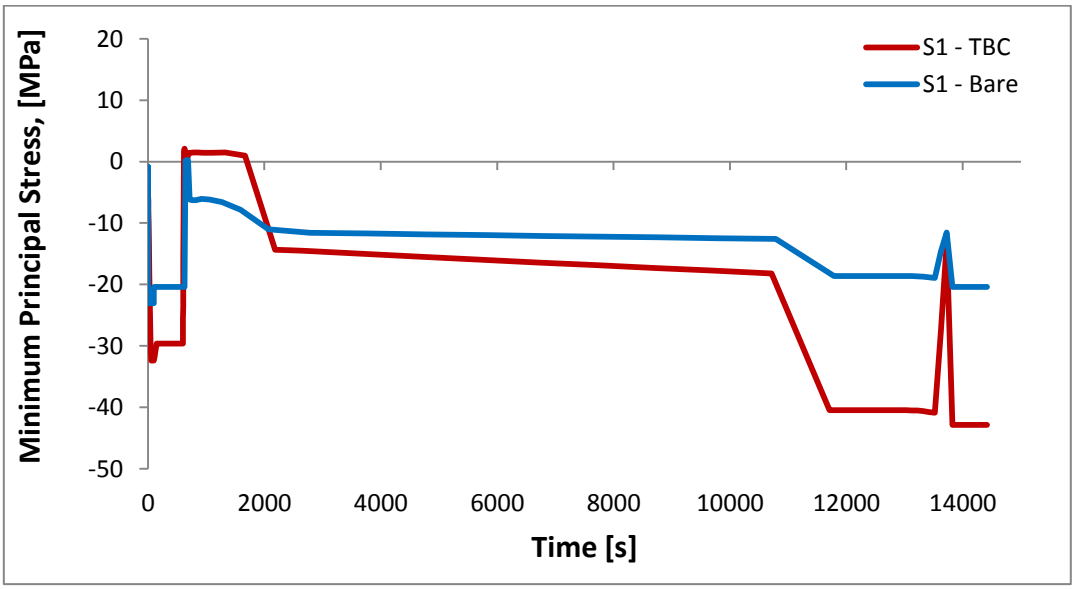

Figure 9-5: Variation of minimum principal stress (S1) along the flight path.

It should be noted different observations have been reported on the impact of TBC on the TMF life of the turbine blade. Bernstein,et al and Heine, et al, [81][56] have reported a decreased life, while others such as Guedou and Honorat [121], have shown that the life could also increase. A further complication is that for the same AM1 SC superalloy material used by Guedou and Honorat[121] [121][123], Chataigner and Remy[122] observed no significant change in the life between bare and coated specimens. Nevertheless, the general view according to Bernstien [81] is that the life reduces due to TBC. This is because the coatings have less ductility than the substrate and begin to crack before the base metal. It is observed that majority of these results have been based on physical testing of coated blade samples. The cracking of the coating or its protective effect becomes an apparent influencing characteristic. Therefore, if the coatings remain intact, as modelled in this research, it is likely that an improved life would result.

9.4 Effect of TBC Thermal Expansion, Conductivity and thickness

Factors such as the thermal conductivity, thermal expansion coefficient and thickness affect the level of thermal protection provided by the TBC system [123]. For instance, a designer could adjust the coating thickness in order to achieve a desired thermal gradient in the turbine blade. However, experiments have shown that TBC failure is highly dependent on the properties of each of its constituent layers. Hence, any changes in these properties would impact the blade life to varying degrees. The following subsections show the potential of the TBC blade model developed in this thesis to examine the impact on blade life due to changes in TBC properties.

9.4.1 Thermal Expansion and Conductivity

The thermal stresses generated by the TBC depend on both the thermal expansion and the conductivity, (which influences the thermal gradient).To optimise a given design for instance, it would be useful for an analyst to identify which of these TBC properties has the dominant effect on the blade life. In this

thesis, the approach used was to calculate the blade life for two cases. First, it was assumed that only thermal expansion affects the blade life and there is no effect of conduction between the TBC and the substrate. Then, it was assumed that only thermal conduction affects the blade life and there is no effect of thermal expansion between the TBC and the substrate. For the first case, the value of the thermal conduction of the substrate was used for the top coat, while keeping the actual coefficient of thermal expansion. In the second case, the value of the coefficient of thermal expansion of the substrate was assigned to the top coat, while maintaining the actual thermal conductivity.

The maximum stress and strains on the blade, due to the individual impacts of thermal conductivity and thermal expansion are summarised in Table 9-1, while Figure 9-6 shows the distribution of the temperature and TMF life along the blade span. The individual impact of thermal conductivity reduces the original blade life by about 40%, while for the effect of only thermal expansion; the blade life reduces by about 8%. Thus the TBC thermal conductivity significantly impacts the TMF life compared to thermal expansion. The impact of thermal conductivity particularly drives the thermal gradient and the resultant strain. Hence, irrespective of the blade expansion, the thermal gradients would drive the overall strain imposed on the blade, as well as the resultant thermal stress. Furthermore, an increase in thermal conductivity will favour an increased thermal gradient, resulting in lower blade lives. This is depicted in Figure 9-7, where, as expected, the blade life progressively reduces with increase in the TBC thermal conductivity from 0.8-1.5 W/m/K.

Table 9-1: Effect of Thermal Expansion and Conductivity on TMF life

Cases	Von Mises Stress (MPa)	Max. Principal Strain (mm)	Thermal Strain (mm)	TMF Life (Cycles)
Actual Thermal Expansion and Conductivity)	317.2	7.89E-03	7.19E-03	18385
Effect of Thermal Expansion	315.0	8.04E-03	7.43E-03	16955
Effect of Thermal Conductivity	323.7	8.63E-03	8.17E-03	11051

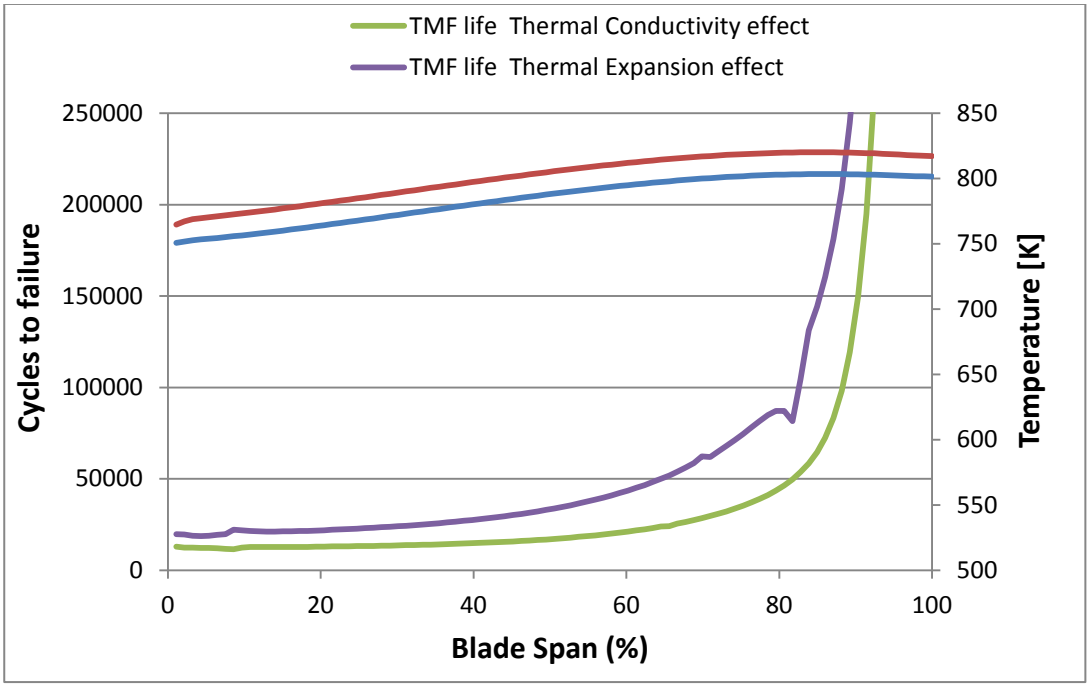

Figure 9-6: Temperature and TMF life distribution for individual impacts of thermal conductivity and thermal coefficient.

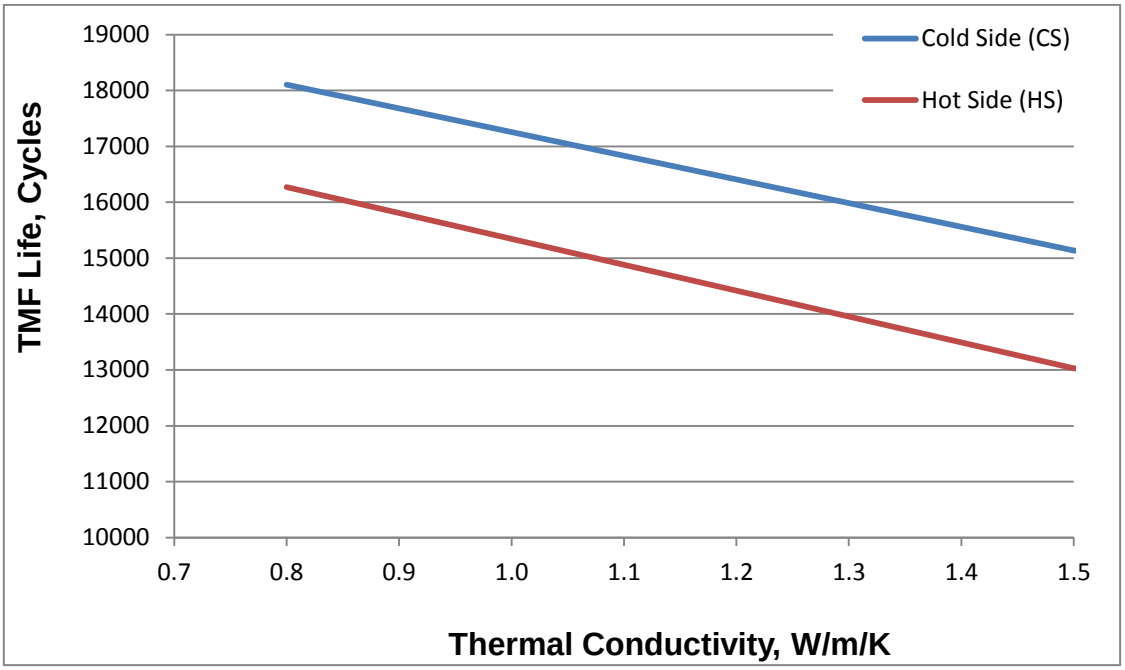

Figure 9-7: TMF life Vs Thermal Conductivity

9.4.2 Effect of TBC Thickness on TMF life

The typical top coat thickness for the electron beam physical vapour deposited (EB-PVD) TBC is 125 µm, while the typical top coat thickness for air-plasma–sprayed (APS) TBC is, 300 µm. In [123] the blade surface temperature was shown to increase as TBC thickness was reduced. Hence, it is expected that the thermal gradients and associated thermal strain/stresses will also increase with reduced TBC thickness, and vice versa. This implies that the blade life should improve as the TBC thickness is increased. Accordingly, Figure 9-8 shows that the blade life increased as the thickness of the TBC was increased from 125 to 300 µm.

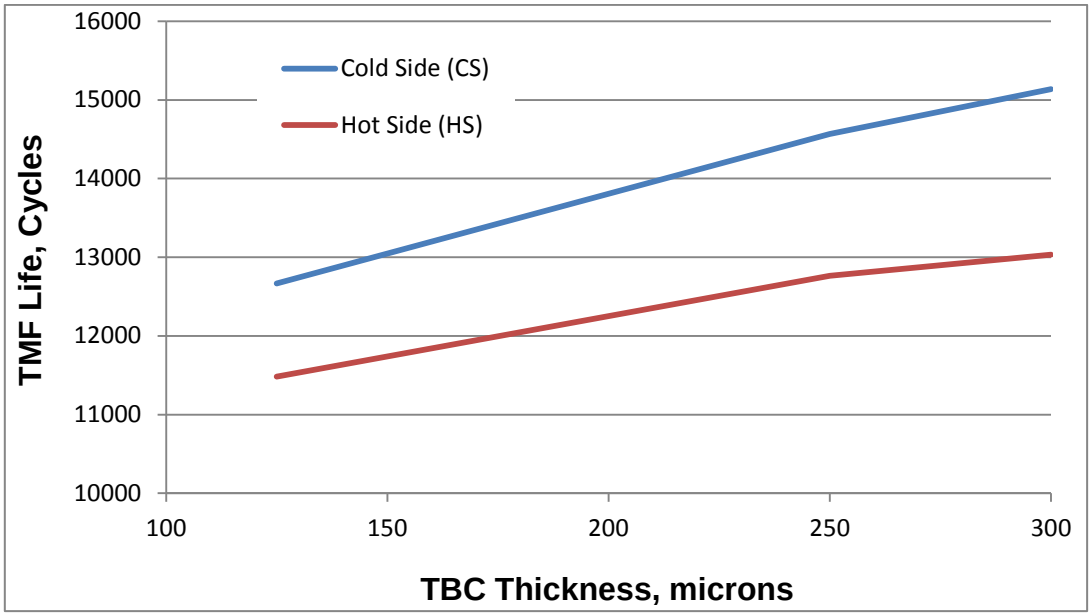

Figure 9-8: TMF life Vs thickness of TBC.

9.5 Chapter Conclusions

The effect of the stresses developed due to the TBC addition could be captured using a FEA model that incorporates the layers of the TBC attached to the substrate. In this research, the TBC FEA model was created from the bare model by including the bond coat, TGO and ceramic top coat layers. The lifing methodology developed in this research was then applied to examine the effects of TBC addition on the blade life. The purpose was to capture the impact on blade life due to the thermo-mechanical stresses generated by the mismatch in thermal expansion between the substrate and the TBC. In addition, the influence of changes in properties of the TBC such as thermal conductivity and TBC thickness (ceramic top coat) were studied.

Majority of the results on the impact of TBC in the literature have been based on physical testing of coated blade samples. How the cracking of the coating or its protective effect is evaluated becomes an apparent influencing factor in determining the life of a coated blade. Therefore, if the coatings remain intact, as modelled in this research, it is likely that an improved life would result.

The current research did not examine the life of the TBC system. Only the influence of the generated strains /stresses due to TBC addition, and the resulting impact on the life of the substrate was examined. This presupposes that the TBC is intact for the coated blade, whereas it has failed in the case of the bare blade. Hence, the analysis of the evolution of the principal stresses and strains in the coated blade gives a plausible explanation for the increased TMF life experienced for the TBC blade model. Nevertheless, recommends that ‘the coatings and substrate must be considered as a single system in order to predict the TMF life of coated turbine blades. To this end, the TMF model developed by kadioghlu and Sehitoghlu[16] for coated turbine blades could be considered. This is beyond the boundaries of this thesis and has been duly recommended for future work.

This research observes that the TBC thermal conductivity significantly impacts the TMF life compared to thermal expansion. The impact of thermal conductivity particularly drives the thermal gradient and the resultant strain. Hence, irrespective of the blade expansion, the thermal gradients would drive the overall strain imposed on the blade, as well as the resultant thermal stress. Furthermore, an increase in thermal conductivity will favour an increased thermal gradient, resulting in lower blade lives.

The blade surface temperature increases as TBC thickness is reduced. Hence, the blade life improves with increase in TBC thickness.

10 CONCLUSIONS AND FUTURE WORK

10.1 Conclusions

One of the major challenges for the development of future higher efficient aero engines is the severe thermal and mechanical loads that the core components have to bear. Especially, the HPT blade that undergoes cyclic variations of both thermal and mechanical loads; resulting in TMF damage. The design parameters and the way the engine is operated affect the severity of the damage of the HPT blade. This would influence the available time on wing, maintenance scheduling and costs. Hence, an appropriate method to assess the impact of the operational and design factors on the blade severity would significantly contribute to enhancing the assessment of turbine blade life.

The aim of this research was therefore to develop a generic Physics based Method for evaluating the influence of design characteristics, technology level and aircraft operating conditions on the life and severity of high pressure turbine blades in jet engines. In order to assess the turbine blade life, the damage due to the combined thermo- mechanical loads needs to be adequately accounted for. This becomes more challenging when detailed component geometry is limited. Therefore, a compromise between the level of geometric detail and the complexity of the lifing method to be implemented would be necessary. This thesis therefore contributes to the development of a lifing approach for aero engine turbine blades that maintains a balance between the necessary level of fidelity and the availability of the design inputs.

The developed approach is based on the engine thermodynamic cycle; as well as incorporating the critical design/technological factors, operational parameters and variable loading cycles that influence the blade TMF. All these were achieved using minimum design inputs, yet maintaining the necessary fidelity.

The developed approach therefore aids design space exploration by enabling improved assessment of the turbine blade durability at preliminary stages. It also would provide a reliable and cost effective means for people who may not be experts in the specific fields, but are involved in gas turbine operations and life assessment (such as performance engineers, maintenance engineers, supervisors and technicians).

The developed methodology comprises six main modules. These are: performance model (aircraft and engine), component sizing, stress model, heat transfer model, FEA model, and TMF damage model. First, the engine performance is done using a representative aero engine and aircraft model. The engine and aircraft performance results provide inputs to the turbine sizing and heat transfer models. Turbine sizing is performed to obtain the basic design dimensions, while a heat transfer analysis gives the spanwise blade metal temperature distribution and heat transfer coefficients across the blade. A sequentially coupled thermal-stress analysis on an idealised blade is then performed with Abaqus FEA software. The FEA was needed to evaluate the variations of temperature along the flight path (thermal transients); the thermal gradients between the hot gas surface and the cooling hole; the thermal induced stresses and the mechanical stresses (due to centrifugal loads). From the FEA stress and strain inputs, the blade life is evaluated based on the Neu-Sehitoglu TMF damage model. The model implicitly and explicitly captures the damage due to creep, low cycle fatigue and oxidation. The model also accounts for the phasing of temperature and mechanical strain, which dictate the damage, induced in the turbine blade. Furthermore, material properties and TMF model parameters form major inputs to the approach

The developed approach enabled the severity analysis of operational, design and technological parameters that significantly affect the life of aero engines. The potential of the approach to examine the impact of TBC was also explored.

10.1.1 Summary of Findings

Turbine Blade Lifing and Heat Transfer.

- Most lifing prediction methods will involve thermal and stress analysis, either by use of analytical or numerical tools to obtain the thermal and mechanical loads of the hot section component. Then a suitable damage model would be applied to predict the remaining life of the component.
- The accuracy of the life prediction would depend on the selection of the appropriate damage mechanisms. A right balance between the available inputs and the level of fidelity required is paramount to achieving an adequate blade life assessment.
- Accurate determination of the turbine blade temperature distribution and heat transfer is very crucial to turbine blade lifing assessments. Precluding advanced numerical heat transfer analysis, such as CFD, an adequate heat transfer analysis can be achieved using analytical models that account for salient blade design parameters and internal geometry of the blade.

Thermo-Mechanical Fatigue.

- As a result of the cyclic thermal and mechanical loads experienced by the turbine blade, thermo-mechanical fatigue is identified as the main damage mechanism affecting the life of the blade.
- TMF is influenced by the thermal gradients, thermal transients, the strain – temperature phasing and the effect of coatings among other factors. Accounting for these effects, as well as the interaction of creep, fatigue and oxidation mechanisms is essential in the TMF life prediction of the turbine blade.
- The Neu/Sehitoglu model is identified as a general TMF model that accounts for arbitrary temperature- strain phasing, strain rate, mechanical strain range and the accumulation of damage due to the influence of creep, fatigue and oxidation. Although the model requires

several parameters to implement, it has found wide application because of its reported accuracy.

Integrated Lifing Approach

- The impact of the thermal gradients and transients, as well as the mechanical loads experienced by the turbine blade are identified as key parameters and accounted for in the developed lifing method. .

- Using minimum design inputs, the developed lifing method successfully integrates a performance model (aircraft and engine), component sizing, stress model, heat transfer model, FEA model, and a TMF damage model to enable the evaluation of the effects of operational and design factors on blade life.

- Eshati's heat transfer model is employed to give the temperature distribution and heat transfer coefficients along the blade hot surface and cooling hole. The model was enhanced in this research to give the time dependent variation of the temperature and heat transfer coefficients along a flight path, necessary to account for the thermal transients. This was achieved by linking the heat transfer model variables to the aircraft performance outputs throughout a flight segment obtained from Hermes.

- An idealised blade geometry was created, which incorporates the cooling hole and root fixing as key features for thermal-stress FEA analysis. The model is divided into the hot gas side (HS) in contact with the combustor and the cooling hole surface (CS).

Tools and Models

- From the engine and aircraft performance simulation, a set of basic aero-thermal data inputs were derived and applied as inputs to an enhanced heat transfer model. The outputs from the heat transfer model are used as thermal BCs for the FEA.

- The thermal BCs are time dependent span wise metal temperature distribution for the blade hot side, and the cooling air temperature and heat transfer coefficients for the cold side. These are applied as 3rd order polynomial correlations in the thermal FEA model.

- The results of the thermal FEA are verified by comparing with the temperature profiles from the analytical heat transfer model. From these temperature distributions the variation of thermal gradients along the blade span and throughout the given flight are captured. These bring about associated thermal stresses that are fundamental to any TMF assessments.

- To generate the thermo-mechanical loads, the blade temperature distribution calculated from the FEA thermal model is used as input For the FEA thermo-mechanical stress analysis. In addition, a rotational body force equivalent to the HPT shaft speed is applied to generate the centrifugal stress.

- The FEA stress results are verified with the hand calculations from the analytical stress model, as well as quantitative and qualitative assessment of the separately applied stress and thermal loads.

- The blade thermo-mechanical stress distribution shows the highest stress occurring in the root and progressively reducing along the blade span. The thermal stress was identified to be critical in the evolution of the overall blade stresses.

- The blade cold side experienced more thermo- mechanical stress. This is because the thermal stresses generated are predominantly tensile in the cold side, while compressive in the hot side. Hence, while the hot side stress are subtracted from the centrifugal stress. The tensile cold side stresses are added; giving a higher stress distribution in the cold side. These counteracting thermal stresses influence the blade TMF life, as well as the impact of the dominant damage mechanisms.

- Using the N/S TMF model, the blade TMF life calculated is conservative compared to IF methods (coffin-manson and LMP).
- The oxidation damage is the main mechanism driving the blade TMF life, while the blade cold side was identified as the critical damage region.

Geometry and Method Verification

- The turbine blade leading edge had to be simplified due to: limitation of design inputs; need to reduce the complexity and computational cost of modelling; ease of modification for design studies and sensitivity analyses, as well as to meet the generic requirement of the blade life assessment approach.
- Six basic cylindrical and elliptical shaped models were therefore created, incorporating critical features such as the cooling hole and root fixing.
  The developed methodology was then applied using each of the models to investigate the influence of the choice of shape on the lifing assessment.
- The results indicate that the variation in temperatures and CF stresses are negligible, while the thermal-mechanical stress varies within a maximum factor of 1.06.
- TMF lives calculated for the various geometries are within a maximum relative factor of 1.3. This is considered a very good agreement; giving that In lifing studies, It is generally acceptable to have variation in life estimates up to a factor of +/-2.
- The use of the idealised geometry was verified by comparing with a detailed NASA E3 blade model. The TMF life obtained from the idealised geometries could vary within a relative factor of 1.3, when compared with the use of detailed blade geometry.
- The results therefore suggest that the selection of a particular shape would not severely affect the TMF life prediction using the developed approach. What would be more significant is accurate definition of the thermal and stress boundary conditions. Hence, provided the blade

temperature distribution and applied loads could be accurately determined, any similar geometry to the idealised ones in this work would give adequate lifing results

Influence of TMF Model Material Parameters

- In addition to 4 earlier reported parameters, the environmental shape factor (ξ_{ox}), which is a phasing constant, was identified as critical to TMF life assessment of aero engines. The other four parameters are; the strain rate sensitivity constant (*b),* activation energy for oxidation (Q_{ox}) and activation energy for γ' depletion ($Q_{\gamma'}$) and time exponent (*β).*

- The impact of a deviation in TMF parameters has more influence on damage severity than changes in the operating conditions considered (TET and PCN).
- Using a given set of TMF parameters, the same severity characteristics can be predicted for different operating conditions. This is very useful at the preliminary design stages were design choices in operating parameters such as TET and PCN could be investigated in terms of severity with some degree of certainty.

Case Studies

- The effects of engine operational parameters such as TO derate, trip length and OAT investigated using the developed methodology reveal:
    - Higher severity results compared to similar study that used Isothermal based lifing methods.
    - Damage on the blade reduces and the severity decreases with increasing TO derate. However, below a certain temperature and stress limit, not much benefit will be further derived from derate at take-off.

- The shorter flight lengths show more damage severity than longer flight lengths. Irrespective of flight length, applying take- off derate is beneficial in reducing the damage severity.
- Engines operated in higher OAT environment will experience more damage severity. The use of take-off derate at airports with high OAT would help reduce the severity, but, applying higher percentage of TO derate would be marginally beneficial at lower OATs.

- The developed approach was found eminently capable to conduct relative blade life and severity assessment; as well sensitivity case studies – particularly, at the conceptual design stages where very little information is available about the component.
- For the design parameters different RTDF, TET, and cooling effectiveness (ε) were investigated:
  - The blade severity increased as RTDF was increased. The severity also increased as cooling effectiveness was reduced. The critical region remained the cold side as the blade life reduced with reduction in cooling effectiveness.
  - Increasing the TET increased the severity impact of the damage mechanisms and reduced the blade life accordingly. However, creep started to drive the total failure at higher TETs, compared to the effects of fatigue and oxidation.

TBC Modelling and Analysis

- The influence of TBC on blade TMF is complex and contrasting results abound in the literature. Invariably, how the cracking of the coating or its protective effect is evaluated becomes an apparent influencing characteristic.
- The capability of the developed model to examine the influence of TBC on the blade TMF life was explored. The TBC FEA model was created

from the bare model by including the bond coat, TGO and ceramic top coat layers.

- This research shows the increase in the TMF life due to addition of TBC. The increased life could be attributed to the reduced thermo-mechanical stresses on the blade substrate due to the constraints (inducing compressive stresses on the substrate surface) imposed by the TBC layers.
- It was observed that the TBC thermal conductivity significantly impacts the TMF life compared to thermal expansion. The impact of thermal conductivity particularly drives the thermal gradient and the resultant strain. Hence, irrespective of the blade expansion, the thermal gradients would drive the overall strain imposed on the blade, as well as the resultant thermal stress.
- The recognised increase in blade life due to a reduction in TBC thermal conductivity and increase in TBC thickness was also demonstrated using the developed lifing approach.

10.2 Future Work

The method developed in this research is a generic but robust approach for the life assessment of HP turbine blades. Despite the simplifications made, the method significantly captures the main physics involved in TMF life assessment of turbine blades. The following are areas for further work using the developed approach:

TBC Modelling

Thermal stresses arise because of the different thermal expansion between the substrate and the various layers of the TBC. Therefore, the interactions between the various layers of the TBC needs to be critically examined and modelled accurately.In the present work, the TBC modelling was implemented to analyse the impact on the thermal and mechanical stresses on the substrate. For the future, it would important to examine the life and thermo-mechanical

behaviour of the TBC and the combination of the TBC-substrate as a whole. The model of Kadioglu and Sehitoglu[16] is suggested as a starting point for this .

Film Cooling Implementation

The impact of film cooling holes on the structure of the blade is an area of current concern. The film cooling holes impose stress concentrations on the blade and the interaction of the film cooling air and hot gases would affect the magnitude of thermal gradients generated. It is therefore expected that the thermo-mechanical stress distributions would change due to the film cooling holes.

This could be implemented for the idealised leading edge model in this thesis by either incorporating series of film cooling holes or using one cooling slot as shown in Figure 10.1 and 10.2 respectively. Tinga et al, [28][28][28] has used the cooling slot successfully for analysing a detailed blade and Cunha et al,[124] implemented the cooling slot for idealised trailing edge geometries.

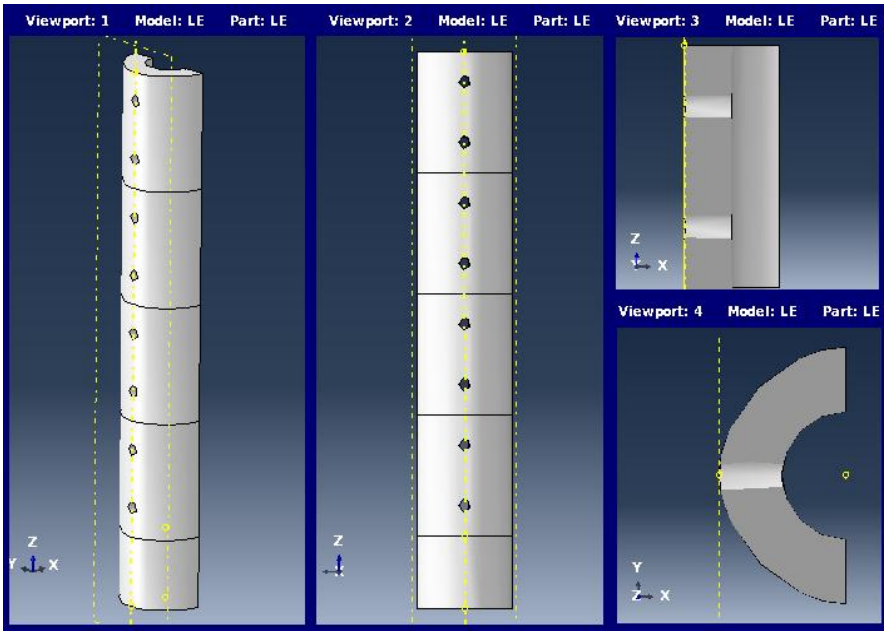

Figure 10-1: Proposed geometry for film cooling addition.

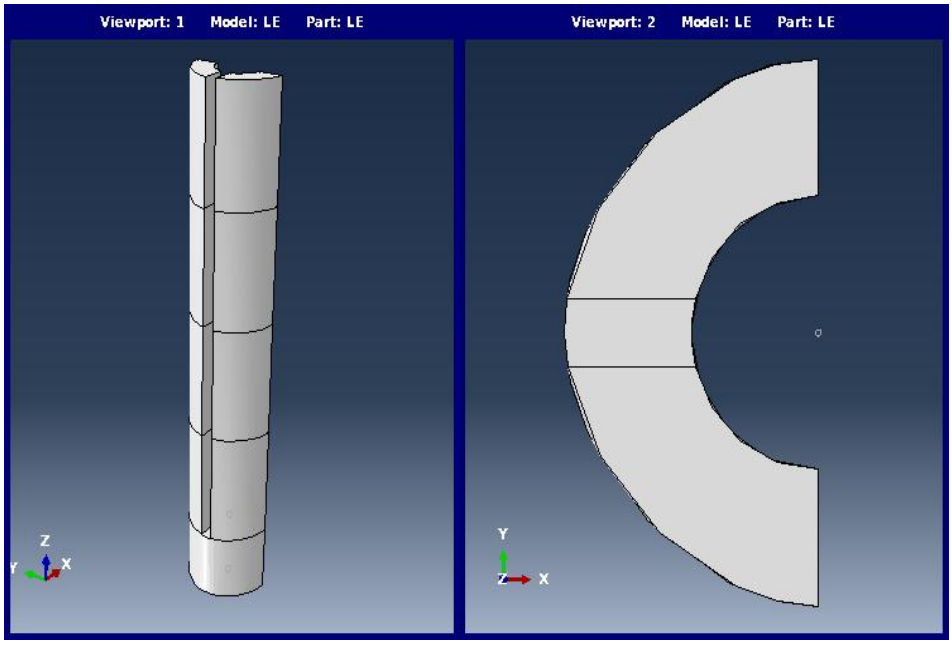

Figure 10-2: Film cooling holes simplified with a slot.

Engine maintenance cost

The engine maintenance cost is an increasingly significant input to engine purchase decisions and is considered one of the major cost drivers. Since the actual engine usage has been identified as a key driver to engine maintenance costs, the relative effect of operational usage can be assessed by severity factors as demonstrated in this thesis. Hence, the impact of factors such as thrust ratings, engine age and operating environment that affect the useable life and deterioration rates of engine components can be represented as severity factors. These severity factors can be factored into maintenance cost calculations to better account for maintenance demand due to actual operation and enable more accurate shop visit predictions.

REFERENCES

[1] Harrison, G. F., Tranter, P. H. and Williams, S. J. (1995), "Modelling of thermomechanical fatigue in aero engine turbine blades", *81st Meeting of the AGARD SMP Panel,* AGARD, Banff, Canada, pp. 16-1 – 16-8.

[2] Boismier, D. A. (1988), *Thermo-mechanical fatigue mechanisms and life prediction for Mar-M247 nickel-based superalloy,* (M.S Thesis), University of Illinois at Urbana-Champaign, Illinois.

[3] Amaro, R. L., Antolovich, S. D., Neu, R. W. and Staroselsky, A. (2010), "On thermo-mechanical fatigue in single crystal Ni-base superalloys", *10th International Fatigue Congress, Fatigue 2010,* Vol. 2, 6-11 June 2010, Prague, pp. 815-824.

[4] Spera, D. A. (1972), *Comparison of experimental and theoretical thermal fatigue lives for five nickel-base alloys*, vol. NASA TM X-68051.

[5] Lupinc, V. (1981), "Creep:Introduction and phenomenology", in *Creep and Fatigue in High Temperature Alloys,* Applied Science Publishers Ltd, Essex, pp. 7-11.

[6] Haslam, A. (2011), *Fatigue and Fracture lecture notes,* Cranfield University, Cranfield,England.

[7] Boyer, H. E. (1988), *Atlas of creep and stress-rupture curves,* ASM International.

[8] Leinster, M. G. (2008), "A method of creep rupture data extrapolation based on physical processes", *International Journal of Pressure Vessels and Piping* vol. 85, no. 10, pp. 701-710.

[9] Viswanathan, R. (1989), *Damage mechanisms and life assessment of high-temperature components,* ASM International, Metals Park, Ohio.

[10] Haslam, A. S. and Cookson, R. A. (2008), *Mechanical Design of Turbomachinery, MSc course notes,* Cranfield University, Cranfield, England.

[11] Nissley, D. M. (1995), "Thermomechanical fatigue life prediction in gas turbine superalloys - A fracture mechanics approach", *AIAA Journal,* vol. 33, no. 6, pp. 1114-1120.

[12] Coffin, L. F. (1969), "Prediction parameters and their application to high temperature low - cycle fatigue", *Proceedings of Second International Conference on Fracture,* Brighton, London, Chapmans Hall, pp. 643-654.

[13] Hanumanthan, H., Stitt, A., Laskaridis, P. and Singh, R. (2012), "Severity estimation and effect of operational parameters for civil aircraft jet engines", Proceedings of the Institution of Mechanical Engineers, Part G: *Journal of Aerospace Engineering,* vol. 226 no. 12 1544-1561.

[14] Manson, S. S. and Halford, G. (1967), *A method of estimating high temperature low cycle*, vol. NASA TM X-52270.

[15] Romeyn, A. (2006), *ATSB transport Safety Investigation Report: Additional Analysis of left Engine Failure VH - LQH,*, Australian Transport Safety Bureau.

[16] Kadioglu, Y. and Sehitoglu, H. (1993), "Modeling of thermomechanical fatigue damage in coated alloys", *Proceedings of the Symposium on Thermomechanical Fatigue Behavior of Materials,* 14-16 October 1991, San Diego, CA, USA, ASTM, pp. 17-34.

[17] Kadioglu, Y. and Sehitoglu, H. (1993), "Modeling of thermomechanical fatigue damage in coated alloys" *ASTM Special Technical Publication*, no. 1186, pp. 17-34.

[18] Izquierdo, A. (2010), *A review of suitable oxidation models for aero gas turbine engines,* (unpublished MSc thesis), Cranfield University.

[19] Swaminathan, V. P., Allen, J. M. and Touchton, G. L. (1997), "Temperature Estimation and Life Prediction of Turbine Blades Using Post-Service Oxidation Measurements", *Journal of Engineering for Gas Turbines and Power, ASME,* vol. 119, no. 4, pp. 922-929.

[20] Fatemi, A. and Yang, L. (1998), "Cumulative fatigue damage and life prediction theories: a survey of the state of the art for homogeneous materials", *International Journal of Fatigue,* vol. 20, no. 1, pp. 9-34.

[21] Richard, M. C. (2008)*, Cumulative damage leading to fatigue and creep failure for general materials*, available at: http://www.failurecriteria.com/Media/Cumulative_Damage_Leading_to_Fatigue_and_Creep_Failure_for_General_Materials.pdf (accessed 14 December 2013).

[22] ETBX (2013)*, Miners rule*, available at: http://www.fea-optimization.com/ETBX/miner_help.html (accessed10 December 2013).

[23] Zhimin, L., Mavris, D. N. and Volovoi, V. V. (2001), "Creep life prediction of gas turbine components under varying operating conditions", *ASME International Joint Power Generation Conference,* June 4-7, New Orleans, Louisiana.

[24] Zhimin, L., Vitali, V. and Dimitri, N. M. (2002), "Probabilistic remaining creep life assessment for gas turbine components under varying operating conditions", *43rd AIAA/ASME/ASCE/AHS/ASC Structures, Structural Dynamics, and Materials Conference,* 22-25, April, Denver, Colorado.

[25] Wallace, J. M. and Dimitri, N. M. (2003), "Creep life uncertainty assessment of a gas turbine airfoil", *Proceeding of 4th AIAA Non-Determinstic Approaches Forum,* 7-10, April, Norfolk, Virginia.

[26] Harris, J. (2001), "Fuzzy logic methods in fatigue and creep", *The Journal of Strain Analysis for Engineering Design,* vol. 36, no. 4, pp. 411-420.

[27] Philip Chen, C. L., Kim, J. and Guo, T. H. (2006), "Monte Carlo Simulation for System Damage Prediction: An Example from Thermo - Mechanical Fatigue (TMF) Damage for a turbine Engine", *Proceedings of the 2006 IEEE/SMC international Conference on System of Systems Engineering,* 26-28, April 2006, Los Angeles, California, pp. 30-34.

[28] Tinga, T., Visser, W. P. J., DE wolf, W. B. and Broomhead, M. J. (2000), *Integrated lifing analysis tool for gas turbine components,* NLR-TP-2000-049, National Aerospace Laboratory NLR.

[29] Tinga, T., De Wolf, W. B., Visser, W. P. J. and Woldendorp, S. (2001), "Integrated Lifing Analysis of a Film-Cooled Turbine Blade", *RTO-AVT Symposium on Monitoring and Management of Gas Turbine Fleets for Extended Life and Reduced Costs,* NATO Research and Technology, Manchester, UK, .

[30] Naeem, M., Singh, R. and Probert, D. (2001), "Consequences of aero-engine deteriorations for military aircraft", *Applied Energy,* vol. 70, no. 2, pp. 103-133.

[31] Naeem, M., Singh, R. and Probert, D. (1998), "Implications of engine deterioration for creep life", *Applied Energy,* vol. 60, no. 4, pp. 183-223.

[32] Pascovici, D. S. (2008), *Thermo economic and risk analysis for advanced long range aero engines* (PhD thesis), Cranfield University, Cranfield, England.

[33] Suria, O. V. (2006), *A Flexible Lifing Model for Gas Turbines:Creep and Low Cycle Fatigue Approach* (MSc thesis), Cranfield University, Cranfield, England.

[34] Wu, F. E. (1994), *Aero Engine's Life Evaluated for Combined Creep and Fatigue, and Extended by Trading-off Excess Thrust* (PhD thesis), Cranfield University, Cranfield, England.

[35] Koehl, M. (2011), *Algorithimic Aero Engine Usage Monitoring Based on Reference Analysis of Design Mission*, available at: http://www.mtu.de/en/technologies/engineering_news/development/Koehl_Algorithmic_aero_engine_en.pdf (accessed 17 January 2012).

[36] Corran, R. S. J. and Williams, S. J. (2007), "Lifing Methods and Safety Criteria in Aero Gas Turbines", *Engineering Failure Analysis,* vol. 14, no. 3, pp. 518-528.

[37] Rubini. (2008), *Turbine Blade Cooling* ,(unpublished MSc Lecture Notes), Cranfield University.

[38] Eshati, S. (2011), *An Evaluation of Operation and Creep life of Stationary Gas Turbine Engine* (PhD thesis), Cranfield University, Cranfield England.

[39] Han, J. and Wright, L., M. (2012), *Enhanced Internal Cooling of Turbine Blades and Vanes*, available at: http://www.netl.doe.gov/technologies/coalpower/turbines/refshelf/handbook/4.2.2.2.pdf (accessed 20 February, 2012).

[40] Padture, N. P., Gell, M. and Jordan, E. H. (2002), "Thermal Barrier Coatings for Gas-Turbine Engine Applications", *Science,* vol. 296, no. 5566, pp. 280-284.

[41] Nissley, D. M. (1997), "Thermal Barrier Coating Life Modeling in Aircraft Gas Turbine Engines", *Journal of Thermal Spray Technology,* vol. 6, no. 1, pp. 91-98.

[42] Brett, S. (2005), *Residual Life Assessment And Microstructure,* AC/MC/93, ECCC, Italy.

[43] Torbidoni, L. and Horlock, J. H. (2005), "A New Method to Calculate the Coolant Requirements of a High-Temperature Gas Turbine Blade", *Journal of Turbomachinary,* vol. 127, no. 1, pp. 191-199.

[44] Eshati, S., Abu, A., Laskaridis, P. and Khan, F. (2013), "Influence Of Water–Air Ratio On The Heat Transfer And Creep Life Of A High Pressure Gas Turbine Blade", *Applied Thermal Engineering,* vol. 60, no. 1–2, pp. 335-347.

[45] Ainley, D. G. (1957), *Internal Air-Cooling for Turbine Blades a General Design Survey,* 3013, Aeronautical Research Council Reports and Memo, London.

[46] Halls, A. G. (1967), "Air Cooling of Turbine Blades and Vanes an account of the history and development of gas turbine cooling", *Aircraft Engineering,* vol. 39, no. 8, pp. 4-14.

[47] Holland, M. J. and Thake, T. F. (1980), "Rotor Blade Cooling in High Pressure Turbine", *Journal of Aircraft,* vol. 17, no. 6, pp. 412-418.

[48] Consonni, S. (1992), *Performance Prediction of Gas/Steam Cycles for Power Generation,*(PhD Thesis), Princeton University, Princeton, USA.

[49] Young, B. J. and Wilcock, C. R. (2002), "Modelling the Air-Cooled Gas Turbine: Part 1-General Thermodynamics", *Journal of Turbomachinary,* vol. 124, no. 2, pp. 207-213.

[50] Young, J. B. and Wilcock, R. C. (2002), "Modeling the Air-Cooled Gas Turbine: Part 2-Coolant Flows and Losses", *Journal of Turbomachinary,* vol. 124, no. 2, pp. 214-222.

[51] Torbidoni, L. and Massardo, F. A. (2004), "Analytical Blade Row Cooling Model for Innovative Gas Turbine Cycle Evaluations Supported by Semi-Empirical Air-Cooled Blade Date", *Journal of Engineering for Gas Turbines and Power,* vol. 3, no. 126, pp. 498-506.

[52] Torbidoni, L. and Horlock, J. H. (2005), "A New Method to Calculate the Coolant Requirements of a High-Temperature Gas Turbine Blade", *Journal of Turbomachinary,* vol. 127, no. 1, pp. 191-199.

[53] Horlock, J. H. and Torbidoni, L. (2006), "Turbine Blade Cooling: The Blade Temperature Distribution", *Journal of Power and Energy,* vol. 220, pp. 343-353.

[54] Eshati et al (2012), "The influence of humidity on the creep life of a high pressure gas turbine blade: Part I Heat Transfer Model, GT2012- 69445", ASME Turbo Expo, Copenhagen, Denmark.

[55] Antolovich, S. D. and Saxena, A. (2002), Thermomechanical fatigue: Mechanisms and practical life analysis, *Failure Analysis and Prevention*, Vol 11, *ASM Handbook*, ASM International, pp. 738–745.

[56] Heine, J. E., Warren, J. R. and Cowles, B. A. (1989), *Thermal Mechanical Fatigue of Coated Blade Materials,* WRDC-TR-89-4027, United Technologies Corporation, Pratt & Whitney.

[57] Zhuang, W. Z. and Swansson, N. S. (1998), *Thermo-Mechanical Fatigue Life Prediciton A Critical Review,* DSTO-RR-0609.

[58] Sehitoglu, H. (1992), "Thermo-mechanical fatigue life prediction methods", *Advances in Fatigue Lifetime Predictive Techniques,* 24 April 1990, San Francisco, CA, ASTM international, pp. 47-76.

[59] Antolovich, S. D., Amaro, R. L., Neu, R. W. and Staroselsky, A. (2011), "On the Development of physically Based life Prediction models in the Thermo Mechanical fatigue of Ni-base Superalloys", *Key Engineering Materials,* vol. 465, pp. 47-54.

[60] Beck, H., et al. (2006), "Thermo-mechanical Fatigue – the route to standardisation ("TMF - Standard" project)", *Materials and Corrosion, Vol.57, pp.53-59.*

[61] Halford, G. R., et al. (1992), "Thermomechanical and Bithermal Fatigue Behavior of cast b1900+hf and wrought haynes 188 ", in Mitchel, M. R. and landgraf, R. W. (eds.) *Advances in Fatigue Lifetime Predictive Techniques,* ASTM, STP 1122 ed, American Society for Testing and Materials, , pp. 120-142.

[62] Ziebs, J., Meersmann, J., Kuhn, H. J. and Klinglehöffer, H. (2000), "Multiaxial thermo-mechanical deformation behavior of in 738 LC and SC16", in Sehitoglu, H. and Maiers, H. J. (eds.) *Thermo-Mechanical Fatigue Behavior of Materials,* Third volume ASTM STP1371 ed, American Society for Testing and Materials, , pp. 257-278.

[63] Kalluri, S. and Bonacuse, P. J. (1997), "An Axial -Torsional, Thermomechanical Fatigue Testing Technique", in Kalluri, S. and Bonacuse, P. J. (eds.) *Multi Axial Fatigue and Deformation Testing Techniques,ASTM STP1280,* American Society for Testing and Materials, , pp. 184-207.

[64] Kraft, S., Zauter, R. and Mughrabi, H. (1993), "Aspects of High-Temperature Low-Cycle Thermomechanical Fatigue of a Single Crystal Nickel-Base Superalloy", *Fatigue & Fracture of Engineering Materials & Structures,* vol. 16, no. 2, pp. 237-253.

[65] Remy, L. (2003), "Thermal-mechanical fatigue (including thermal shock)", in *Comprehensive Structural Integrity,* Vol 5, Elsevier Applied Science Publishers, pp. 113-199.

[66] Martinez-Esnaola, J. M., Arana, M., Bressers, J., Timm, J., Martin-Meizoso, A., Bennett, A. and Affeldt, E. E. (1996), "Crack Initiation in an Aluminide Coated Single Crystal During Thermomechanical Fatigue", *ASTM Special Technical Publication,* vol. 1263, pp. 68-81.

[67] Hales, R. (1983), "A Method of Creep Damage Summation Based on Accumulated Strain For The Assessment Of Creep-Fatigue Endurance",

Fatigue & Fracture of Engineering Materials & Structures, vol. 6, no. 2, pp. 121-135.

[68] Saxena, A. and Bassani, J. L. (1984), "Time Dependent Fatigue Crack Growth Behaviour at Elevated Temperature", in Wells, J. M. and Landes, J. D. (eds.) *Fracture: Interactions of Microstructure, Mechanisms and Mechanics,* TMS-AIME, pp. 357-383.

[69] Lasalmonie, A., Pellerin, F. and Fournier, d. (1996), "Thermomechanical fatigue in gas turbine engines: the reasons of a concern", in *Thermal Mechanical Fatigue of Aircraft Engine Materials,* AGARD, , pp. 1.1-1.2.

[70] Fleury, E. and Remy, L. (1991), "Behavior of nickel-base superalloy single crystals under thermal-mechanical fatigue", *Fatigue and Fracture of Engineering Materials and Structures,* vol. 14, no. 1, pp. 115-129.

[71] McDowell, D. L., Antolovich, S. D. and Oehmke, R. L. T. (1992), "Mechanistic considertaions for TMF life predicntion of nickel-base superalloys", *Nuclear Engineering and Design,* vol. 133, pp. 383-399.

[72] Miller, M. P., McDowell, D. L., Oehmke, R. L. T. and Antolovich, D. D. (eds.) (1993), *Life Prediction Model for Thermomechanical Fatigue Based on Microcrack Propagation,* ASTM STP 1186 ed, American Society for Testing and Materials.

[73] Sehitoglu, H. and Boismier, D. A. (1990), "Thermo-mechanical fatigue of Mar-M247. Part 2. Life prediction", *Journal of Engineering Materials and Technology, Transactions of the ASME,* vol. 112, no. 1, pp. 80-89.

[74] Cai, C., Liaw, P. K. and Ye, M. Y. J. (1999), *Recent Developments in the Thermomechanical Fatigue Life Prediction of Superalloys*, available at: http://www.tms.org/pubs/journals/JOM/9904/Cai/Cai-9904.html (accessed 27 September, 2008).

[75] Christ, H., Jung, A., Maier, H. J. and Teteruk, R. (2003), "Thermomechanical Fatigue-Damage Mechanisms and Mechanism-Based Life Prediction Methods", *Sadhana - Academy Proceedings in Engineering Sciences* vol. 28, no. 1&2, pp. 147-165.

[76] Chaboche, J. L. and Lesne, P. M. (1988), "A Non-Linear Continuous Fatigue Damage Model", *Fatigue & Fracture of Engineering Materials & Structures,* vol. 11, no. 1, pp. 1-17.

[77] ASME (1994), *Rules for Construction of Nuclear Power Plant Components,* ASME Boiler and Pressure Vessel Code: Section 3, ASME.

[78] Halford, G. R. and Manson, S. S. (1976), "Life Prediction of Thermal - Mechanical Fatigue Using Strain Range Partitioning", in Spera, A. and Mowbray, D. F. (eds.) *Thermal Fatigue of Materials and Components,* ASTM STP 612, American Society for Testing and Materials, pp. 239-254.

[79] Zamrik, S. Y. and Renauld, M. L. (2000), "Thermo-mechanical out-of-phase fatigue life of overlay coated in-738lc gas turbine material", *In Thermo-Mechanical Fatigue Behavior of Materials, ASTM,* vol. 3, pp. 119-137.

[80] Ellison, E. G. and Al-Zamily, A. (1994), "Fracture And Life Prediction Under Thermal-Mechanical Strain Cycling", *Fatigue & Fracture of Engineering Materials & Structures,* vol. 17, no. 1, pp. 53-67.

[81] Bernstein, H. L., Grant, T. S., McClung, R. C. and Allen, J. M. (1993), “Prediction of Thermal-mechanical Fatigue life for Gas Turbine Blades in Electric Power Generation. (1993), 212–238.", in Sehitoglu, H. (ed.) *Thermo-mechanical Fatigue Behavior of Materials, ASTM STP 1186,* American Society for Testing and Materials, , pp. 212-238.

[82] Woodford, D. A. and Mowbray, D. F. (1974), "Effect of Material Characteristics and Test Variables on Thermal Fatigue of Cast Superalloys. A Review ", *Materials Science and Engineering,* no. 16, pp. 5-43.

[83] Halford, G. R., Lerch, B. A. and Arya, V. K. (2000), "Thermal Strain Fatigue Modelling of a Matrix Alloy for a Metal Matrix Composite", in Sehitoglu, H. and Maier, H. J. (eds.) *Thermomechanical fatigue Behaviour of Materials,* volume 3 ASTM STP 1371 ed, pp. 186-203.

[84] Koberl, H., Winter, G. and Eichlseder, W. (2012), "Valuation of TMF Lifetime Calnculation Methods and their Limitations of Usability", *Key Engineering Materials* vol. 488-489, pp. 403-406.

[85] Taira, S. (1962), "Lifetime of Structures Subjected to varying load and temperature", in Hoff, N. J. (ed.) *Creep in structures IUTAM Symposia,* Springer Berlin Heidelberg, pp. 96-124.

[86] Coffin, L. F. (1976), "The concept of Frequency Seperation in life Prediction for Time Dependent Fatigue", in *ASME-MPC Symposium on Creep-Fatigue Interaction,* MPC-3 ed, American Society of Mechanical Engineers, pp. 349-364.

[87] Priest, R. H. and Ellison, E. G. (1981), "A Combined Deformation Map-Ductility Exhaustion Approach to Creep-Fatigue Analysis", *Materials Science and Engineering,* vol. 49, no. 1, pp. 7-17.

[88] Manson, S. S., Halford, G. R. and Hirschberg, M. H. (1971), *Creep-Fatigue Analysis by Strain Range Partitioning,* NASA TM X-67838, NASA Technical Memorandum, Cleveland,Ohio.

[89] Nitta, A., Kuwabara, K. and Kitamura, T. (1984), "The characteristics of thermal-mechanical fatigue strength in superalloys for gas turbine", *1983 Tokyo International Gas Turbine Congress, Tokyo, Japan,* pp. 765.

[90] Neu, R. W. and Sehitoglu, H. (1989), "Thermomechanical Fatiuge, Oxidaiton, and Creep: Part II. Life Prediction", *Metallurgical Transactions,* vol. 20A, no. 9, pp. 1769-1783.

[91] Neu, R. W. and Sehitoglu, H. (1989), "Thermomechanical Fatigue, Oxidation, and Creep: Part I. Damage mechanisms", *Metallurgical Transactions,* vol. 20A, no. 9, pp. 1755-1767.

[92] Blanchard, A. (2011), *Review of Thermomechanical Fatigue Models for Aero- Engines, MSc Thesis,* Cranfield University, Cranfield, England.

[93] Boismier D A , Sehitoglu Huseyin (1990), "Thermo-mechanical Fatigue of Mar-M247: part 1 - Experiments", *Jounal of Engineering Materials and Technology,* vol. 112, pp. 68-79.

[94] Zamrik, S. Y., Asok, R. and Koss, D. A. (1995), "Life Prediction of Advanced Materials for Gas Turbine Application ", *Advanced Turbine Systems Annual Program Review,* October 17-19,1995, Morgantown, West Virginia, .

[95] Bernstein, H. L. and Allen, J. M. (1992), "Analysis of Cracked Gas Turbine Blades", *Journal of Engineering for Gas Turbine and Power,* vol. 114, no. 2, pp. 293-301.

[96] Heine, J. E., Ruano, E. and DeLaneuville, R. E. (1996), "TMF life prediction approach for turbine blades", in *Thermal Mechanical Fatigue of Aircraft Engine Materials,* AGARD, , pp. 20.1-20.6.

[97] Palmer, J. R. (1990), *The Turbomatch scheme for aero/industrial gas turbine engine design point/off-design performance calculation for aero/industrial gas turbineengine designpoint/off-design performance calculation,* Cranfield University, Cranfield, Bedfordshire.

[98] IHS Janes (2010), *Aero-Engines,* 28th ed.

[99] Roux, E. (2007), *Turbofan and turbojet engines: database handbook,* Lulu.com, Blagnac, France.

[100] CFM International (2012), *CFM Technical Data*, available at: www.cfm56.com/products/cfm-technical-data.pdf (accessed 22 December 2012).

[101] Laskaridis, Pilidis, P., and Kotsiopoulos, P. (2005), "An integrated engine-aircraft performance platform for assessing new technologies in aeronautics.ISABE2005-1165", *17th International Symposium on Air Breathing Engines,* International Society for Air Breathing Engines, Munich, Germany, .

[102] Aircraft Commerce (2010), *Owner's & Operator's Guide: 737NG Family*, available at: http://www.aircraft-commerce.com/articles (accessed 14 August 2012).

[103] Boeing International, (2013), *737 Airplane Characteristics for Airport Planning*, available at: http://www.boeing.com/assets/pdf/commercial/airports/acaps/737.pdf (accessed 11 September 2013).

[104] Saravanamuttoo, H., Rogers, G., Cohen, H. and Straznicky, P. (2009), *Gas Turbine Theory,* Prentice Hall imprint, Great Britain.

[105] Walsh, P. P. and Fletcher, P. (2004), *Gas Turbine Performance,* second edition ed, Blackwell Science, Fairfield, NJ.

[106] Ramsden, K. (2008), *Gas Turbine Fundamentals and Turbomachinery(unpublished MSc lecture notes),* Cranfield University, Cranfield, England.

[107] Cookson and Haslam, A. S. (2008), *Mechanical Design of Turbomachinery* (unpublished MSc Lecture Notes), Cranfield University.

[108] Bunker, R. S. (2006), "Cooling Design Analysis", in *The Gas Turbine Handbook,* The National Energy Technology Laboratory, USA, pp. 296-308.

[109] Thulin, R. D., Howe, D. C. and Singer, I. D. (1982), *NASA Energy Efficient Engine High - Pressure Turbine Detailed Design Report NASA CR - 165608,* , NASA, Cleveland.

[110] Nickel Development Institute, (1995), *High-Temperature, High-Strength Nickel Base Alloys Nº393*, Nickel Development Institute, courtesy of Inco Limited.

[111] Gordon, A. P. (2006), *Crack Initiation Modeling of a Directionally - Solidified Ni-Based Superalloy* (PhD thesis), Georgia Institute of Technology, Atlanta, Georgia.

[112] Jones, M. J., Bradbrook, S. J. and Nurney, K. (2002), "A Preliminary Engine Design Process for an Affordable Capability", *Reduction of Military Vehicle Acquisition Time and Cost through Advanced Modelling and Virtual Simulation - RTO AVT Symposium ,* 22-25 April 2002, Paris, France, pp. 52-1.

[113] Carter, T. J. (2005), "Common failures in gas turbine blades", *Engineering Failure Analysis,* vol. 12, no. 2, pp. 237-247.

[114] AGARD, (1971), "High Temperature Turbines", *AGARD Conference Proceedings No. 73 36th Meeting of the AGARD Propulsion and Energetics Panel,Florence, Italy,* Vol. 73, 21-25 September 1970, .

[115] Incropera, F. P. and et al (2007), *Introduction to heat transfer,* 5th ed, John Wiley and Sons, USA.

[116] Frank, M. W. (1988), *Heat and Mass Transfer,* Addison-Wesley, USA.

[117] Minichmayr, R., Riedler, M., Winter, G., Leitner, H. and Eichlseder, W. (2008), "Thermo-mechanical Fatigue life Assessment of Aluminium Components Using the Damage Rate Model of Sehitoglu", *International Journal of Fatigue,* vol. 30, no. 2, pp. 298-304.

[118] Ackert, S. (2013)*, Engine Maintenance Concepts for Financiers*,

available at:

http://www.aircraftmonitor.com/uploads/1/5/9/9/15993320/engine_mx_concepts_for_financiers___v2.pdf (accessed 1 December 2013).

[119] Hanumanthan, H. (2009), *Severity Estimation and Shop Visit Prediction of Aero engines* (PhD thesis), Cranfield University, Cranfield, England.

[120] Gomes, E. E. B. (2007), *Operational optimisation of gas turbine distributed generation systems in a competitive electricity market* (PhD thesis), Cranfield University.

[121] Guedou, J. and Honnorat, Y. (1993), "Thermomechanical fatigue of turbo-engine blade superalloys. , ASTM (1993), 157–175.", in Sehitoglu, H. (ed.) *Thermomechanical Fatigue Behavior of Materials,* ASTM STP 1186 ed, American Society for Testing and Materials, Philadelphia, pp. 157-175.

[122] Chataigner, E. and Remy, L. (1996), "Thermomechanical Fatigue Behaviour of Coated and Bare Nickel-Based Superalloy Single Crystals", in Verrilli, V. M. and Castelli, M. G. (eds.) *Thermomechanical Fatigue Behavior of Materials,* Second Volume. ASTM STP 1263, American Society for Testing and Materials, pp. 3-26.

[123] Miller, R. A. (1987), "Current status of thermal barrier coatings - An Overview", *Surface and Coatings Technology,* vol. 30, no. 1, pp. 1-11.

[124] Cunha, F. J., Dahmer, M. T. and Chyu, M. K. (2006), "Analysis of Airfoil Trailing Edge Heat Transfer and Its Significance in Thermal-Mechanical Design and Durability", *Journal of Turbomachinery,* vol. 128, pp. 738-746.

[125] Busso, E P, Wright, L, Evans, H E, McCartney, L N, Saunders, S R J, Osgerby, S, Nunn, J (2007,), "A physics-based life prediction methodology for thermal barrier coating systems", *Acta Materiala*, vol. 55, pp. 1491-1503.

Appendix A

A.1 Description of the Neu/Sehitoglu TMF Model

The Neu and Sehitoglu model was developed for high-temperature fatigue and TMF. This thesis uses the model that was applied to Mar – M247 Nickel based superalloy. The model considers damage accumulation due to fatigue, oxidation, and creep processes. Damages per cycle from fatigue (D^{fat}), oxidation (D^{ox}) and creep (D^{creep}) are summed to obtain a total damage per cycle (D^{tot}). The model assumes that linear damage is equal to one at failure.

$$D^{tot} = D^{fat} + D^{ox} + D^{creep} \quad \text{(A- 1)}$$

Equation A-1 can be rewritten in terms of life, N_f where damage is taken as $1/N_f$.

$$\frac{1}{N_f} = \frac{1}{{N_f}^{fat}} + \frac{1}{{N_f}^{ox}} + \frac{1}{{N_f}^{creep}} \quad \text{(A- 2)}$$

Where; $\boldsymbol{{N_f}^{fat}}$, $\boldsymbol{{N_f}^{ox}}$ and $\boldsymbol{{N_f}^{creep}}$ represent the number of cycles to failure from fatigue damage, environmental damage (oxidation) and creep damage, respectively.

Fatigue Damage Terms

The fatigue life term**,** N_f^{fat} is estimated from the strain - life equation, which is the most common description of the process:

$$\frac{\Delta\varepsilon_{mech}}{2} = \frac{{\sigma'}_f}{E}(2{N_f}^{fat})^b + {\varepsilon_f}'(2{N_f}^{fat})^c \quad \text{(A-3)}$$

Where: $\Delta\varepsilon_m$ is the mechanical strain, σ'_f is the fatigue strength coefficient, *b* is the fatigue strength exponent and ε_f' is the fatigue ductility coefficient. *c* is the fatigue ductility exponent and *E* is the elastic modulus. Boismier and Sehitoglu [93] used the corresponding pure fatigue life correlation in Equation A- 4, where *C* and *d* are material constants. The mechanical strain was taken as the key variable precluding any thermally-induced strain. The model assumes that the inelastic strain is relatively negligible for nickel-based superalloys under isothermal fatigue loading at low temperatures.

$$\frac{\Delta\varepsilon_m}{2} = C(2N_f^{fat})^d \qquad \text{(A- 4)}$$

Oxidation Damage Terms

If $\Delta\varepsilon_{mech} > \varepsilon_0$, the oxidation life term is given as:

$$\frac{1}{N_f^{ox}} = \left[\frac{h_{cr}\delta_0}{B\,\Phi^{ox}\left(K_{peff}^{ox}+K_{peff}^{\gamma'}\right)}\right]^{-1/\beta} \frac{2(\Delta\varepsilon_m)^{\frac{2}{\beta}+1}}{\dot{\varepsilon}^{1-\frac{b}{\beta}}} \qquad \text{(A- 5)}$$

Where: ε_0 is the threshold strain for oxide cracking, h_{cr} is a critical crack length where environmental (oxidation) attack trails behind crack growth and δ_0 is a measurement of oxide plus γ' depleted zone ductility. *B* is a material coefficient, Φ^{ox} is the phasing factor for oxidation damage and β is the time related mechanical strain range exponent. $\dot{\varepsilon}$ is the mechanical strain rate, *b* represents the thermal strain rate sensitivity exponent, while K_{peff}^{ox} and $K_{peff}^{\gamma'}$ are the effective parabolic constants for oxidation and γ' depletion, respectively. It should be noted that the oxidation damage in this model is based on measurements of surface and crack tip oxidation and γ' depletion kinetics. The oxidation and γ' depletion have been frequently assumed to follow the parabolic growth law:

$$h = \sqrt{K_p t} \qquad \text{(A- 6)}$$

Where: h represents the total oxidation induced crack length, K_p is the parabolic constant that is a function of temperature, and t is the time measured from the instant fresh metal is exposed to the environment. For varying temperature conditions, (such as TMF) an effective parabolic constant, K_{peff}, that accounts for the cycle period is defined as

$$K_{peff} = \frac{1}{t_c}\int_0^{t_c} D_0 e^{\frac{-Q}{RT(t)}}\, dt \qquad \text{(A- 7)}$$

D_0 and Q are the diffusion constant and activation energy, respectively, while t_c is the cycle time. From Equation A-5, K_{peff}^{ox} and $K_{peff}^{\gamma'}$ were derived with respect to the two oxidation – related mechanisms (general matrix oxidation and γ' depletion). The Arrhenius term in the expression of Equation A-7 can also be noted; as such a term has been quite frequently introduced into TMF or isothermal high-temperature LCF models, to account for high-temperature damage mechanisms

The oxidation damage term reflects both the environmentally induced crack nucleation and growth. To account for the type of oxide cracking that occurs (in IP or OP loading), the phasing factor (Φ^{ox}) was included in the model. Hence, any history will have a unique Φ^{ox}defined by integrating the phasing, $\emptyset_{ox}$, which relates to the ratio of thermal and mechanical strain rates ($\dot{\varepsilon}_{\mathrm{th}}/\dot{\varepsilon}_{\mathrm{m}}$) over the period of the history.

$$\emptyset_{ox} = \exp\left[-\frac{1}{2}\left(\frac{(\dot{\varepsilon}_{\mathrm{th}}/\dot{\varepsilon}_{\mathrm{m}}) + 1}{\xi^{\mathrm{ox}}}\right)^2\right] \qquad \text{(A-8)}$$

$$\Phi^{\mathrm{ox}} = \frac{1}{\mathrm{t_c}}\int_0^{\mathrm{t_c}} \exp\left[-\frac{1}{2}\left(\frac{(\dot{\varepsilon}_{\mathrm{th}}/\dot{\varepsilon}_{\mathrm{m}}) + 1}{\xi^{\mathrm{ox}}}\right)^2\right] \mathrm{dt} \qquad \text{(A-9)}$$

Where, ξ^{ox} is a constant introduced as a measure of the relative amount of damage due to the different phasings.

Experimental tests have shown that the most oxidation damage occurs in OP-TMF when $\emptyset_{ox} = 1$, at $(\dot{\varepsilon}_{th}/\dot{\varepsilon}_{mech} = -1)$. The limiting case of free expansion is when $\dot{\varepsilon}_{th}/\dot{\varepsilon}_{mech} = \pm\infty$ and $\emptyset_{ox} = 0$ For any arbitrary history of $\dot{\varepsilon}_{th}/\dot{\varepsilon}_{mech}$ the

range of $\emptyset_{ox}$ will be between 0 to 1, and the maximum damage occurring at $\dot{\varepsilon}_{th}/\dot{\varepsilon}_{mech} = -1$ (Figure 10.5).

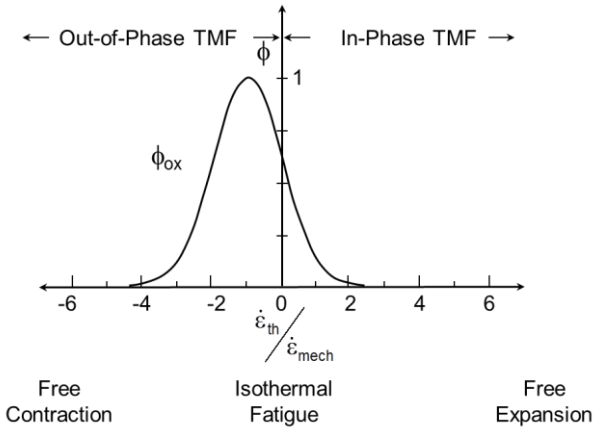

Figure A-1 Phasing constants for oxidation

Creep Damage Terms

The derivation of the creep life term was largely influenced by the fact that creep mechanisms could operate both in compression and tension. To account for this asymmetry, Neu and Sehitoglu [91] defined a creep damage term as a function of both effective and hydrostatic stresses.

$$\frac{1}{N_f^{creep}} = \int_0^{t_c} A_{cr\Phi_{cr}} \exp\left(\frac{-\Delta H}{RT}\right)\left(\frac{\alpha_1\bar{\sigma} + \alpha_2\sigma_H}{K}\right)^m dt \qquad \text{(A-10)}$$

Where: *ΔH* is the activation energy for creep, *R* is the gas constant, *T* is the temperature, *Acr* is a scaling constant for creep, and *m* is the creep stress exponent. K represents the drag stress, while $\bar{\sigma}$ and σ_H are the effective and

hydrostatic stress components, respectively. α_1 is the stress state constant and α_2 is the hydrostatic stress sensitivity constant. In addition, a phasing factor, Φ_{cr} was defined as:

$$\Phi_{cr} = \frac{1}{t_c}\int_0^{t_c} \exp\left[-\frac{1}{2}\left(\frac{\dot{\varepsilon}_{th}/\dot{\varepsilon}_{mech} - 1}{\xi^{cr}}\right)^2\right] \qquad \text{(A- 11)}$$

Where, ξ^{cr} is the creep phasing constant for thermal and mechanical strains. If no creep occurs in compression, α_1 = 1/3 and α_2 =1. The phasing factor accounts for different creep damage mechanisms such as intergranular or transgranular cracking.

A.2 Effect of cycle counting variables

In Chapter 5, three cycle counting variables, namely temperature, mechanical strain and stress that could be employed in the TMF damage calculation were identified. The Influence of each of these variables on the predicted TMF results have been evaluated in Figure 10.4 and Figure 10.5 for the cold and hot side, respectively

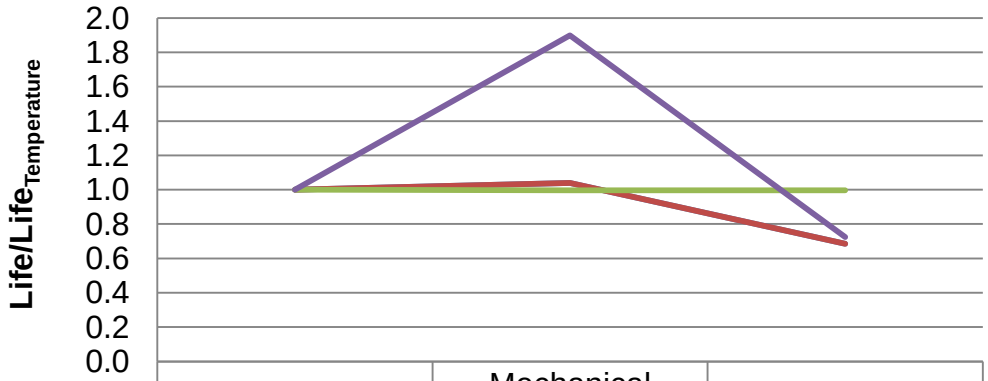

	Temperature	Mechanical strain	Stress
Total	1.000E+00	1.040E+00	6.856E-01
Oxidation	1.000E+00	1.040E+00	6.855E-01
Fatigue	1.000E+00	9.959E-01	9.959E-01
Creep	1.000E+00	1.899E+00	7.238E-01

Figure A-2: Effect of cycle variables in the Cooling Hole.

The life estimated from the cycle counting variables are plotted relative to the life predicted using temperature as the counting variable for all the counting variables, oxidation damage drives the TMF life calculation. The cold side is generally observed to experience lower life, although the cold side life for the mechanical strain variable was slightly higher than the hot side.

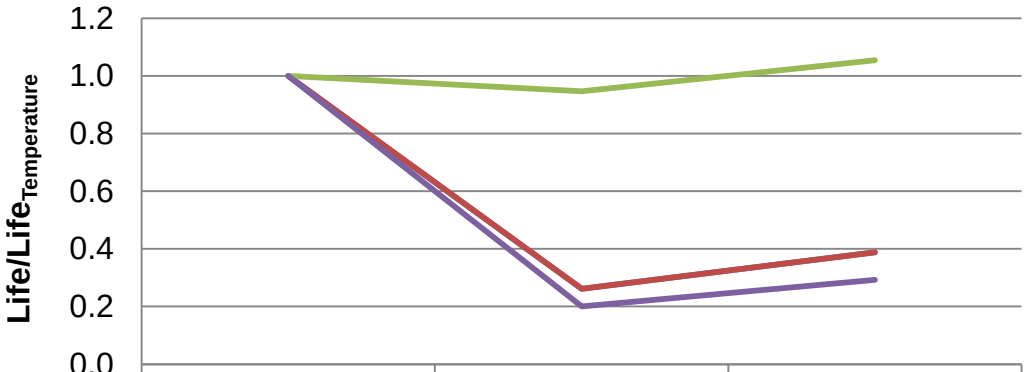

	Temperature	Mechanical strain	Stress
Total	1.000E+00	2.618E-01	3.886E-01
Oxidation	1.000E+00	2.618E-01	3.886E-01
Fatigue	1.000E+00	9.465E-01	1.054E+00
Creep	1.000E+00	2.001E-01	2.923E-01

Figure A-3: Effect of cycle variables in the Hot Side

Temperature cycle counting variable gives the least conservative values for TMF life, while Stress is the most conservative .The model appears therefore to be more sensitive to changes in applied stress as shown in the consistent low life values obtained for oxidation and creep damage, as well as total damage severity in the hot and cold sides unlike stress, the mechanical strain variable gives the most conservative results for the hot side only. It could also be noted that the choice of counting variable has negligible influence on fatigue damage. The TET is a key parameter that is explored in aero engine performance analysis. In terms of operating conditions, Thus, the influence of temperature could be independently assessed from a cycle analysis .On the other hand, the mechanical strain, and stress are not readily available, but depend on further

analysis from FEA. This makes these two cycle counting variables more difficult to control. Hence, temperature was selected as the suitable counting variable for this study.

Appendix B

B.1 FEA MODELLING AND PROCEDURES

Introduction

This section covers the key FEA procedures conducted for the idealised turbine blade leading edge in this research. Essentially, a sequentially coupled thermal stress analysis was implemented using Abaqus CAE. A transient thermal analysis was performed, then the thermal-mechanical (static stress) analysis. A formal documentation of these procedures will give a good basis for those doing similar research in the future. This document can also be used to introduce FEA to the students of the department of power and propulsion.

Structure of Analysis in Abaqus

Any Abaqus analysis will have the structure shown in Figure B-1; comprising three stages: pre-processing, processing/analysis and post-processing. It is important to note that each of these stages has its associated files.

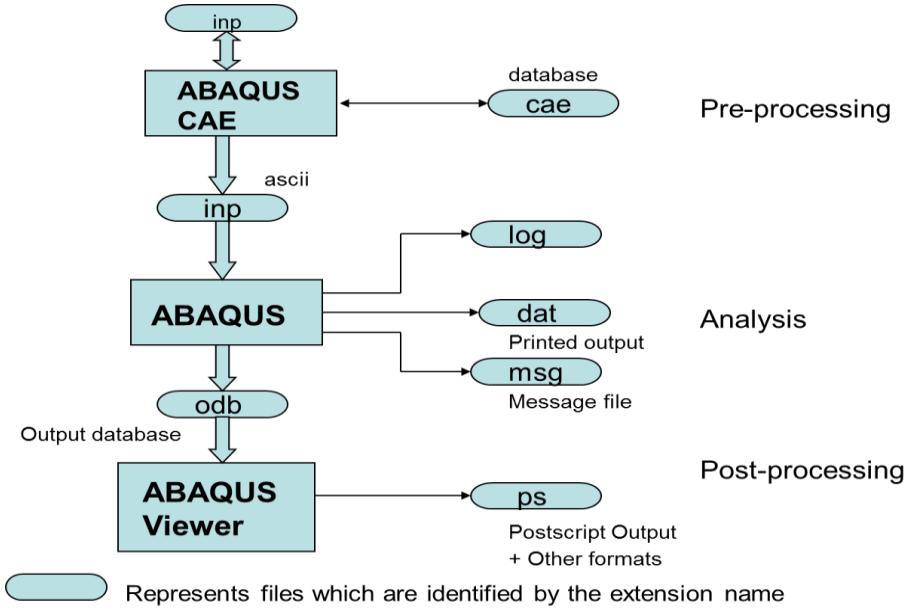

Figure B-1: Stages of analysis in Abaqus CAE

- **Pre-processing**: This is the first stage where the model defining the physical problem is graphically created and the input file is generated using Abaqus CAE or an alternative pre-processor.
- **Simulation**: The simulation process is run in the background. At this stage, Abaqus solves the numerical problem earlier defined in the pre-processor. The duration of a simulation depends largely on the complexity of the problem and the computational power available.
- **Post-processing**: The outputs, (such as temperature, stress, strains and displacements), from a successful simulation can be evaluated using Abaqus/CAE visualization module or other post-processor. The Visualization module enables the results to be displayed and analysed using contour plots, charts and animations.

FEA Model development

In developing the FEA model, different Abaqus/CAE modules are required. These are provided in the model tree as shown in Figure B -2. It is suggested that the model tree is followed sequentially, leaving out aspects not required for a particular model. As mentioned earlier, a sequential coupled heat transfer analysis was conducted. This type of analysis is required when the stress/displacement solution is dependent on the temperature field. The various procedures involved in the analysis are detailed subsequently.

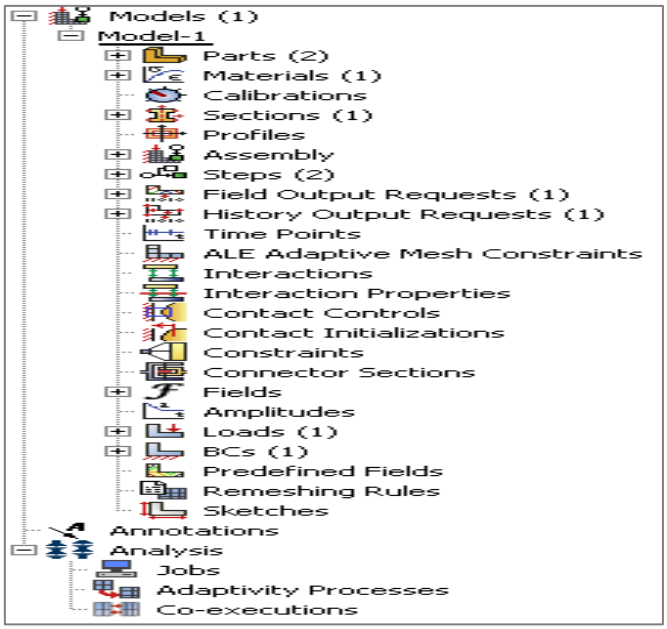

Figure B-2: Abaqus CAE model tree**.**

Part

The idealised geometry considers only the blade leading edge (metal substrate) with a cooling hole passage. Two models were developed; an un-coated model and another with TBC. The un-coated model comprises a single part with the root region, hot side (outer surface in contact with the hot gas) and cold side (internal surface that interacts with the cooling air), defined as separate sets shown in Figure B-3. The root region is an extension of the blade to represent its fixing into the blade disc.

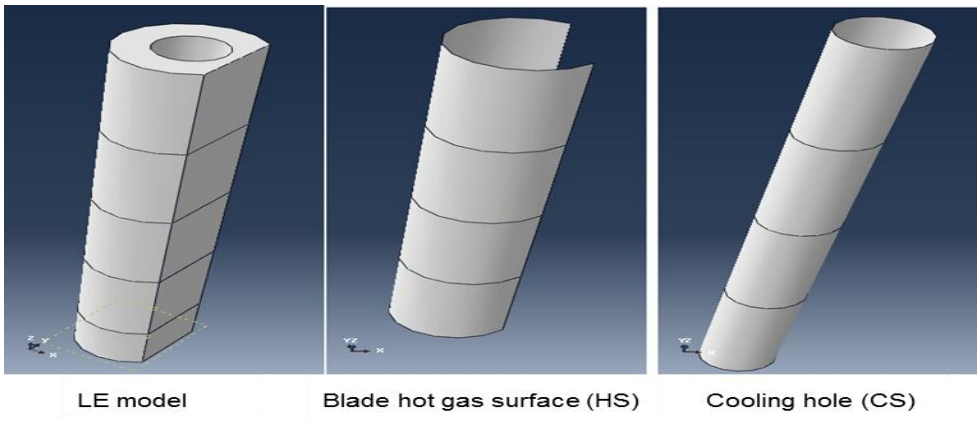

Figure B-3: Parts of the coated blade.

The uncoated LE model consist of four different parts representing the metal substrate, bond-coat, TGO layer and the ceramic top-coat as shown in Figure B-4. Various sets were also created to allow

easy application of loads, BCs, and visualisation/ extraction of results.

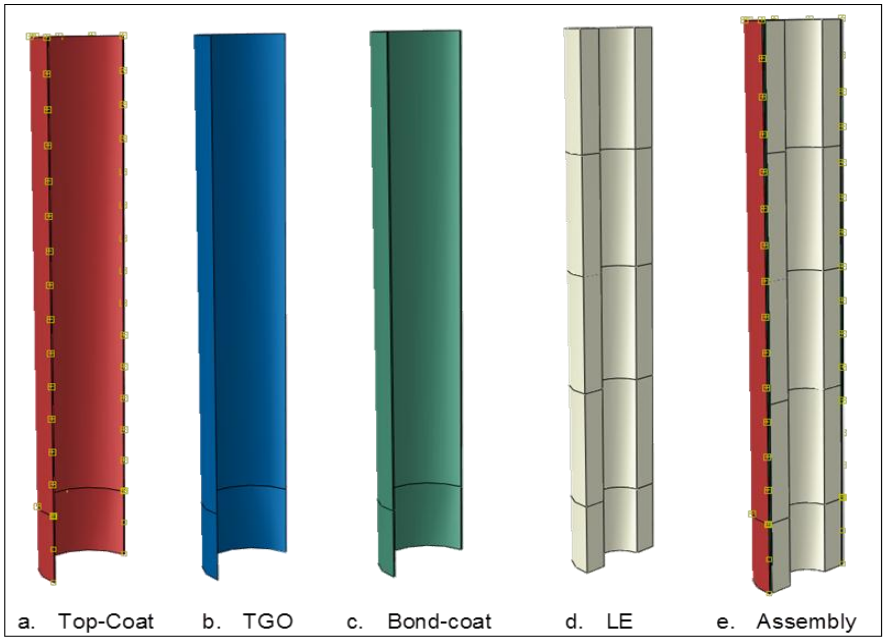

Figure B-4: Parts and assembly of the TBC model

Materials

MAR-M247 material properties were used for the metal substrate in all the idealised blade geometries. The TBC system layers were assigned material properties as follows: NiCoCrAlY for bond-coat, alumina (Al_2O_3) for TGO and yttria-stabilised Zirconia (YSR) for ceramic top-coat **(**Table B-1). All the materials were assigned elasto-plastic behaviour. The key temperature dependent material properties are: thermal conductivity, thermal expansion and density for the thermal analysis. In addition, specific heat capacity, yield stress, young's modulus and Poisson's ratio, are used for the thermal- mechanical analysis (thermal stress model).

Table B-1: Table of Materials for idealised Leading edge parts.

Parts	Material	Type
Leading Edge (Metal Substrate)	MAR-M247	Solid-Homogenous
Bond-Coat	NiCoCrAlY	
Top-Coat	yttria-stabilised Zirconia (YSR)	
TGO	Alumina (Al_2O_3)	Shell-Homogenous

Meshing

The FE model in Abaqus is meshed to divide the geometry into smaller elements and nodes (point were elements are connected). The collection of elements and nodes in the model is referred to as the mesh.Meshing for the thermal analysis requires heat transfer elements; while for the thermal-mechanical analysis, static stress elements are used. Table B-2 presents the element types used in the thermal and thermal mechanical analyses conducted in this research. The element shape, type, and location, as well as the total number of elements affect the results obtained from a simulation. The finer the mesh density (i.e., the greater the number of elements) the more accurate the results will be, but the computational time also increases. Therefore an optimum mesh size needs to be selected which optimizes both the mesh size and the computational time. Figure B-5 illustrates the mesh assembly for the TBC model in this research.

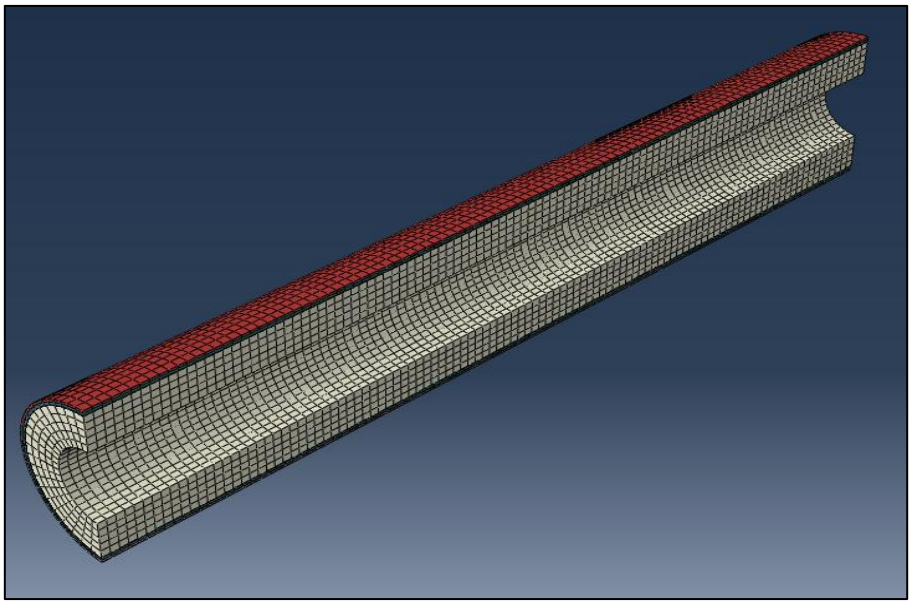

Figure B-5: Mesh plot of the TBC Assembly

Table B-2: Table of Element types

Parts	Mesh size	Element Type	
		Thermal Analysis	Mechanical Analysis
Leading Edge (Metal Substrate)	0.00044m	DC3D8: linear 8-node heat transfer brick	C3D8R: linear 8-node brick with reduced integration and hourglass control
Bond-Coat	0.00044m		
Ceramic Top-Coat	0.00044m		
TGO	0.00044m	DS4: Heat transfer Quadrilateral Shell	S4R: 4-node doubly curved thick or thin shell

Assembly

In the assembly module, instances of the individual parts are combined to form one whole model. Datum planes are first created for the part instances; and then the instances are positioned using face to face, parallel face and coaxial constraints (Figure B-6). For the TBC systems, tie constraints were used

between the layers to implement the contact between the surfaces. In this case, master and slave surfaces need to be defined. A general rule is to assign the thicker instance as the master. Figure B-7 shows the constraints definition for the bond coat and TGO; where the bond coat is assigned as master surface while the TGO is the slave surface.

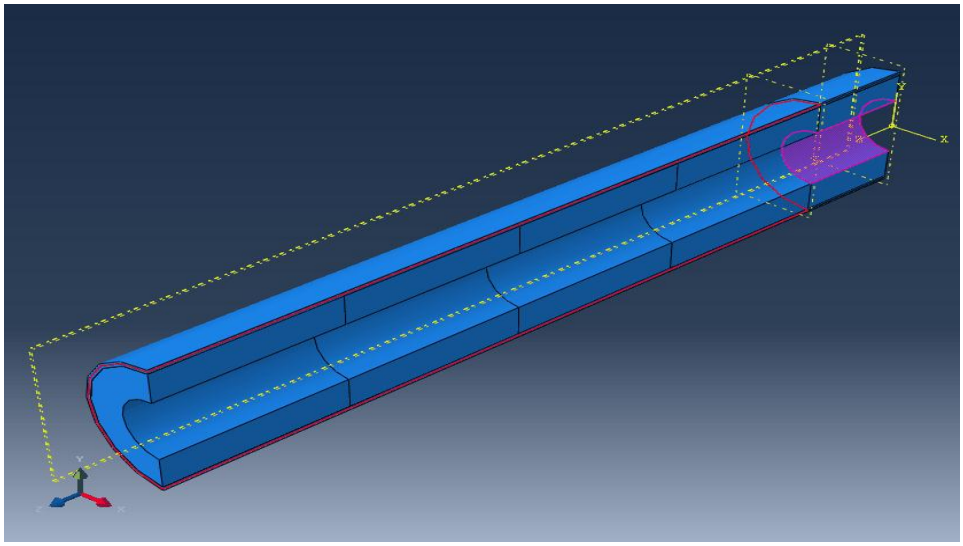

Figure B-6: Assembly position constraints implementation

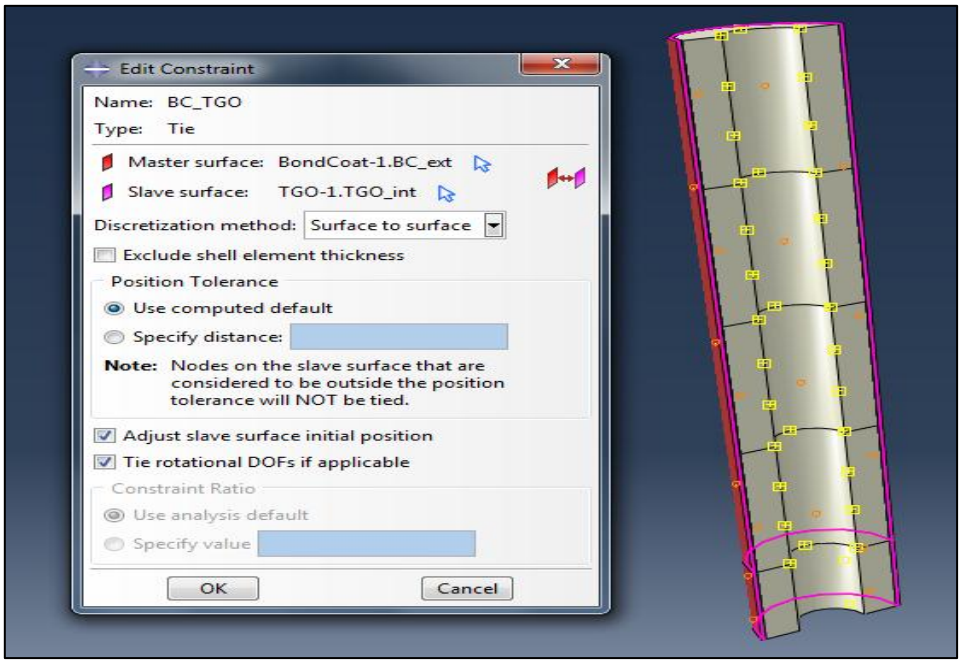

Figure B-7: Constraints definition between bond coat and TGO surfaces

Steps

The steps are used to implement the sequence and duration of an analysis procedure; in terms of how the loads and BCs are applied and their variation. The needed outputs and the solution controls are also specified in the step module. Abaqus/CAE creates a default initial step where, at the start of the analysis, the boundary conditions, predefined fields, and interactions could be applied. The user then creates other steps required for the analysis, which could either be static or transient. The analyses performed in this research include static stress analysis, transient heat transfer analysis and transient thermal stress analysis.

Output Requests

The results computed from an analysis include many variables. Hence, in Abaqus, the user can request specific variables/outputs from any selected region of interest via the Field output request the rate at which the variables are written to the output database can also be specified.

Interactions

Interactions are normally used to define the relationship between surfaces of a model that are in contact. This could be mechanical, thermal or combination of both. ‘Tie’ interaction was used for the TBC system layers as earlier highlighted in the Assembly Section.

Amplitude

Amplitudes are used to implement a time or frequency variation of an applied load or BC, such as temperature, heat transfer coefficient and centrifugal stress applied in this research. The amplitude could be defined over a specific analysis step time or the total time.

Fields

The spatial variation of a load, BC, or interaction could be defined using an analytical field. Either an expression field or mapped analytical field could be used in Abaqus/CAE. In this work, an expression field using the polynomial expression derived from the analytical heat transfer model was implemented for the FEA thermal analysis.

Loads

The load module is where the applied loads are specified. The loads are to be specified in the appropriate step in which they are active.

Job

The Job module is where the input files for a specific analysis is created. From the Job module, an analysis can be submitted and monitored until completion.

Visualization

It is in the visualisation module that the results of an FE analysis are graphically displayed. The required outputs for any step of the analysis can be extracted in several formats, such as reports, X-Y data and graphical plots. the output files are controlled by selecting the appropriate output requests in the step module.

Mesh Convergence study

In order to get satisfactory results, a mesh convergence study is required to select the optimum mesh size for an analysis. However, this is a trade off between accuracy, computing resources and time. Nevertheless, previous experience is usually the first and cheapest option. In a mesh convergence study, the mesh density is increased until a level where further mesh refinements give negligible change in the results. The converged mesh size is then selected from a judgement of the computing time, resources and level of accuracy needed. The mesh convergence study in this research was conducted

for three identical geometries to Geometry 0, Geometry 1, and Geometry 2 (Figure B-8). The total time taken by the computer processor to complete the analysis and the relative difference in maximum von mises stress were plotted against the different mesh sizes as shown in Figure B-8. The mesh could be observed to converge from a mesh size of 0.37mm to 0.30mm for Geometry 0; 0.40mm to 0.45mm for Geometry 1 and Geometry 2; and 0.5mm to 0.55mm for Geometry 3.Within the aforementioned ranges of mesh sizes a compromise between the computing time and accuracy had to be made in selecting the mesh sizes used for the various geometries. To this end, an optimal mesh size could be taken as the point where the two curves intersect. However, due to the need to run numerous cases and additional time to process results for the lifing calculations, reducing computing time was more favourable.

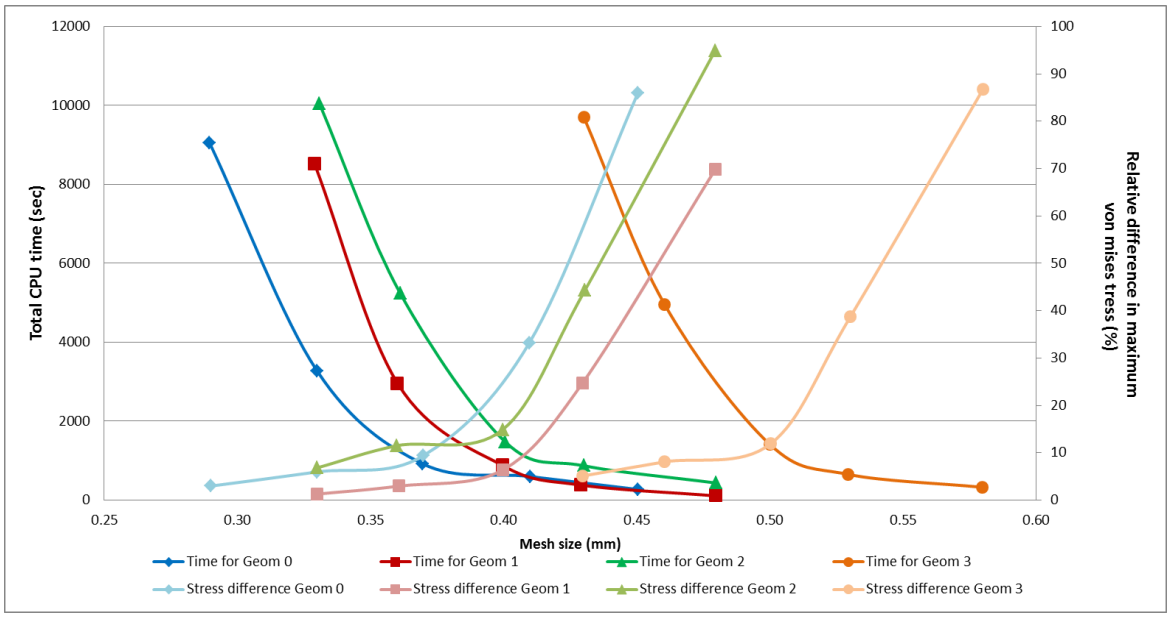

Figure B-8: Mesh convergence study

For Geometry 0, a finer mesh of 0.35mm was preferred to the optimal of 0.37mm, as the difference in computing time was not very significant. For Geometry 1 and Geometry 2, a mesh size of 0.44mm was selected because of the benefits of the reduction of computing time from the optimal point of

0.40mm. The optimal mesh size of 0.5mm was chosen for Geometry 3, due to the significant difference in the results for coarser mesh sizes. Furthermore, the mesh size for Geometry 3 was used for the Geometries 4 and 5 due to their similarity. The mesh sizes for the various geometries used in this thesis are presented in Table B-3.

Table B-3: chosen mesh sizes for geometries.

Geometry	Mesh size (mm)
Geometry 0	0.35
Geometries 1 and 2	0.44
Geometries 3,4 and 5	0.5

Having selected a mesh size a detailed analysis of the available elements could be conducted to select the appropriate element type for the analysis. Figure B-9, shows the results for the elements selection study where; C3D8 and C3D20 represent hexahedral static linear and quadratic elements, respectively. The letter R means reduced integration.

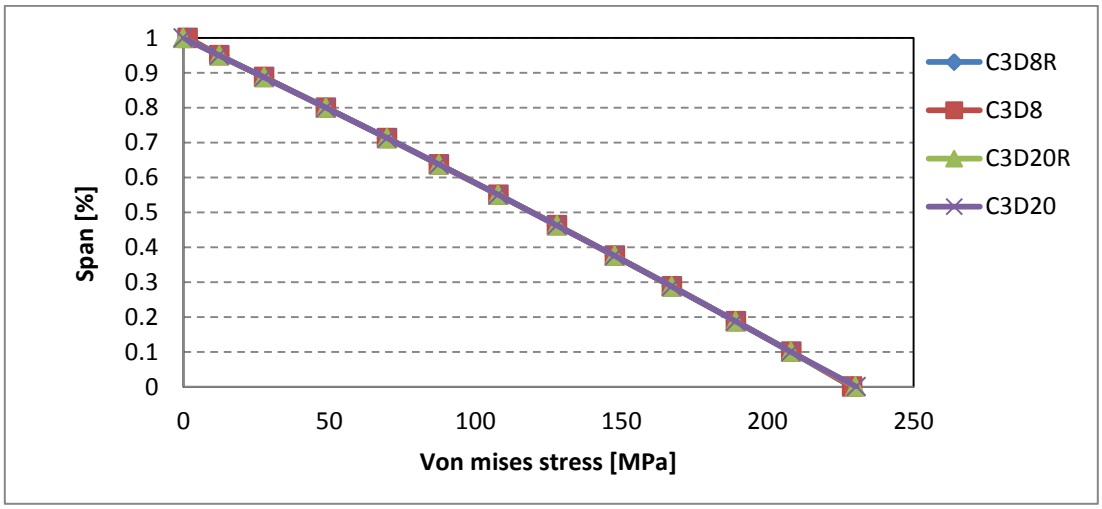

Figure B-9: Element selection study

Again, a cheaper element (linear elements) that gives reasonable accuracy would be preferred over a more accurate element type (quadratic elements) that

is computationally expensive. Linear elements, (C3D8), were selected in this research as they gave equally good accuracy and were computationally more efficient than the quadratic elements.

Root Fixing Method

A method was evolved for fixing the root of the idealised blade using an extended portion that is constrained in all directions (Encastre) .This however results in abnormally high stresses and strains at the root of the blade. A sensitivity analysis had to be conducted to obtain the optimum extended length of the root. The length was varied from 0% to 50% of the blade span until the relative change in von mises stress was less than 1% to obtain the curve in Figure B-10. An optimum root length of 15% was therefore selected. This was further verified in Figure B-11 by comparing the results to the analytical stress calculation.

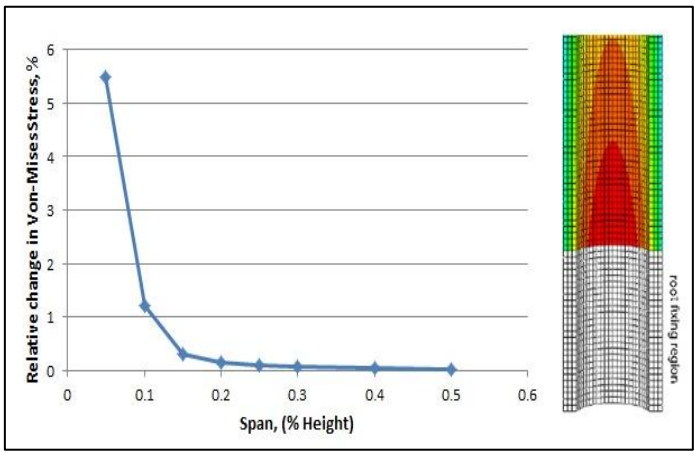

Figure B-10: Selection of optimum root length [Blanchard,2009]

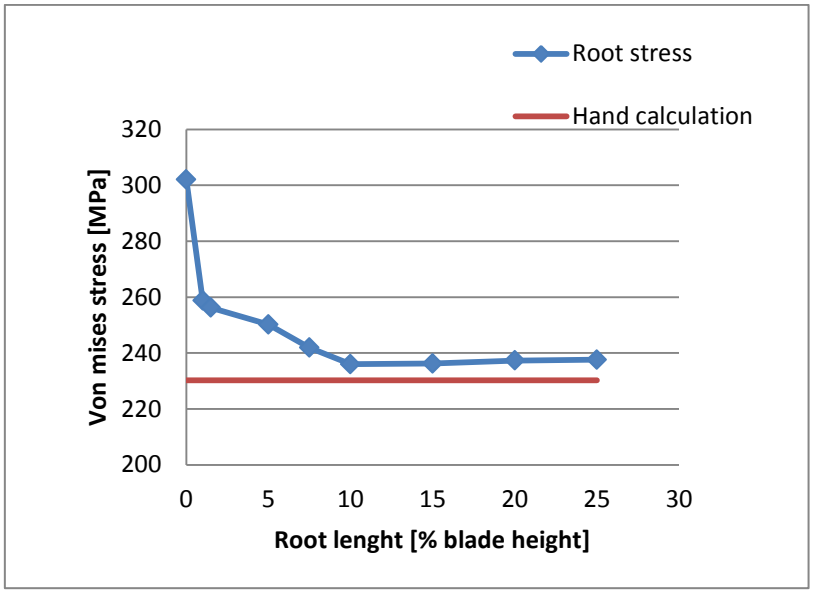

Figure B-11: Verification of root length

FEA Analysis

The following sections highlight the key thermal and mechanical analysis procedures. A concise summary is also provided at the end of the chapter.

Thermal Analysis

Steps

Four steps were created to cover the entire flight profile using a transient thermal analysis: Taxi –ground idle (initial_th) idle-to-climb, cruise and descend-landing. The transient analysis accounts for the time dependent variation of temperature and not transient performance. Field output requests: Nodal (NT) and element (TEMP) temperatures are selected as the outputs to be calculated and written to the database:

Amplitudes

The amplitude is created as a tabular input that specifies the variation of temperature with the total time along the flight as shown in Figure B-12.

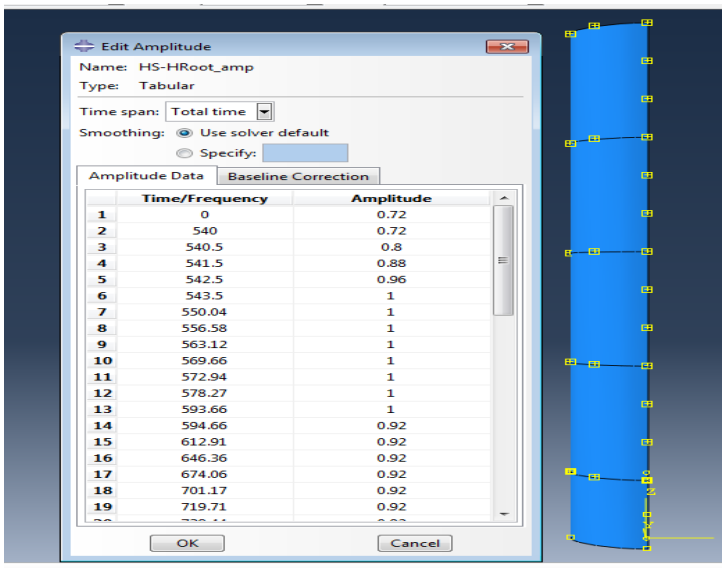

Figure B-12: Amplitudes implementation for thermal analysis.

Fields

Three analytical expression fields for the external metal temperature, coolant temperature and coolant heat transfer coefficients were applied in the model. Figure B-13 shows the menu in which the analytical fields are implemented

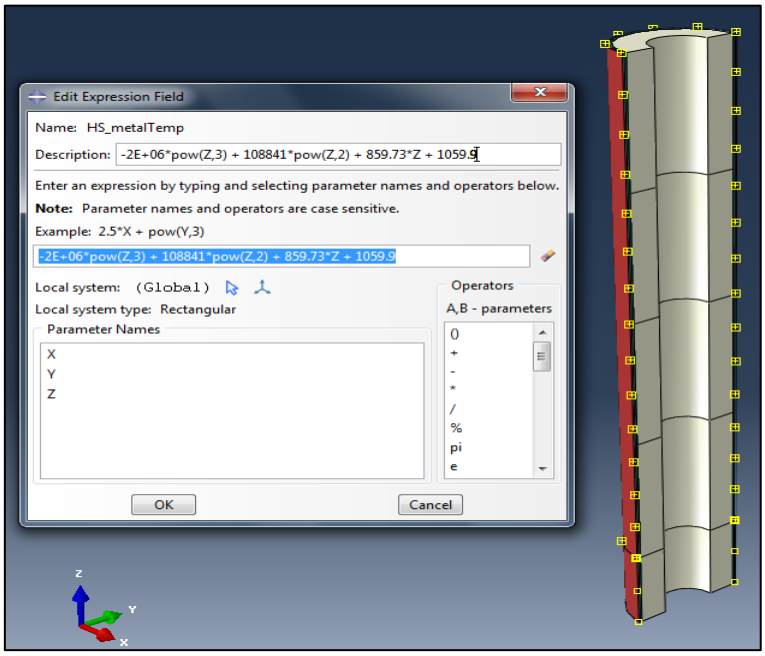

Figure B-13: Analytical Expression Field.

Thermo-mechanical Analysis

The same key steps for the thermal analysis are followed in the thermo-mechanical analysis. However, in the thermo-mechanical analysis, the temperature distribution from the heat transfer analysis is used as a predefined field. A rotational body force (centrifugal load) is applied using the blade angular velocity as shown in Figure B-14 , and the root of the blade is constrained in all degrees of freedom (DOF) 'Encastre'.

In terms of the field outputs, the stress and strain components are the variables to be calculated and written to the database. However, a verification practice is to include the nodal or element temperatures in the output requests. This way, a confirmation can be done to ascertain that the model has captured the thermal inputs. Similar to the thermal analysis; the amplitude for the variation of the centrifugal force is also applied. The other steps are the same with the thermal analysis.

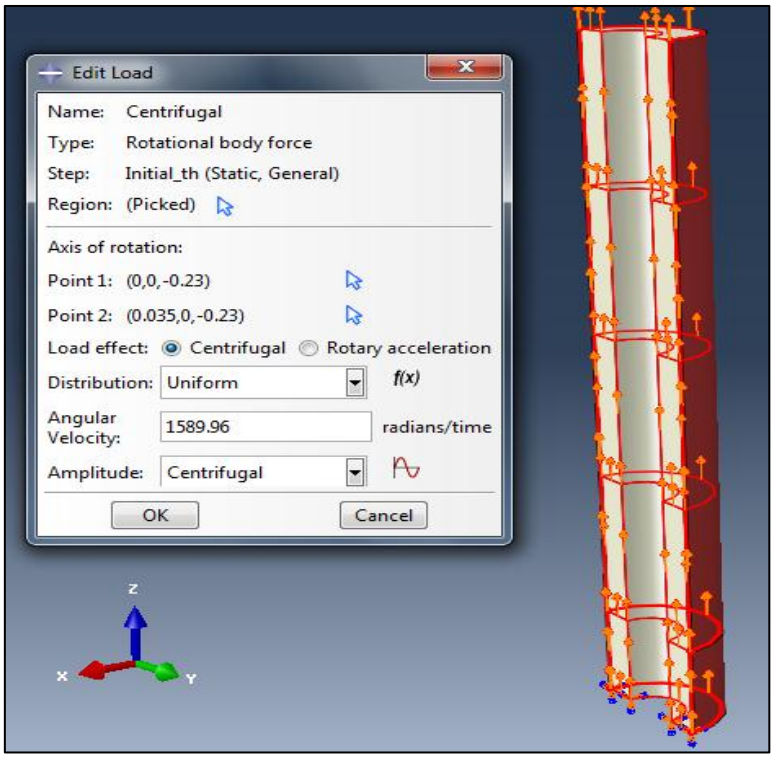

Figure B-14: Centrifugal Load definition.

Summary of FEA models and procedures

				Abaqus FEA Thermal Analysis (TH) -No TBC			
Models	**LE**	**Parts**	**Features**	Solid Extrude	Sketch	Extrude-0.046 (B-0.04, E-0.006)	
				Partition Edge-1		Straight Line	
				Datum Pt-1	(0,0,0)		
				Datum Plane-1		Bottom Plane	
				Datum Pt-2	(0,0,0.006)	Divides root fixing from blade	
				Partition Cell-1		Divide whole blade into encastre	
				Partition Cell-2			
				Partition Cell-3			
				Partition Cell-4			
			Sets	CRoot	Cooling passage - Root	Apply BC (Uniform Temp)	
				CS	Cooling passage-Blade	Apply BC (Temp Loads)-Amp.	
				Encastre	Datum Plane for Root BC	Applying BC - THM Analysis	
				HRoot	External (Gas) path area of Root	Apply BC (Uniform Temp)	
				HS	External (Gas) path area of LE along Blade	Apply BC (Temp Loads)-Amp.	
				LE	Solid Volume of blade including Encastre	Useful in apply in CF Load	
				LE_AIRFOIL	Solid Volume of blade excluding Root	Useful in extracting results	
			Surfaces	CRoot	Cooling passage - Root		
				CS	Cooling passage - blade		
			Section Assign	MARM	Solid, Homogenous Type		
		Materials	Conductivity	Type-Isotropic	**Conductivity**		**Temp**
		MARM-247		Temp Dependent	8.648		366.48
					24.214		1283.15
			Density	Distribution-Uniform	8525.41		
			Elastic	Type-Isotropic	**Elastic modulus**	**Poisson Ratio**	**Temp**
				Temp Dependent	1.4479E+11	0.29	255.37
					1.31E+11	0.29	533.15
					1.1514E+11	0.29	810.93
					86184000000	0.29	1088.71
			Expansion	Type-Isotropic	**Coeff of thermal exp**		**Temp**
				Temp Dependent	1.57E-05		922.04
					2.03E-05		1255.37
			Plasticity	Hardening-Isotropic	**Yield**	**Plastic Strain**	**Temp**
				Temp Dependent	8.53E+08	0	271.48
					9.37E+08	0	1042.59
					7.47E+08	0	1194.26
			Specific Heat	Constant Volume	5.02E+02		
		Section	Name	MAR M-247			
			Type	Solid Homogenous			
			Material	MAR M-247			
		Assembly	Instances	LE	Mesh	Standard, Linear, Heat Transfer	
						DC3D8 - 8 node linear heat transfer	
						Size-0.00044	
			Features	Datum Co-ordinate System			
			Sets	Created default as in Parts			
			Surfaces	Created default as in Parts			
		Steps	Step	**Initial_th**	**Idle-TO-Cruise**	**Cruise**	**Desc-Land**
			Type	Heat Trasfer	Heat Trasfer	Heat Trasfer	Heat Trasfer
			Response	Transient	Transient	Transient	Transient
			Time	100	500	12000	1820
			NL Geom	Off	Off	Off	Off
			Type	Automatic	Automatic	Automatic	Automatic
			Max No. of Increments	1.00E+08	1.00E+08	1.00E+08	1.00E+08
			Initial	0.5	5	5	5
			Min	1.00E-09	1.00E-09	1.00E-09	1.00E-06
			Max	10	100	1000	100
			Max Allowable Temp Change	5	2	2	2
			Max Allowable Emmissivity	1.00E-01	0.1	0.1	0.1
			Method	Direct	Direct	Direct	Direct
			Matrix Storage	Default	Default	Default	Default
			Solution Technique	Full Newton	Full Newton	Full Newton	Full Newton

		Field O/P Request	Name	Output-1		
			Step	Initial_th		
			Procedure	Heat Transfer		
			Domain	Model		
			Frequency	Every n increments	n=1	Every time step X =10 (alternative)
			Output Variables	Select from List	Thermal	NT, Nodal Temperatures
						TEMP, Element Temp
						HFL, Heat Flux Vector
		Interactions	Name	CRoot	CS	
			Type	Surface Film Condition	Surface Film Condition	
			Step	Initial_th	Initial_th	
			Surface	LE-1.CRoot	LE-1.CS	
			Definition	Embedded Coefficient	CS_Htc	
			Film Coeff	5123	1	
			Film Coeff Amp	hc_amp	hc_amp	
			Sink Defn	Uniform	CS_Tcool	
			Sink Temp	821	1	
			Sink Amp	TC_amp	TC_amp	
		Fields	Analytical Fields	CS_HTc	3E6*pow(Z,3)-172785*pow(Z,2)-924.25*Z+5123.4	
				CS_Tcool	(-2E6*pow(Z,3)+128189*pow(Z,2)+237.07*Z+820.91)	
				HS_MetalTemp	(-2E6*pow(Z,3)+108380*pow(Z,2)+682.53*Z+1036.4)	
		Amplitude	Name	HS_Hroot_amp	TC_amp	HC_amp
			Type	Tabular	Tabular	Tabular
			Time Span	Total Time	Total Time	Total Time
			0	0.7239	0.7177	1
			630	0.7239	0.7177	1
			630.5	0.7979	0.8054	0.9401
		BC	Name	HS_Metal Temp	Root_Metal Temp	
			Type	Temp	Temp	
			Step	Initial_th	Initial_th	
			Region	LE-1.HS	LE-1.Hroot	
			Distribution	HS_Metal Temp	Uniform	
			Magnitude	1	1037	
			Amplitude	HS-Hroot_amp	HS_Hroot_amp	
		Predefined Field	Name	Initial_T		
			Type	Temp		
			Step	Intial		
			Region	LE-1.LE		
			Distribution	Direct Specification		
			Magnitude	869.02		
	Analysis	**Jobs**	TH_Geom2b	Job name		
			Right Click and write input file			

Abaqus FEA Thermal-mechanical Analysis (THM) -No TBC

Models	LE	Parts					
			Features	Solid Extrude	Sketch	Extude-0.046 (B-0.04, E-0.006)	
				Partition Edge-1		Straight Line	
				Datum Pt-1	(0,0,0)		
				Datum Plane-1		Bottom Plane	
				Datum Pt-2	(0,0,0.006)	Dividing Encastre from Blade	
				Partition Cell-1		Divide whole blade into encastre (0.006) and 4 equal parts	
				Partition Cell-2			
				Partition Cell-3			
				Partition Cell-4			
			Sets	CRoot	Cooling passage of root	Apply BC (Uniform Temp)	
				CS	Cooling passage of blade	Apply BC (Temp Loads)-Amp.	
				Encastre	Datum Plane area of root	Applying BC - THM Analysis	
				HRoot	External (Gas) path area of root	Apply BC (Uniform Temp)	
				HS	External (Gas) path area of LE along Blade	Apply BC (Temp Loads)-Amp.	
				LE	Solid Volume of blade including Encastre	Useful in apply in CF Load	
				LE_AIRFOIL	Solid Volume of blade excluding Encastre	Useful in extracting results	
			Surfaces	CRoot	Cooling passage along encastre		
				CS	Cooling passage of blade		
			Section Assign	MARM	Solid, Homogenous Type		
		Materials	Conductivity	Type-Isotropic	**Conductivity**		**Temp**
		MARM-247		Temp Dependent	8.648		366.48
					24.214		1283.15
			Density	Distribution-Uniform	8525.41		
			Elastic	Type-Isotropic	**Elastic modulus**	**Poisson Ratio**	**Temp**
				Temp Dependent	1.4479E+11	0.29	255.37
					1.31E+11	0.29	533.15
					1.1514E+11	0.29	810.93
					86184000000	0.29	1088.71
			Expansion	Type-Isotropic	**Coeff of thermal exp**		**Temp**
				Temp Dependent	1.57E-05		922.04
					2.03E-05		1255.37
			Plasticity	Hardening-Isotropic	**Yield**	**Plastic Strain**	**Temp**
				Temp Dependent	8.53E+08	0	271.48
					9.37E+08	0	1042.59
					7.47E+08	0	1194.26
			Specific Heat	Constant Volume	5.02E+02		
		Section	Name	MARM-247			
			Type	Solid Homogenous			
			Material	MARMM-247			
		Assembly	Instances	LE	Mesh	Standard, Linear, 3D Stress	
						C3D8R - 8 node linear brick, reduced integration	
						Size-0.00044	
			Features	Datum Co-ordinate System			
			Sets	Created default as in Parts			
			Surfaces	Created default as in Parts			
		Steps	Step	**Initial_th**	**Idle-TO-Crusie**	**Cruise**	**Desc-Land**
			Type	Static General	Static General	Static General	Static General
			Response	Transient	Transient	Transient	Transient
			Time	100	500	12000	1820
			NL Geom	Off	Off	Off	Off
			Type	Automatic	Automatic	Automatic	Automatic
			No. of Increments	1.00E+08	1.00E+08	1.00E+08	1.00E+08
			Initial	0.1	1	0.01	0.01
			Min	1.00E-09	1.00E-09	1.00E-09	1.00E-06
			Max	10	50	1000	100
			Method	Direct	Direct	Direct	Direct
			Matrix Storage	Default	Default	Default	Default
			Solution Technique	Full Newton	Full Newton	Full Newton	Full Newton

		Field O/P Request	Name	Output-1		
			Step	Initial_th		
			Procedure	Static General		
			Domain	Set	LE-1.LE_Airfoil	
			Frequency	Every n increments	n=1	
			Output Variables	Select from List	Stress	S-Stress components and invariants
					Strain	E-Total Strain
						PE-Plastic Strain
						PEEQ-Eqv. Plastic strain
						PEMAG-Plastic strain magnitude
						THE-Thermal Strain
						LE-Logarthimic Strain
						ER-Mechanical Strain rate
					Displacement	U-Translation & Rotational
					Thermal	NT, Nodal Temperatures
						TEMP, Element Temp
						HFL, Heat Flux Vector
		History O/P Reque	Name	Output-1		
			Step	Initial_th		
			Procedure	Static General		
			Domain	Whole Model		
			Frequency	Every n increments	n=1	
			Output Variables	Preselect defaults	Energy	All
		Amplitude	Name	Centrifugal		
			Type	Tabular		
			Time Span	Total Time		
			0	0.757		
			630	0.757		
			630.5	0.8857		
		Loads	Name	Centrifugal		
			Type	Rotational Body Force		
			Step	Initial_th		
			Region	LE-1.LE		
			Axis			
			Point 1	0,0,-0.23		
			Point 2	0.035,0,-0.23		
			Distribution	Uniform		
			Angular Vel	1589.96		
			Amplitude	Centrifugal		
		BC	Name	Encastre		
			Type	Symm/AxisSymm/Encastre		
			Step	Initial		
			Region	LE-1.Encastre		
			Encastre	Encastre (u1=u2=u3=r1=r2=r3=0)		
		Predefined Field	Name	Initial_T	Name	Temperature
			Type	Temp	Type	Temp
			Step	Intial	Step	Intial_th
			Region	Read from file	Region	Read from file
			Distribution	Read from results or od	Distribution	Read from results or odb
			File name	TH_Geom2b.odb	File name	TH_Geom2b.odb
			Step	1	Begin Step	1
			Increment	0	End Step	1
			Mesh Compatible	Yes	Mesh Compatible	Yes
					Note : Go to Steps and modify for steps 2 to 4 for the begin and end steps.	
	Analysis	**Jobs**	THM_Geom2b			
			Right Click and write input file			
	Note :	Any changes carried, regenerate both the parts and assembly				

Abaqus FEA Thermal Analysis (TH) - TBC

Models	LE	Parts		LE	BC	TBC	TGO
			Features	Solid Extrude	Solid Extrude	Solid Extrude (T-0.00015)	Shell Extrude
				Partition Edge-1	Datum Plane-1	Datum Plane-1	Datum Plane-1
				Datum Pt-1	Datum Plane-2	Partition Cell	
				Datum Plane-1		Datum pt-1	
				Datum Pt-2			
				Partition Cell-1			
				Partition Cell-2			
				Partition Cell-3			
				Partition Cell-4			
			Sets	CRoot			
				CS			
				Encastre			
				HRoot			
				HS			
				LE			
				LE_AIRFOIL			
			Surfaces	LE_Ext	BC_ext	Blade_ext	TGO_ext
				Root_int	BC_int	Root_ext	TGO_int
				Cooling_1 - 8		TBC_int	
			Section Assign	MARM	Bond Coat		
			Mesh	0.002	0.002	0.002	0.002
				Heat Transfer	Heat Transfer	Heat Transfer	Heat Transfer
				Linear	Linear	Linear	Linear
				DC3D8	DC3D8	DC3D8	DS4
		Materials	Conductivity	Type-Isotropic	**Conductivity**		**Temp**
		MARM-247		Temp Dependent	8.648		366.48
					24.214		1283.15
			Density	Distribution-Uniform	8525.41		
			Elastic	Type-Isotropic	**Elastic modulus**	**Poisson Ratio**	**Temp**
				Temp Dependent	1.4479E+11	0.29	255.37
					1.31E+11	0.29	533.15
					1.1514E+11	0.29	810.93
					86184000000	0.29	1088.71
			Expansion	Type-Isotropic	**Coeff of thermal exp**		**Temp**
				Temp Dependent	1.57E-05		922.04
					2.03E-05		1255.37
			Plasticity	Hardening-Isotropic	**Yield**	**Plastic Strain**	**Temp**
				Temp Dependent	8.53E+08	0	271.48
					9.37E+08	0	1042.59
					7.47E+08	0	1194.26
			Specific Heat	Constant Volume	5.02E+02		
		Section	Name	MARM-247	BC	TBC	TGO
			Type	Solid Homogenous	Solid Homogenous	Solid Homogenous	Shell, Homogenous
			Material	MARMM-247	BC	TBC	TGO
			Thickness				5.00E-07
			Integration Points				5
		Assembly	Instances	LE	BC	TBC	TGO
			Position Constraints	Parallel Face	Co-axial	Face to Face	Face to Face-2
			Surfaces				
		Steps	Step	**Initial_th**	**Idle-TO-Cruise**	**Cruise**	**Desc-Land**
			Type	Heat Trasfer	Heat Trasfer	Heat Trasfer	Heat Trasfer
			Response	Transient	Transient	Transient	Transient
			Time	100	500	12000	1820
			NL Geom	Off	Off	Off	Off
			Type	Automatic	Automatic	Automatic	Automatic
			No. of Increments	1.00E+08	1.00E+08	1.00E+08	1.00E+08
			Initial	5.00E-01	5	5	5
			Min	1.00E-09	1.00E-06	1.00E-06	1.00E-06
			Max	10	100	100	100
			Max Allowable Temp Chang	5	2	2	2
			Max Allowable Emmissivity	1.00E-01	0.1	0.1	0.1
			Method	Direct	Direct	Direct	Direct
			Matrix Storage	Default	Default	Default	Default
			Solution Technique	Full Newton	Full Newton	Full Newton	Full Newton

		Field O/P Request	Name	Output-1		
			Step	Initial_th		
			Procedure	Heat Transfer		
			Domain	Model		
			Frequency	Every n increments	n=1	Every time step X =10 (alternative)
			Output Variables	Select from List	Thermal	NT, Nodal Temperatures
						TEMP, Element Temp
						HFL, Heat Flux Vector
		Interactions	Name	CRoot	CS	
			Type	Surface Film Condition	Surface Film Condition	
			Step	Initial_th	Initial_th	
			Surface	LE-1.CRoot	LE-1.CS	
			Definition	Embedded Coefficient	CS_Htc	
			Film Coeff	5123	1	
			Film Coeff Amp	hc_amp	hc_amp	
			Sink Defn	Uniform	CS_Tcool	
			Sink Temp	821	1	
			Sink Amp	TC_amp	TC_amp	
		Fields	Analytical Fields	CS_HTc	3E6*pow(Z,3)-172785*pow(Z,2)-924.25*Z+5123.4	
				CS_Tcool	(-2E6*pow(Z,3)+128189*pow(Z,2)+237.07*Z+820.91)	
				HS_MetalTemp	(-2E6*pow(Z,3)+108380*pow(Z,2)+682.53*Z+1036.4)	
		Amplitude	Name	HS_Hroot_amp	TC_amp	HC_amp
			Type	Tabular	Tabular	Tabular
			Time Span	Total Time	Total Time	Total Time
			0	0.7239	0.7177	1
			630	0.7239	0.7177	1
			630.5	0.7979	0.8054	0.9401
		BC	Name	HS_Metal Temp	Root_Metal Temp	
			Type	Temp	Temp	
			Step	Initial_th	Initial_th	
			Region	LE-1.HS	LE-1.Hroot	
			Distribution	HS_Metal Temp	Uniform	
			Magnitude	1	1037	
			Amplitude	HS-Hroot_amp	HS_Hroot_amp	
		Predefined Field	Name	Initial_T		
			Type	Temp		
			Step	Intial		
			Region	LE-1.LE		
			Distribution	Direct Specification		
			Magnitude	869.02		
	Analysis	**Jobs**	TH_Geom2b	Job name		
			Right Click and write input file			

Abaqus FEA Thermal-mechanical Analysis (THM) -TBC

Models	LE	Parts		LE	BC	TBC	TGO
			Features	Solid Extrude	Solid Extrude	Solid Extrude (T-0.00015)	Shell Extrude
				Partition Edge-1	Datum Plane-1	Datum Plane-1	Datum Plane-1
				Datum Pt-1	Datum Plane-2	Partition Cell	
				Datum Plane-1		Datum pt-1	
				Datum Pt-2			
				Partition Cell-1			
				Partition Cell-2			
				Partition Cell-3			
				Partition Cell-4			
			Sets	CRoot	BC_Encastre	TBC_Encastre	TGO_Encastre
				CS			
				Encastre			
				HRoot			
				HS			
				LE			
				LE_AIRFOIL			
			Surfaces	LE_Ext	BC_ext	Blade_ext	TGO_ext
				Root_int	BC_int	Root_ext	TGO_int
				Cooling_1 - 8		TBC_int	
			Section Assign	MARM	Bond Coat		
			Mesh	0.002	0.002	0.002	0.002
				Heat Transfer	Heat Transfer	Heat Transfer	Heat Transfer
				Linear	Linear	Linear	Linear
				DC3D8	DC3D8	DC3D8	DS4
		Materials	Conductivity	Type-Isotropic	**Conductivity**		**Temp**
		MARM-247		Temp Dependent	8.648		366.48
					24.214		1283.15
			Density	Distribution-Uniform	8525.41		
			Elastic	Type-Isotropic	**Elastic modulus**	**Poisson Ratio**	**Temp**
				Temp Dependent	1.4479E+11	0.29	255.37
					1.31E+11	0.29	533.15
					1.1514E+11	0.29	810.93
					86184000000	0.29	1088.71
			Expansion	Type-Isotropic	**Coeff of thermal exp**		**Temp**
				Temp Dependent	1.57E-05		922.04
					2.03E-05		1255.37
			Plasticity	Hardening-Isotropic	**Yield**	**Plastic Strain**	**Temp**
				Temp Dependent	8.53E+08	0	271.48
					9.37E+08	0	1042.59
					7.47E+08	0	1194.26
			Specific Heat	Constant Volume	5.02E+02		
		Section	Name	MARM-247	BC	TBC	TGO
			Type	Solid Homogenous	Solid Homogenous	Solid Homogenous	Shell, Homogenous
			Material	MARMM-247	BC	TBC	TGO
			Thickness				5.00E-07
			Integration Points				5
		Assembly	Instances	LE	BC	TBC	TGO
			Position Constraints	Parallel Face	Co-axial	Face to Face	Face to Face-2
			Surfaces				
		Steps	Step	**Initial_th**	**Idle-TO-Crusie**	**Cruise**	**Desc-Land**
			Type	Heat Trasfer	Heat Trasfer	Heat Trasfer	Heat Trasfer
			Response	Transient	Transient	Transient	Transient
			Time	100	500	12000	1820
			NL Geom	Off	Off	Off	Off
			Type	Automatic	Automatic	Automatic	Automatic
			No. of Increments	1.00E+06	1.00E+06	1.00E+07	1.00E+06
			Initial	1.00E+00	5	5	5
			Min	1.00E-10	1.00E-05	1.00E-05	1.00E-05
			Max	100	100	100	100